Supported Gold Catalysts for Selective Oxidation and Hydrogenation Reactions

Thesis Submitted to AcSIR
for the Award of the Degree of

Doctor of Philosophy

in

Chemical Sciences

AcSIR

By

Devadutta Nepak

(AcSIR Roll No.: 10CC11J26087)

Under the Guidance of
Dr. D. Srinivas

CSIR- National Chemical Laboratory
Pune-411008, India

December 2015

Certificate

This is to certify that the work incorporated in this Ph.D. thesis entitled **"Supported Gold Catalysts for Selective Oxidation and Hydrogenation Reactions"** submitted by **Mr. Devadutta Nepak** to Academy of Scientific and Innovative Research (AcSIR) in fulfillment of the requirements for the award of the Degree of **Doctor of Philosophy**, embodies original research work under my supervision. I further certify that this work has not been submitted to any other University or Institution in part or full for the award of any degree or diploma. Research material obtained from other sources has been duly acknowledged in the thesis. Any text, illustration, table etc., used in the thesis from other sources, have been duly cited and acknowledged.

Devadutta Nepak

(Research Student)

Dr. D. Srinivas

(Research Guide)

Date: 28-12-2015

Place: Pune

Dedicated to

My Beloved Parents

"Fight! In this life, you have to fight for your career and pursue lofty dreams that may or may not take you to the finish line. It is worth giving it a try. The beginning is always hard and, at times, discouraging, but you cannot give up."

– Jenny Lovell

Acknowledgements

First and foremost, I would like to acknowledge my research advisor, Dr. D. Srinivas. I am especially thankful for the great interest he showed in my work and the freedom I enjoyed in his group. He challenged me continuously. He was my toughest critic and at the same time my biggest supporter. My deepest personal regards are due for him forever.

My heartfelt thanks are due to my Doctoral Advisory Committee (DAC) members Dr. M. V. Badiger, Dr. B. L. V. Prasad and Dr. A. K. Kumbhar for their invaluable suggestions, support and encouragement during each stage of this work.

I extend my sincere thanks to Dr. C.V.V. Satyanarayna, Dr. C. S. Gopinath, Dr. T. Raja, Dr. K.R. Patil, Dr. C. P. Vinod, Dr. P. Dhepe, Dr. Nandini Devi, Dr. Subhangi Umberkar, Dr. S. S. Deshpande, Mr. R. K. Jha and Ms. Violet Samuel. I also like to thank Mr. Purushothaman, Mr. Madhu, Mr. Milind, and all other scientific and non-scientific staff for their help and support during my tenure as a research student.

I am really thankful to my teachers, Prof. Someswararao, Prof. Syambabu, Dr. Lokanadham, Mr. Simhachalam and Mr. R. Mohanty for their encouragement and motivation The single largest contribution in shaping my present comes from the faith, hope, encouragement and affection of my parents and I am grateful to them. Special thanks to my brothers Bibhu and Gyan for their support.

I sincerely thank all my seniors, labmates and friends especially Dr. Jithendra, Dr. Anuj, Dr. Bhogesh, Dr. Jabeen, Dr. Joby, Unni, Sagar, Ravi, Bineesh, Anthony, Vikram, Navya, Dr. Ramesh, Dr. Vilas, Dr. Raj, Dr. Kanna, Devraji, Atul, Laxmi, Ashok, Srikant, Pravat, Khiro, Prabha, Rami, Rayavarapu, Chaitu, Bala, Babu, Kasi, Narendra, Sinu, Sati, Ramu, Santu, Koti, Venki, Santi, Inniah, Anji, Jani, and all other telugu speaking community, who helped me during my research.

It is indeed my privilege to thank the Director, CSIR-NCL and Chairman, Catalysis Division for giving me this opportunity and extending all possible infrastructural facilities at CSIR-NCL open for the research work.

Finally, I thank the Council of Scientific and Industrial Research, New Delhi for financial assistance.

Devadutta Nepak

iv

Abbreviations

ATNT	Alkali & alkaline earth metal ion exchanged titanate nanotubes
BaTNT	Barium titanate nanotubes
BE	Binding energy
BET	Brunauer, Emmett and Teller
BJH	Barrett-Joyner-Halenda
Bzh	Benzaldehyde
CA	Cinnamaldehyde
CAL	Cinnamyl alcohol
DP	Deposition-Precipitation
DR UV-vis	Diffuse reflectance Ultraviolet-Visible
ESR	Electron spin resonance
GC	Gas chromatography
GC-MS	Gas chromatography-mass spectroscopy
$HAuCl_4$	Tetrachloroauric acid
HCA	Hydrocinnamaldehyde
HDP	Homogeneous deposition-precipitation
ICP-OES	Inductively coupled plasma-optical emission spectroscopy
IEP	Isoelectric point
IMP	Impregnation
$NaBH_4$	Sodium borohydride
NaTNT	Sodium titanate nanotubes
PPL	3-Phenylpropanol
SO	Styrene oxide
TBHP	*tert.*-Butylhydroperoxide
TEM	Transmission electron microscopy
THPC	Tetrakis(hydroxymethyl)phosphonium chloride
TOF	Turnover frequency
TPD	Temperature-programmed desorption
TPR	Temperature-programmed reduction
XPS	X-ray photoelectron spectroscopy
XRD	Powder X-ray diffraction

Table of Contents

Chapter-4:   Selective Oxidations over Au/Titanate Nanotubes: Effect of Pd & Alkali (Earth) Metal Ions   85

List of Figures

List of Schemes

List of Tables

Chapter - 1

General Introduction

1.1. Introduction

Nanocatalysis is one of the significant and oldest branches of nanotechnology. The era of nanocatalysis began in 19th century with the very first application of silver nanoparticles in photography and platinum nanoparticles in the decomposition of hydrogen peroxide [1]. Rampino and Nord [2] in 1941 reported the reduction of nitrobenzene over Pd and Pt and Cha and Parravano [3] in 1970 reported hydrogen-atom transfer between benzene and cyclohexane and oxygen-atom transfer between CO and CO_2 in presence of gold (Au) nanoparticles. A real breakthrough in the catalysis by Au nanoparticles came in 1980's from the pioneering works of Hutchings [4] and Haruta et al. [5] on acetylene hydrochlorination and low-temperature CO oxidation, respectively. These contemporaneous discoveries attracted a great deal of research interest probing into the causes for the unexpected catalytic activity of nano-Au, as the bulk Au is catalytically inert [6]. This discovery led to undertake tremendous research activities in the design of nanocatalysts with the aspiration to improve their stability, activity, and selectivity. This thesis reports metal oxide- and titanate nanotubes-supported nano-gold and its catalytic applications in selective oxidation (alcohols and styrene) and hydrogenation (cinnamaldehyde) reactions. Factors controlling the catalytic activity of the supported gold are probed.

1.2. Gold

Gold is a glittering metal having a range of applications in coinage to jewellery. It is also used in some advanced technologies viz., gold coated visors (used by astronauts to protect them from the sunlight) [5], nanoscale electronic devices [7] and medicine (for the treatment of rheumatoid arthritis) [8]. The astonishing catalytic behaviour of this ductile and malleable metal in a nano state made many researchers to go back to corroborate the physical and chemical properties of gold to understand how it is different from other metals. Bulk gold is distinctive among all the metals due to its high resistance towards oxidation and corrosion. According to Tanaka-Tamaru rule [9], the initial enthalpies of chemisorption of oxygen and other molecules are linearly related to the enthalpies of formation of the most stable oxides. This states that the energy of these chemisorbed oxygen atoms are similar to that of atoms or ions in bulk oxides. For example, silver has negative free energy of formation of oxides whereas the instability of gold oxide (Au_2O_3; $\Delta H_f = +19.3$ kJ.mol^{-1}) is unique for the inertness of gold. The properties of gold compared to its neighbouring metals are unexpected in many other respects [10].

The electronic configuration of Au (atomic number (Z) = 79) is [Xe]$4f^{14}5d^{10}6s^1$. It is a Group 11 (IB) element lies below copper and silver, which are known as the ''coinage

metals'' and placed in between platinum (Group 10) and mercury (Group 12). Fig. 1.1 presents the properties of these five metals. A dramatic increase in nuclear charge with increase in the number of valence electrons is observed in this region. The parameters such as melting temperature and vaporization energy are high for gold than for silver which points out the stronger inter-atomic bonding in gold [10]. The metallic radius of gold is slightly smaller than that of silver. This trend is same even in their + 1 oxidation state [11].
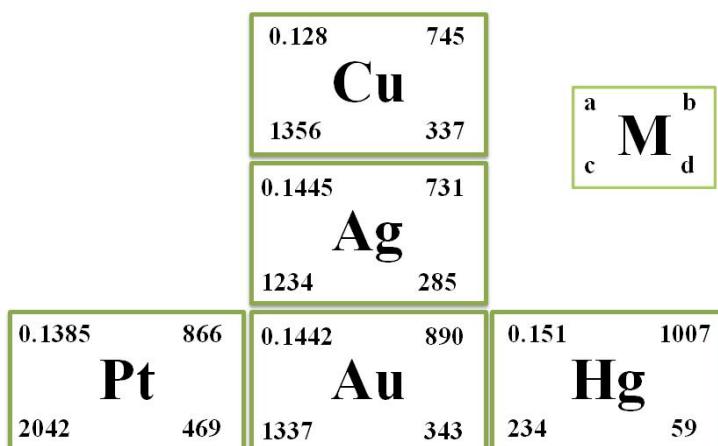
Fig. 1.1. Physical properties of Pt, Hg and the metals of group 11: (a) Metallic radius (nm), (b) First ionization potential (kJ.mol^{-1}), (c) Melting temperature (K) and (d) Sublimation enthalpy (kJ.mol^{-1}) [10].

Unlike alkali metals (Group 1), the Group 11 metals exist in various oxidation states (> 1) due to their low second and third ionization potential energies compared to alkali metals. Copper is known for its common oxidation state of +2. It also exists in +3 and +4 oxidation states in the complex fluoride anions $[CuF_6]^{3-}$ and $[CuF_6]^{2-}$, respectively. For silver, the +3 oxidation state is known. Gold exists in much wider range of oxidation states: commonly in +1 and +3 states. Unlike other Group 11 metals, in $[AuF_6]^{-}$, it exists in +5 oxidation state. The existence of auride anion (Au^-) in the form of a compound CsAu is also known due to its high electronegativity [12]. For this reason, other electronegative elements like sulfur or oxygen do not react with bulk gold. The chemistry of organo-gold has been explored recently [13].

Einstein's theory of special relativity on the energies of electron orbits postulates that the mass of an electron (*m*) increases as its speed (*v*) approaches towards the velocity of light (*c*) as per the following equation:

$$m = \frac{m_0}{\left(1-(c/v)\right)^{1/2}}$$ (1)

where m_0 is rest mass of electron. In fact, the impact of relativity on chemical phenomena was not considered in the Schrodinger equation and its relativistic analogue derived by Dirac. The theory describes that as the mass of the nucleus increases, the innermost $1s$ electrons have to increase their speed to maintain their position, therefore this orbital contracts, and the outer s shells shrinks in sympathy. The electrons in p orbitals are also affected to some extent, but the probability of being close to nucleus is low in the case of d and f orbitals so they are not affected. Thus, this relativistic effect is more apparent for atoms with atomic number above 50 (Sn). In consequence, the $6s$ orbital contracts across the third transition series and is greatest for gold, while for platinum the value is similar. Subsequently, as the $6p$ electron shell is filled, the effect becomes less noticeable (Fig. 1.2). These properties are very helpful in understanding why gold varies so much from its neighbours in its reactivity [13].
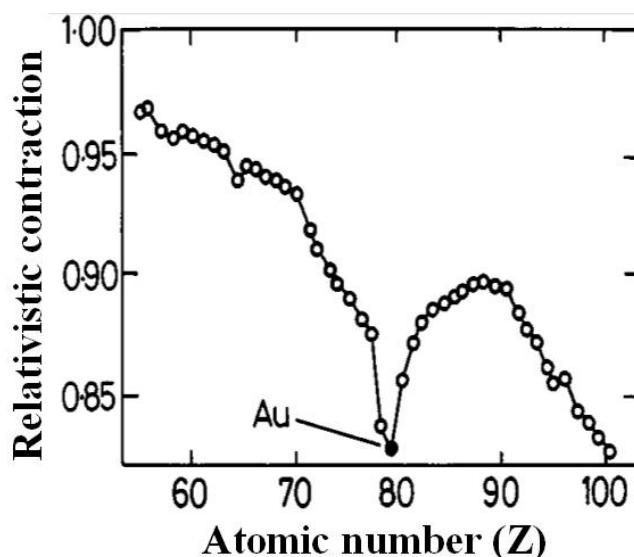
Fig. 1.2. Relativistic contraction (r_{rel}/r_{nonrel}) for $6s$ orbitals of heavy elements as a function of the atomic number (Z) [13].

1.3. Catalysis by Gold

Dulong and Thenard [14] in 1823 found that gold among the metals catalyzes the decomposition of ammonia. In fact, this gave away the idea of developing the concept of catalytic action to J. J. Berzelius. A few years later, Michael Faraday in 1834 observed the reaction of hydrogen with oxygen at room temperature catalyzed by gold [15, 16]. Later, this reaction was studied over gold gauze in 1906 and on gold powder in 1925 [17, 18]. A report on gold gauze catalyzed CO oxidation at 300 ºC was presented by Beaton and Elgin in 1927 [19]. Application of gold powder as a catalyst in ethene hydrogenation at 100 ºC was reported in 1925 [20]. In 1973, Bond and Sermon [21] reported that small gold particles dispersed on

SiO_2 and Al_2O_3 catalyze the hydrogenation of alkenes and alkynes. After a long history of minor interest in the application of the noblest metal (gold) in catalysis, the exceptional activity of nano-sized gold in acetylene hydrochlorination and CO oxidation reported by Hutchings [4] and Haruta et al. [22], respectively, in the late 1980s, had awakened the interest in the catalysis by gold.

1.4. Methods for Preparation of Supported Gold Catalysts

One of the features of nano-gold catalysis is the dependence of catalytic performance on Au particle size. The method of preparation and the nature of support have significant influence on the Au particle size and electronic properties. The supported Au catalysts can be prepared by several methods, which fall into the category of physical or chemical methods. In general, the chemical methods adopt simple approaches using relatively cheap and common Au precursors, such as tetrachloroauric acid ($HAuCl_4$) and $AuCl_3$ in aqueous solution. Further, Au precursors such as dimethylgold acetylacetonate [23] and phosphinegold complex [24] are also employed. Impregnation, co-precipitation, deposition-precipitation (DP), grafting and reduction-deposition are the wet chemical methods, in which aqueous solution of $HAuCl_4$ is used as a precursor.

1.4.1. Impregnation Method

An early attempt to make the supported Au catalysts employed one of the simplest classical methods i.e., impregnation (IMP). This method of preparation is frequently used because of its ease and low cost of production [25]. In general, a catalyst support has to be added into an aqueous Au precursor solution followed by drying of the suspension. Then, the material is calcined at a required temperature to obtain a supported metallic Au catalyst. If the liquid phase volume is equal to the pore volume of the support then, it is called conventional impregnation or dry impregnation method. In case, the liquid phase volume is higher than the support's pore volume, it is known as incipient wetness impregnation. The main disadvantage of this method is the poor control on particle size. In particular, the removal of residual chloride is difficult in this process, which causes aggregation of Au particles. Furthermore, the presence of residual chloride causes suppression in the reducibility of Au and hence, a significant amount of oxidized Au is observed even after calcination [26]. Because of the above mentioned noticeable disadvantages, this method has not been considerably investigated in the preparation of supported Au catalysts.

1.4.2. Co-Precipitation and Deposition–Precipitation Methods

These are the regular methods employed in the preparation of supported gold catalysts. In particular, deposition-precipitation (DP) method provides Au nanoparticles of

size 2-3 nm. In co-precipitation (CP) method, Au precursor ($HAuCl_4$) and a support precursor (metal nitrate) are mixed together in water to hydrolyze. They are precipitated using alkali (Na_2CO_3 and NaOH) [27, 28]. While in DP method, metal oxide or metal hydroxide is taken as a support instead of metal nitrate. Commonly, in both methods, an alkali (NaOH or Na_2CO_3) is used as a precipitating agent. The pH value of the synthesis mixture should be close to or a little higher than the support's isoelectric point (IEP) value (usually above 7) by which, low chlorine content and well distributed Au nanoparticles with smaller size can be obtained [29]. In DP method, the surface of the support acts as a nucleating agent. However, in these methods complete Au loading is not possible, which means that, a part of Au is washed away during the catalyst preparation [30]. DP method is advantageous than CP method as the entire active components stay on the surface of the support and none is buried in the metal hydroxide matrix.

It is possible to prevent the precipitation away from the support surface by avoiding local high concentrations of alkali. The DP method was modified using urea as precipitating agent [31], which avoids elegantly the local high concentrations of alkali by slow decomposition. In this way, hydroxyl ions generated slowly and uniformly throughout the process are consumed almost as soon as they are formed. This modified version of DP method is called "homogeneous deposition-precipitation method" [32].

Conventional DP method is not appropriate for the supports with low IEP values, as at high pH, the negatively charged support surface has strong electrostatic repulsion with the anionic Au precursor species. In those circumstances ion exchange reactions [33] or grafting method [34, 35] are necessary to obtain a high dispersion of Au nanoparticles on low IEP supports.

1.4.3. Reduction–Deposition Method

In all the methods mentioned above, adsorption and/or anchoring of Au ions onto the support surfaces is done prior to that they are converted into Au nanoparticles following by several surface reaction steps and heat treatment. Reduction-deposition method is an alternative approach, in which pre-formed Au colloidal solution is reduced to obtain Au nanoclusters / nanoparticles and then, it is deposited onto the support surface. In particular, this approach is called sol-immobilization method [36]. Sometimes, the reduction of Au can be done in presence of supports. The Au nanoparticles can be post-deposited onto a support surface in a separate step, which is known as a colloid-based method.

For the preparation of gold colloidal solution, many kinds of amines, thiols, organic acids and polymers such as tetrakis(hydroxymethyl)phosphonium chloride (THPC) [37],

polyvinylpyrrolidone (PVP) [38] and polyvinylalcohol (PVA) [36, 39] are used as capping agents. Capping agents are chosen to obtain very small nanoparticles with required diameter and which can be removed easily at lower temperatures without any obvious alteration in metal particle size. Reducing agents such as $NaBH_4$ and NH_2NH_2 (hydrazine) or photoreduction [40] procedures are employed to get the nanoparticles from the colloidal solution.

1.5. Catalysis by Supported Gold

In the late 1980s, Hutchings [4] realized that $AuCl_3$ is a very efficient catalyst for acetylene hydrochlorination due to the very high standard electrode potential of Au (+1.5 V). However, the era of nano-gold catalysis came into limelight after 1987, when Haruta et al. [22] demonstrated, for the first time, that the supported Au catalysts prepared by DP method are highly active for low-temperature CO oxidation reaction. Since then, nano-gold catalysis has emerged as a fascinating research globally [27, 41]. Supported gold and gold-based catalysts were tested for several other reactions such as: NO_x reduction [42, 43], water-gas shift (WGS) reaction [44], NH_3 oxidation [45], total oxidation of volatile organic compounds (VOCs) [46], preferential oxidation of CO in the presence of H_2 (PROX) [47], oxidation of alcohols [48], oxidation of olefin [49] and hydrogenation [50] (Fig. 1.3).
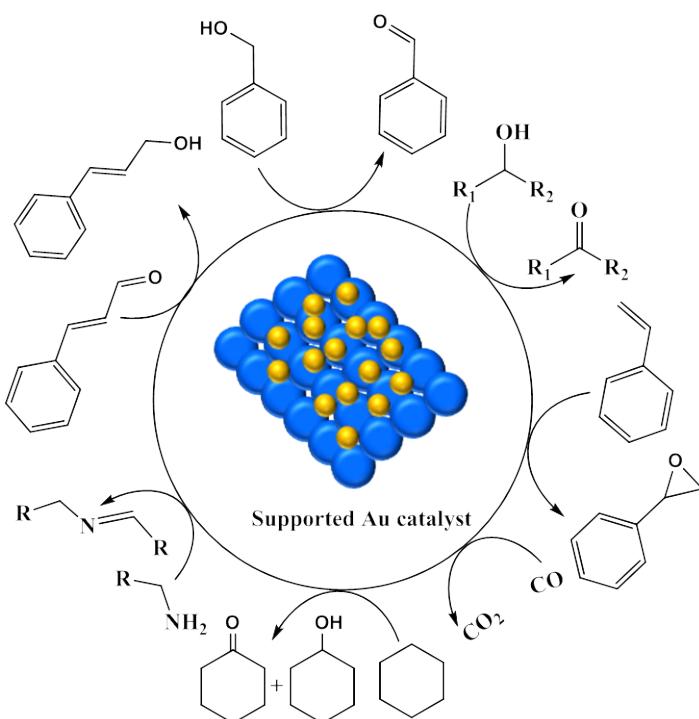
Fig. 1.3. Reactions over supported Au catalysts.

In addition, the unexpectedly high catalytic behavior of gold-based catalysts attained industrial importance in chemical processing reactions such as hydrogen purification, water pollution control and in the production of vinyl acetate monomer using ethene and acetic acid in the presence of oxygen [51]. These heterogeneous gold catalysts are highly active in various chemical transformations [52, 53]. The significant use of supported gold catalysts is clearly evidenced from an upsurge in the number of academic publications reported in recent times (Fig. 1.4). However, due to the large number of reports, here the explanation is confined to only some selected examples which have been investigated in this thesis. For instance, the selective oxidation of alcohols, oxidation of styrene and hydrogenation of α, β-unsaturated aldehydes catalyzed by gold are discussed below.
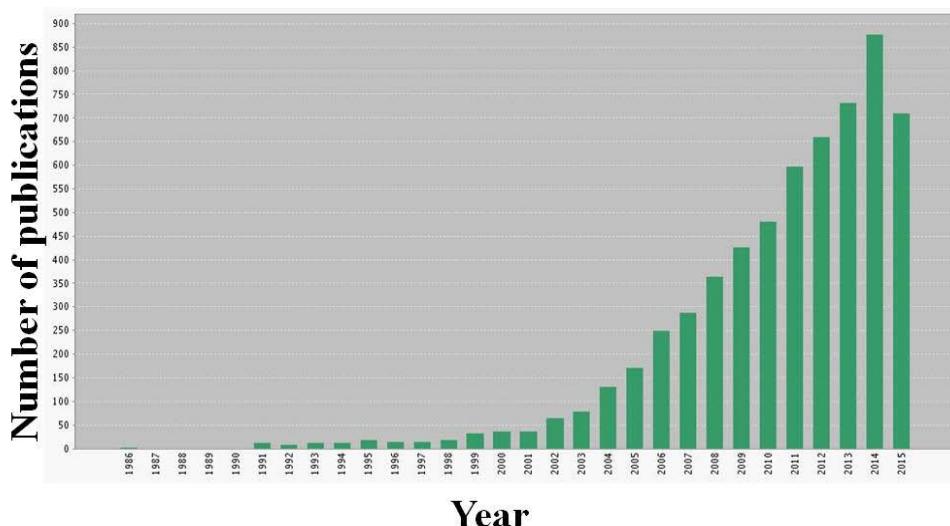
Fig. 1.4. Publications on catalysis by gold (source: Web of Science).

1.5.1. Selective Oxidation Reactions

Oxidation is a key process for producing oxygenates employed as valuable intermediates in the production of pharmaceuticals and bulk chemicals [54]. These reactions are often carried out using stoichiometric metal containing reagents (such as permanganate, dichromate, etc) as oxidants. These conventional methods are not eco-friendly [55]. Use of greener oxidants such as air, molecular oxygen and/or H_2O_2 and reusable heterogeneous oxidation catalysis make the oxidation processes more attractive [56]. Oxidation of alcohols and epoxidation of olefins are the widely studied oxidation reactions over gold catalysis. However, in olefin oxidation, it is very difficult to achieve higher reaction rates and selectivity to epoxide while using molecular oxygen instead of peroxides as oxidant.

1.5.1.1. Alcohol Oxidation

The selective oxidation of alcohols to aldehydes is an important reaction in both academia and industry [57]. The product aldehydes are used as intermediates in pharmaceuticals and perfumery [58]. Supported metal catalysts can efficiently oxidize alcohols to corresponding aldehydes [59]. Gold in its nano-state was found to be highly active for the oxidation of alcohols with air/molecular oxygen (O_2) in presence of an aqueous base (as promoter) [60]. This reaction may also proceed in the absence of a base [61]. In fact, oxidation of diols and triols under these conditions, produce the corresponding mono-acid, rather than aldehydes [62]. Prati and co-workers [62 - 64] illustrated that selective oxidation of alcohols and polyols proceeds well with Au/C catalysts. They demonstrated the gas-phase oxidation of volatile alcohols to selectively carbonyl compounds (aldehydes and ketones) over supported Au catalysts [64]. Carrettin et al. [65, 66] reported the oxidation of glycerol to glyceric acid with 100% selectivity using Au/graphite as a catalyst. Abad et al. [67] described the high activity of Au/CeO_2 catalyst in selective oxidation of alcohols. The challenge lies in the design of stable oxidation catalysts that enable high conversion and selectivity. The probable way of resolving this challenge is by developing bimetallic catalysts, such as Au promoted with Pd [68].

1.5.1.1.1. Liquid-Phase Oxidation of Benzyl Alcohol

Partial oxidation of benzyl alcohol leads to benzaldehyde (Scheme 1.1) which finds use in agrochemical, dyes and perfumery industries. It is used as an intermediate for aromatic talc, as a solvent for oils and in the manufacturing of benzoic acid, pharmaceuticals and photographic chemicals. The consumption pattern of benzaldehyde in several sectors is as shown in Fig. 1.5 [69].
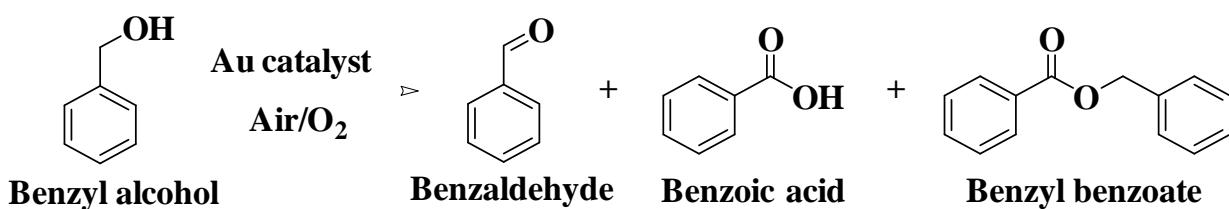
Scheme 1.1. Benzyl alcohol oxidation.
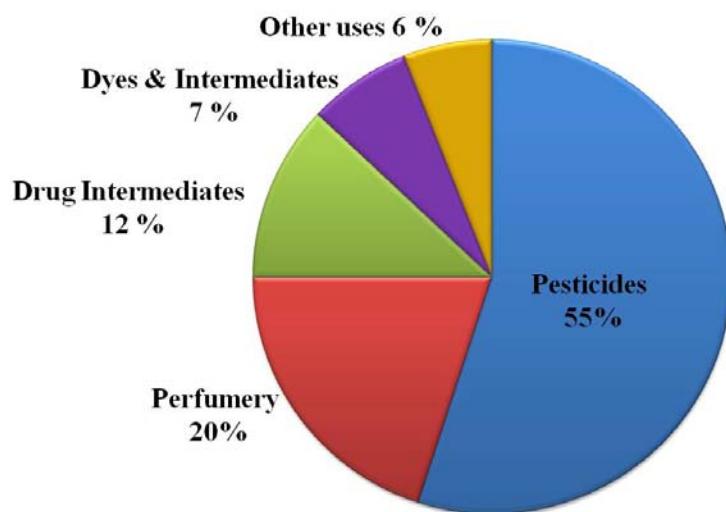
Fig. 1.5. Utility of benzaldehyde [69].

The main processes for the manufacturing of benzaldehyde are from the hydrolysis of benzal chloride and the air oxidation of toluene. Other old processes, including the oxidation of benzyl alcohol, the reduction of benzoyl chloride and the reaction of carbon monoxide and benzene are no longer used in industry. In 1950s and early 1960s, most of the world's synthetic benzaldehyde was produced from the air oxidation of toluene by both vapour and liquid-phase oxidation processes [69]. A catalyst consisting of the oxides of uranium, molybdenum or related metals was used in the vapour-phase process [70]. High temperatures and short contact times are the optimized conditions to obtain maximum yields. A by-product, maleic anhydride formed in the process can be reduced by adding small amounts of copper oxide to the catalyst mixture, even though; it is difficult to prevent over-oxidation to carbon oxide products [71]. In late 1950s, Dow Chemical Company developed a liquid-phase process wherein both benzaldehyde and benzoic acid were recovered. Then Viscosa developed a liquid-phase process for the synthesis of benzaldehyde during the work on toluene-to-caprolactam process. The benzaldehyde recovered from the liquid-phase air oxidation of toluene was purified by either batch or continuous distillation [69]. Choudhary et al. [72] reported a liquid-phase benzyl alcohol oxidation process using mixed metal oxides. High catalytic activity was obtained over Cu or Mn containing catalysts but with low selectivity towards benzaldehyde.

Enache et al. [73] reported that Au/Fe_2O_3 prepared by co-precipitation method shows highest conversion, while Au/TiO_2 prepared by impregnation method gives the highest selectivity to benzaldehyde. Au/C shows a poor activity and selectivity towards

benzaldehyde. Moreover, best results were obtained on Au/CeO_2. They observed a decrease in benzaldehyde selectivity over Au supported on acidic support. Choudhary et al. [74] studied the activity of Au supported on several alkali, alkaline earth and transition metal oxides prepared by homogeneous deposition-precipitation (HDP) method. Au/ZrO_2 was highly active in terms of turnover frequency (TOF). Au/Al_2O_3 was the best in terms of benzyl alcohol conversion. Highest conversion and benzaldehyde selectivity was obtained on Au/U_3O_8 catalyst. These reports presented the influence of preparation method and support on Au particle size and catalytic performance.

Kimmerle et al. [75] investigated several supported gold catalysts prepared by colloid deposition method and tested for benzyl alcohol oxidation activity under supercritical CO_2 medium. Best results were obtained on Au (1 wt.%)/TiO_2 catalyst. Table 1.1 lists the reports on selective oxidation of benzyl alcohol over Au catalysts.

1.5.1.1.1a. Effect of Co-added Metal - Palladium (Pd)

One of the ways to improve the catalytic activity and selectivity of supported metal catalysts is to promote with a second metal [76, 77]. Thus formed bimetallic nano-catalyst systems show high catalytic activity and selectivity compared to their monometallic counterparts. This high activity and selectivity are specifically obtained due to ensemble and/or ligand (electronic) effects [78, 79]. The platinum-group metals (Ni, Pd and Pt) are well known for their catalytic activity in many reactions. Particularly, considering the electron-band theory, the electronic interactions can be tuned by adding a Pt-group metal such as Pd (having an incompletely filled d-orbital) with Au (having a filled d-orbital). Thus by varying the alloy composition, one can alter the electronic interactions due to change in d band structure, which results in promotion of catalytic activity [80]. There are several reports explaining such effects influencing the activity and selectivity. Marx and Baiker [81] reported a bimetallic Au-Pd (1:9) system with increased benzaldehyde selectivity in the oxidation of benzyl alcohol. Chen et al. [82] observed this effect in the synthesis of vinyl acetate from acetoxylation of ethylene over Pd-Au alloys.

Over the years, Au-Pd bimetallic systems have become a fascinating area of research. Enache et al. [68] reported the enhanced activity of Au-Pd catalysts in the oxidation of benzyl alcohol to benzaldehyde as compared to the monometallic Au or Pd catalysts. The extensive characterization studies revealed the presence of Au rich-core surrounded by a Pd-rich shell. Moreover, Enache et al. [83] studied the effect of composition in Au-Pd/TiO_2 catalyst prepared by impregnation method and found that the 2.5wt%Au+2.5wt%Pd/TiO_2 was the most active catalyst in benzyl alcohol oxidation.

Table 1.1. Literature survey on supported Au catalysts for benzyl alcohol oxidation

Catalyst	Reaction conditions (benzyl alcohol, catalyst mass, solvent, oxidant, temperature (T) and reaction time (t))	Conversion (%)	Aldehyde selectivity (%)	TOF (h^{-1})	Reference
Au(0.7 wt.%)/SiO$_2$	Substrate = 40 ml, catalyst = 0.2 g, no solvent, P(O$_2$) = 2 bar, T = 100 °C, t = 3 h. TOF = moles of benzyl alcohol converted per mole of Au per unit time.	1.9	100	-	[73]
Au(2 wt.%)/CeO$_2$	"	3.4	100	150	[73]
Au(2 wt.%)/TiO$_2$	"	0.65	100	-	[73]
Au(5 wt.%)/Fe$_2$O$_3$	"	7.1	87.6	-	[73]
Au(2 wt.%)/C	"	2.3	90.4	-	[73]
Au(8 wt.%)/U$_3$O$_8$	Substrate = 29 mmol, catalyst = 0.1 g, no solvent, P(O$_2$) = 1.5 atm, T = 130 °C, t = 5 h. TOF = moles of benzaldehyde formed per unit mass of the deposited gold per unit time	53.0	95.0	0.37	[74]
Au(7.5 wt.%)/MgO	"	51.0	86.0	0.34	[74]
Au(6.4 wt.%)/Al$_2$O$_3$	"	68.9	65.0	0.41	[74]
Au(3 wt.%)/ZrO$_2$	"	50.7	87.0	0.85	[74]
Au(1 wt.%)/TiO$_2$(coll)	Substrate = 7 mmol, catalyst = 0.1 g, O$_2$ (14 mmol) + CO$_2$ (1591 mmol) at 150 bar, T = 100 °C, t = 3 h. (TOF = mol$_{product}$ mol$_{Au}$$^{-1}$ h^{-1})	16.0	99.0	161	[75]
Au(2.5 wt.%)TiO$_2$	Substrate = 20 ml, catalyst = 0.2 g, base (K$_2$CO$_3$) = 0.280 g, P(O$_2$) = 2 atm, T = 100 °C, t = 5 h.	35.0	55.0	534	[84]
Au(2.5 wt.%)MgO	"	47.4	58.0	723	[84]
Au(2.5 wt.%)Co$_3$O$_4$	"	65.8	55.7	1003	[84]
Au(1wt.%)/K$_2$Ti$_6$O$_{13}$ nanowires	Substrate = 1 mmol, catalyst = 0.1 mol% Au, methanol = 30 mmol, base (KOH) = 10 mol%, P(O$_2$) = 1 bar, T = RT, t = 24 h. * Yield of main product methyl benzoate, the value in parenthesis is obtained after 48 h without any added base.	>99.0	93.0 (13%)*	-	[85]

5Au/MnO$_2$-Rod	Substrate = 200 mmol, catalyst = 0.2 g, no solvent, P(O$_2$) = 0.3 MPa, T = 120 °C, t = 8 h. TOF = moles of benzyl alcohol converted per mole of Au present per unit time.	55.3	96.9	320	[86]
Au(2.5 wt.%)/γ-Ga$_2$O$_3$	Substrate = 20 ml, catalyst = 0.2 g, P(O$_2$) = 5 atm, T = 130 °C, t = 5 h	40.0	97.7	606	[87]
Au (1 wt.%)/Ga$_3$Al$_3$O$_9$	Substrate = 1 mmol, catalyst = 0.1 g, toluene = 10 ml, P(O$_2$) = 20 mLmin^{-1}, T = 80 °C, t = 2 h	98.0	>99.0	-	[88]
Au(1 wt.%)/APS-S16	Substrate = 50 mmol, catalyst = 0.02 g, P(O$_2$) = 20 ml/min, T = 140 °C, t = 1 h	2.5	86.1	1937	[89]
Au/MgCr–HT	Substrate = 1 mmol, catalyst = 0.2 mol% Au, toluene = 10 ml, O$_2$ = 20 mLmin^{-1}, T = 100 °C, t = 1 h	96.0	>99.0	1880	[90]
Au/LDH	Substrate = 0.6 mmol, catalyst = 0.08 g, toluene = 10 ml, O$_2$ = 30 ml/min, T = 80 °C, t = 20 h	89.0	93.0		[90]
Au/NG-4.0	Substrate = 0.1 mmol, catalyst = 0.03 g, H$_2$O = 80 ml, P(O$_2$) = 1 atm, T = 70 °C, t = 6 h	67	40	-	[90]
Au(2.76 wt.%)/Mn–CeO$_2$	Substrate = 4 mmol, catalyst = 0.1 g, toluene = 4 ml, P(O$_2$) = 50 ml/min, T = 90 °C, t = 3 h, Mn/Ce mol/mo = 6/100	43.22	>99.0	-	[91]
Au(4 wt.%)/CuO	Substrate = 10 mmol, catalyst = 0.01 g, P(O$_2$) = 5 ml/min, T = 80 °C, t = 5 h. TOF was calculated on the basis of total loading of gold.	58.5	98.2	56	[92]
Au(4.4 wt.%)/NiO	"	40.7	68.7	25	[93]
Au(3.4 wt.%)/MCM-41	"	71.1	92.2	5.6	[94]
Au(1 wt.%)/MnO$_2$-12 h	Substrate = 2 g, catalyst = 0.02 g, P(O$_2$) = 0.2 MPa, T = 120 °C, t = 4 h	8.8	98.5	-	[95]
Au(1.97 wt.%)-100CeO$_2$@SBA-15	Substrate = 2.5 mmol, catalyst = 0.01 mmol of Au, P(O$_2$) = 20 ml/min, T = 90 °C, t = 4 h	18.0	>99.0	270	[96]

They have also explored the application of Au-Pd bimetallic catalysts in the direct synthesis of H_2O_2 [97, 98], oxidation of glycerol [99], hydrochlorination of acetylene [100] and many other reactions [101-103].

Li et al. [104] investigated the catalytic activity of the Au and Au-Pd supported on zeolites in oxidation of benzyl alcohol and explained that the acidity of support leads to by-product formation and addition of Pd brings high conversion while maintaining the aldehyde selectivity. Miedziak et al. [105] demonstrated the high stability of Au-Pd/CeO_2. Table 1.2 lists the catalytic activity of Au-Pd systems in benzyl alcohol oxidation.

1.5.1.1.2. Nature of Active Au Sites and Activation of O_2

The transition-metal oxidation catalysts follow the Mars-van-Krevelen mechanism, where O^{2-} is a key intermediate involved in oxidation [106], while the formation of O^{2-} species is thermodynamically prohibited on gold and the mechanism by which gold nanoparticles activate O_2 remains unclear. For various oxidation reactions over supported Au catalysts, their active sites and reaction pathways are probably different. According to the theoretical calculations and experimental results, the interaction of Au and O_2 elaborately summarised as follows:

(1) The reactivity towards O_2 is dominated by Au clusters possessing an odd number of electrons, i.e., the odd-numbered clusters.

(2) For most small cluster sizes, O_2 is energetically favoured to be dissociatively bound, although the barriers to dissociation are expected to be large (in the order of 1 eV and greater) and thus may not be observed experimentally owing to kinetic trapping.

(3) In the cases where O_2 adsorption is observed, charge transfer to O_2 occurs with an increase of the O-O distance, suggesting activation towards a superoxo-like state.

(4) The extent of activation (for molecular adsorption) is predicted to be less for the neutral clusters than the anionic ones [107-109].

Van Bokhoven et al. [110] probed the charge transfer from small Au particles to oxygen using in situ XANES, when Au/Al_2O_3 was exposed to oxygen. Other findings suggest that the activation of O_2 on supported Au particles occurs at the three-phase boundary between the Au cluster, the metal oxide, and the gas phase [111]. The mostly acceptable activation of O_2 on even-sized Au cluster anions was correlated to the alternating electron affinities [112, 113] of the gold clusters which arise from their alternating closed- and open-shell electronic structure. Therefore, the single-electron donation from the anionic cluster into the O_2 π^* orbital forming a superoxo (O_2^-) moiety was proposed [114].

Table 1.2. An overview on supported Au-Pd catalysts for benzyl alcohol oxidation

Catalyst	Reaction conditions (benzyl alcohol, catalyst mass, solvent, oxidant, temperature (T), reaction time (t))	Conversion (%)	Aldehyde selectivity (%)	TOF (h^{-1})	Reference
1% Pd_{20}@Au_{80}/AC	Substrate = 0.3 M, alcohol/metal 1/500 mol/mol, were mixed in distilled water (total volume 10 ml), T = 60 °C, $P(O_2)$ = 1.5 atm. TOF calculated after 15 min of reaction	90.0	>99.0	1021	[115]
1% Pd_{20}@Au_{80}/AC	Same as above with the addition of the appropriate amount of NaOH (alcohol/NaOH = 1 mol/mol). TOF calculated after 15 min of reaction.	90.0	46.0	1189	[115]
Au^0–Pd^0/HSA-$BaAl_2O_4$	Substrate = 1.25 mmol, catalyst = 0.5 μmol metal, DMF = 5 ml, $P(O_2)$ = 2.0 MPa, T = 80 °C, t = 55 min. TOF was calculated on the basis of total loading of gold	98.0	100	2680	[116]
0.1%Bi@ 1% Au–Pd/C	Substrate/metal = 5000/1 (mol/mol), $P(O_2)$ = 2 atm, T = 80 °C. TOF calculated after 15 min of reaction.	90.0	85.0	2546	[117]
1%Au–Pd/MgAl-MMO	Substrate = 1 ml, catalyst = 0.01 g, $P(O_2)$ = 1 bar, T = 120 °C, t = 240 min	90.0	93.0	325	[118]
$Pd_{0.2}$Au/MSN	Substrate = 5 ml, catalyst = 0.2 g (m_{BzOH}/m_{Metal} = 1000/1), $P(O_2)$ = 0.5 MPa, T = 90 °C, t = 1 h. TOF in g g^{-1}_{metal} h^{-1}	98.0	>95.0	1320	[119]
Au–Pd@ZrO_2	Substrate = 3 mmol, catalyst = 0.05 g, ethanol = 10 ml, $P(O_2)$ = 1 atm, T = 40 °C, t = 7 h. TOF at 1 h	91.0	97.0	79	[120]
1Au5Pd/APS-S16	Substrate = 50 mmol, catalyst = 0.02 g, $P(O_2)$ = 20 ml/min, T = 140 °C, t = 1 h	22.3	94.4	8667	[89]
1% Au + Pd/TiO_2	Substrate = 40 ml, catalyst = 0.1 g, $P(O_2)$ = 150 psi, T = 120 °C, t = 2 h. TOF after 0.5 h.	61.2	69..2	15400	[121]
1% Au + Pd/C	"	81.1	55.0	35400	[121]

1.5.1.2. Oxidation of Olefins

Oxidation of alkenes is an important reaction as the product - epoxides and aldehydes is used as an intermediate in the manufacture of pharmaceuticals, agrochemicals, food additives, sweeteners, perfumes, epoxy resins, plasticizers, etc. The production of epoxide by the electrophilic addition of oxygen to an olefinic C=C bond is still a challenging reaction in oxidation catalysis. Many oxidation reactions proceed well with the most environmentally benign oxidant - molecular oxygen. However, in many other cases, such as epoxidation reactions, the molecular oxygen does not work efficiently. In such conditions, a far more reactive form of oxygen species is necessary to produce epoxides. Epoxidation of several olefinic compounds such as styrene, cyclohexene, allyl chloride, etc by solid catalysts using various epoxidizing agents has been described in the literature [122]. The earliest reports on the silver-based catalysts [123-125] for gas-phase propylene epoxidation using molecular oxygen had shown poor propylene oxide (PO) selectivity. However, these catalysts were explored extensively, till Sinha et al. [126] discovered the potential of Au nanoparticles as epoxidation catalyst in gas-phase epoxidation of ethene using molecular oxygen, where hydrogen was used as sacrificial reducing agent. It was one of the breakthroughs in the catalysis of Au for epoxidation.

1.5.1.2.1. Oxidation of Styrene

Liquid-phase epoxidation of styrene is of immense interest due to its selective product styrene oxide (Scheme 1.2), which is a versatile and useful intermediate for the production of UV-absorbers, perfumes, pharmaceuticals, sweeteners and epoxy resins. The traditional method of epoxidation of styrene utilizes stoichiometric amount of peracid as oxidant [127].
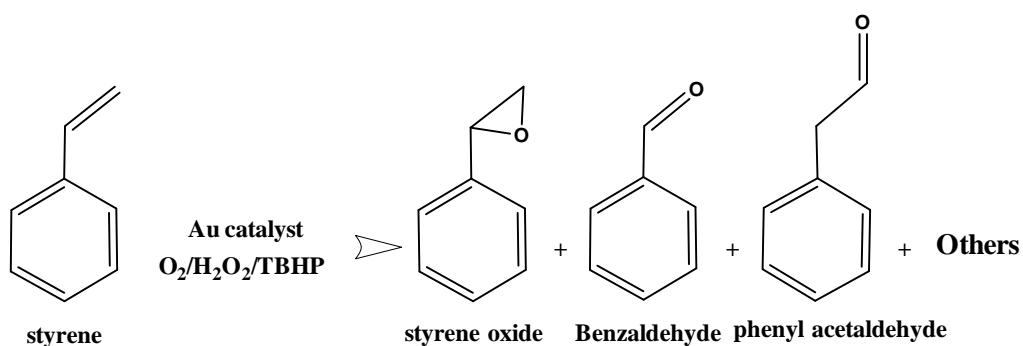
Scheme 1.2. Styrene oxidation.

The reaction safety concerns led many researchers to develop a better catalyst for epoxidation. Herrmann epoxidation system is one of such inventions, where methyl-

trioxorhenium was used as a catalyst along with H_2O_2 as oxidant [128, 129]. Furthermore, many solid catalysts such as TS-1 [130, 131], Ti-MCM-41 and Ti-HMS [132], Ti-beta, Cu-HMS [133] and transition metals supported on metal oxides (SiO_2, Al_2O_3, ZrO_2, MgO) and activated carbon [134] have been used for this reaction. Leaching of incorporated metal is the main problem with these catalyst systems.

A number of studies on supported Au catalysts for the epoxidation of styrene have been reported by Patil et al. [135]. They evidenced the effectiveness of homogeneous deposition-precipitation (HDP) method, which is having a fine control to obtain well dispersed, smaller size Au nanoparticles. Moreover, they identified the presence of both metallic and cationic Au species. They found that Au/TiO_2 shows better catalytic performance compared to Au/CeO_2, where the conversion of styrene over Au/TiO_2 was 60% with the epoxide selectivity being 53% using TBHP (in benzene) as oxidant. The activity and selectivity towards epoxide over gold supported on group IIIA metal oxides (γ-Al_2O_3, Ga_2O_3, In_2O_3, and Tl_2O_3) prepared by HDP method followed the order: Al_2O_3 < Ga_2O_3 < In_2O_3 < Tl_2O_3 [136]. The order obtained was well correlated with the ability of support oxide to stabilize cationic Au. Yin et al. [137] studied the epoxidation of styrene over Au/mesoporous Al_2O_3 using TBHP as oxidant at 82 °C. Styrene conversion of 68% with selectivity towards epoxide of 74% was achieved. The catalytic performance was influenced by the surface basicity. Similar observations were reported on Au supported on MgO, CaO, SrO, and BaO [138, 139] and also on many rare-earth oxides and transition metal oxides, such as Yb_2O_3, Tb_2O_3, Eu_2O_3, Sm_2O_3, NiO, CuO, and U_3O_8 by Choudhary and co-workers [140-142]. Zhang et al. [143] elucidated the crystal face selective deposition of Au and the higher activity of Au nanoparticles of 2-3 nm deposited at lateral faces {10$\bar{1}$0} of a layered double hydroxide compound (LDH) in the oxidation of styrene by TBHP. Au_{25} clusters were immobilized on hydroxyapatite (HAP) using $Au_{25}(SG)_{18}$ precursor. It showed best catalytic performance for epoxidation of styrene in toluene medium and TBHP as oxidant [144].

There are very few investigations on the liquid-phase styrene oxidation with molecular oxygen as oxidant catalyzed by supported gold catalysts. Turner et al. [145] illustrated that Au_{55} nanocrystals supported on carbon and BN are catalytically active for styrene oxidation using O_2 as sole oxidant, without any radical initiator. However, the major product obtained was benzaldehyde. Zhu et al. [146] reported that the unsupported $Au_{25}(SR)_{18}$ nanoclusters are catalytically active for oxidation of styrene with a selectivity towards benzaldehyde of 70%, epoxide of 25% and others of 5%. SiO_2-supported $Au_{25}(SR)_{18}$

nanoclusters showed a comparable performance to that of support free nanoclusters. The effect of oxidants such as TBHP and O_2 on the catalytic performance of SiO_2 supported $Au_{25}(SR)_{18}$ nanoclusters was also investigated by the same group [147]. Their results indicated that the type of oxidant plays a vital role in styrene oxidation. Moreover, the activation of O_2 and type of oxygen species formed influenced the styrene conversion and product selectivity. Table 1.3 presents a list of supported catalysts used in styrene oxidation.

1.5.1.3. Titanate Nanotubes as Support

Among metal oxides, titanium oxide is one of the predominantly studied support material because of its reducible nature, low cost and abundance. But its low surface area is one of the disadvantages to accommodate more number of active sites [148]. During 1991, the discovery of carbon nanotubes by Iijima [149] gave an idea to elevate the development of a new synthesis procedure to prepare higher specific surface area titanate nanotubes by Kasuga [150] using a simple alkali hydrothermal synthesis procedure.

The characteristic properties such as high surface area, basicity and mesoporous nature of these materials made them suitable and promising supports in heterogeneous catalysis. A variety of catalytic applications of alkali as well as protonated titanate nanotubes as catalyst supports and also as catalysts have been reported [151]. Catalytic performance of Au supported titanate nanotubes are reported for CO oxidation, alcohol oxidation, CO_2 reduction by hydrogen and water-gas shift reaction [151, 152]. All these reports led our attention to use the sodium titanate nanotubes, and alkali and alkaline earth metal ion-exchanged titanate nanotubes as support to synthesize Au, Au-Pd supported catalysts for selective oxidation of alcohols and oxidation of styrene and to emphasize the effect of their characteristic properties on the catalytic performance of Au.

Table 1.3. Literature reports on the oxidation of styrene over supported Au catalysts

Catalyst	Oxidant	Reaction conditions (styrene, catalyst mass, solvent, temperature (T) and reaction time (t))	Conversion (%)	Selectivity (%)		TOF (h^{-1})	Reference
				SO	Bzh		
Au(1 wt.%)/TiO$_2$	TBHP	Substrate = 10 mmol, catalyst = 0.1 g, 26% TBHP in benzene = 5.7 ml (15 mmol), T = 82-83 °C, t = 3 h	60.0	53.0	7.0	-	[135]
Au(5.4 wt.%)/Tl$_2$O$_3$	TBHP	"	60.5	56.9	7.6	-	[136]
Au(7.5 wt.%)/MgO	TBHP	"	62.6	54.3	10.8	29.8	[138]
Au(4.7 wt.%)/Yb$_2$O$_3$	TBHP	Substrate = 10 mmol, catalyst = 0.1 g, 26% TBHP in benzene = 5.7 ml (15 mmol), T = 82 °C, t = 3 h	42.0	60.1	7.1	-	[142]
Au(0.66 wt.%)/LDH	TBHP	Substrate = 10.18 mmol, catalyst = 0.1 g, benzene = 5 ml, TBHP 65% in water = 2.8 ml (28.6 mmol), T = 80 °C, t = 8 h	67. 4	73.5	21.3	157.2	[143]
Au(0.5 wt.%)/HAP	TBHP	Substrate = 0.04 g, catalyst = 0.05 g, anhydrous TBHP = 0.2 g, toluene = 10 ml, T = 80 °C, t = 12 h	100	92.0		114.0	[144]
0.6-wt.% Au$_{55}$/BN	O$_2$	Substrate = 12 mmol, catalyst = 0.1 g, toluene = 20 ml, P(O$_2$) = 0.5 bar, T = 100 °C, t = 15 h	19.2	14.0	82.3	-	[145]
Au-2S-IL-(4.5 wt.%)	H$_2$O$_2$	Substrate = 1.04 g, catalyst = 0.05 g, acetonitrile = 5 g, H$_2$O$_2$/styrene = 2 (mol),T = 70 °C, t = 6 h	50.4	92.1	1.7	81.9	[153]
Au(0.3 wt.%)/CNTs	TBHP	Substrate = 4 mmol, catalyst = 0.05 g, acetonitrile = 5 ml, TBHP 70% in water = 3 ml, T= 82 °C, t=10 h	67.2	77.5	13.1	2733	[154]
Au/SBA-15-N	TBHP	Substrate = 6 mmol, catalyst = 0.08 g, toluene = 10 ml, TBHP = 3 mol% based on substrate, T = 100 °C, t = 8 h	15.6	3.0	86.0	-	[155]
Au$_{25}$–CeO$_2$ NRs(1 wt.%)	O$_2$	Substrate = 12 mmol, catalyst = 0.1 g, pure O$_2$ stream or 36 mmol TBHP, acetonitrile = 15 ml, T = 80 °C, t = 24 h	~5	0	100	-	[156]
Au$_{25}$–CeO$_2$ NRs(1 wt.%)	TBHP	"	99.0	44	32	-	[156]

1.5.2. Hydrogenation Reactions

Besides oxidation reactions, the interest in the catalysis by supported gold was driven by its enhanced selectivity towards the desired product in a variety of hydrogenation reactions including hydrodechlorination [157] and hydrogenation of nitro compounds [158, 159], alkenes [160, 161], alkadiens [162, 163], alkynes [164, 165] and α,β-unsaturated carbonyl compounds. The study on hydrogenation of alkenes and alkynes over Au/SiO_2 was first reported by Bond and Sermon [166]. Later, Parrvano et al. [167, 168] reported hydrogen and oxygen transfer reactions over Au/Al_2O_3 and Au/MgO catalysts. The characteristic metal-support interactions of supported nano-gold influenced the rate of dissociative adsorption of H_2. Theoretical studies revealed that hydrogen chemisorption is favoured on smaller Au particles and is enhanced with increase in low coordinated corner and edge sites [169]. Hydrogenation of α,β-unsaturated carbonyl compounds over supported gold catalysts yields the corresponding unsaturated alcohols which are intermediates in the formation of fine chemicals and pharmaceuticals [170, 171]. Supported gold catalysts catalyze the hydrogenation of nitro compounds to yield selectively the corresponding substituted aromatic amines [158].

1.5.2.1. Hydrogenation of Cinnamaldehyde

Chemoselective hydrogenation of α,β-unsaturated aldehydes (e.g., cinnamaldehyde) to its semi-hydrogenated products viz., saturated aldehydes (from C=C hydrogenation) and unsaturated alcohols (from C=O hydrogenation) (Scheme 1.3) is of great interest as the hydrogenated products are used in fragrances, pharmaceuticals and other applications [172]. However, the challenge lies in selective hydrogenation of C=O, which is thermodynamically unfavourable compared to C=C bond hydrogenation [173].
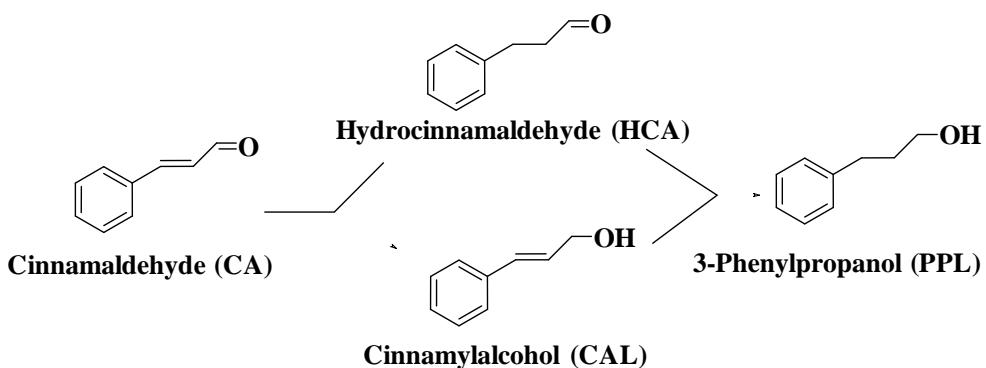
Scheme 1.3. Hydrogenation of cinnamaldehyde

Chemoselective hydrogenation of α,β-unsaturated aldehydes is a structure sensitive reaction. The catalytic activity and selectivity have strong dependence on the size and electronic effect arises from metal-support interactions. According to Bond [174], the contribution of smaller particles towards catalytic activity is more. Claus et al. illustrated the effects of particle size, geometry and electronic structure on activity and selectivity in crotonaldehyde hydrogenation using nano-gold supported on various supports [50]. Milone et al. [175] studied the liquid-phase hydrogenations over several gold catalysts with supports like goethite (FeOOH), maghemite (g-Fe_2O_3), hematite (γ-Fe_2O_3), TiO_2 and Al_2O_3. They reported that high activity and C=O hydrogenation selectivity was achieved over Au/FeOOH, while Au/γ-Fe_2O_3 catalyst was least active/selective. Bus et al. [171] reported that the Au particle size of 2 nm or less over Au/Al_2O_3 is more active and selective in cinnamaldehyde hydrogenation compared to Pt/Al_2O_3 catalyst. Milone et al. [176] specified that the acidic sites over Au/TiO_2 prompted the formation of cinnamyl ethyl ether rather than cinnamyl alcohol in the hydrogenation of cinnamaldehyde. Rojas et al. [177] studied the hydrogenation of cinnamaldehyde over Au/SiO_2 and Ir/SiO_2. They observed that Au/SiO_2 catalyst was more selective towards unsaturated alcohol compared to Ir/SiO_2. This increase in selectivity towards C=O hydrogenation was correlated with the presence of negatively charged Au. Table 1.4 presents the literature on supported Au catalysts for hydrogenation of cinnamaldehyde. Support material influences the physical and electronic structure of Au nanoparticles which in turn dictate the selective interaction of Au with a specific functional group (C=C or C=O) [178].

1.5.2.2. Interaction of Gold with Hydrogen

Hydrogen (H_2) chemisorption and dissociation are the crucial initial steps involved in hydrogenation reactions. Weak adsorption of a small amount of hydrogen was found on low coordinated gold atoms on the film surface at a temperature of -195 °C and desorbed at around -148 °C. [179] Lin and Vannice [180] detected weak, reversible adsorption of hydrogen on 30 nm gold particles on TiO_2 at 27 and 127 °C. H_2 chemisorption properties of Au/Al_2O_3 and Au/SiO_2 catalysts were investigated by Bus et al. [181] in a temperature range of 25 to 250 °C. They observed that only 10-30% of the total adsorbed hydrogen was not desorbed while evacuating for 2 h at the analysis temperature. The shapes of the hydrogen adsorption isotherms indicated the dissociative chemisorption of hydrogen. It was also proved by H/D isotopic exchange experiments. As the hydrogen uptake was found to increase with temperature, it was suggested that the adsorption of hydrogen is an activated process and very

Table 1.4. Literature on hydrogenation of cinnamaldehyde (CA) over supported Au catalysts

Catalyst	Reaction conditions	Conversion (%)	Selectivity (%)		Reference
			CAL	HCA	
Au(3.4 wt.%)/ZnO$_c$	CA = 1 g in 25 ml isopropanol, catalyst = 0.044 g in 25 ml isopropanol, H$_2$ pressure = 20 bar, T = 70 °C, t = 4 h	45.7	99.0	-	[182]
Au(1.62 wt.%)/CNTs	CA = 0.2 mmol, catalyst = 0.005 g, toluene = 1.0 ml, H$_2$ pressure = 0.8 MPa, T = 90 °C, t = 2 h	95.0	-	91.0	[183]
Au(1.2 wt.%)/HDAE	CA = 20 ml of 0.08 M isopropanol, catalyst = 0.2 g, H$_2$ pressure = 1 MPa, T = 100 °C, t = 3 h	28.0	88.0	-	[184]
Au(1.1 wt.%)/5FeAl	"	20.0	67.0	-	[184]
Au(1.5 wt.%)/Al	"	16.0	26.0	-	[184]
AF5.3	CA = 0.6 mmol, catalyst = 0.500 g, ethanol = 25 ml, H$_2$ pressure = 1 atm, T = 60 °C, t = 1 h	50.2	83.8	13.6	[185]
AAl2.3dp	"	50.1	60.3	33.9	[185]
Au(1 wt.%)/SiO$_2$	CA = 4 mmol, catalyst = 0.050 g, toluene = 5 ml, H$_2$ pressure = 1 MPa, T = 150 °C, t = 12 h	11.0	23.0	73.0	[186]
Au(1 wt.%)/Al$_2$O$_3$	CA = 4 mmol, catalyst = 0.050 g, toluene = 5 ml, H$_2$ pressure = 1 MPa, T = 150 °C, t = 2 h	5.0	28.0	65.0	[186]
Au (5 wt.%)/XC-72	CA = 4 mmol, catalyst = 0.050 g, toluene = 5 ml, H$_2$ pressure = 1 MPa, T = 150 °C, t = 4 h	15.0	32.0	63.0	[186]
Au(2 wt.%)/Mg$_2$AlO	CA = 2 ml, catalyst = 0.500 g, ethanol = 78 ml, H$_2$ pressure = 929 kPa, T = 120 °C, t = 2 h	77.8	84.8	6.5	[187]
ExPVA(Au-Citr, 1 wt.%)/SiO$_2$	CA= 4 mmol, catalyst= 0.050 g, p-xylene= 5 ml, H$_2$ pressure= 2 MPa, T= 150 °C, t= 4 h.	11.0	20	76	[188]
Au(1.73 wt.%)/MAC-1 (15:4:1Mg: Al: Ce mol ratio)	CA = 0.8 mmol, catalyst = 0.200 g, ethanol = 60 ml, H$_2$ pressure = 1 MPa, T = 120 °C, t = 6 h	91	41	44	[189]
Au(5.6 wt.%)/P25	CA = 1.2 g, catalyst = 0.150 g, methanol = 16 ml, H$_2$ pressure = 20 kg/cm^2, T = 120 °C, t = 1 h	25.4	18.1	74.1	[190]

likely associated with hydrogen dissociation. The Au/Al$_2$O$_3$ catalyst with the smallest particle size of about 1 nm exhibited the highest hydrogen uptake per surface atom. At this size, most of the surface consists of atoms at corner and edge positions are active. Thus, both the hydrogen uptake and the strength of adsorption are influenced by particle size effect. Fujitani et al. [191, 192] proposed that Au$^{\delta+}$-O$^{\delta-}$-Ti sites, formed at the perimeter interface between Au and stochiometric TiO$_2$ were the active sites for the dissociation of H$_2$ on Au/TiO$_2$ catalysts.

1.5.2.3. The Oxidation State of Active Gold Species

According to literature on immensely studied CO oxidation reaction over gold catalysts, there is no consensus on the oxidation state of the catalytically active Au species. The cationic [193], reduced [194] and negatively polarized [195] gold species have been proposed to be catalytically active. Moreover, the cationic [163] and reduced [196] Au species have been confessed as catalytically active sites in hydrogenation reactions [110].

1.6. Scope and Objectives of the Work

The overall aim of this work is fundamental understanding of the catalysis by nano-gold and the factors affecting the catalysis of Au. With this broad scope, the objectives of the thesis are: (i) to prepare catalysts of gold of varying content supported on various reducible and non-reducible oxides like CeO$_2$, TiO$_2$, ZrO$_2$, SiO$_2$, MgO, Al$_2$O$_3$ and sodium and alkali/alkaline earth metal ion-exchanged titanate nanotubes, (ii) to probe their physicochemical characteristic and (iii) to investigate their catalytic activities in liquid-phase, selective oxidation of benzyl alcohol (with air/molecular oxygen as oxidant), oxidation of styrene and hydrogenation of cinnamaldehyde. The influence of support, base, co-added metal and nature of oxidant (O$_2$, H$_2$O$_2$ and TBHP) on the oxidation activity of supported gold will be explored. Some structure-function correlations in these catalysts will be established.

1.7. Organization of Thesis

This thesis is divided into six chapters. A brief description of each chapter is given below.

Chapter 1 narrates a brief introduction for the catalysis by gold, methods of gold catalyst preparation and review of literature on the catalytic activity of gold, in particular, in oxidation and hydrogenation reactions. The scope and objectives of the present work are presented.

Chapter 2 gives a detailed description of the synthesis methodologies of the supported gold catalysts studied in this work. The catalysts investigated in the present study include:

(i) Au supported on CeO_2, TiO_2, ZrO_2, SiO_2, MgO, Al_2O_3, sodium titanate nanotubes (NaTNT), and alkali, alkaline earth metal ion-exchanged titanate nanotubes, and

(ii) Au-Pd supported on TiO_2, NaTNT and BaTNT.

A brief note on the working principle of each instrumental technique used for the characterization of catalysts is provided. A detailed experimental procedure for catalytic activity evaluation in the oxidation of benzyl alcohol, oxidation of styrene and hydrogenation of cinnamaldehyde is also reported.

Chapter 3 provides the catalytic performance of Au nanoparticles supported on metal oxides (CeO_2, TiO_2, ZrO_2, SiO_2, MgO and Al_2O_3) in liquid-phase, aerial oxidation of benzyl alcohol and hydrogenation of cinnamaldehyde. Influence of support on the particle size and electronic and catalytic properties of Au are reported. Further, the influence of acid-base properties of the support on the product selectivity is studied. The oxidation activity (in terms of turnover frequency, TOF) of Au supported on reducible oxides is found higher than that on non-reducible oxides. Benzaldehyde selectivity is low in the case of acidic supports (SiO_2, CeO_2 and Al_2O_3). Au supported on reducible oxides (TiO_2, ZrO_2 and CeO_2) show higher conversion and turnover frequency with selectivity for C=C hydrogenation of cinnamaldehyde while Au/Al_2O_3 is selective for C=O hydrogenation yielding cinnamyl alcohol (50 wt.%). Influence of base addition on the hydrogenation activity is studied.

Chapter 4 presents the influence of co-added metal (Pd) and alkali / alkaline earth metal ions exchange on the catalytic activity of Au supported on titanate nanotubes in liquid-phase aerobic oxidation of 1° and 2° alcohols. The activity of Au-Pd/NaTNT is found higher than their monometallic counterparts Au/NaTNT, Pd/NaTNT and Au-Pd/TiO_2. The composition of Au-Pd affects benzyl alcohol conversion and benzaldehyde selectivity. A composition with 1:1 wt./wt.% of Au and Pd is found highly active and selective. Physicochemical studies reveal that the particles of Au are smaller and uniformly dispersed on the support in presence of Pd. Au atoms on NaTNT in the presence of Pd are richer in electron density and thereby enhance the activation of molecular oxygen enabling higher oxidation activity. Among Au on alkali and alkaline earth metal ions (A = Li^+, K^+, Cs^+, Mg^{2+}, Ca^{2+}, Sr^{2+} and Ba^{2+})-exchanged NaTNT (Au/ATNTs), Au/BaTNT having higher basicity, smaller Au particles and higher metal dispersion shows enhanced catalytic activity than the other Au/ATNT catalysts. Pd addition to Au leading to Au-Pd/BaTNT increases the activity (TOF) but lowers the selectivity for benzaldehyde (from 99 to 80 wt.%). The influence of reaction parameters is also investigated.

Chapter 5 deals with the application of Au/BaTNT catalyst for the liquid-phase oxidation of styrene. The effect of reaction parameters such as solvent, nature of oxidant, catalyst concentration, temperature and reaction time is systematically investigated and reaction conditions are optimized. Recyclability of the catalysts is also investigated.

Chapter 6 provides an overall summary and conclusions of the work presented in the thesis.

By and large, this thesis describes the synthesis, characterization and catalytic performance of supported Au catalysts in three industrially important reactions viz., liquid-phase selective oxidation of alcohols, oxidation of styrene and hydrogenation of cinnamaldehyde. The inferences derived enhance the understanding of the unusual catalytic power of nano-gold.

1.8. References

[1]   D. Astruc, F. Lu, J. R. Aranzaes, Angew. Chem., Int. Ed. 44 (2005) 7852-7872.

[2]   L. D. Rampino, F. F. Nord, J. Am. Chem. Soc. 63 (1941) 2745-2749.

[3]   D. Y. Cha, G. Parravano, J. Catal. 18 (1970) 200-211.

[4]   G.J. Hutchings, J. Catal. 96 (1985) 292–295.

[5]   R. C. Langley, Gold Bull. 4 (1971) 62-66.

[6]   A. Taketoshi, M. Haruta, Chem. Lett. 43 (2014) 380-387.

[7]   A. Laguna, Modern Supramolecular Gold Chemistry: Gold-Metal Interactions and Applications, Wiley-VCH, Weinheim (2008).

[8]   S. Y. Ho, E. R. T. Tiekink, in Metallotherapeutic Drugs and Metal-based Diagnostic Agents: The Use of Metals in Medicine (Eds.: M. Gielen, E. R. T. Tiekink), John Wiley & Sons Ltd., Chichester (2005) p-507.

[9]   K. Tanaka and K. Tamaru, J. Catal. 2 (1963) 366-370.

[10]   G. C Bond, Gold Bull. 34 (2001) 117-119.

[11]   A. Bayler, A. Schier, G. A. Bowmaker, H. Schmidbaur, J. Am. Chem. Soc., 118 (1996) 7006-7007.

[12]   J. J. Lagowski, Gold Bull. 16 (1983) 8-11.

[13]   H. Schmidbaur, Gold Bull. 23 (1990) 11-21.

[14]   P. L. Dulong, L. G. Thenard, Ann. Chim. Phys. 23 (1823) 440-443.

[15]   P. A. Sermon, Gold Bull. 9 (1976) 129-131.

[16]   M. Faraday, Experimental Researches in Electricity, J. M. Dent, London (1914) p-94.

[17] W. A. Bone, R.V. Wheeler, Phil. Trans. 206A (1906) p-1.

[18] D. L. Chapman, J. E. Ramsbottom, C. G. Thomas, Proc. Roy. Soc. A207 (1925) 92.

[19] A. F. Beaton, J. C. Elgin, J. Am. Chem. Soc. 49 (1927) 2426-2438.

[20] O. Schmidt, Zeit. Phys. Chem. 118 (1925) 193.

[21] G. C. Bond, P. A. Sermon, Gold Bull. 6 (1973) 102-105.

[22] M. Haruta, T. Kobayashi, H. Sano, N. Yamada, Chem. Lett. (1987) 405-408.

[23] T. Ishida, M. Nagaoka, T. Akita, M. Haruta, Chem. Eur. J. 14 (2008) 8456-8460.

[24] Z. Yan, S. Chinta, A. Mohamed, J. Fackler, Jr., D. W. Goodman, Catal. Lett. 111 (2006) 15-18.

[25] G.C. Bond, D.T. Thompson, Catal. Rev.-Sci.Eng. 41 (1999) 319-388.

[26] M. Haruta, CATTECH 6 (2002) 102-115.

[27] M. Haruta, N. Yamada, T. Kobayashi, S. Iijima, J. Catal. 115 (1989) 301-309.

[28] M. Haruta, S. Tsubota, T. Kobayashi, H. Kageyama, M. J. Genet, B. Delmon, J. Catal. 144 (1993) 175192.

[29] F. Moreau, G. C. Bond, Catal. Today 122 (2007) 260-265.

[30] M. Khoudiakov, M. C. Gupta, S. Devi, Appl. Catal. A: Gen. 291 (2005) 151-161.

[31] J. W. Geus, in Preparation of Catalysts III (G. Poncelet, P. Grange, and P. A. Jacobs, eds.), Elsevier, Amsterdam (1983) p-1.

[32] R. Zanella, S. Giorgio, C. R. Henry, C. Louis, J. Phys. Chem. B. 106 (2002) 7634-7642.

[33] H. Zhu, C. Liang, W. Yan, S. H. Overbury, S. Dai, J. Phys. Chem. B. 110 (2006) 10842-10848.

[34] A. Simon, T. C.-Bouhacina, M. C. Porte, J. P. Aime, C. Baquey, J. Colloid Interface Sci. 251 (2002) 278-283.

[35] M. Date, M. Okumura, S. Tsubota, M. Haruta, Angew. Chem. Int. Ed. 43 (2004) 2129-2132.

[36] J. Pritchard, M. Piccinini, R. Tiruvalam, Q. He, N. Dimitratos, J. A. Lopez-Sanchez, D. J. Morgan, A. F. Carley, J. K. Edwards, C. J. Kiely, G. J. Hutchings, Catal. Sci. Technol. 3 (2013) 308-317.

[37] J.-D. Grunwaldt, M. Maciejewski, O. S. Becker, P. Fabrizioli, A. Baiker, J. Catal. 186 (1999) 458-469.

[38] G. M. Lari, E. Nowicka, D. J. Morgan, S. A. Kondrat, G. J. Hutchings, Phys. Chem. Chem. Phys. 17 (2015) 23236-23244.

[39]   F. Porta, L. Prati, M. Rossi, G. Scari, J. Catal. 211 (2002) 464-469.

[40]   S. C. Chan, M. A. Barteau, Langmuir 21 (2005) 5588-5595.

[41]   M. Haruta, Gold Bull. 37 (2004) 27-36.

[42]   A. Ueda, T. Oshima, M. Haruta, Appl. Catal. B: Env. 12 (1997) 81-93.

[43]   M. A. P. Dekkers, M. J. Lippits, B. E. Nieuwenhuys, Catal. Today 54 (1999) 381-390.

[44]   D. Andreeva, V. Idakiev, T. Tabakova, A. Andreev, J. Catal. 158 (1996) 354-355.

[45]   S. D. Lin, A. C. Gluhoi, B. E. Nieuwenhuys, Catal. Today 90 (2004) 3-14.

[46]   S. Minico, S. Scire, C. Crisafulli, R. Maggiore, S. Galvagno, Appl. Catal. B: Env. 28 (2000) 245-251.

[47]   M. Haruta, A. Ueda, S. Tsubota and R. M. Torres Sanchez, Catal. Today 29 (1996) 443-447.

[48]   T. Mallat, A. Baiker, Annu. Rev. Chem. Biomol. Eng. 3 (2012)11-28.

[49]   A. Arcadi, Chem. Rev. 108 (2008) 3266-3325.

[50]   P. Claus, A. Bruckner, C. Mohr, H. Hofmeister, J. Am. Chem. Soc. 122 (2000) 11430-11439.

[51]   W. D. Provine, P. L. Mills, J. J. Lerou, Stud. Surf. Sci. Catal. 101 (1996) 191-200.

[52]   L. McEwan, M. Julius, S. Roberts, J. C.Q. Fletcher, Gold Bull. 43 (2010) 298-306.

[53]   M. Stratakis, H. Garcia, Chem. Rev. 112 (2012) 4469-4506.

[54]   P. Gunawan, R. Xu, Z. Zhong, Heterogeneous Gold Catalysts and Catalysis (2014) 288-400.

[55]   B.S. Lane, K. Burgess, Chem. Rev. 103 (2003) 2457-2474.

[56]   R.A. Sheldon, in: L.I. Simandi (Ed.), Dioxygen Activation and Homogeneous Catalytic Oxidation, Elsevier, Amsterdam, 199, p. 573.

[57]   L.-C. Wang, Y.-M. Liu, M. Chen, Y. Cao, H.-Y. He, K.-N. Fan, J. Phys. Chem. C. 112 (2008) 6981-6987.

[58]   G.-j. ten Brink, I. W. C. E. Arends, R. A. Sheldon, Science 287 (2000) 1636-1639.

[59]   H. Wang, W. Fan, Y. He, J. Wang, J. N. Kondo, T. Tatsumi, J. Catal. 299 (2013) 10-19.

[60]   J. Zhu, J. L. Figueiredo, J. L. Faria, Catal. Commun. 9 (2008) 2395-2397.

[61]   A. S. K. Hashmi, G. J. Hutchings, Angew. Chem. Int. Ed. 45 (2006) 7896-7936.

[62]   L. Prati, M. Rossi, J.Catal. 176 (1998) 552-560.

[63]   F. Porta, L. Prati, M. Rossi, S. Colluccia, G. Martra, Top. Catal. 13 (2000) 231-236.

[64]   L. Prati, Gold Bull. 32 (1999) 96-101.

[65]   S. Carrettin, P. McMorn, P. Johnston, K. Griffin, G. J. Hutchings, Chem. Commun. 4 (2002) 696-697.

[66]   S. Carretin, P. McMorn, P. Johnston, K. Griffin,C. J. Kiely, G. J. Hutchings, Phys. Chem. Chem. Phys. 5 (2003) 1329-1336.

[67]   A. Abad, P. Concepcion, A. Corma, H. Garcia, Angew. Chem. Int. Ed. 44 (2005) 4066-4069.

[68]   D.I. Enache, J.K. Edwards, P. Landon, B. Solsona-Espriu, A.F. Carley, A.A. Herzing, M. Watanabe, C.J. Kiely, D.W. Knight, G.J. Hutchings, Science 311 (2006) 362-365.

[69]   P. Dutia, Chemical Weekly (2008) 195-198.

[70]   F. Wang, J. Xu, X. Li, J. Gao, L. Zhou, R. Ohnishi, Adv. Synth. Catal. 347 (2005) 1987-1992.

[71]   M. Arai, S. Nishiyama, S. Tsuruya, M. Masai, Faraday Trans. 92 (1996) 2631-2636.

[72]   V. R. Choudhary, P. A. Chaudhari, V. S. Narkhede, Catal. Commun. 4 (2003) 171-175.

[73]   D. I. Enache, D. W. Knight, G. J. Hutchings, Catal. Lett. 103 (2005) 43-52.

[74]   V. R. Choudhary, A. Dhar, P. Jana, R. Jha, B. S. Uphade, Green Chem. 7 (2005) 768-770.

[75]   B. Kimmerle, J.-D. Grunwaldt, A. Baiker, Top. Catal. 4 (2007) 1-2.

[76]   N. Toshima, T. Yonezawa, New J. Chem. 22 (1998) 1179-1201.

[77]   J.H. Sinfelt, J. Catal. 29 (1973) 308-315.

[78]   N. Toshima, (L. M. Liz-Marzan, P. V. Kamat) Nanoscale Materials, Academic Pub. Boston (2003) p-79-96.

[79]   J.H. Sinfelt, Bimetallic Catalysts Wiley, New York 1983.

[80]   J.H. Sinfelt, Acc. Chem. Res. 20 (1987) 134-139.

[81]   S. Marx, A. Baiker, J. Phys. Chem. C. 113(2009) 6191-6201.

[82]   M. S. Chen, D. Kumar, C.W. Yi, D.W. Goodman, Science 310 (2005) 291-293.

[83]   D. I. Enache, D. Barker, J. K. Edwards, S. H. Taylor, D.W. Knight, A. F. Carley, G. J. Hutchings, Catal. Today. 122 (2007) 407-411.

[84]   N. Zheng, G. D. Stucky, Chem. Commun. (2007) 3862-3864.

[85]   S. K. Klitgaard, A. T. D. Riva, S. Helveg, R. M. Werchmeister, C. H. Christensen, Catal. Lett. 126 (2008) 213-217.

[86]   L.-C. Wang, L. He, Q. Liu, Y.-M. Liu, M. Chen, Y. Cao, H.-Y. He, K.-N. Fan, Appl. Catal. A: Gen. 344 (2008) 150-157.

[87]   F.-Z. Su, M. Chen, L.-C. Wang, X.-S. Huang, Y.-M. Liu, Y. Cao, H.-Y. He, K.-N. Fan, Catal. Commun. 9 (2008) 1027-1032.

[88]   F.-Z. Su, Y.-M. Liu, L.-C. Wang, Y. Cao, H.-Y. He, K.-N. Fan, Angew. Chem. Int. Ed. 120 (2008) 340-343.

[89]   Y. Chen, H.Lim, Q. Tang, Y. Gao, T. Sun, Q. Yan, Y. Yang, Appl. Catal. A: Gen. 380 (2010) 55-65.

[90]   P. Liu, Y. Guan, R. A. van Santen, C. Li, E. J. M. Hensen, Chem. Commun. 47 (2011) 11540-11542.

[91]   L.Wang, J. Zhang, X. Meng, D. Zheng, F.-S. Xiao, Catal. Today. 175 (2011) 404-410.

[92]   X. Xie, J. Long, J. Xu, L. Chen, Y. Wang, Z. Zhang, X. Wang, RSC Adv.2 (2012) 12438-12446.

[93]   S. Mandal, C. Santra, K. K. Bando, O. O. James, S. Maity, D. Mehtad, B. Chowdhury, J.Mol. Catal. A: Chem. 378 (2013) 47-56.

[94]   H. Wang, W. Fan, Y. He, J. Wang, J. N. Kondo, T. Tatsumi, J. Catal. (2013) 299 10-19.

[95]   M. Alhumaimess, Z. Lin, Q. He, L. Lu, N. Dimitratos, N. F. Dummer, M. Conte, S. H. Taylor, J. K. Bartley, C. J. Kiely, G. J. Hutchings, Chem.Eur. J. 20 (2014) 1701-1710.

[96]   T. Wang, X. Yuan, S. Li, L. Zeng, J. Gong, Nanoscale 7(2015) 7593-7602.

[97]   J. K. Edwards, A. F. Carley, A.A. Herzing, C. J. Kiely, G. J. Hutchings, Faraday Discuss.138 (2008) 225-239.

[98]   P. Landon, P.J. Collier, A. J. Papworth, C. J. Kiely, G. J. Hutchings, Chem. Commun. (2002) 2058-2059.

[99]   W.C. Ketchie, M. Murayama, R.J. Davis, J. Catal.250 (2007) 264-273.

[100]   M. Conte, A. F. Carley, G. Attard, A. A. Herzing, C. J. Kiely, G. J. Hutchings, J. Catal. 257 (2008) 190-198.

[101]   R.W. J. Scott, C. Sivadinarayana, O. M. Wilson, Z.Yan, D. W. Goodman, R. M. Crooks, J. Am. Chem. Soc. 127 (2005) 1380-1381.

[102]   J.A. Lopez-Sanchez, N. Dimitratos, P. Miedziak, E. Ntainjua, J. K. Edwards, D. Morgan, A. F. Carley, R. Tiruvalam, C. J. Kiely, G. J. Hutchings, Phys. Chem.

Chem. Phys. 10 (2008) 1921-1930.

[103] A. A. Herzing, A. F. Carley, J. K. Edwards, G. J. Hutchings, C. J. Kiely, Chem. Mater. 20 (2008) 1492-1501.

[104] G. Li, D.I. Enache, J. K. Edwards, A. F. Carley, D.W. Knight, G. J. Hutchings, Catal. Lett. 110 (2006) 7-13.

[105] P. J. Miedziak, Z. Tang, T. E. Davies, D.I. Enache, J. K. Bartley, A. F. Carley, A. A. Herzing, C. J. Kiely, S. H. Taylor, G. J. Hutchings, J. Mater. Chem. 19 (2009) 8619-8627.

[106] P. Mars, D. van Krevelen, Chem. Eng. Sci. 3 (1954) 41-59.

[107] G. Mills, M. S. Gordon, H. Metiu, Chem. Phys. Lett. 359 (2002) 493-499.

[108] A. Franceschetti, S. J. Pennycook, S. T. Pantelides, Chem. Phys. Lett. 374 (2003) 471-475.

[109] X. Ding, Z. Li, J. Yang, J. G. Hou, Q. Zhu, J. Chem. Phys. 120 (2004) 9594-9600.

[110] J. A. van Bokhoven, C. Louis, J. T. Miller, M. Tromp, O. V. Safonova, P. Glatzel, Angew. Chem. Int. Ed. 45 (2006) 4651-4654.

[111] I. X. Green, W. Tang, M. Neurock, J. T. Yates, Science 333 (2011) 736-739.

[112] D. M. Cox, R. Brickman, K. Creegan, A. Kaldor, Z. Phys. D 19 (1991) 353-355.

[113] B. Salisbury, W. Wallace, R. Whetten, Chem. Phys. 262 (2000) 131-141.

[114] L. M. Molina, B. Hammer, J. Chem. Phys. 123 (2005) 161104(1)-161104(5).

[115] A. Villa, N. Janjia, P. Spontoni, D. Wang, D. S. Su, L. Prati, Appl. Catal. A: Gen. 364 (2009) 221-228.

[116] P. G. N. Mertens, S. L. F. Corthals, X. Ye, H. Poelman, P. A. Jacobs, B. F. Sels, I .F. J. Vankelecom, D. E. De Vos, J.Mol. Catal. A: Chem. 313 (2009) 14-21.

[117] A. Villa, D. Wang, G. M. Veith, L. Prati, J. Catal. 292 (2012) 73-80.

[118] J. Feng, C. Ma, P. J. Miedziak, J. K. Edwards, G. L. Brett, D. Li, Y. Du, D. J. Morgan, G. J. Hutchings, Dalton Trans. 42 (2013) 14498-14508.

[119] X. Yang, C. Huang, Z. Fu, H. Song, S. Liao, Y. Su, L. Du, X. Li, Appl. Catal. B: Env. 140 (2013) 419- 425.

[120] W. Cui, Q. Xiao, S. Sarina, W. Ao, M. Xie, H. Zhu, Z. Bao, Catal. Today. 235 (2014) 152-159.

[121] R. C. Tiruvalam, J. C. Pritchard, N. Dimitratos, J. A. Lopez-Sanchez, J. K. Edwards, A. F. Carley, G. J. Hutchings, C. J. Kiely, Faraday Discuss. 152 (2011) 63-86.

[122] V. N. Shetti, P. Manikandan, D. Srinivas, P. Ratnasamy, J. Catal. 216 (2003) 461-

467.

[123] M. Akimoto, K. Ichikawa, E. Echigoya, J. Catal. 76 (1982) 333-344.

[124] M. A. Barteau, R. J. Madix, J. Am. Chem. Soc. 105 (1983) 344-349.

[125] J. Lu, J. J. Bravo-Suaez, A. Takahashi, M. Haruta, S. T. Oyama, J. Catal. 232 (2005) 85-95.

[126] A. K. Sinha, S. Seelan, S. Tsubota M. Haruta, Angew. Chem. Int. Ed. 43 (2004) 1546-1548.

[127] D. Swern, Organic Peroxides, Wiley, New York and London, 1961.

[128] C. Coperet, H. Adolfsson, K. B. Sharpless, Chem. Commun., 16 (1997) 1565-1566.

[129] J. Rudolph, K. L. Reddy, J. P. Chiang, K. B. Sharpless, J. Am. Chem. Soc. 119 (1997) 6189-6190.

[130] J. Yu, Z. Feng, L. Xu, M. Li, Q. Xin, Z. Liu, C. Li, Chem. Mater. 13 (2001) 994-998.

[131] T. Kitano, Y. Kituzono, Stud. Surf. Sci. Catal. 121 (1999) 355-358.

[132] W. Zhang, M. Froeba, J. Wang, P. T. Tanev, J. Wong, T. J. Pinnavaia, J. Am. Chem. Soc. 118 (1996) 9164-9171.

[133] E. A. Blyumberg, S. Y. Zasedatelev, T. V. Filippova, E. S. Smirnov, A. G. Merzhanov, I. P. Borovinskaya , I. E. Pokrovskaya, U.S.S.R. Patent, (1981) U.S.S.R. SU 810691.

[134] C. Li, Q. Yang, P. Ying , Q. Xin, CN Patent (2000) CN 1253033.

[135] N. S. Patil, B. S. Uphade, P. Jana, R. S. Sonawane, S. K. Bhargava ,V. R. Choudhary, Catal. Lett. 94 (2004) 89-93.

[136] N. S. Patil, R. Jha, B. S. Uphade, S. K. Bhargava and V. R. Choudhary, Appl. Catal. A: Gen.275 (2004) 87-93.

[137] D. Yin, L. Qin, J. Liu, C. Li, Y. Jin, J. Mol. Catal. A: Chem. 240 (2005) 40-48.

[138] N. S. Patil, B. S. Uphade, P. Jana, S. K. Bharagava, V. R. Choudhary, J. Catal.223 (2004) 236-239.

[139] V. R. Choudhary, P. Jana, S. K. Bhargava, Int. J. Nanopart. 2009, 2, 11-19.

[140] N. S. Patil, B. S. Uphade, D. G. McCulloh, S. K. Bhargava, V. R. Choudhary, Catal. Commun. 5 (2004) 681-685.

[141] N. S. Patil, B. S. Uphade, P. G. Jana, S. K. Bhargava, V. R. Choudhary, Chem. Lett. 33 (2004) 400-401.

[142] V. R. Choudhary, D. K. Dumbre, N. S. Patil, B. S. Uphade, S. K. Bhargava, J. Catal. 300 (2013) 217-224.

[143] F. Zhang, X. Zhao, C. Feng, B. Li, T. Chen, W. Lu, X. Lei, S. Xu, ACS Catal. 1 (2011) 232-237.

[144] Y. Liu, H. Tsunoyama, T. Akita, T. Tsukuda, Chem. Commun., 46 (2010) 550-552.

[145] M. Turner, V. B. Golovko, O. P. H. Vaughan, P. Abdulkin, A. B.-Murcia, M. S. Tikhov, B. F. G. Johnson, R. M. Lambert, Nature 454 (2008) 981-983.

[146] Y. Zhu, H. Qian, M. Zhu, R. Jin, Adv. Mater. 22 (2010) 1915-1920.

[147] Y. Zhu, H. Qian, R. Jin, Chem. Eur. J.16 (2010) 11455-11462.

[148] A. Fernandez, J. Leyrer, A. Gonzalez, G. Munera and H. Knozinger, J. Catal. 112 (1988) 489.

[149] S. Iijima, Nature 354 (1991) 56.

[150] T. Kasuga, M. Hiramatsu, A. Hoson, T. Sekino, K. Niihara, Langmuir 14 (1998) 3169.

[151] D. V. Bavykin, F. C. Walsh, Titanate and Titania Nanotubes Synthesis, Properties and Applications, RSC publishing, Cambridge, UK 12 (2010) p-121.

[152] L. T.-Murciano, T. Villager, D. Chadwick, ChemCatChem 7 (2015) 925-927.

[153] Y. Jina, D. Zhuang, N. Yu, H. Zhao, Y. Ding, L. Qin, J. Liu, D. Yin, H. Qiu, Z. Fu, D. Yin, Microporous and Mesoporous Materials 126,(2009), 159-165.

[154] J. Liu, F.Wang, T. Xu, Z. Gu, Catal. Lett. 134 (2010) 51-55.

[155] L. Wang, H.Wang, P. Hapala, L. Zhu, L. Ren, X. Meng, J. P. Lewis, F.-S. Xiao, J. Catal. 281 (2011) 30-39.

[156] P. Huang, G. Chen, Z. Jiang, R. Jin, Y. Zhu, Y. Sun, Nanoscale 5 (2013) 3668-3672.

[157] M. Conte, C. J. Davies, D. J. Morgan, T. E. Davies, D. J. Elias, A. F. Carley, P. Johnston, G. J. Hutchings, J. Catal. 297 (2013) 128-136.

[158] A. Corma, P. Serna, Science 313 (2006) 332-334.

[159] F. Cardenas-Lizana, N. P. S. Gomez-Quero, M. A. Keane, Gold Bull. 42 (2009) 124-132.

[160] G. C. Bond, P. A. Sermon, Gold Bull. 6 (1973) 102-105.

[161] J. Guzman, B.C. Gates, Angew. Chem. Int. Ed. 42 (2003) 690-693.

[162] X. Zhang, H. Shi, B.-Q. Xu, Angew. Chem. Int. Ed. 44 (2005) 7132-7135.

[163] X. Zhang, F. X. Llabres i Xamena, A. Corma, J. Catal. 265 (2009) 155-160.

[164] T. V. Choudhary, C. Sivadinarayana, A. K. Datye, D. Kumar, D. W. Goodman, Catal. Lett. 86 (2003) 1-8.

[165] Y. Segura, N. Lopez, J. Perez-Ramirez, J. Catal. 247 (2007) 383-386.

[166] G. C. Bond, P. A. Sermon, Gold Bull. 6 (1973) 102-105.

[167] D. Y. Cha, G. Parravano, J. Catal. 18 (1970) 200-211.

[168] S. Galvano, G. Parravano, J. Catal. 55 (1978) 178-190.

[169] M. Boronat, P. Concepcion, A. Corma, S. Gonzalez, F. Illas, P. Serna, J. Am. Chem. Soc. 129 (2007) 16230-16237.

[170] R. Zanella, C. Louis, S. Giorgio, R. Touroude, J. Catal. 223 (2004) 328-339.

[171] E. Bus, R. Prins, J. A. van Bokhoven, Catal. Commun. 8 (2007) 1397-1402.

[172] J. Grolig, Ullmann's Encyclopedia of Industrial Chemistry; Wiley- VCH: Weinheim, Germany, 2003.

[173] P. Claus, Appl. Catal. A: Gen. 291 (2005) 222-229.

[174] G. Bond, Gold Bull. 43 (2010) 88-93.

[175] C. Milone, C. Crisafulli, R. Ingoglia, L. Schipilliti, S. Galvagno, Catal. Today 122 (2007) 341-351.

[176] C. Milone, M.C. Trapani, S. Galvagno, Appl. Catal. A: Gen. 337 (2008) 163-167.

[177] H. Rojas, G. Diaz, J. J. Martinez, C. Castaneda, A. G.-Cortes, J. A.-Alatorre, J. Mol. Catal. A: Chem. 363(2012) 122-128.

[178] A. G.-Fendler, D. Richard, P. Gallezot, in Heterogeneous Catalysis and Fine Chemicals (M. Guisnet, J. Barrault, C. Bouchoule, D. Duprez, C. Montassier, G. Perot, eds.), Studies in Surface Science and Catalysis, Elsevier, Amsterdam 41 (1988) p-171.

[179] L. Stobinsky, L. Zommer, R. Dus, Appl. Surf. Sci. 141 (1999) 319-325.

[180] S. Lin, M. A. T. Vannice, Catal. Lett. 10 (1991) 47-61.

[181] E. Bus, J. T. Miller, J. A. van Bokhoven, J. Phys. Chem. B 109 (2005) 14581-14587.

[182] E. Castillejos, E. G.-Suarez, B. B. -Baeza, R. Bacsa, P. Serp,A. G.-Ruiz, I. R.-Ramos, Catal. Commun. 22 (2012) 79-82.

[183] X. Zhang , Y. C. Guo, Z. C. Zhang, J. S. Gao, C. M. Xu, J. Catal. 292 (2012) 213-226.

[184] J. Lenz, B. C. Campo, M. Alvarez, M. A. Volpe, J. Catal. 267 (2009) 50-56.

[185] C. Milone, R. Ingoglia, A. Pistone, G. Neri, F. Frusteri, S. Galvagno, J. Catal. 222 (2004) 348-356.

[186] K.-Q. Sun, Y.-C. Hong, G. Zhang, B. Xu, ACS Catal.1 (2011) 1336-1346.

[187] K.-J. You, C.-T. Chang, B.-J. Liaw, C.-T. Huang, Y.-Z. Chen, Appl. Catal. A: Gen.

361 (2009) 65-71.

[188] R.-Y. Zhong, X.-H. Yan, Z.-K. Gao, R.-J. Zhang, B.-Q. Xu, Catal. Sci. Technol. 3 (2013) 3013-3019.

[189] Z. Tian, X. Xiang, L. Xie, F. Li, Ind. Eng. Chem. Res. 52 (2013) 288-296.

[190] M. G. Prakash, R. Mahalakshmy, K. R. Krishnamurthy, B. Viswanath, Catal. Today. 2015.

[191] I. Nakamura, H. Mantoku, T. Furukawa, T. Fujitani J. Phys. Chem. C 115 (2011) 16074-16080.

[192] T. Fujitani, I. Nakamura, T. Akita, M. Okumura, M. Haruta, Angew. Chem. Int. Ed. 48 (2009) 9515-9518.

[193] J. Guzman, B. C. Gates, J. Am. Chem. Soc. 126 (2004) 2672-2673.

[194] Y. Hao, M. Mihaylov, E. Ivanova, K. Hadjiivanov, H. Knözinger, B. C. Gates, J. Catal. 261 (2009) 137-149.

[195] Z. Yan, S. Chinta, A. A. Mohamed, J. P. Fackler, D. W. Goodman, J. Am. Chem. Soc. 127 (2005) 1604-1605.

[196] Y. Guan, E. J. M. Hensen, Phys. Chem. Chem. Phys. 11 (2009) 9578-9582.

Chapter - 2

Experimental Methods and Characterization Techniques

2.1. Introduction

This chapter gives a detailed account of the synthesis procedure of supported metal catalysts investigated in this work. It also describes the instrumental techniques used for characterization of the catalysts and the experimental procedure adopted to evaluate the catalytic activity of the synthesized materials. The catalysts investigated in the present work include:

(i) Au supported on CeO_2, TiO_2, ZrO_2, SiO_2, MgO and Al_2O_3, and

(ii) Au & Au-Pd supported on sodium titanate nanotubes (NaTNTs) and alkali and alkaline earth metal ion (Li^+, K^+, CS^+, Mg^{2+}, Ca^{2+}, Sr^{2+} and Ba^{2+})-exchanged titanate nanotubes (ATNTs).

The metal oxides were prepared by precipitation method. NaTNTs were prepared under hydrothermal conditions by alkali treatment of titana. The other titanate nanotubes were prepared by ion-exchange of Na^+ in NaTNTs with several alkali and alkaline earth metal ions. Au and Au-Pd were deposited on the pre-formed supports by a deposition-precipitation (DP) method.

The elemental composition, structural and textural properties of the catalysts were determined by using various physicochemical techniques, which include inductively-coupled plasma-optical emission spectroscopy (ICP-OES), powder X-ray diffraction (XRD), N_2-physisorption, transmission electron microscopy (TEM), diffuse reflectance UV-visible (DR UV-vis), Fourier transform laser Raman spectroscopy (FT-Raman), electron paramagnetic resonance (EPR), X-ray photoelectron spectroscopy (XPS), temperature-programmed desorption (TPD of NH_3 and CO_2) and temperature-programmed reduction with H_2 as probe molecule (H_2-TPR). The catalytic performances of these catalysts were investigated in liquid-phase for the reactions:

(i) selective oxidation of benzyl alcohol

(ii) selective oxidation of styrene, and

(iii) selective hydrogenation of cinnamaldehyde (CA).

2.2. Catalyst Preparation

2.2.1. Preparation of Support Materials

2.2.1.1. Metal Oxides

Six types of metal oxides *viz.*, CeO_2, TiO_2, ZrO_2, SiO_2, MgO and Al_2O_3 were prepared by simple precipitation technique. To prepare these metal oxides, specified amount of a metal precursor (Table 2.1) was dissolved in 145 ml of deionized water taken in a triple-necked, glass, round-bottom flask (2 l) fitted with a water-cooled condenser, pH electrode and burette

containing 1 M aqueous NaOH solution and placed in an temperature controlled oil bath. The contents of the flask were heated to 80 °C. NaOH solution was added drop-wise while stirring and maintaining the pH of the solution at 8-9. The precipitate is in the form of its hydroxide. The suspension was digested at 80 °C for 3 h while stirring. Then, it was cooled down to room temperature (25 °C). The precipitate was filtered out, washed with distilled water (until all the Na^+ ions were removed), dried at 80 °C overnight and then at 200 °C for 4 h in an electric oven to get the final support metal oxide.

Table 2.1. Metal oxides, corresponding precursors and the amount of precursors used in preparation

Metal oxide	Precursor	Amount (g)	Remarks
CeO_2	$Ce(NO_3)_3 \cdot 6H_2O$	6.31	Loba Chemie Pvt. Ltd.
TiO_2	Titanium(IV) isopropoxide	9.10	Aldrich Co.
ZrO_2	$ZrO(NO_3)_2 \cdot xH_2O$	4.71	Loba Chemie Pvt. Ltd.
SiO_2	Tetraethyl orthosilicate	8.80	Aldrich Co.
MgO	$Mg(NO_3)_2 \cdot 6H_2O$	11.10	Thomas Baker
Al_2O_3	$Al(NO_3)_3 \cdot 9H_2O$	9.60	Thomas Baker

2.2.1.2. Sodium Titanate Nanotubes (NaTNTs)

NaTNTs were prepared following the method reported by Kasuga et al. [1]. In a typical preparation, anatase TiO_2 (1 g) and 10 M aqueous solution of NaOH (80 ml, Thomas Baker Chemicals Ltd.) were mixed together in a glass beaker, transferred into a Teflon-lined, stainless-steel autoclave (100 ml) and hydrothermally treated at 110 °C while stirring (50 rpm) for 7 days. The solid formed was separated and washed with deionized water till the pH of washings was 7. It was dried at 110 °C overnight. The sample obtained was designated as NaTNT.

2.2.1.3. Alkali and Alkaline Earth Metal Ion-Exchanged Titanate Nanotubes (ATNTs)

The ion-exchanged titanate nanotubes (ATNTs, where A = Li^+, K^+, Cs^+, Mg^{2+}, Ca^{2+}, Sr^{2+} and Ba^{2+}) were formed by an ion-exchanging the pre-formed NaTNTs. In the typical preparation, 2.5 g of dried NaTNT was suspended in 120 ml of 1.0 M aqueous solution of alkali and alkaline earth metal nitrates. The suspension was stirred for 8 h while maintaining the temperature at 80 °C. The solid was separated and the ion-exchange was repeated for another two times. The solid isolated was washed with deionized water, filtered and dried at 110 °C overnight to obtain ATNTs. In the case of Cs^+, Sr^{2+} and Ba^{2+} exchanged materials the

concentration of the nitrate solution used was 0.5 M (instead of 1.0 M), as solubility is an issue with those salts.

2.2.2. Preparation of Supported Metal Catalysts

2.2.2.1. Metal Oxide-Supported Au

Gold nanoparticles were deposited by a modified deposition-precipitation (DP) method [2]. A known quantity of aqueous $HAuCl_4 \cdot 3H_2O$ solution (HiMedia Laboratories Pvt. Ltd., India; 2 mM) was taken in a beaker kept at 80 °C; pH of the solution was adjusted to 8 using 0.2 M NaOH solution. In another flask, 1 g of the support was suspended in 100 ml of deionized water and maintained at 80 °C. To it, the above gold precursor solution was added drop-wise while stirring. Then, an aqueous trisodium citrate salt solution (2 mM, 4 molar equivalents of gold) was added while continuing the stirring for 4 h. The solid formed was filtered and washed thoroughly with deionized water till the washings contained no traces of chloride ions (confirmed by the $AgNO_3$ test). It was dried at 80 °C for 12 h and calcined at 400 °C for 4 h. Catalysts with Au loadings of 1, 3 and 5 wt.% were prepared by taking appropriate amounts (31, 93 and 155 ml, respectively) of 2 mM precursor solution.

2.2.2.2. Titanate Nanotubes-Supported Au and Au-Pd

To synthesize the supported catalysts, NaTNT (1 g) was suspended in deionized water (100 ml) heated to 80 °C. A known quantity of 2 mM aqueous $HAuCl_4$ $3H_2O$ solution (HiMedia Chemicals Ltd.) was added drop by drop. The suspension was stirred for 12 h at 80 °C while maintaining the pH at 7 to 8. The preparation was done in dark. The solid obtained was separated, washed with deionized water and dried at 110 °C for 12 h to obtain Au/NaTNT.

A set of Au–Pd/NaTNT with three different Au:Pd weight ratio (0.5:1, 1:1 and 1:0.5; keeping total amount of metal on support at 2 wt.%) was prepared in the same manner taking a pre-mixed aqueous solution (2 M) of required quantities of $HAuCl_4 \cdot 3H_2O$ and $Pd(OAc)_2$ (Aldrich Co.). The materials were then reduced in flowing hydrogen at 250 °C for 2 h to yield the Au and Au-Pd catalysts. Similar procedure was followed for the preparation of Au, Au-Pd supported TiO_2 and ATNT catalysts.

2.3. Catalyst Characterization Techniques

The materials prepared following the procedures mentioned above were characterized by various physicochemical techniques. It was necessary to check the formation and properties of the catalysts so as to correlate them with the catalytic performance. Such an understanding helps designing improved catalysts. A brief account of the theory and principle of various characterization techniques used in the current study are discussed below.

2.3.1. Powder X-ray Diffraction

Powder X-ray diffraction (XRD) is a common technique used to determine the structure of the materials. It provides information on the phase purity, crystallinity and crystallite size of the prepared materials [3]. In this technique, elastic diffraction of a monochromatic X-ray beam (CuK_{α} or MoK_{α}) by atoms arranged in a periodic lattice results in a series of reflected beams when the Bragg equation is satisfied:

$$n\lambda = 2\mathrm{dsin}\theta \tag{2.1}$$

where n is the order of reflection (n = 1, 2, 3,…), λ is the wavelength of incident X-ray, d is the inter planar spacing and θ is the angle between the incident X-rays and the normal to the reflecting lattice plane [4]. The XRD measures the intensity of diffracted radiation as a function of 2θ. The X-ray beam encounters crystallites of all possible random (hkl) plane orientations, resulting in a cone of diffracted beams at characteristic 2θ values. The width of the characteristic diffraction peak increases when the crystallite size is reduces below a certain limit (<100 nm). Therefore, the average crystallite size of specimen can be estimated by measuring the resulting broadening of XRD peaks by using Scherrer equation [5]:

$$t = \frac{K\lambda}{\beta \cos\theta} \tag{2.2}$$

where t is the size of the crystallites (Å), K is the shape factor (taken to be 0.9 for spherical crystallites), λ is the X-ray wavelength of X-rays, β is the full width at half maximum (FWHM) of diffraction peak and θ is the diffraction angle.

The surface area of gold was estimated from the crystallite size (XRD). Considering the gold particles as hemispheres in shape, the metal surface area was calculated using the following formula [6]:

$$S_{Au} = \frac{50000 \cdot W}{\rho \cdot d} \tag{2.3}$$

where W corresponds to the gold loading, ρ is the density of gold (19.3 cm^3g^{-1}) and d is the diameter of gold particles as determined by XRD (Å). X-ray diffraction pattern of all the powdered catalysts used in the present study were measured in the 2θ range of 5-90° at a scan rate of 4°/min, using a PANalytical X'pert Pro dual goniometer X-ray diffractometer with Ni-filtered CuK_{α} radiation (40 kV, 30 mA).

2.3.2. Nitrogen Physisorption

The general method of measuring textural characteristics (specific surface area, average pore volume and pore size distribution) of catalyst materials is the one that works based on the theory of multilayer physisorption developed by Brunauer, Emmett and Teller in

1938. It was postulated that (i) the adsorption energy remains constant from zero coverage to full coverage for the primary layer of the adsorbate and each of the layers above, (ii) the lateral interactions are ignored, though the molecules attract and retain molecules striking them from the gas phase, (iii) enthalpy of adsorption is the same for any layer other than the first, and (iv) a new layer can be initiated before completion of the one under formation. Brunauer, Emmett and Teller (BET) derived an equation for calculating the monolayer coverage of the adsorbate which is represented as [7]:

$$P/V(P_0 - P) = 1/CV_m + [(C - 1)/CV_m] P/P_0 \qquad (2.4)$$

where P is adsorption equilibrium pressure, P_0 is saturation vapor pressure of the adsorbate at the experimental temperature, V is total volume adsorbed (STP) at pressure P, V_m is the volume of adsorbate at monolayer coverage and C is a constant related to the heat of adsorption and liquefaction. A linear relationship between $P/V(P_0/P)$ and P/P_0 is required to obtain the quantity of nitrogen adsorbed. This linear portion of the curve is restricted to a limited portion of the isotherm, generally between 0.05-0.30. The monolayer volume, V_m is given by $1/(S+I)$, where S is the slope and it is equal to $(C-1)/CV_m$ and I is the intercept and it is equal to $1/CV_m$. With N_2 and many other adsorbates C >> 1, thus to a good approximation the slope equals $1/V_m$. Based on the equation: $C = e^{(q_1 - q_L)/RT}$, where q_1 is the heat of adsorption in the 1st monolayer and q_L is the heat of liquefaction (condensation) of the adsorbate . The values obtained for C and q_L, heats of physisorption represented by q_1 are typically below 10 kcal/mole. Then the specific surface area of the catalyst (S_{BET}) is calculated from V_m, by the equation,

$$S_{BET} = (V_m/22414)N_a\sigma \qquad (2.5)$$

where N_a is Avogadro number and σ is mean cross sectional area covered by one adsorbate molecule. The commonly considered value of σ for N_2 is 0.162 nm^2. Among the several methods Barrett-Joyner-Halenda (BJH) model is the most reliable procedure for determination of pore size distribution, which is typically applied to nitrogen desorption data measured at -196 ℃ on porous materials. It uses the modified Kelvin equation to relate the amount of adsorbate removed from the pores of the material, as the relative pressure (P/P_0) is decreased from a high to low value, to the size of the pores [8]. The pore size distribution can be obtained from the plot of $\Delta V_p/\Delta r_p$ versus r_p, where V_p is pore volume and r_p is pore radius.

A NOVA 1200 Quanta Chrome instrument was used for the textural characterization of the catalysts reported in this thesis. Specific surface area was determined as the total surface area per unit weight of the sample. About 0.1 g of the sample was taken in a quartz

cell and evacuated at 250 °C for 3 h for Au/metal oxides and at 200 °C for 2 h in the case of Au/ATNTs. After that, the quartz cell was fixed at the sample port to dip the sample into a liquid nitrogen container and then, nitrogen was passed through it. Then, adsorption and desorption of nitrogen was measured. The specific surface area of the samples was determined using the data points in the relative pressure (P/P$_0$) of 0.05-0.3. The total pore volume was determined from the uptake of adsorbate (N$_2$) at a relative pressure (P/P$_0$) of 0.99.

2.3.3. Transmission Electron Microscopy (TEM)

A majority of industrial catalytic systems are supported metals, where the metal nanoparticles are dispersed on a high surface area support. The reaction rate (TOF) is proportional to the active metal surface area (m^2/g). In the case of structure-sensitive reactions, it also depends on crystallite size and exposed crystal plane. Thus, it is important to know the metal surface area, metal dispersion and crystallite size [9].

Transmission electron microscopy (TEM) is a versatile technique to determine the particle size, shape, metal dispersion and chemical composition of heterogeneous catalysis. The operating principle of TEM is same as the light microscope, where electron beam is used instead of light. High-energy electrons emitted from a gun through electromagnetic lenses are focused into a fine beam. Interaction of this beam with the sample surface gives reflected electrons. The electrons that transmit through a two-dimensional projection of the sample are magnified by electromagnetic lenses and then hit a fluorescent screen generating the bright field TEM image. Based on atom density, metals generally have a higher electron density than supports and thus, they appear darker in the TEM image. The dark field TEM image is obtained from the diffracted electron beam which is slightly off-angled from the transmitted beam.

TEM instrument is operated generally under the following conditions: the high energy100-200 keV electrons, 10^{-6} mbar vacuum, 5 nm resolution and magnification of about 3 x 10^5 or 10^6. A high resolution transmission electron microscopy (HRTEM) operates at 100-300 keV electrons, 10^{-6} vacuum, 0.5 nm resolution and magnification of about 3 x 10^5 (or) 10^6. The crystallographic planes and various phases can be identified using the topographic information obtained from TEM or HRTEM [10].

Average metal particle size ($\bar{d}$) can be obtained based on a count of many particles. The experimental data are typically represented as a number average ($\overline{dn}$) or surface-weighted average diameter ($\bar{d}s$):

$$\overline{d_n} = \sum_i n_i d_i / \sum_i n_i \tag{2.6}$$

$$\overline{d_s} = \sum_i n_i d_i^3 / \sum_i n_i d_i^2 \tag{2.7}$$

or $$\overline{d_s} = 6 \sum_i n_i V_i / \sum_i n_i A_i = 6 \, V_m N_T / a_m N_S \tag{2.8}$$

where, n_i is the number of particles with diameter d_i, V_i is the volume of ith particle and A_i is the surface area of ith particle. V_m is the volume occupied by Au atom (1.69×10^{-23} cc), a_m is the area occupied by Au atom (0.869×10^{-15} cm^2), N_S is the total number of metal atoms present on the surface and N_T is the total number of metal atoms (surface and bulk).

The d values obtained using above formulae are often in good agreement with the average value determined by chemisorption and XRD measurements. The metal dispersion (D) can be defined as the fraction of surface metallic atoms exposed, which determines their catalytic properties. Thus, the metal dispersion can be expressed as $D = N_S/N_T$. The relation between average metal particle size ($\overline{d}$) and dispersion (D) is as follows:

$$D = 6 \, (V_m/a_m)/\overline{d} \tag{2.9}$$

TEM images presented in this dissertation were recorded using a JEOL (model 1200 EX) instrument operating at 100 KV. A small amount (0.001-0.005 g) of the catalyst was taken in 5 ml of iso-propanol/ethanol solvent and sonicated for 0.5 h at room temperature. Then, a drop of the sample suspension was placed on a carbon coated Cu grid (200 mesh, ICON Analytical) and dried for 4 h at room temperature, then it was used in TEM analysis.

2.3.4. *Diffuse Reflectance UV-vis Spectroscopy (DR UV-vis)*

DR UV-vis spectroscopy is an important spectroscopic tool for characterization of solid catalysts. It is based on the electronic transitions involving σ and π electrons, transitions involving charge-transfer and transitions involving d and f electrons. UV-visible spectra provide the information on the (1) oxidation state and coordination number of metals (from the metal-centred and charge transfer transitions), (2) dispersions of supported oxide moieties (from charge transfer transitions), (3) particle size and shape of dispersed (coinage) metals (from surface plasmon resonance), (4) band gaps of semiconductors (from the analysis of the absorption edge), and (5) nature of surface functional groups (from overtone and combination modes of the vibrations). A strong point of UV-visible spectroscopy in catalysis research is that the spectra of a solid can be recorded in the presence of a gas or liquid-phase over a wide range of temperature and with a time resolution of less than a second. The method is thus highly suitable for the investigation of catalysts as they work [11].

In particular, the surface plasmon absorption in the metal nanoparticles arises from the collective oscillations of the free conduction band electrons that are induced by the

incident electromagnetic radiation. Such resonances are seen when the wavelength of the incident light far exceeds the particle diameter. The reflectance determined is related to two sample properties, namely, the scattering and the absorption coefficient, denoted as the Kubelka–Munk function (sometimes also called remission function). Metallic gold shows distinct and well-defined plasmon absorption in the visible region of the spectra. In addition, the plasmon absorption of gold nanoparticles is sensitive to the surrounding environment and the interaction between gold and support [12].

A Shimadzu UV-2550 spectrophotometer equipped with an integrating sphere attachment (ISR 2200) was used to identify the presence of Au nanoparticles. The spectral grade $BaSO_4$ was used as the reference material. Certain experiments on Au/BaTNT were carried on contacting the sample with oxidants like H_2O_2 and TBHP or the styrene + oxidant reaction mixture (Chapter 5), in particular to identify the oxo-species formed during the reaction.

2.3.5. Fourier Transform Laser Raman Spectroscopy (FT-Raman)

Raman spectroscopy is one of the most versatile techniques for characterization of solid catalysts and surface species formed under reaction conditions. Raman spectroscopy works on the principle of light scattering. Scattering of light is observed, when the incident beam of light (photons) interacts with the electron cloud of a molecule. Most of the collisions between photons and molecules are elastic (no change in frequency of incident and scattered light), also known as Rayleigh scattering. Raman effect occurs while the frequency of the scattered light is different to the frequency of the incident light (inelastic scattering). The change in energy of the vibrational and rotational energy levels of the molecule is responsible for this inelastic scattering [13].

Absorption of energy from the incident beam by a molecule or solid in the ground state causes it to be raised to higher (virtual) energy level, and then it rapidly relaxes to a lower energy level, with emission of low energy photon, is called as Stokes scattering. A photon of energy greater than the incident photon emerges while the photon is absorbed by a molecule which is already at an excited level and immediately relaxed back to the ground state. This is specified as Anti-Stokes scattering. A vibration is Raman active if there is a change in the polarizability. The selection rule of vibrational Raman spectroscopy is the change of the vibrational quantum number υ by ± 1.

FT-Raman spectra were recorded on a Horiba JY LabRaman HR 800 MicroRaman spectrometer using 630 nm wavelength generated by a He-Ne laser operating at 20 mV.

2.3.6. Electron Spin Resonance (ESR)

Electron Spin Resonance (ESR) spectroscopy is a powerful tool for investigating the structure, location and dispersion of paramagnetic active sites in solid catalysts. The conduction ESR (CESR) technique is one of the potential methods to gain valuable information on structure–reactivity relationships. From the information obtained for conduction electron spin resonance (CESR) of the metal and paramagnetic F-centers (trapped electrons in oxygen vacancies) of the support, the metal particle size (EPR active) and the metal-support interactions can be determined [12].

In the present study, Electron spin resonance (ESR) spectra of supported gold samples were recorded at -196 °C on a Bruker EMX X-band spectrometer. The ESR spectra were recorded taking the samples in suprasil quartz tubes (~ 4 mm o.d.).

2.3.7. X-ray Photoelectron Spectroscopy (XPS)

Siegbahn and co-workers developed X-Ray photoelectron spectroscopy (XPS) in the mid 1960's. XPS is also known as electron spectroscopy for chemical analysis (ESCA) and can provide information for oxidation state and surface compositions of materials. The basic principle involved in this technique is the photoelectric effect. The monochromatic aluminium K_α or non-monochromatic magnesium K_α X-rays are used as source to eject electrons from inner-shell orbitals. An electron from a higher energy level then falls to fill the hole left behind and it emits radiation energy, which can be used to eject an electron called Auger electron. These photoelectrons are collected and analyzed by the instrument to produce a spectrum of emission intensity versus electron binding (or kinetic) energy [14].

The photoelectrons emitted have characteristic kinetic energy corresponding to a particular element and their bonding states. The kinetic energy, E_k of these photoelectrons determined from the energy of the incident X-ray radiation (hv) and the electron binding energy (E_b) is given as:

$$E_k = h\nu - E_b \qquad (2.10)$$

The experimentally determined energies of the photoelectrons are obtained using the equation:

$$E_k = h\nu - E_b - E_w \qquad (2.11)$$

where E_w is the work function of the spectrometer. The ejected electrons can escape only from a depth of few nanometers or less, making electron spectroscopy a versatile surface sensitive tool to study surfaces of solid materials.

XPS spectra of the catalyst samples were obtained using a VG Microtech Multilab ESCA 3000 with Mg K_α radiation (hυ = 1253.6 eV). Base pressure in the analysis chamber was maintained at 3-6 x 10^{-10} mbar. The energy resolution of the spectrometer was set at 0.8 eV at pass energy of 20 eV. The binding energy (BE) values of various elements in the material were estimated considering the reference carbon 1s at 285 eV. The relative percentage concentration of metal in different oxidation states present on the surface of the material were obtained by deconvolution of XPS spectra.

2.3.8. Temperature-Programmed Desorption (TPD)

This technique can be used to obtain information about the strength and number of acidic and basic sites. In general, NH_3 and CO_2 are used as probe molecules to determine the acidity and basicity of different catalyst samples, respectively. Initially, catalyst sample was contacted with probe molecules at 50 °C. Then the temperature is raised at a constant rate and the amount desorbed is recorded to characterize the surface properties of the catalysts [15].

The acidity and basicity of the catalyst materials were determined using a Micromeritics Auto Chem 2910 instrument. In a typical experiment, 0.1 g of the catalyst was taken in a U-shaped, flow-through, quartz sample tube. Prior to measurements, the catalyst was pre-treated in He (30 ml/min) at 400 °C (for Au/metal oxides) or 250 °C (Au/ATNT) for 1 h. It was then cooled to 25 °C and a mixture of NH_3 in He (10 vol%) was fed to the sample (30 ml/min) for 1 h. Then, the sample was flushed with He (30 ml/min) for 1 h at 100 °C. Before starting the desorption analysis, baseline was checked for stability. NH_3-TPD measurements were then carried out on this activated material in the temperature range of 50 – 400 °C at a heating rate of 10 °C/min. The CO_2-TPD measurements were carried out in the temperature range of 100 – 700 °C using a gas mixture of CO_2 in He (10 vol%). NH_3 or CO_2 concentration in the effluent was monitored with a thermal conductivity detector (TCD). The amount of desorbed ammonia or carbon dioxide was determined based on the area of the desorption peak.

2.3.9. Temperature-Programmed Reduction (TPR)

H_2-temperature programmed reduction (H_2-TPR) is a useful technique for the characterization of supported catalysts. During a TPR experiment, the catalyst is exposed to hydrogen gas while the temperature is increased linearly. The difference between the inlet and outlet concentration of the hydrogen gas is measured as function of time using a thermal conductivity detector (TCD). This gives the information about the presence of reducible species [16].

A Micromeritics Auto Chem 2920 instrument was used in the present study. In a typical analysis, 0.1 g of the catalyst taken in a U-shaped quartz tube was treated initially in a 5% O_2 in He (50 ml/min) flowing gas mixture at 250 °C for 1 h and then, in pure He gas (20 ml/min) at 200 °C for 1 h. The temperature was lowered, cooled to 25 °C using N_2 gas as a coolant. A gas mixture of H_2(5%) – Ar(95%) was then passed (20 ml/min) through the quartz reactor at 40 °C for 1 h. The temperature was raised to 950 °C at a heating rate of 10 °C/min and held at that temperature for 10 min. The amount of hydrogen consumed was estimated and the degree of reduction for the metal oxide supported Au catalysts was determined. A standard Ag_2O powder was used to calibrate the amount of H_2 consumption.

2.3.10. Inductively-Coupled plasma-Optical Emission Spectroscopy (ICP-OES)

ICP-OES is one of the powerful analytical tools for the determination of trace elements in a myriad of sample types. The technique is based upon the spontaneous emission of photons from atoms and ions that have been excited in a radio frequency (RF) discharge. Liquid and gas samples may be injected directly into the instrument, while solid samples require extraction or acid digestion so that the analytes will present in a solution. The solution converted as aerosol is introduced into Ar plasma and then the ionization process takes place. Further, the exited ions relax to the ground state via the emission of a photon. The characteristic photon determined by photodiode quantifies the specific element [17].

In a typical sample preparation, a known quantity of catalyst material was digested in aquaregia (HNO_3: HCl, 1:3 mol) and a known ppm solution was prepared by making up to 100 ml with deionized water. ICP-OES analysis was carried out on a Spectro Arcos instrument equipped with the Winlab software. Metals can be analyzed by either a radial or an axial plasma configuration. Standard solutions containing different elements were used for the calibration purpose.

2.4. Reaction Procedure

2.4.1. Oxidation of Alcohols

The experimental procedure followed while using Au/metal oxide as catalyst is as follows. Benzyl alcohol [10 mmol, Thomas Baker (Chemicals) Pvt. Ltd., India], K_2CO_3 (1 mmol), toluene [5 ml, Thomas Baker (Chemicals) Pvt. Ltd., India] and catalyst (0.1 g) were taken in a glass, round-bottom flask fitted with a reflux condenser and placed in temperature-controlled oil bath. The reactor was connected with an air filled balloon. The oxidation reactions were conducted for a known period of time while stirring at 80 °C. Aliquots of the samples were withdrawn at different time intervals, the solid catalyst was separated by centrifugation and the liquid product was analyzed and quantified by gas chromatography

(Varian 3800; CP-8907 column; 15 m × 0.25 mm × 0.25 μm) fitted with flame -ionization detector.

The following procedure was used to test the catalytic performance of Au supported on titanate nanotubes. In a typical experiment, a known quantity of catalyst (0.05 g) and benzyl alcohol (25 mmol) were charged into a triple necked, glass, round-bottom flask (25 mL) placed in a temperature controlled oil bath. The reactor was connected with a water-cooled reflux condenser, a molecular oxygen/air-filled rubber balloon and a magnetic stirrer. Temperature of the reactor was raised to 80-120 °C and the reaction was conducted for a specific time. It was then cooled to 25 °C and the catalyst was separated by centrifugation. For identification and quantification of products a GC–MS (Varian CP-3800; CP-Sil8CB — 30 m × 0.25 mm × 0.25μm capillary column) and a gas chromatography (Varian 3800; CP-8907 — 15 m × 0.25 mm × 0.25 μm column and flame ionization detector) were employed.

2.4.2. Hydrogenation of Cinnamaldehyde

Cinnamaldehyde (1 g; Aldrich Co.; CA), isopropanol (25 ml; s.d. fine Chem Ltd., India) and 0.05 g of catalyst were taken in a 100 ml stainless-steel Parr bench-top reactor (Paar 4875 power controller and 4871 process controller). The reactor was initially flushed and then pressurized to a desired value (5–30 atm) with hydrogen. Temperature of the reactor was raised to 50-200 °C and the reaction was conducted while stirring (600 revolutions per minute) for 0.5 to 4 h. The liquid product was analyzed and quantified by gas chromatography (Varian 3400; CP-SIL5CB column; 30 m-long and 0.53 mm i.d.). The products were identified by GC–MS (Shimadzu GCMS-QP5050A; HP-5 column; 30 m-long × 0.25 mm i.d. × 0.25 μm thickness).

2.4.3. Oxidation of Styrene

Oxidation of styrene over supported Au catalysts was performed at atmospheric pressure by taking 0.05 g of catalyst along with 10 mmol of styrene and 10 mmol of anhydrous t-butyl hydroperoxide [TBHP (5.5 M) in decane]/ aqueous TBHP (70%)/ aqueous H_2O_2 (30%) in a magnetically stirred glass reactor (capacity: 25 cm^3) placed in an oil bath at 80 °C, under reflux condition for a period of 15 h. After the completion of the reaction, the reactor was cooled to room temperature and the catalyst was separated out by centrifugation. The reaction products and unconverted styrene were analyzed by gas chromatography (GC) [Varian 3400; column - CP-SIL 5 CB (30 m-long and 0.53 mm i.d x 0.25 μm)] and products were identified by GC-MS [Shimadzu GCMS-QP5050A; column-HP-5 (30 m-long x 0.25 mm i.dx 0.25 μm thickness)].

2.5. References

[1]   T. Kasuga, M. Hiramatsu, A. Hoson, T. Sekino, K. Niihara, Langmuir 14 (1998) 3160-3163.

[2]   M. Haruta, T. Kobayashi, H. Sano, N. Yamada, Chem. Lett. 16 (1987) 405-408.

[3]   J. W. Niemantsverdriet, Spectroscopic methods in Heterogeneous catalysis, VCH, Weinheim (1993).

[4]   W.H. Bragg, W.L. Bragg, The Crystalline State, Vol. 1, McMillan, New York (1949).

[5]   N. F. M. Henry, J. Lipson and W. A. Wooster, The interpretation of x-ray diffraction photographs, Macmillan and Co Ltd., London, (1951).

[6]   A. C. Gluhoi, X. Tang, P. Marginean, B. E. Nieuwenhuys, Top. Catal. 39 (2006) 101-110.

[7]   S. Brunauer, P.H. Emmett, E. Teller, J. Am. Chem. Soc. 60 (1938) 309-319.

[8]   E.P. Barrett, L.G. Joyner, P.P. Halenda, J. Am. Chem. Soc. 73 (1951) 373-380.

[9]   M. Boudart, Adv. Catal. Relat. Subj. 20 (1969) 153-166.

[10]   J.M. Thomas, O. Terasaki, P.L. Gai, W. Zhou, J. Gonzalez-Calbet, Acc. Chem.Res. 34 (2001) 583-594.

[11]   F. C. Jentoft in: Advances in Catalysis 52 (2009) p-129.

[12]   P. Claus, A. Bruckner, C. Mohr, H. Hofmeister, J. Am. Chem. Soc. 122 (2000) 11430-11439 and refs. therein.

[13]   M. A. Banares, G. Mestl, Advances in Catalysis 52 (2009) p-43.

[14]   (a) T. A. Carlson, X-ray Photoelectron Spectroscopy, Dowden, Hutchinson & Ross: Stroudsburg, PA, 1978. (b) D. Briggs and M. P. Seah, Practical Surface Analysis, Vol. 1: Auger and X-ray Photoelectron Spectroscopy, 2nd edition, Wiley, New York, 1990.

[15]   V. Rakic, L. Manjanovic, in: Calorimetry and Thermal Methods in Catalysis, Springer 154 (2013) p-131.

[16]   A. Jones, B. D. McNicol, Temperature Programme Reduction for Solid Material Characterization, Marcel Dekker, New York, 1986.

[17]   C.B. Boss, K.J. Fredeen, Concept, Instrumentation and Techniques in Inductively Coupled Plasma Optical Emission Spectrometry, 2nd edition, Perkin-Elmer, Norwalk, CT, 1997.

Chapter - 3

Oxidation of Benzyl Alcohol and Hydrogenation of Cinnamaldehyde over Au/Metal Oxides

3.1. Introduction

Since the discovery of Haruta et al. [1] and Hutchings [2] that supported gold catalysts are highly active for CO oxidation and acetylene hydrochlorination reactions, respectively, there has been great upsurge in the catalysis by gold. Gold nanoparticles supported on metal oxides have emerged as powerful heterogeneous catalysts for various chemical transformations such as oxidation, hydrogenation, hydrochlorination, water-gas shift and coupling reactions [1-9]. Nanogold catalysts have found commercial application in gas sensors, CO safety masks, unheated CO_2 lasers and pollutant abatement [10]. Liquid-phase, selective oxidation of alcohols is a fascinating route for the synthesis of carbonyl compounds, which are used as fine chemicals and pharmaceutical intermediates [11]. In particular, oxidation of benzyl alcohol (a primary alcohol) is a practically important reaction for the production of chlorine-free benzaldehyde required in food, perfumery and pharmaceutical industries. The vapour-phase oxidation process is not atom efficient. It is preferred to produce benzaldehyde more selectively by catalytic liquid-phase oxidation processes [12]. Such oxidations are conventionally carried out using stoichiometric oxidizing reagents e.g., permanganate and dichromate, which are expensive and produce toxic waste [13]. Several homogeneous Pd, Cu and Ru catalysts have been reported, but recovery and reuse of those catalysts was an issue [14, 15]. Reusable solid catalysts capable of performing this reaction with air at mild/moderate conditions as well as replacement of stoichiometric oxidizing agent with molecular oxygen/air are important steps to develop a sustainable oxidation process. In this context, several metal catalysts have been examined.

Au/CeO$_2$, Au/TiO$_2$, Au/MgO, Au/NiO, Au/hydrotalcite (HT), Au/BaTNT (barium titanate nanotubes) and Au/C showed good catalytic performance for the aerobic oxidation of alcohols [16-21]. High activity and selectivity towards benzaldehyde was obtained over bimetallic Au-Pd, Au-Pt and Au-Cu catalysts [22-24]. Presence of base enhanced the catalytic performance of Au [25-27]. The role of metal promoters in bimetallic systems is not completely understood. However, the role of base was considered important for dehydrogenation of the alcohol [28]. Abad et al. [17] reported that Au supported on CeO$_2$ exhibits high activity because of the collaborative effect between gold and the support. Formations of metal-alcoholate, β-hydride shift from carbon to metal and Au-H oxidation have been invoked in alcohol oxidation reactions over Au/CeO$_2$ catalysts. The catalytic performance of the gold is sensitive to the support oxide [27-30]. Detailed understanding of factors influencing the catalytic activity is important towards developing efficient supported Au catalysts.

In recent times, gold has also emerged as a hydrogenation catalyst. Selective hydrogenation of cinnamaldehyde (CA; a representative α,β-unsaturated aldehyde) is an interesting reaction from both fundamental and commercial aspects [31]. The hydrogenation of olefinic (C=C) group in CA produces hydrocinnamaldehyde (HCA, Scheme 1.3 in Chapter 1), which is an important intermediate in the preparation of pharmaceuticals used in the treatment of HIV [32]. However, the challenge lies in selective hydrogenation of the carbonyl (C=O) group to yield unsaturated alcohol, a key intermediate in the manufacture of chemicals for pharmaceuticals, flavours and fragrances [33]. While there have been several reports on the use of Pd, Pt and Ru catalysts, such reports on supported Au catalysts are scarce [34]. Even the best Au catalysts reported for these transformations are still less selective. Hence, development of improved catalysts is desired. While Pd and Ru catalysts are selective for C=C hydrogenation, Pt with its selectivity for C=O hydrogenation forms cinnamyl alcohol (CAL) from CA. Gold is a cheaper metal than Pt for use in such selective hydrogenation reactions.

In this study, gold (1-5 wt.%) deposited on six metal oxides of varying acid-base properties were synthesized by deposition-precipitation (DP) method and their catalytic activity for the liquid-phase benzyl alcohol oxidation (with air) and hydrogenation of cinnamaldehyde (with hydrogen) was investigated. Factors influencing activity and selectivity of gold catalysts are examined.

3.2. Experimental

Gold nanoparticles were supported on CeO_2, TiO_2, ZrO_2, SiO_2, MgO and Al_2O_3 by deposition-precipitation (DP) method as described in detail in Chapter 2 (sections 2.2.1.1 and 2.2.2.1). These catalysts were characterized by several physicochemical techniques (Chapter 2, section 2.3). The catalytic performance of these catalysts was studied in benzyl alcohol oxidation and in hydrogenation of cinnamaldehyde. Details of the reaction procedures are presented in Chapter 2 (sections 2.4.1 and 2.4.2).

3.3. Results and Discussion

3.3.1. Catalyst Characterization

3.3.1.1. ICP-OES

The composition of Au in the catalysts was determined by inductively-coupled plasma-optical emission spectroscopy (ICP-OES). It was found that the actual amount of gold deposited on metal oxides was lower than the nominal value (Table 3.1). For samples with 1 wt.% nominal loading, support showed a marked influence on the actual deposited amount, with CeO_2, TiO_2 and MgO enabling more amount of Au deposition (80-98%) than Al_2O_3,

ZrO_2 and SiO_2 (60-65%). However, the influence of support was not clearly obvious at higher Au loadings (3 and 5 wt.%, Table 3.1).

3.3.1.2. Surface area analysis

Specific surface area (S_{BET}) of the calcined samples (determined from N_2-physisorption studies) decreased with increasing metal loading. Except for Au(1, 3 and 5 wt.%)/Al_2O_3 (336, 240 and 186 m^2/g, respectively) and Au (1 wt.%)/SiO_2 (168 m^2/g), S_{BET} for rest of Au catalysts are in the range 40-93 m^2/g. A reduction in the surface area was noted after the deposition of Au (Table 3.1).

3.3.1.3. XRD

X-ray powder diffraction (XRD) patterns of Au (1 wt.%) supported on metal oxides are shown in Fig. 3.1(a). Except for the supports peaks, no additional peaks due Au were observed. It was also likely that the XRD peaks due to Au overlapped with those of the support oxides. However, at higher Au loading (3 and 5 wt.% on MgO, TiO_2 and Al_2O_3) distinct reflections at 38.2°, 44.6°, 64.6° and 77.8° arising from (111), (200), (220) and (311) planes of metallic gold (JCPDS-ICDD index-pattern 04-0784) were detected (Fig. 3.1(b)). Using the Scherrer formula, the average crystallite size of gold was determined (Table 3.1; the peak at 44.6° was considered in the calculations). Au/MgO exists in a different phase compared to bare MgO (Fig. 3.1(b)). This observation is in agreement with that reported by others [23, 35]. Assuming that nano-gold particles have hemispherical morphology with the flat side on the support, metal surface area (S_{Au}) of Au(3 wt.%)/Al_2O_3 and Au(5 wt.%)/Al_2O_3 was determined using the formula [36],

$$S_{Au} = \frac{50000 \cdot W}{\rho \cdot d}$$

where, W corresponds to gold loading (output), ρ is density of gold (19.3 g/cm^3) and d is diameter of gold crystals in Å determined by XRD. The S_{Au} values of Au (3 wt.%)/Al_2O_3 and Au (5 wt.%)/Al_2O_3 are 1.8 and 2.8 m^2/g, respectively. In the case of other supported Au catalysts, the peaks due to gold could not be discerned as they were masked by the peaks of the support oxide.

3.3.1.4. TEM

The TEM images provided evidence for the presence of nano-Au supported on metal oxides (Fig. 3.2). TEM depicted the influence of support on Au particle size. The average particle size of Au (1 wt.%) on different oxide supports decreased in the order: CeO_2 ~ ZrO_2 (10 nm) > TiO_2 (7 nm) > SiO_2 (6 nm) > Al_2O_3 ~ MgO (5 nm) (Table 3.1). In case of higher loadings, the average particle size of Au on the Au(3 wt.%)/TiO_2, Au(3 wt.%)/MgO and

Table 3.1. Physical properties supported Au catalysts

S.No.	Catalyst[a]	Actual Au loading (wt%)[b]	S_{BET} $(m^2/g)^c$	TEM		Acidity (mmol/g)[e]	Basicity (mmol/g)[f]
				Mean Au particle size (nm)[d]	Metal dispersion (%)		
1	Au(1 wt.%)/CeO$_2$	0.98	87 (96)	10	10.1	0.187	0.025
2	Au(1 wt.%)/TiO$_2$	0.90	82 (120)	7	12.0	0.546	0.050
3	Au(3 wt.%)/TiO$_2$	2.50	63	9	10.0	0.580	0.038
4	Au(5 wt.%)/TiO$_2$	4.30	48	10 (9.6)	9.9	0.545	0.025
5	Au(1 wt.%)/ZrO$_2$	0.60	56 (80)	10	8.4	0.313	0.003
6	Au(1 wt.%)/SiO$_2$	0.60	168 (188)	6	12.4	0.127	0.008
7	Au(1 wt.%)/MgO	0.80	93 (124)	5	14.1	0.668	0.156
8	Au(3 wt.%)/MgO	2.67	65	7	11.2	0.647	0.121
9	Au(5 wt.%)/MgO	4.52	41	9 (9.4)	11.7	0.590	0.089
10	Au(1 wt.%)/Al$_2$O$_3$	0.65	336 (355)	5	17.3	0.593	0.070
11	Au(3 wt.%)/Al$_2$O$_3$	2.60	240	4 (3.8)	19.7	0.601	0.017
12	Au(5 wt.%)/Al$_2$O$_3$	4.50	186	- (4.2)	-	0.849	-

[a]Value in the parenthesis represents the nominal value of Au. [b]Determined by ICP-OES. [c]Determined from N$_2$-physisorption study. Values in parenthesis are for the bare supports. [d]Values in parenthesis denote crystallite size of Au determined from XRD. [e]Determined from NH$_3$-TPD study. [f]Determined from CO$_2$-TPD study.
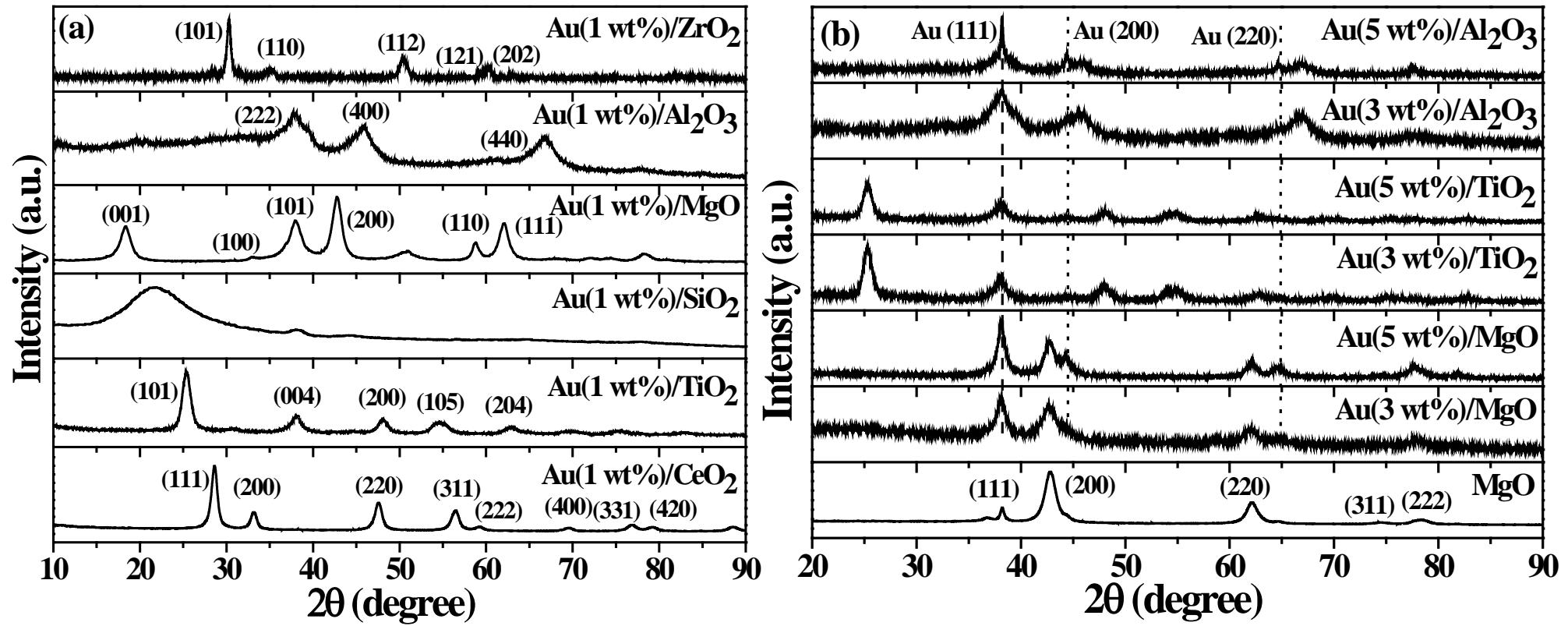
Fig. 3.1. XRD profiles of metal oxide-supported Au catalysts.
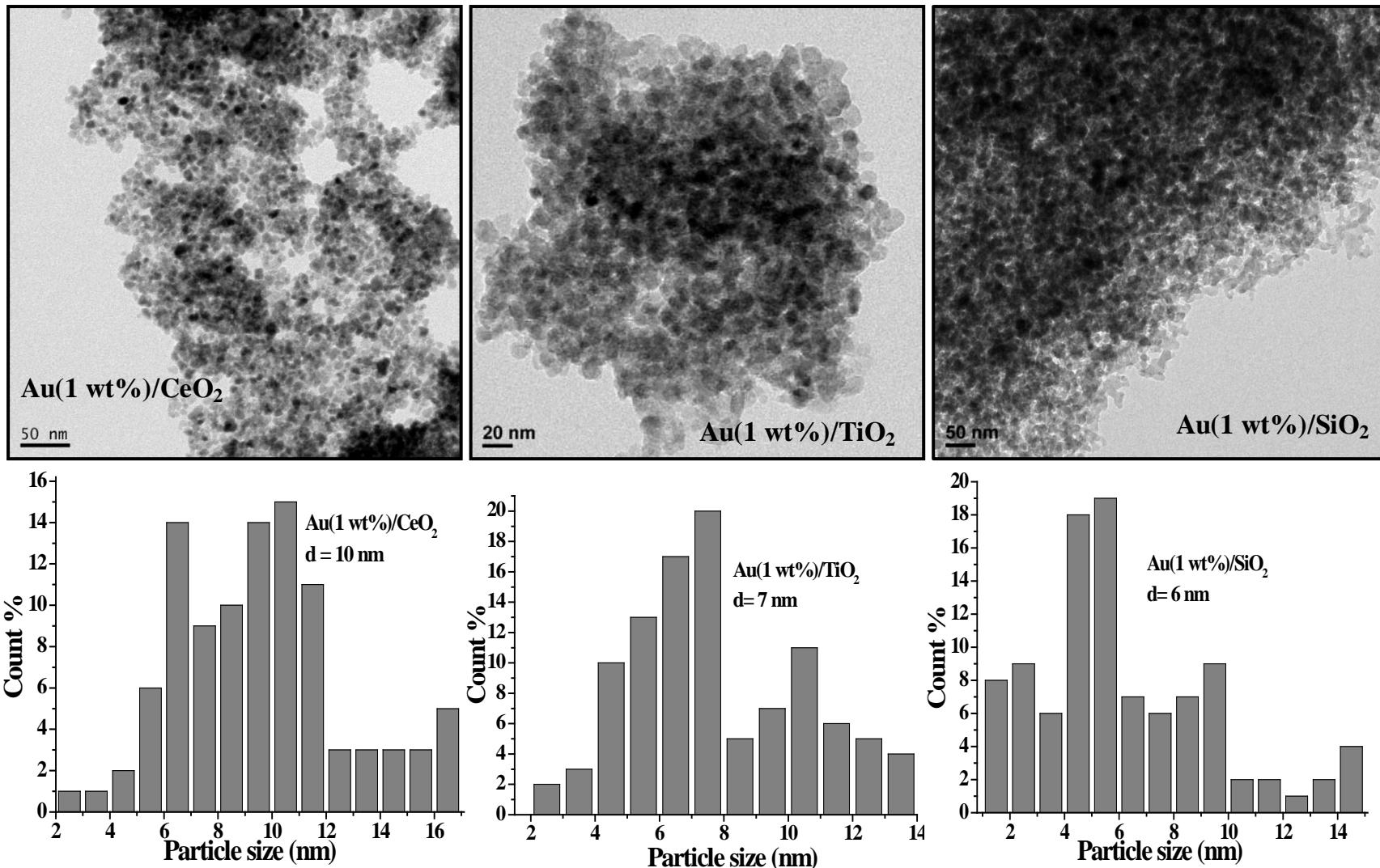
Fig. 3.2. TEM images and Au particle size distributions of supported Au catalysts (cont.).
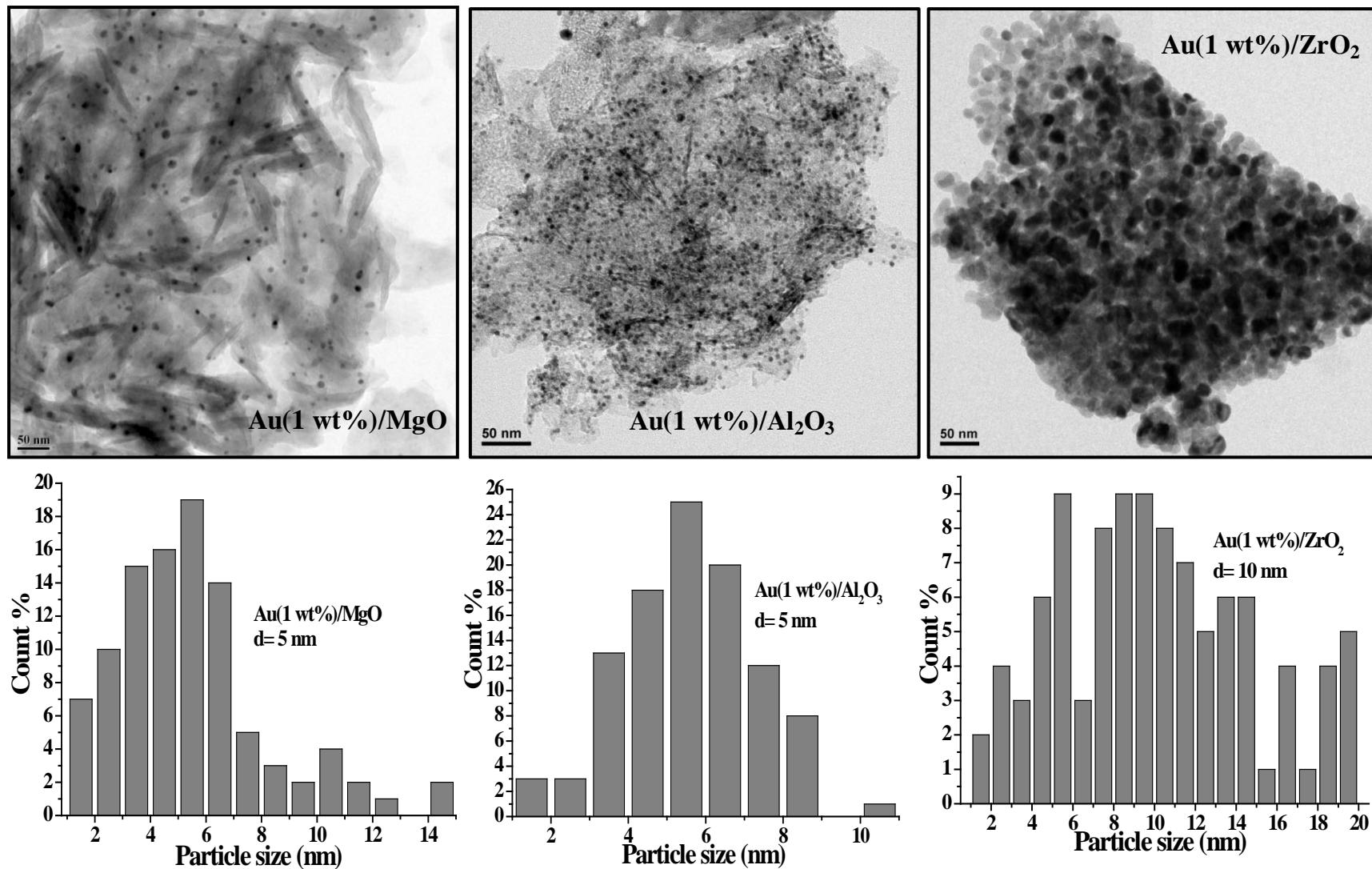
Fig. 3.2. TEM images and Au particle size distributions of supported Au catalysts (cont.).
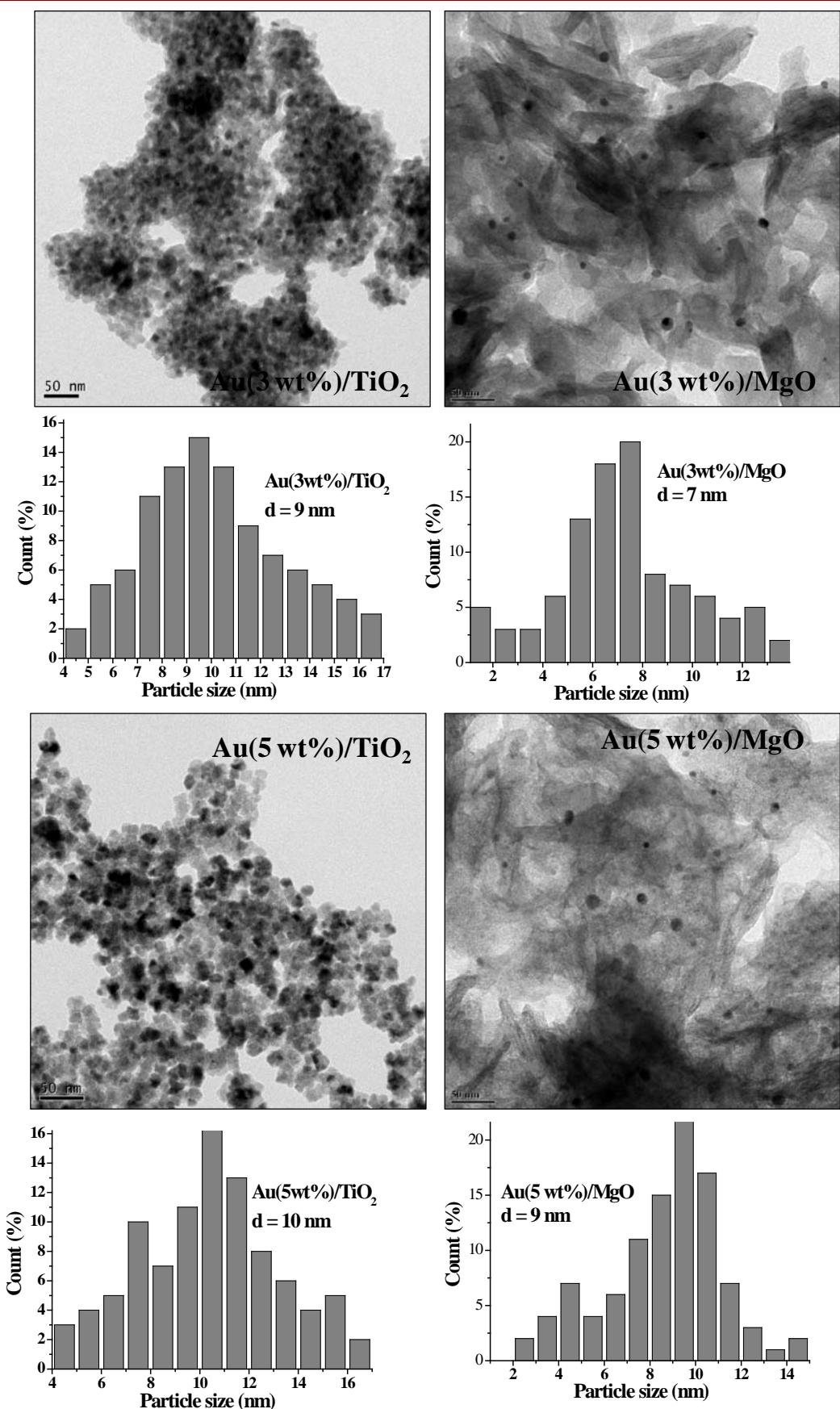
Fig. 3.2. TEM images and Au particle size distributions of supported Au catalysts (contd.).
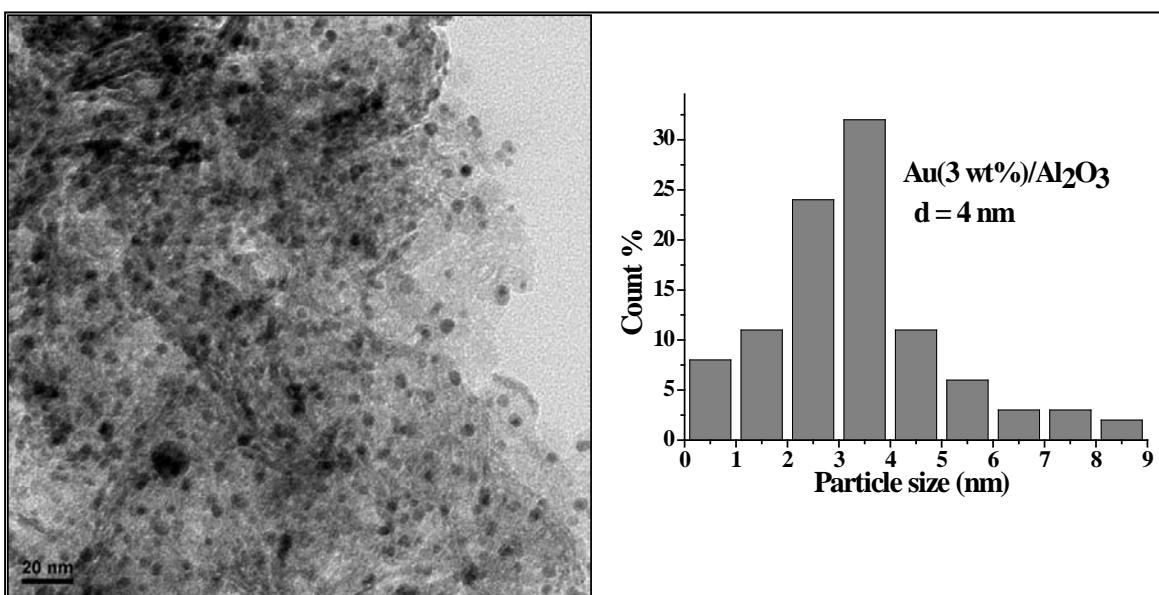
Fig. 3.2. TEM images and Au particle size distributions of supported Au catalysts.

Au(3 wt.%)/Al$_2$O$_3$ was 9, 7 and 4 nm, respectively and that on Au(5 wt.%)/TiO$_2$ and Au(5 wt.%)/MgO was 10 and 9 nm, respectively. These values agree closely with the crystallite size determined from XRD (Table 3.1). Considering that the supported Au particles have hemispherical shape, the exposed surface Au atoms and metal dispersion were determined. However, some deviation from this morphology on some supports cannot be ruled out. On different supports, dispersion of Au decreased as follows: Au(3 wt.%)/Al$_2$O$_3$ (19.7%) > Au(1 wt.%)/Al$_2$O$_3$ (17.3%) > Au(1 wt.%)/MgO (14.1%) > Au(1 wt.%)/SiO$_2$ (12.4%) > Au(1 wt.%)/TiO$_2$ (12.0%) > Au(5 wt.%)/MgO (11.7 %) > Au(3 wt.%)/MgO (11.2 %) > Au(1 wt.%)/CeO$_2$ (10.1%) > Au(3 wt.%)/TiO$_2$ (10.0%) > Au(5 wt.%)/TiO$_2$ (9.9%) > Au(1 wt.%)/ZrO$_2$ (8.4%). The number average Au particle size was determined from TEM using the formula:

$$\bar{d}_n = \sum_i n_i d_i \Big/ \sum_i n_i$$

where n_i represents the number of particles with a diameter d_i.

3.3.1.5. DR UV-vis Spectroscopy

Nano-Au exhibits a localized surface plasmon resonance (LSPR) in visible region due to absorption arising from the collective oscillations of the free conduction band electrons that are induced by the incident electromagnetic radiation. Neither bulk gold nor atoms of gold exhibit this resonance. It is characteristic of Au particles of nano dimension. The catalysts of this study showed this band in the diffused reflectance UV-vis spectrum in the range
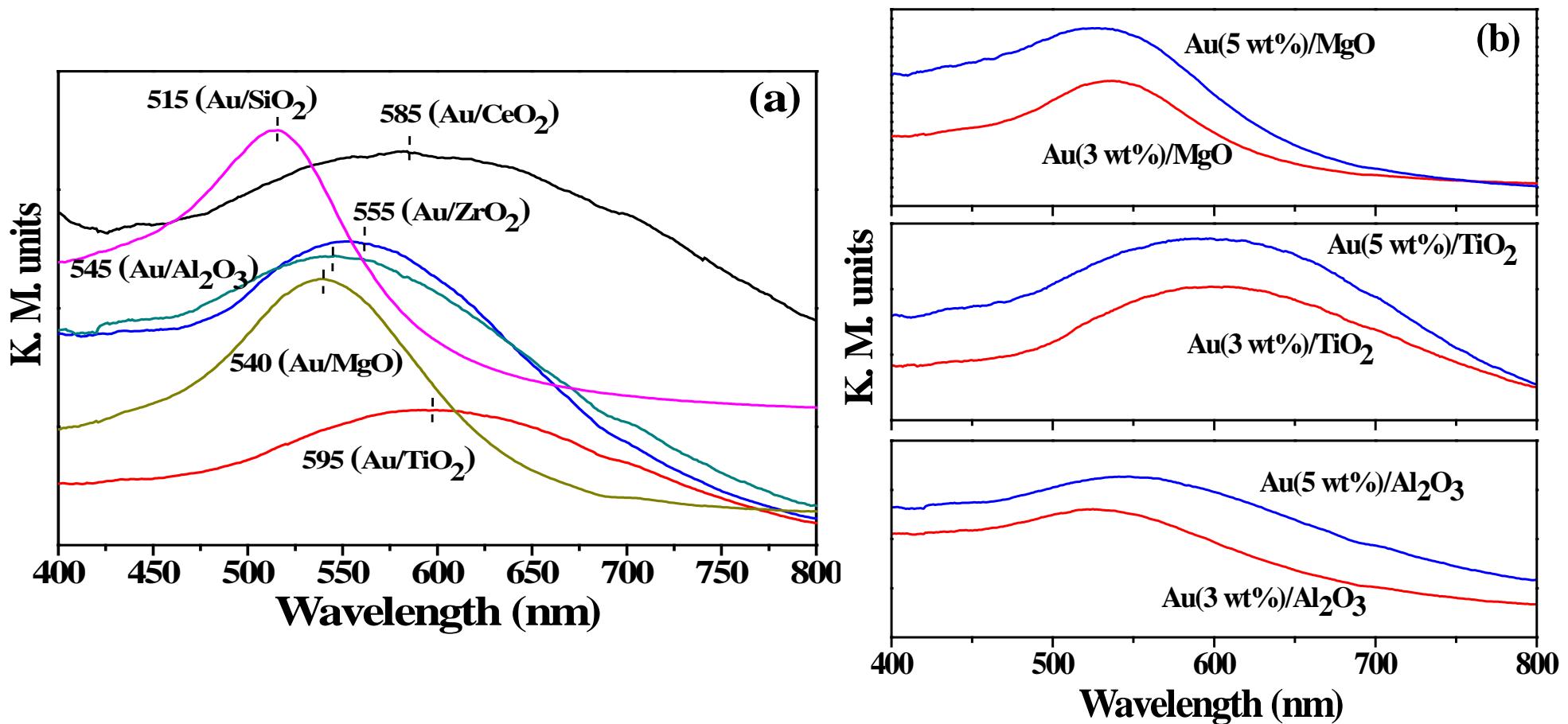
Fig. 3.3. DR UV-vis spectra: (a) Au(1 wt.%)/metal oxides, (b) supported Au(3 and 5 wt.%) catalysts.

515-595 nm (Fig. 3.3 (a)) [34, 37, 38]. LSPR of metallic nanoparticles is sensitive to the particle size, shape, loading and dielectric function of the supporting and surrounding environment. The spectra presented in Fig. 3.3, indeed reveal that support and gold particle size have notable effects on the position and shape of this band. While this band for Au(1 wt.%)/SiO$_2$, Au(1wt.%)/Al$_2$O$_3$ and Au(1 wt.%)/MgO occurred below 550 nm, for Au(1 wt.%)/CeO$_2$, Au(1 wt.%)/TiO$_2$ and Au(1 wt.%)/ZrO$_2$, it occurred above 550 nm (Fig. 3.3(a)). It is broad for Au supported on reducible oxides like CeO$_2$, TiO$_2$ and ZrO$_2$ (line width at half maximum = 150-200 nm) whereas it is narrower for Au supported on SiO$_2$, Al$_2$O$_3$ and MgO (line width at half maximum ~ 100 nm). The variation in LSPR band position is in agreement with the change in gold particle size determined from TEM [39]. The broad, asymmetric LSPR band for Au on CeO$_2$ and TiO$_2$ cannot rule out the presence of an overlapping band at around 630 nm which belongs to the longitudinal plasmon resonance band of aggregates that deviate from the spherical geometry [34]. The Au particle size increased with increase in the nominal Au loading. This should result in a red shift of the LSPR band [40], which was observed from 545 to 550 nm on Au/Al$_2$O$_3$ and from 595 to 600 nm on Au/TiO$_2$ as the gold loading increased from 1 to 5 wt.% (Fig. 3.3 (b)). The spectral line broader in the case of 5 wt.% Au loaded catalysts, indicating the existence of larger Au particles compared to low Au loadings. However, we observed a marginal blue shift in the band position for Au supported on MgO (Fig. 3.3 (b)). In the case of supported Au catalysts, at lower nominal loadings, support-metal interactions possibly play a dominant role and influence the optical band position. As the loading increased, this effect was minimized and hence, an imprecise trend (i.e., blue shift in band position) was observed for higher loading of Au. It was reported that Au$^+$ ions and small clusters such as Au$_n^{\delta+}$ show bands at 240 and 390 nm, respectively [41]. Even if they were present, they could not be identified due to their overlap with the bands from the support oxide.

3.3.1.6. ESR

Electron spin resonance (ESR) spectroscopy is a highly sensitive and powerful tool that bridges the gap in detecting nanoparticles and clusters containing a few atoms. It is also used to study metal-support interactions. With too small particles detecting between them and the support material by electron microscopic techniques becomes difficult. ESR spectroscopy is a complementary technique in those cases. The magnetic and electric properties of those nanoparticles differ significantly from the bulk metal due to quantum size effects [42]. In nanoparticles, the conduction electron band is not a continuum as in the bulk metal but splits into discrete energy levels separated by an energy gap of δ. As a consequence of this,

conduction electron spin resonance (CESR) signals are usually observed for nanoparticles of heavy metals. With increasing δ, linewidth decreases due to long relaxation time [43]. Further, δ is inversely related to the volume of the nanoparticle. Metal particle size is small enough to show the quantum size effects and CESR signals, provided the conditions: hν/δ >> 1 and h/τδ >> 1 are satisfied, where h is Planck constant, ν is microwave frequency and τ is spin relaxation time [44]. Claus and co-workers [34, 45] reported the application of this technique to investigate Au nanoparticles supported on TiO_2 and ZrO_2. According to TEM, the percentage of Au particles with diameter below 5 nm on different supports varies in the order: Au(1 wt.%)/MgO (67%) > Au(1 wt.%)/Al_2O_3 (62%) > Au(1 wt.%)/SiO_2 (60%) > Au(1 wt.%)/TiO_2 (28%) > Au(1 wt.%)/ZrO_2 (24%) > Au(1 wt.%)/CeO_2 (10%). All these particles are, in principle, amenable for detection by ESR spectroscopy provided the above conditions are satisfied. Representative ESR spectra of Au(1 wt.%)/ZrO_2 recorded at liquid nitrogen temperature was shown in Fig. 3.4. The former showed a quartet line hyperfine splitting pattern in the ESR spectrum centred at g_{iso} = 2.0594. This hyperfine splitting (A_{iso} = 29.1 G) due to ^{197}Au (I = 3/2; 100% natural abundance) was more visible in the 2nd derivative plot. "Neat" ZrO_2 support (without Au) did not show this signal confirming its origin as due to CESR of nano-gold particles. Au(1 wt.%)/Al_2O_3 and Au(1 wt.%)/MgO (Fig. 3.4) showed the CESR signal at g_{iso} = 2.0611 and 2.0768 with the corresponding A_{iso}(Au) of 29.0 and 23.3 G, respectively. Lower hyperfine splitting constant for Au supported on MgO (23.3 G) indicates higher support-metal interaction than on ZrO_2 and Al_2O_3. Au(1 w.t%)/CeO_2 showed a complex spectrum (Fig. 3.4). By comparison with the ESR spectrum of neat CeO_2 and based on the reported data it is concluded that the sextet line hyperfine pattern marked by asterisk (*) is due to Mn^{2+} ion impurity in CeO_2 and the two signals (perpendicular and parallel g features) marked by the symbol # are due to Ce^{3+} sites in CeO_2. A signal detected at g = 2.003 (~3380 G) is attributed to O$^-$ species. A relatively broader signal centred at 3273 G with partially resolved quartet hyperfine features is attributed to CESR signal of nano-Au^0 particles. From the linewidth of the CESR signal (ΔH_{pp}) and using the following equation, the diameter of ESR detected nano-Au particle was determined (Table 3.2).

$$d^2 = \frac{3.82 \; x \; 10^{-47} \; . \; \gamma \; . \; \Delta H_{pp}}{v_F \; . \; hv \; . \; \Delta g^2}$$

Here, γ is magnetogyric ratio of electron (1.76 x 10^{11} sec^{-1}.tesla^{-1}), ΔH_{pp} is linewidth of CESR (in units of tesla), v_F is Fermi velocity of electron (10^6 m/sec), h is Plank constant (6.627 x 10^{32} m^2.kg/sec), ν is microwave frequency (in hertz), Δg = g_{iso} – 2.0023 and particle size (d) is calculated in meters.
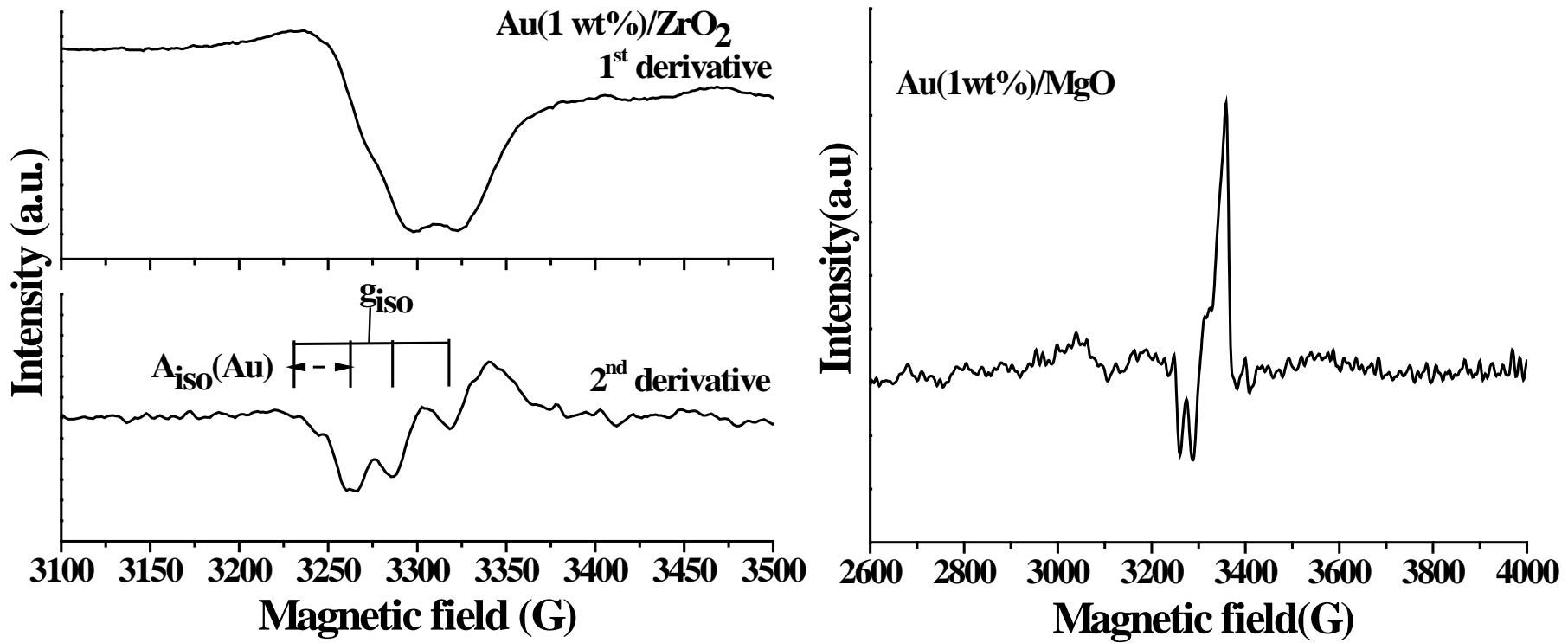
Fig. 3.4. X-band ESR spectra at -196 ºC of Au(1 wt.%)/ZrO$_2$, Au(1 wt.%)/MgO, Au(1 wt.%)/CeO$_2$ and Au(1 wt.%)/Al$_2$O$_3$ (Cont.).
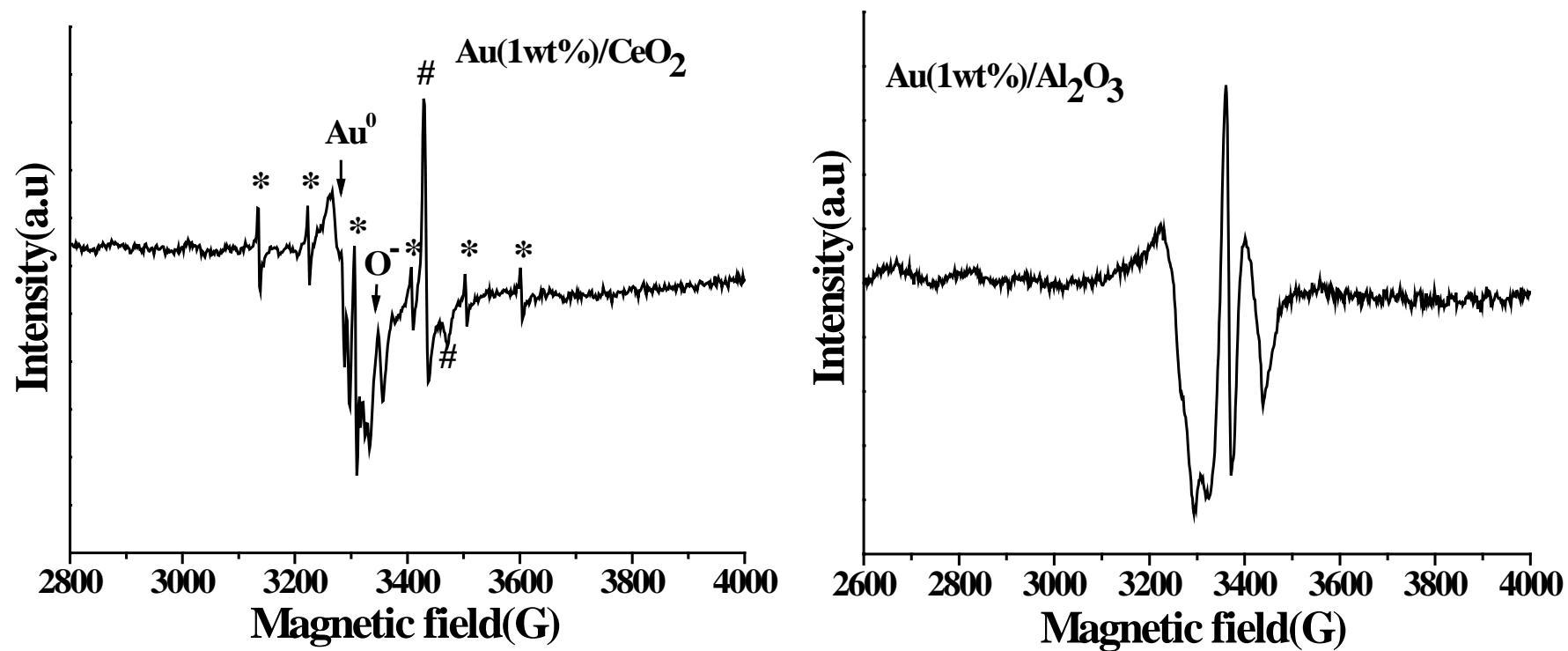
Fig. 3.4. X-band EPR spectra at -196 °C of Au(1 wt.%)/ZrO$_2$, Au(1 wt.%)/MgO, Au(1 wt.%)/CeO$_2$ and Au(1 wt.%)/Al$_2$O$_3$.

Table 3.2. EPR and XPS parameters

Catalyst	Spin Hamiltonian parameters (EPR)			Binding energy values (eV, XPS)		
	g_{iso}	A_{iso} (G)	Au size (d; nm)	Au $4f_{7/2}$	Au $4f_{5/2}$	Support
Au(1 wt.%)/TiO$_2$	-	-	-	83.4	87.0	459.1 (Ti 2p$_{3/2}$)
Au(1 wt.%)/MgO	2.0768	23.3	1.2	83.7	-	49.5 (Mg 2p)
Au(1 wt.%)/Al$_2$O$_3$	2.0611	29.0	1.8	84.0	87.5	74.8 (Al 2p)
Au(1 wt.%)/ZrO$_2$	2.0594	29.1	1.7	-	-	-

3.3.1.7. XPS

The Au 4f core level X-ray photoelectron spectra (XPS) of Au(1 wt.%)/TiO$_2$ and Au(1 wt.%)/MgO (Fig. 3.5) showed two peaks corresponding to $4f_{7/2}$ and $4f_{5/2}$, and reveal that gold is in metallic state. XPS lines due to oxidic gold species (Au$^+$ and Au^{3+} at 85.5 and 89.1 eV, respectively) were not observed [45]. The spectral lines of Au 4f in Au(1 wt.%)/MgO overlapped partly with those of Mg 2s peaks. Only the peak corresponding to Au $4f_{7/2}$ could be resolved. Similar findings were also reported by Rahim et al. [35]. Support has a major effect on the binding energy (BE) of Au $4f_{7/2}$, where in the case of Au(1 wt.%)/TiO$_2$ the BE value was 83.4 eV and for Au(1 wt.%)/MgO it was 83.7 eV. Unsupported, neat gold showed this peak at 84.0 eV. A shift toward lower binding energy for Au 4f core electron level in the case of Au(1 wt.%)/TiO$_2$ and Au(1 wt.%)/MgO indicates support-metal interactions and electron rich Au nanoparticles because of the charge transfer from TiO$_2$ and MgO substrates. This charge transfer occurs due to large difference in the work function of Au and support oxide. Thus, electron transfer is facilitated from the support oxide to Au [35, 45-47]. There are reports for the presence of Au°, Au$^+$ and Au^{3+} species in uncalcined Au/TiO$_2$ samples. Upon calcination, the oxidized gold transformed into Au°. The observations in this study on calcined samples agree well with the other reports [27].

3.3.1.8. NH$_3$ & CO$_2$-TPD

The acid-base properties of supported Au catalysts were examined by temperature-programmed desorption (TPD) of NH$_3$ and CO$_2$. NH$_3$-TPD studies revealed that the acidity (per gm of catalyst) decreases in the order: Au(5 wt.%)/Al$_2$O$_3$ > Au(1 wt.%)/MgO > Au(3 wt.%)/MgO > Au(3 wt.%)/Al$_2$O$_3$ > Au(1 wt.%)/Al$_2$O$_3$ > Au(5 wt.%)/MgO > Au(3 wt.%)/TiO$_2$ > Au(1 wt.%)/TiO$_2$ > Au(5 wt.%)/TiO$_2$ > Au(1 wt.%)/ZrO$_2$ > Au(1 wt.%)/CeO$_2$
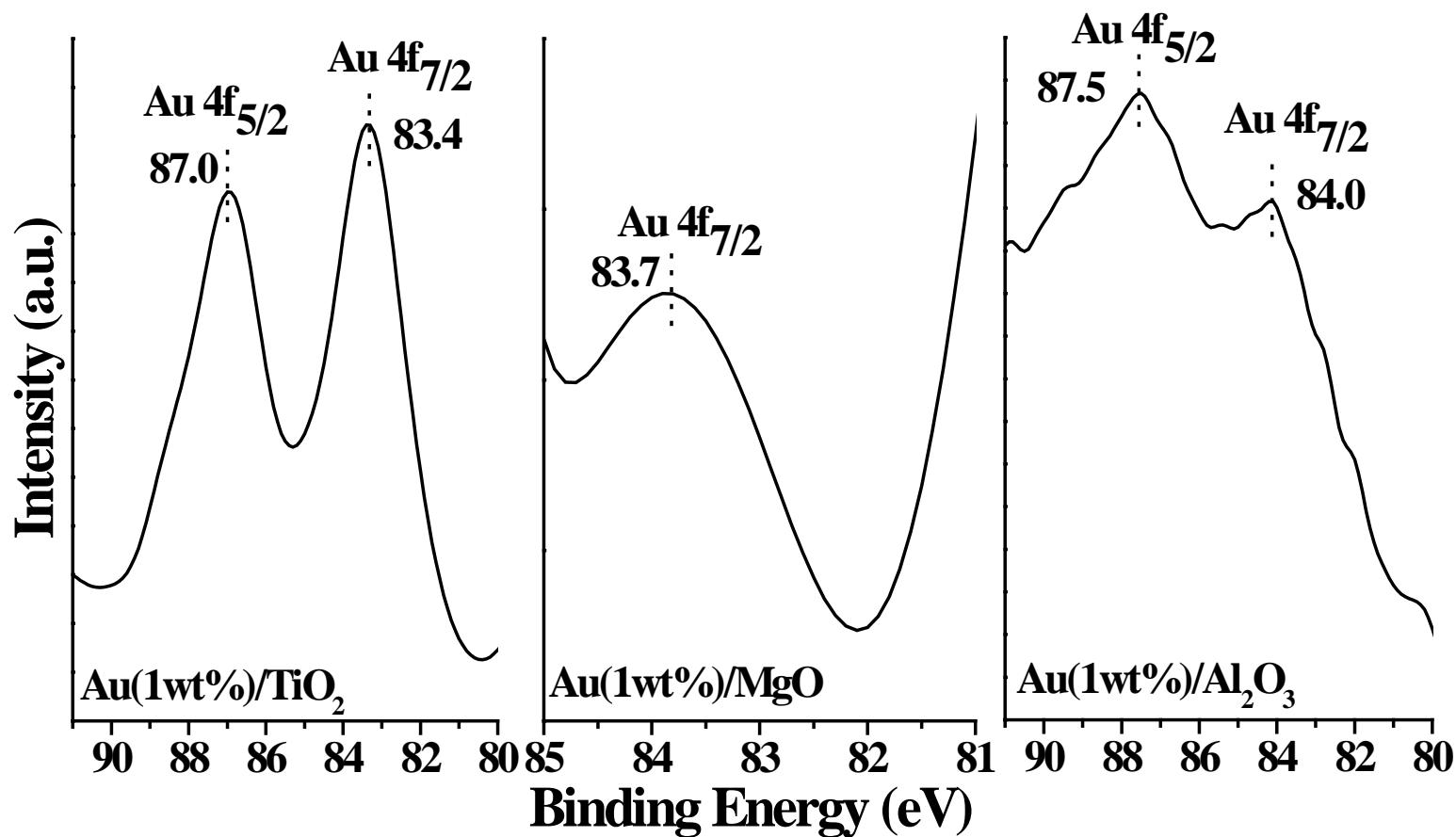
Fig. 3.5. X-ray photoelectron spectra of TiO$_2$, MgO and Al$_2$O$_3$-supported Au catalysts.
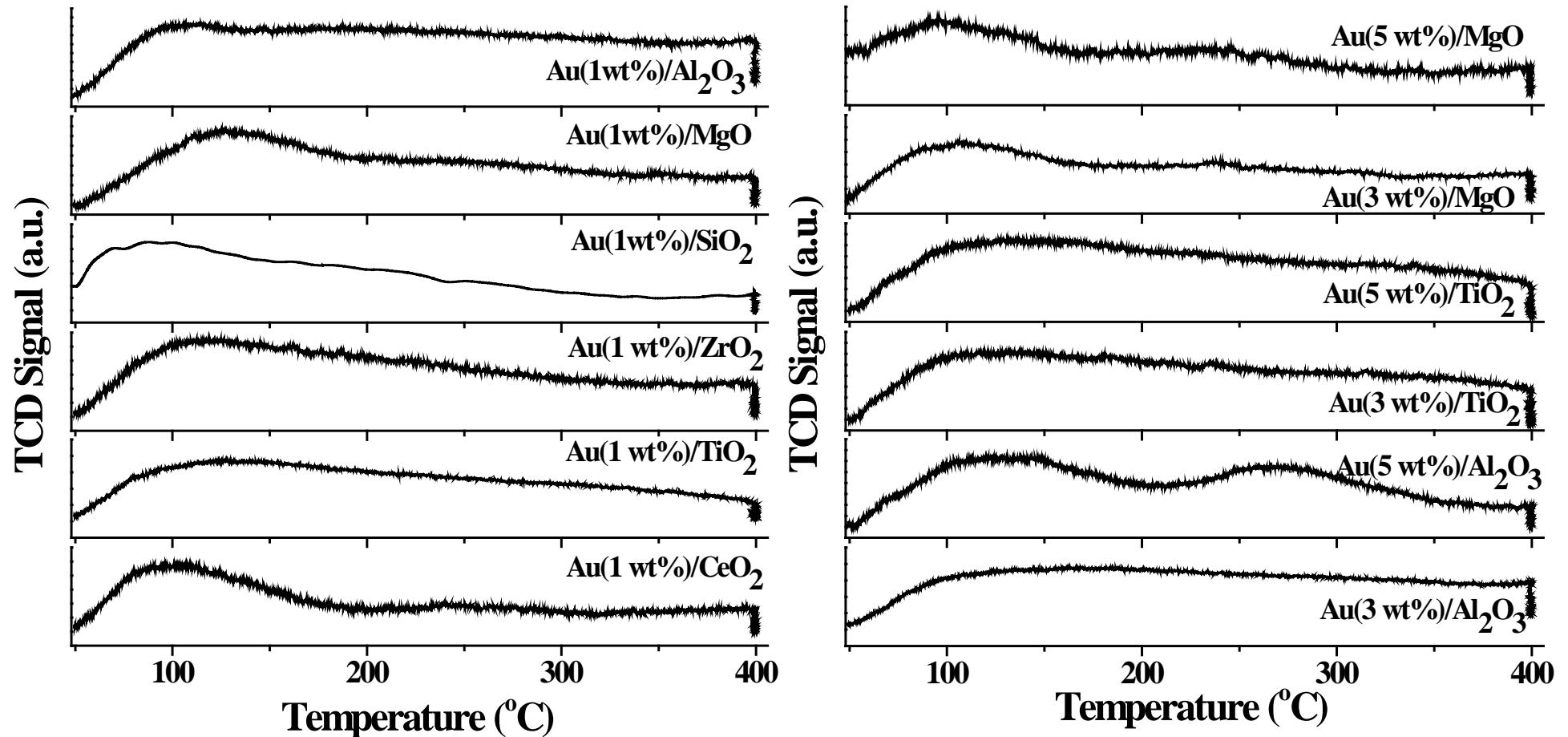
Fig. 3.6. NH_3-TPD profiles of metal oxide-supported Au catalysts.

> Au(1 wt.%)/SiO_2 (Table 3.1 and Fig. 3.6). ICP-OES analysis revealed that MgO support contained a small quantity of aluminium as impurity, which is the possible cause of higher acidity of Au supported on MgO catalyst. CO_2-TPD analysis showed that basicity (per gm of the catalyst) decreases in the order: Au(1 wt.%)/MgO > Au(3 wt.%)/MgO > Au(5 wt.%)/MgO >Au(1 wt.%)/Al_2O_3 > Au(1 wt.%)/TiO_2 > Au(3 wt.%)/TiO_2 > Au(5 wt.%)/TiO_2 ~ Au(1 wt.%)/CeO_2 > Au(3 wt.%)/Al_2O_3 > Au(1 wt.%)/SiO_2 > Au(1 wt.%)/ZrO_2 (Table 3.1 and Fig. 3.7). Moreover, the particle size of Au nanoparticles and the significant support effects observed due to the acid-base properties of support play pivotal role in determining both the activity and the selectivity.

3.3.1.9. H_2-TPR

Representative H_2-temperature-programmed reduction (TPR) profiles of Au(1 wt.%) supported on metal oxides are presented in Fig. 3.8. The supported Au catalysts showed two reduction peaks, one in the temperature region of 40-200 °C with peak maximum at 55-108 °C and the other above 400 °C (Table 3.3). While, the low temperature peak is attributed to reduction of the oxidic nano-gold, the high temperature peak is corresponded to reduction of support oxide. Support had a marked effect on position and shape of the low temperature reduction peak. The peak corresponding to Au(1 wt.%) on TiO_2, ZrO_2 and SiO_2 was asymmetric and broader than that for Au(1 wt.%) on CeO_2 and Al_2O_3 indicating the presence of a broad distribution of Au particles reducing in a larger temperature range. TEM images indeed confirmed the presence of broad particle size distribution. The reducibility of Au on different supports decreased as Au(1 wt.%)/MgO (T_{max} = 130 °C) > Au(3 wt.%)/Al_2O_3 (108 °C) > Au (1 wt.%)/CeO_2 (87 °C) > Au(1 wt.%)/Al_2O_3 (83 °C) > Au(1 wt.%)/TiO_2 (70 °C) > Au(1 wt.%)/ZrO_2 (60 °C) > Au(1 wt.%)/SiO_2 (56 °C). While it is not clear at this point, the causes for the difference in reducibility, it is believed that particle size of Au as well as acid-base properties of the support oxide influence the reducibility of Au. While, the support CeO_2 showed reduction peaks at around 400 and 780 °C due to reduction of surface and bulk sites, TiO_2 showed this peak at 630 °C. The reduction peak of ZrO_2 occurred above 900 °C. MgO and Al_2O_3 showed their surface and bulk oxygen reduction peaks at (240 and 560 °C) and (400 and 650 °C), respectively. The overall H_2 consumption on Au(1 wt.%)/TiO_2 was higher than on Au(1 wt.%)/MgO. The peak corresponding to reduction of gold observed at 70 °C and130 °C for Au(1 wt.%)/TiO_2 and Au(1 wt.%)/MgO, respectively, indicating the presence of highly reducible gold on TiO_2. This reducible nature of Au on TiO_2 perhaps results in high oxidation activity.
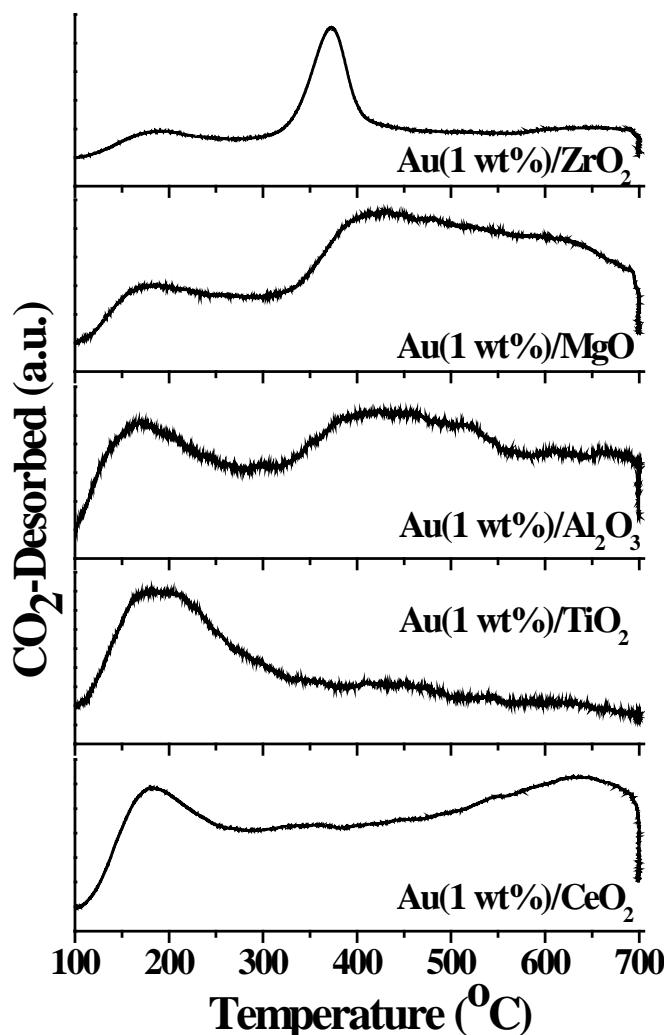
Fig. 3.7. CO_2-TPD profiles of metal oxide-supported Au catalysts.

Table 3.3. H_2-uptake of catalysts obtained from TPR study.

S.No.	Catalyst	H_2-uptake (TPR; mmol/g)	
		Overall	Au
1	Au(1 wt.%)/CeO$_2$	0.567	0.152
2	Au(1 wt.%)/TiO$_2$	0.131	0.077
3	Au(1 wt.%)/ZrO$_2$	0.044	0.029
4	Au(1 wt.%)/SiO$_2$	0.018	0.018
5	Au(1 wt.%)/MgO	0.086	0.018
6	Au(1 wt.%)/Al$_2$O$_3$	0.131	0.060
7	Au(3 wt.%)/Al$_2$O$_3$	0.305	0.190
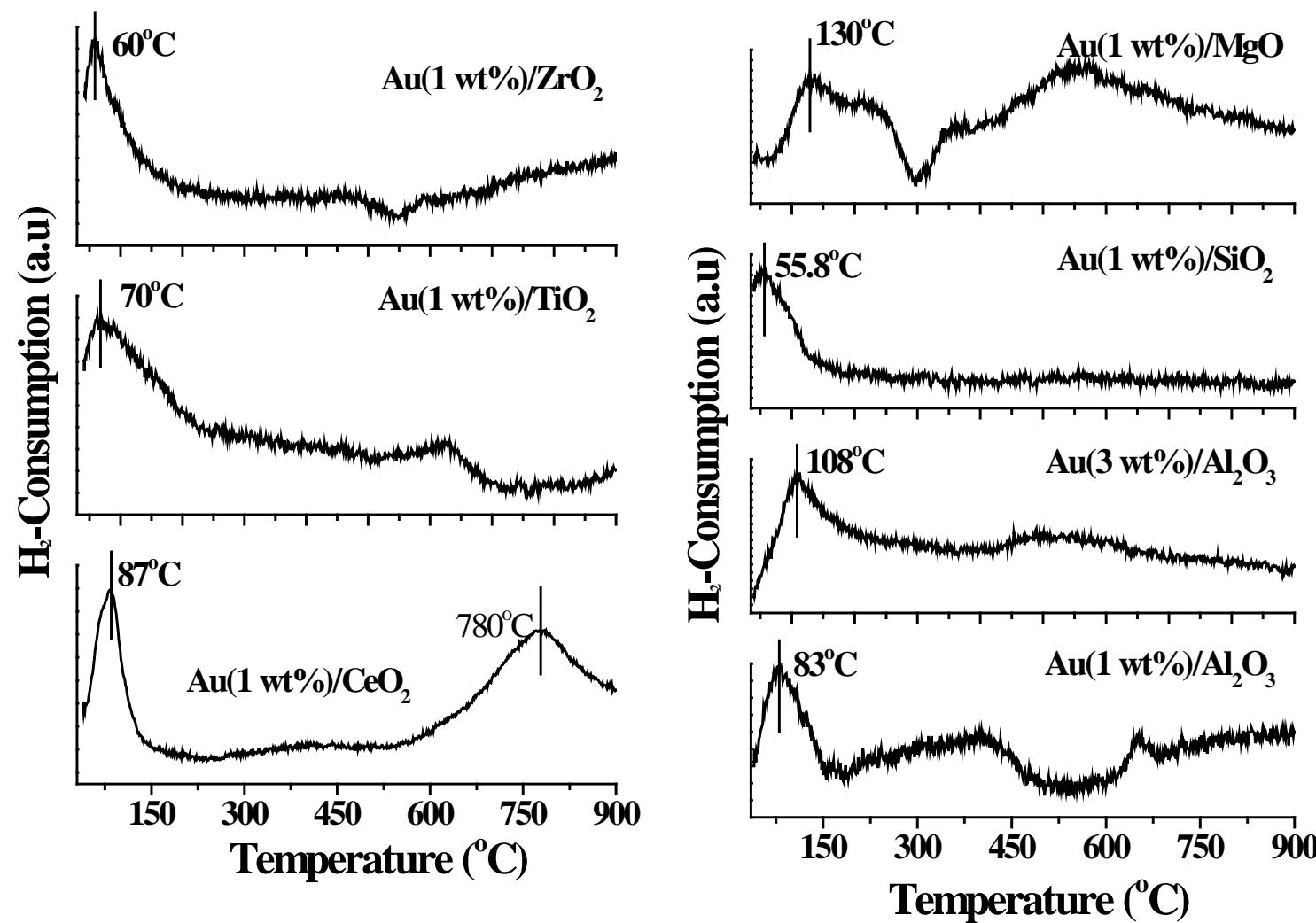
Fig. 3.8. H_2-TPR of metal oxide supported Au catalysts.

3.3.2. Catalytic Activity - Selective Oxidation of Benzyl Alcohol

Oxidation of benzyl alcohol with aerial oxygen over supported Au catalysts was carried out in toluene medium at 80 °C and atmospheric pressure (Table 3.4). Benzaldehyde was the main product. Benzoic acid and benzyl benzoate were the minor products formed due to further reactions (over oxidation and esterification). Gold loading had a marked effect on the activity and selectivity towards benzaldehyde. At higher loadings (3 and 5 wt.%) of Au on TiO_2 and MgO, there was a decrease in the activity (in terms of turnover frequency (TOF), compare entry nos. 3 and 4 with 2 and 7 and 8 with 6 in Table 3.4) and selectivity to benzaldehyde (from 94.0 to 67.4 wt.% and 95.0 to 63.2 wt.%, respectively). Catalysts with Au(1 wt.%) showed better catalytic activity and selectivity perhaps due to smaller size of Au nanoparticles present in those catalysts and because of high dispersion of Au and effective metal-support interactions. Catalytic activity of Au [turnover frequency (TOF) = moles of benzyl alcohol converted per mole of surface Au atoms (estimated from TEM studies) per hour] over different supported Au decreased in the order: Au(1 wt.%)/ZrO_2 > Au(1 wt.%)/TiO_2 > Au(1 wt.%)/MgO > Au(1 wt.%)/CeO_2 > Au(1 wt.%)/Al_2O_3 > Au(1 wt.%)/SiO_2. Selectivity for benzaldehyde decreased in the order: Au(1 wt.%)/MgO > Au(1 wt.%)/TiO_2 > Au(1 wt.%)/SiO_2 > Au(1 wt.%)/CeO_2 > Au(1 wt.%)/ZrO_2 > Au(1 wt.%)/Al_2O_3. TOF values of these supported gold catalysts prepared by deposition-precipitation method were higher than those reported by others [48-50] indicating that the method of preparation has an effect on the activity of gold.

3.3.2.1. Effect of Reaction Parameters

Temperature had a positive effect on benzyl alcohol conversion and TOF (Figs. 3.9 and 3.10), but the selectivity towards benzaldehyde decreased with increase in temperature (due to over oxidation). The conversion of benzyl alcohol increased with increasing reaction time (Fig. 3.11). But at longer durations (9 h) over Au(1 wt.%)/TiO_2 catalyst, the selectivity for benzaldehyde decreased (from 95 to 80 wt.%) and that of benzyl benzoate increased (from 5 to 20 wt.%). The activity of both Au(1 wt.%)/TiO_2 and Au(1 wt.%)/MgO enhanced in the presence of a base (K_2CO_3) (Fig. 3.11). Base facilitated abstraction of alcoholic proton and attack of reactive alkoxide species on catalytic sites. Benzyl alcohol conversion increased (from 20 to 64 wt.%) with increasing amount of the catalyst (from 0.05 to 0.4 g; Table 3.5).

A comparison of the results reveals that both particle size and acid-base properties of the support influencing electronic structure of Au have marked effects on catalytic activity and aldehyde selectivity. Au $4f_{7/2}$ line in XPS for Au(1 wt.%) on TiO_2 and MgO occurred at

70

Table 3.4. Selective oxidation of benzyl alcohol over different supported Au catalysts[a]

Run no.	Catalyst	Conversion (wt.%)	TOF (h^{-1})[b]	Product selectivity (wt.%)		
				Benzaldehyde	Benzyl benzoate	Benzoic acid
1	Au(1 wt.%)/CeO$_2$	27.0	694	88.2	11.8	0
2	Au(1 wt.%)/TiO$_2$	41.5	814	94.0	6.0	0
3	Au(3 wt.%)/TiO$_2$	67.3	612	81.2	18.8	0
4	Au(5 wt.%)/TiO$_2$	78.5	289	67.4	31.0	1.6
5	Au(1 wt.%)/ZrO$_2$	41.2	1735	86.2	13.8	0
6	Au(1 wt.%)/SiO$_2$	11.0	278	90.0	10.0	0
7	Au(1 wt.%)/MgO	44.0	695	95.0	5.0	0
8	Au(3 wt.%)/ MgO	69.4	460	77.5	22.5	0
9	Au(5 wt.%)/ MgO	83.2	418	63.2	34.1	2.7
10	Au(1 wt.%)/Al$_2$O$_3$	25.5	496	84.2	15.8	0

[a]Reaction conditions: Benzyl alcohol = 10 mmol, catalyst = 0.1 g, toluene = 5 ml, K$_2$CO$_3$ = 1 mmol, temperature = 80 ^{o}C, p(air) = 1 atm, time = 5 h. [b]Turnover frequency (TOF) = moles of benzyl alcohol converted per mole of surface Au atoms measured from TEM per hour.

Table 3.5. Effect of catalyst amount on benzyl alcohol oxidation[a]

Catalyst amount (g)	Conversion (wt.%)	Product selectivity (wt.%)	
		Benzaldehyde	Benzyl benzoate
Au(1 wt.%)/MgO			
0.05	22.0	98.3	1.7
0.1	44.0	95.0	5.0
0.2	61.8	86.8	13.2
0.4	66.5	75.5	24.5
Au(1 wt.%)/TiO$_2$			
0.05	20.0	97.0	3.0
0.1	41.5	94.0	6.0
0.2	58.0	88.0	12.0
0.4	64.0	79.5	20.5

[a]Reaction conditions: Benzyl alcohol = 10 mmol, catalyst = 0.05 – 0.4 g, solvent (toluene) = 5 ml, K$_2$CO$_3$ = 1 mmol, temperature = 80 ^{o}C, p(air) = 1 atm, time = 5 h.
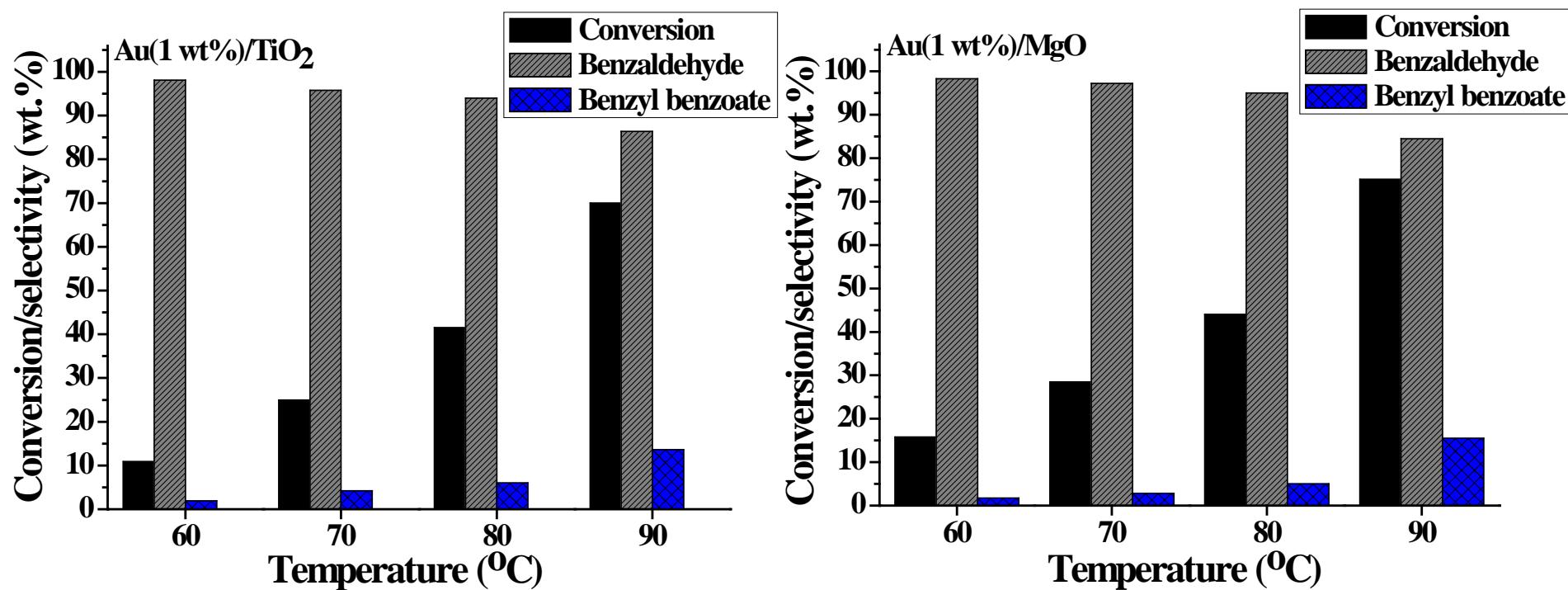
Fig. 3.9. Effect of temperature in benzyl alcohol oxidation over Au(1 wt.%)/TiO$_2$ and Au(1 wt.%)/MgO. Reaction conditions: Benzyl alcohol = 10 mmol, catalyst = 0.1 g, solvent (toluene) = 5 ml, p(air) = 1 atm, reaction time = 5 h, K$_2$CO$_3$ = 1 mmol.
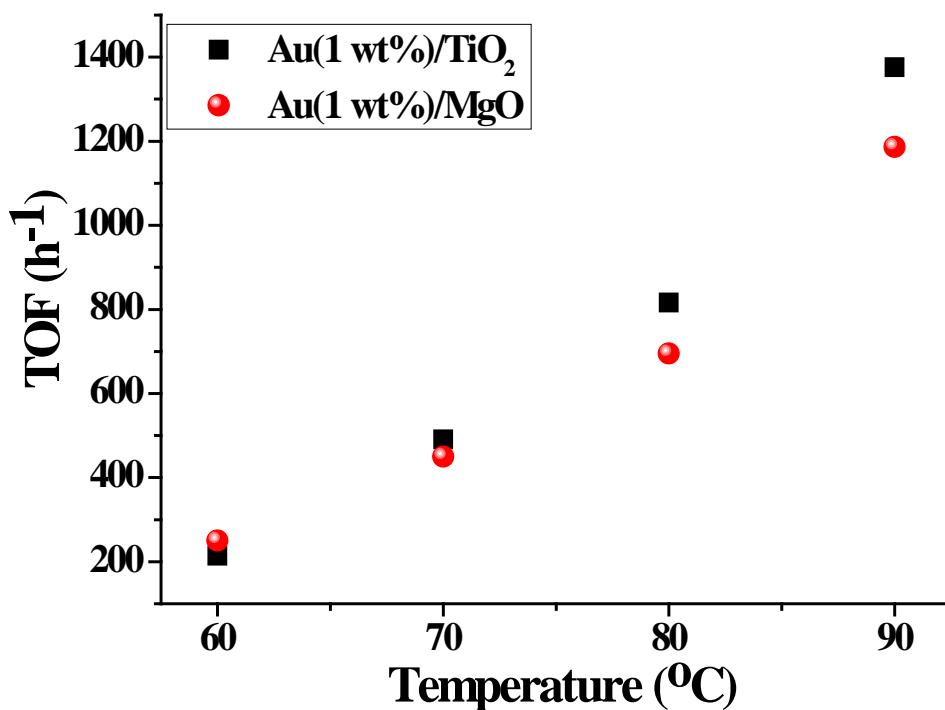
Fig. 3.10. Effect of temperature on activity of Au(1 wt.%)/TiO$_2$ and Au(1 wt.%)/MgO.

lower binding energy values (83.4 eV) revealing that gold is more electronegative on the former than on the latter oxide. A synergistic or cooperative effect of the support and the metal particles is possibly the cause for the high catalytic activity of Au. Abad et al. [17] reported high benzyl alcohol oxidation activity (conversion = 98% and benzaldehyde selectivity = 99%; TOF = 167 h^{-1}) for Au(1.8 wt.%) supported nanoparticle CeO$_2$. According to them, catalytic oxidation of alcohols goes through three main reaction steps: (i) M-alcoholate species formation, (ii) metal hydride intermediate and carbonylic product formation from M-alcoholates through β-hydride shift (rate determining step), and (iii) rapid oxidation of metal hydride by molecular oxygen forming water and the active metal site. When the composition of Au was 1 wt.%, no traces of benzoic acid were detected in product. At higher metal loading (5 wt.%), a small quantity of benzoic acid was also detected (1.6-2.7 wt.%). The by-product benzyl benzoate can form through two reaction pathways: (1) by esterification of benzoic acid with benzyl alcohol, (2) by disproportionation of an aldehyde and alcohol (Cannizzaro reaction, Tishchenko reaction). To probe this further, the esterification reaction taking benzoic acid and benzyl alcohol was performed. None of the catalysts in this study produced benzyl benzoate. Hence, ester is formed by coupling of adsorbed benzyloxy group with benzaldehyde and not through esterification of benzoic acid.
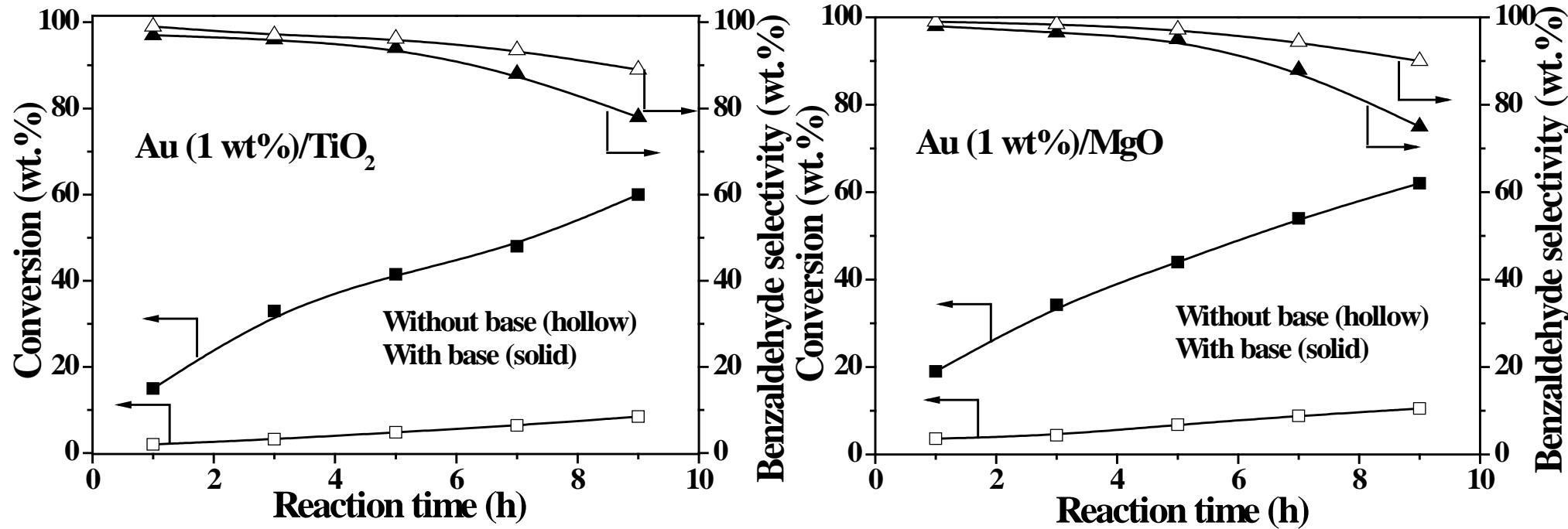
Fig.3.11. Performance of Au(1 wt.%)/MgO and Au(1 wt.%)/TiO$_2$ catalyst with time in presence and absence of base. Reaction conditions: Benzyl alcohol = 10 mmol, catalyst = 0.1 g, solvent (toluene) = 5 ml, temperature = 80 $^\circ$C, p(air) = 1 atm, reaction time = 5 h, K$_2$CO$_3$ = 1 mmol.

A similar observation for the formation of benzyl benzoate through the surface adsorbed benzyloxy group was reported also by Abad et al. [17].

3.3.2.2. Structure-activity Correlations

Considering that Au of particle size < 5 nm is catalytically highly active, a correlation between activity (TOF) and percentage of particle size having < 5 nm diameter was probed (Fig. 3.12). In general, TOF increased with increase in % of Au particles of size < 5 nm. Catalytic activities of Au on ZrO_2, TiO_2 and CeO_2 were higher even though the Au particle size was higher. Perhaps, the reducible nature of support was the cause for their higher catalytic activity. Catalytic activity increased with increase in acidity and basicity. However, the selectivity of benzaldehyde increased with increasing basicity and decreasing acidity. Thus, the correlations reveal that a unique combination of high basicity and low acidity of the support and particle size of Au lower than 5 nm is ideal for developing efficient and selective alcohol oxidation catalysts.
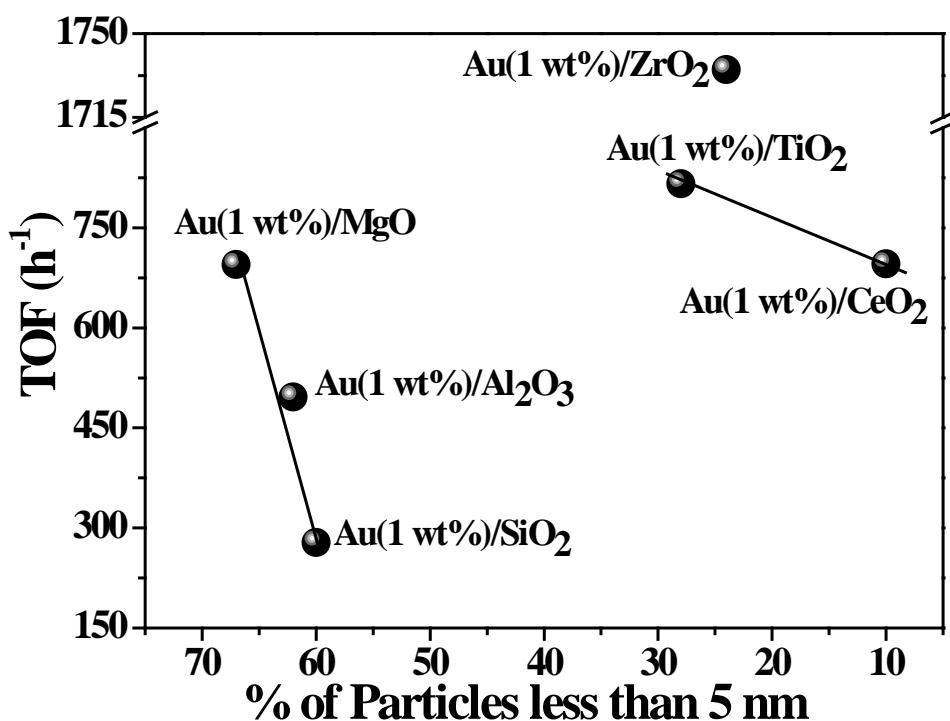
Fig.3.12. Correlation between activity (TOF) and % of Au particle size having < 5 nm.

3.3.2.3. Catalyst Recyclability

Reusability of Au(1 wt.%)/TiO_2 and Au(1 wt.%)/MgO in alcohol oxidation were tested in three recycling experiments (Fig. 3.13). At the end of each run, the catalyst was separating by centrifugation. It was washed with water followed by ethanol and dried at 100 °C for 5 h. Then, it was used in the next recycle experiment. Even after the 3rd recycle,
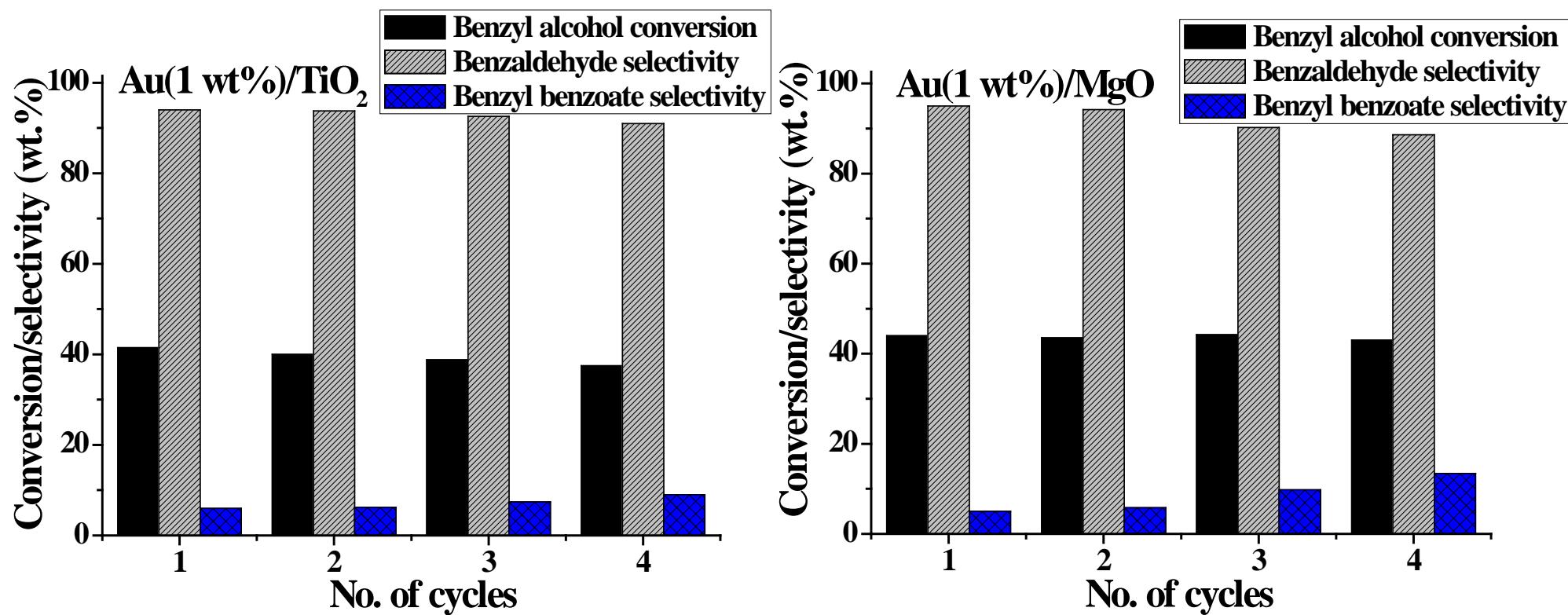
Fig.3.13. Catalyst recycle study. Reaction conditions: Benzyl alcohol = 10 mmol, catalyst = 0.1 g, solvent (toluene) = 5 ml, K_2CO_3 = 1 mmol, temperature = 80 ^{o}C, p(air) = 1 atm, reaction time = 5 h.

Fig. 3.14. TEM images of recycled catalysts. (a) Au(1 wt.%)/TiO$_2$ and (b) Au(1 wt.%)/MgO.

conversion of benzyl alcohol and benzaldehyde selectivity remained the same (within experimental error), inferring that these catalyst are stable and recyclable. ICP-OES analysis of spent catalyst confirmed that chemical composition (Au content) is intact. However, TEM analysis (Fig. 3.14) revealed a marginal increase in the particle size of Au after three recycles.

3.3.3. Catalytic Activity - Hydrogenation of Cinnamaldehyde

Hydrocinnamaldehyde (HCA), 3-phenyl propanol (PPL) and cinnamyl alcohol (CAL) were the major products in the hydrogenation of cinnamaldehyde (CA). A small fraction of high molecular weight condensation products (others) were also observed. Over different supports, TOF for the conversion of CA decreased as follows (Table 3.6): Au(1 wt.%)/ZrO$_2$ > Au(1 wt.%)/TiO$_2$ > Au(1 wt.%)/Al$_2$O$_3$ > Au(1 wt.%)/SiO$_2$ > Au(1 wt.%)/CeO$_2$ > Au(1 wt.%)/MgO. TOF values for the Au catalysts are significantly high and are in the range 218-661 h^{-1}. Except Au (1 wt.%)/Al$_2$O$_3$ and Au (1 wt.%)/MgO, rest all catalysts yielded HCA as main product (selectivity 84.0 -98.8 wt.%). Au (1 wt.%)/MgO led to a large amount of high molecular weight condensation products (76.2 wt.%). Interestingly, Au (1 wt.%)/Al$_2$O$_3$, formed cinnamyl alcohol (C=O hydrogenation product) with a selectivity of 28.9 wt%. Accordingly to XPS studies (Table 3.2), Au is in zero valent oxidation state in all these catalysts but Au supported on MgO and TiO$_2$ (Au 4f$_{7/2}$ peak appearing below 84.0 eV) is richer in electron density. This difference in electronic properties is the possible cause for the difference in the selectivity of Au supported on Al$_2$O$_3$ compared to other catalysts.

Table 3.6. Selective hydrogenation of cinnamaldehyde over supported Au catalysts[a]

Catalyst	CA conversion (wt.%)	TOF (h^{-1})	Products selectivity (wt.%)			
			HCA	PPL	CAL	Others
Au(1 wt.%)/CeO$_2$[b]	12.5	95	79.5	9.9	5.1	5.5
Au(1 wt.%)/CeO$_2$	30.0	228	84.0	4.8	6.7	4.5
Au(1 wt.%)/TiO$_2$	61.3	507	98.8	1.2	0	0
Au(1 wt.%)/ZrO$_2$	53.3	661	98.4	0.7	0.9	0
Au(1 wt.%)/SiO$_2$	27.2	337	89.6	3.3	7.1	0
Au(1 wt.%)/MgO	6.0	56	23.8	0	0	76.2
Au(1 wt.%)/Al$_2$O$_3$	25.2	361	67.7	3.4	28.9	0
Au(3 wt.%)/Al$_2$O$_3$[b]	38.1	109	61.2	12.4	25	1.4
Au(3 wt.%)/Al$_2$O$_3$	76.1	218	40.2	8.2	50	1.6
Au(5 wt.%)/Al$_2$O$_3$	81.0	135	56.8	14.2	26.1	2.9

[a]Reaction conditions: Catalyst = 0.05 g, cinnamaldehyde (CA) = 1 g, solvent (iso propanol) = 25 ml, alkali (NaOH) = 0.01 g in 5 ml water, p(H$_2$) = 20 atm, reaction temperature = 150 °C, reaction time = 4 h, HCA = hydrocinnamaldehyde, PPL = 3-phenyl propanol, CAL = cinnamyl alcohol. Others include higher molecular weight condensation products. [b]Runs without alkali.

3.3.3.1. Effect of Reaction Parameters

Base addition has a marked effect on the hydrogenation reaction (Fig. 3.15). CA conversion and CAL selectivity were higher in the presence of base. The effect of reaction temperature was studied in the absence of alkali promoter.The reactions were conducted at 50, 100, 150 and 200 °C. Conversion of CA increased from 6.5% to 63.4% in 4 h as the temperature was raised from 50 to 200 °C. Increase in CAL selectivity from 14.9% to 29% at the expense of HCA + PPL product selectivity was also noted.

This study thus reveals that temperature facilitates selective hydrogenation of the carbonyl group of CA. With increasing reaction temperature (from 50 to 150 °C), CAL selectivity increased to as high as 50 wt.%. While CA conversion increased with increasing hydrogen pressure (5-20 atm), product selectivity was little affected. The increase in catalyst amount (0.025-0.075 g) had a positive influence on the CA conversion (57.3-88.5 wt.%) and CAL selectivity (25.5-46.2 wt.%). The effect of catalyst amount, H$_2$ pressure and temperature on the catalytic activity of Au(3 wt.%)/Al$_2$O$_3$ in CA hydrogenation are presented in Table

3.7. In other words, this work reveals that support and electronic structure of gold have notable effects on the activity and selectivity in the hydrogenation reaction.
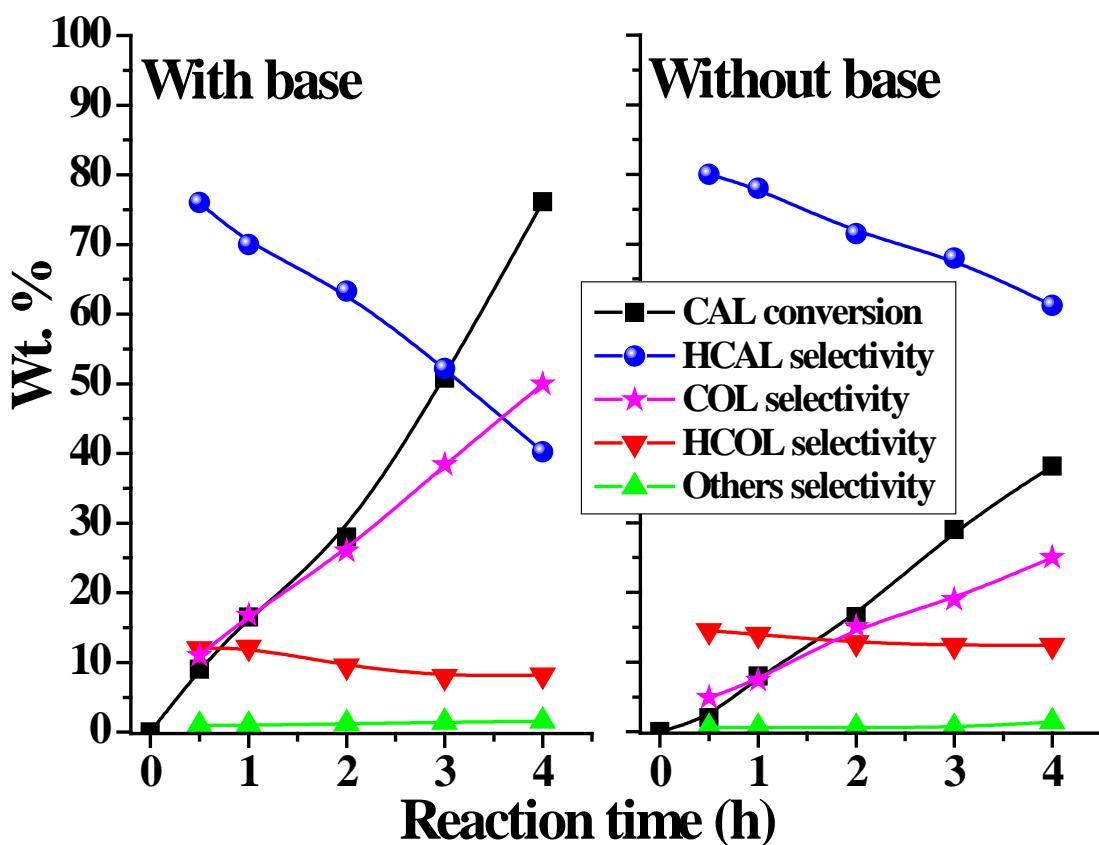
Fig. 3.15. Influence of alkali on the hydrogenation of CA over Au(3 wt.%)/Al$_2$O$_3$ catalyst as a function of reaction time. Reaction conditions: Catalyst = 0.05 g, CA = 1 g, solvent (iso-propanol) = 25 ml, alkali = 0 or 0.01 g in 5 ml water, p(H$_2$) = 20 atm, temperature = 150 °C. HCA = hydrocinnamaldehyde, PPL = 3-phenil propanol, CAL = cinnamyl alcohol and others include higher molecular weight condensation products.

Although Au leads to lower hydrogenation rates as a consequence of its completely filled d-orbitals than the other noble metals (Pt, Pd and Ru), depending on the support and size, the supported Au catalysts do exhibit reasonably good hydrogenation activity. In general, supported Au catalysts favoured hydrogenation of C=C in CA yielding HCA product [51-53]. Only a few catalysts (*ca*., Au supported on ZnO and iron oxy-hydroxide) led to unsaturated alcohol products. In the present study, Au supported on Al$_2$O$_3$ was selective for C=O hydrogenation while rest of the catalysts facilitated C=C hydrogenation in CA.

Table 3.7. Influence of reaction conditions on the hydrogenation activity of Au(3 wt.%)/Al$_2$O$_3$[a]

Catalyst amount (g)	Temperature (°C)	H$_2$ pressure (atm)	CA conversion (wt.%)	TOF (h^{-1})	Products selectivity (%)			
					HCA	PPL	CAL	Others
0.05	50[b]	20	6.5	19	72.0	12.2	14.8	1.0
0.05	100[b]	20	25.0	72	68.6	13.0	17.6	0.8
0.05	150[b]	20	38.1	109	61.2	12.4	25.0	1.4
0.05	200[b]	20	63.4	182	54.0	15.0	29.0	2.0
0.05	150	5	29.0	83	48.0	6.5	43.5	2.0
0.05	150	10	48.0	138	43.0	7.0	48.6	1.4
0.05	150	20	76.1	218	40.2	8.2	50.0	1.6
0.05	150	30	88.5	254	42.0	10.0	46.2	1.8
0.025	150	20	57.3	328	68.4	5.1	25.5	1.0
0.075	150	20	88.0	168	45.0	12.0	41.2	1.8

[a]Reaction conditions: Catalyst = 0.025 – 0.075 g, cinnamaldehyde (CA) = 1 g, solvent (iso-propanol) = 25 ml, alkali (NaOH) = 0.01 g in 5 ml water, H$_2$ pressure = 5 - 30 atm, reaction temperature = 50 - 200 °C, reaction time = 4 h, HCA = hydrocinnamaldehyde, PPL = 3-phenyl propanol, CAL = cinnamyl alcohol. Others include higher molecular weight condensation products. [b]Without base. Turnover frequency (TOF) = moles of reactant converted per mole of metal in the catalyst per hour.

Higher activity (CA conversion = 76-81 wt.%) and unsaturated alcohol (CAL) selectivity (50 wt.%) of Au/Al$_2$O$_3$ can be corresponded to lower particle size (4-5 nm) and higher dispersion (17-19%) of the supported nano gold. These factors facilitate hydrogen dissociation and low electron density at gold (XPS) which in turn promote CA activation through C=O instead of C=C group. Support-metal interaction altering the electronic structure of interfacial gold atoms is the cause for higher catalytic activity (CA conversion and TOF) of Au on reducible supports.

3.4. Conclusions

Gold (1-5 wt.%) supported on six different metal oxides (CeO$_2$, TiO$_2$, ZrO$_2$, SiO$_2$, MgO and Al$_2$O$_3$) were prepared by a modified deposition-precipitation method. Their structural, spectroscopic, reduction and acid-base properties were determined using various characterization techniques. Their application as efficient catalysts for oxidation of benzyl alcohol and hydrogenation of cinnamaldehyde was investigated. Au(1 wt.%)/ZrO$_2$ showed high benzyl alcohol oxidation activity (TOF= 1735 h^{-1}) but the selectivity for benzaldehyde was low (86.2 wt.%). Au(1 wt.%)/TiO$_2$ and Au(1 wt.%)/MgO exhibited highest selectivity for benzaldehyde (94 and 95 wt.%, respectively) while the TOF was 814 and 695 h^{-1}, respectively. The catalysts Au(1 wt.%)/TiO$_2$ and Au(1 wt.%)/MgO were reusable in oxidation reactions. TiO$_2$ and ZrO$_2$-supported Au catalysts exhibited higher TOF values with HCA as the main product. Al$_2$O$_3$-supported Au was more selective for CAL than the other catalysts. Particle size and electronic properties of Au and acid-base properties of support had a marked effect on the catalytic performance of Au in oxidation and hydrogenation reactions.

3.5. References

[1]   M. Haruta, S. Tsubota, T. Kobayashi, H. Kageyama, M. J. Genet, B. Delmon, J. Catal. 144 (1993) 175-192.

[2]   G. J. Hutchings, J. Catal. 96 (1985) 292-295.

[3]   M. Haruta, Angew. Chem. Int. Ed. 53 (2014) 52-56.

[4]   M. Haruta, Catal. Today 36 (1997) 153-166.

[5]   M. Conte, C. J. Davies, D. J. Morgan, T. E. Davies, D. J. Elias, A. F. Carley, P. Johnston, G. J. Hutchings, J. Catal. 297 (2013) 128-136.

[6]   J. K. Edwards, J. Pritchard, M. Piceinini, G. Shaw, Q. He, A. F. Carley, C. J. Kiely, G. J. Hutchings, J. Catal. 292 (2012) 227-238.

[7]   G. C. Bond, Catal. Rev. Sci. Eng. 41 (1999) 319-388.

[8]   N. Semagine, L. Kiwi-Minsker, Catal. Rev. 51 (2009) 147-217.

[9]   C. W. Corti, R. J. Holliday, D. T. Thompson, Top. Catal. 44 (2007) 331-343.

[10]   M. Alden, X. Lai, D.W. Goodman, Science 281 (1999) 1647-1650.

[11]   R. A. Sheldon, I. W. C. E. Arends, G. J. Ten Brink, A. Dijksman, Acc. Chem. Res. 35 (2002) 774-781.

[12]   V.R. Choudhary, D.K. Dumbre, Catal. Commun. 10 (2009) 1738-1742.

[13]   G. Cainelli, G. Cardillo, Chromium Oxidant in Organic Chemistry, Springer, Berlin, 1984.

[14]   G. J. Ten Brink, I. W. C. E. Arends, R. A. Sheldon, Science 287 (2000) 1636-1639.

[15]   T. Iwasawa, M. Tokunaga, Y. Obora, Y. Tsuiji, J. Am. Chem. Soc. 126 (2004) 10657-10666.

[16]   S. E. Davis, M. S. Ide, R. J. Davis, Green Chem. 15(2013) 17-45.

[17]   A. Abad, A. Corma, H. Garcia, Chem. Eur. J. 14 (2008) 212-222.

[18]   A. Villa, C. E. C.-Thaw, G. M. Veith, K. L. More, D. Ferri, L. Prati, ChemCatChem 3 (2011) 1612-1618.

[19]   D. Nepak, D. Srinivas, RSC Adv. 5 (2015) 47740-47748.

[20]   T. Mitsudome, A. Noujima, T. Mizugaki, K. Jitsukawa, K. Kaneda, Adv. Synth. Catal. 351 (2009)1890-1896.

[21]   S. Wang, Q. Zhao, H. Wei, J.-Q. Wang, M. Cho, H. S. Cho, O. Terasaki, Y. Wan, J. Am. Chem. Soc. 135 (2013) 11849-11860

[22]   A. Villa, N. Janjic, P. Spontoni, D. Wang, D. S. Su, L. Prati, Appl. Catal. A: Gen. 364 (2009) 221-228.

[23]   T. A. G. Silva, R. Landers, L. M. Rossi, Catal. Sci. Technol. 3 (2013) 2993-2999.

[24]   V. Peneau, Q. He, G. Shaw, S. A. Kondrat, T. E. Davies, P. Miedziak, M. Forde, N. Dimitratos, C. J. Kiely, G. J. Hutchings, Phys. Chem. Chem. Phys. 15 (2013) 10636-10644.

[25]   E. M. de Moura, M. A. S. Garcia, R. V. Gonçalves, P. K. Kiyohara, R. F. Jardimc, L. M. Rossi, RSC Adv. 5 (2015) 15035-15041.

[26]   Y. Kwon, S. C. S. Lai, P. Rodriguez, M. T. M. Koper, J. Am. Chem. Soc. 133 (2011) 6914-6917.

[27]   N. Zheng, G. D. Stucky, chem. commun. 113 (2007) 3862- 3864.

[28]   T. Mallat, A. Baiker, Chem Rev. 104 (2004) 3037-3058.

[29]   D. I. Enache, D.W. Knight, G. J. Hutchings, Catal. Lett. 103 (2005) 43-52.

[30] A. Abad, P. Concepcion, A. Corma, H. Garcia, Angew. Chem. Int. Ed. 44 (2005) 4066-4069.

[31] P. Maki-Arvela, J. Hajek, T. Salmi, D. Y. Murzin, Appl. Catal. A: Gen. 292 (2005) 1-49.

[32] S. Mahmoud, A. Hammoudeh, S. Gharaibeh, J. Melsheimer, J. Mol. Catal. A: Chem. 178 (2002) 161-167.

[33] K. Weissermel, H. J. Arpe, Industrial Organic Chemistry, Verlag Chemie, Weinheim (1978).

[34] P. Claus, A. Bruckner, C. Mohr, H. Hofmeister, J. Am. Chem. Soc. 122 (2000) 11430-11439.

[35] M.H.A. Rahim, Q. He, J.A. Lopez-Sanchez, C. Hammond, N. Dimitratos, M. Sankar, A.F. Carley, C.J. Kiely, D.W. Knighta, G.J. Hutchings, Catal. Sci. Tech. 2 (2012) 1914-1924.

[36] A. C. Gluhoi, X. Tang, P. Marginean, B. E. Nieuwenhuys, Top. Catal. 39 (2006) 101-110.

[37] C. G. Silva, R. Juarez, T. Marino, R. Molinari, H. Garcia, J. Am. Chem. Soc. 133 (2011) 595–602.

[38] E. Kowalska, O. O. P. Mahaney, R. A. B. Ohtani, Phys. Chem. Chem. Phys. 12 (2010) 2344-2355.

[39] W. Haiss, N.T.K. Thanh, J. Aveyard, D.G. Fernig, Anal. Chem. 79 (2007) 4215-4221.

[40] F. Wu, Q. Yang, Nano Res. 4 (2011) 861-869.

[41] J. L. Margitfalvi, A. Fasi, M. Hegedus, F. Lonyi, S. Gobolos, N. Bogdanchikova, Catal. Today 72 (2002) 157-169.

[42] R. Kubo, J. Phys. Soc. Jpn.17 (1962) 975-986.

[43] W. P. Halperin, Rev. Mod. Phys. 58 (1986) 533-606.

[44] A. Kawabata, J. Phys. Soc. Jpn. 29 (1970) 902-911.

[45] S. Schimpf, M. Lucas, C. Mohr, U. Rodemerck, A. Bruckner, J. Radnik, H. Hofmeister, P. Claus, Catal. Today 72 (2002) 63-78.

[46] L.F. Liotta, G. Di Carlo, G. Pantaleo, A. M. Venezia, Catal. Today 158 (2010) 56-62.

[47] B. Tian, J. Zhang, T. Tong, F. Chen, Appl. Catal. B: Environ. 79 (2008) 394-401.

[48] V. V. Costa, M. Estrada, Y. Demidova, I. Prosvirin, V. Kriventsov, R. F. Cotta, S.

Fuentes, A. Simakov, E. V. Gusevskaya, J. Catal. 292 (2012) 148-156.

[49]   S. Arrii, F. Morfin, A. J. Renouprez, J. L. Rousset, J. Am. Chem. Soc. 126 (2004) 1199-1205.

[50]   M. Estrada, V. V. Costa, S. Beloshapkin, S. Fuentes, E. Stoyanov, E. V. Gusevskaya, A. Simakov, Appl. Catal. A: Gen. 473 (2014) 96-103.

[51]   X. Zhang, Y. C. Guo, Z. C. Zhang, J. S. Gao, C. M. Xu, J. Catal. 292 (2012) 213-226.

[52]   Y.-C. Hong, K.-Q. Sun, G.-R. Zhang, R.-Y. Zhong, B.-Q. Xu, Chem. Commun. 47 (2011) 1300-1302.

[53]   H. Shi, N. Xu, D. Zhao, B.-Q. Xu, Catal. Commun. 9 (2008) 1949-1954.

Chapter - 4

Selective Oxidations over Au/Titanate Nanotubes: Effect of Pd & Alkali (Earth) Metal Ions

4.1. Introduction

Heterogeneous catalysis by gold is now a well fascinating research topic. Previously it was ignored for a long time as bulk gold is chemically inert. The exploration and exploitation of nano-gold in catalysts (in oxidation, epoxidation, direct synthesis of hydrogen peroxide, hydrogenation, coupling and water-gas shift reactions) led to new chemistry practices [1]. Selective oxidation of alcohols is a commercially important organic transformation as its products are intermediates in the manufacture of pharmaceuticals, agrochemicals and perfumeries [2]. This reaction is conventionally performed with stoichiometric oxidation reagents which are expensive and associated with toxicity issues. Liquid-phase, aerobic oxidation of alcohols to corresponding carbonyl compounds using nano-gold catalysts under moderate conditions is attractive from economic and environmental perspectives [1, 3]. However, considerable focus is necessary to improve the catalytic performance and the stability of the gold catalysts. The catalytic performance of supported gold nanoparticles (Au NPs) can be tuned by controlling the particle size and by altering the electronic properties of Au. This can be achieved by (i) the addition of a second metal (Pd), which leads to geometric and electronic effects and (ii) by choosing the right kind of support material, which can introduce suitable contact of gold with the support (through metal-support peripheral interface or via charge transfer from the support to gold) [4].

In recent times interest in catalysis by supported gold-palladium nanoparticles has expanded dramatically. Owing to the ensemble (geometric) and ligand (electronic) effects between these two metals [5], bimetallic Au-Pd NPs can have much improved activity and selectivity compared to their monometallic counterparts. In particular different groups showed that, the alloying of gold with palladium leads to many fold enhancement in activity with simultaneous retention of selectivity [6] and resistance to deactivation [7, 8] as compared to monometallic gold [9]. Enache et al. [6] concluded that the addition of Au into Pd/TiO$_2$ catalyst decreases the activity, but the Au-Pd/TiO$_2$ catalyst retained high selectivity to benzaldehyde at a higher conversion rate. This feature was not observed with supported pure-Au and pure-Pd catalysts. They reported that, the Au-Pd/TiO$_2$ catalysts were very active for this reaction and the selectivity to benzaldehyde was $>$ 96% with benzyl benzoate as the only by-product. In particular, 2.5 wt.% Au-2.5 wt. % Pd/TiO$_2$ catalyst is highly active with a turnover frequency (TOF) as high as 269,000 h^{-1} at 160 $^{\circ}$C, which was over 25 times more active for the selective oxidation of phenylethanol when compared with the Au/CeO$_2$ [9] or Pd/hydroxyapatite catalysts under the same reaction conditions.

The effect of strong metal-support interactions (SMSI) was first observed in TiO_2-supported noble metal systems reported by Tauster et al. in 1978 [4]. One of the early hypotheses for this effect was that the alteration of the charge state of the metal by electron transfer from or to a support leads to an improvement in the ability to activate reactants and thereby influencing the catalytic properties of the metal [10]. This hypothesis was reconfirmed experimentally by several researchers. Bruix et al. [11] successfully interpreted the enhanced activity of platinum particles supported on ceria in water-gas shift reaction as the "electronic metal-support interaction" (EMSI), a term that was recently coined by Campbell [12]. However, intrinsic metal effects, such as the electronic quantum size effect [13] and the structure-sensitivity geometrical effect [14] should be ruled out for a complete understanding of the EMSI effect. For supported metal particle/cluster catalysts, a complete elimination of the intrinsic metal effects is particularly difficult or even impossible. Milone et al. [15] reported that the catalytic properties of supported gold catalysts strongly depend on the type and structure of the support. From the comparative study of Fe_2O_3-, ZnO-, CaO-, and Al_2O_3-supported gold catalysts, they found that the basicity and lattice oxygen of support have significant effects on the catalytic performance.

Recently, the 1-D nanoscale alkali titanates such as nanotubes, nanoribbons and nanowires have attracted much interest in heterogeneous catalysis as catalyst supports, due to their unique physicochemical properties (high specific surface area and hollow morphology). In particular, after the simple alkaline hydrothermal synthesis, sodium titanate nanotubes (NaTNTs) reported by Kasuga et al. [16] have emerged as promising functional materials. The NaTNTs have well-defined mesopores with a wall thickness of a few nanometers. They expose a large proportion of the Na^+ counterions on the inner and outer surfaces of the nanotubes. These Na^+ ions are ion-exchangeable [17]. Ion-exchange has been established as an effective method for preparing highly dispersed supported metal catalysts with a narrow metal particle size distribution for use in heterogeneous catalysis [18] Moreover, the semiconducting properties of titanate nanotubes may lead to strong electronic interaction between the support and metal, which could improve catalytic performance in redox reactions. Specifically, titanate nanotubes have been used as catalyst support for platinum catalyzed cyclohexene hydrogenation-dehydrogenation [19], iridium and cobalt catalyzed water splitting for hydrogen production [20], gold catalyzed water-gas shift reaction [21] and CO oxidation [22, 23] and bimetallic gold-palladium catalyzed direct synthesis of hydrogen peroxide [24].

Here the application of Au-Pd/sodium titanate nanotubes (NaTNT) for the selective oxidation of alcohols under solvent and alkali-free conditions is investigated. The influence of reaction conditions and composition of Au and Pd on the oxidation activity and selectivity is reported. In addition, the effect of alkali and alkaline earth metal ions on benzyl alcohol oxidation activity of titanate nanotubes-supported Au catalysts is also investigated. The structure-activity correlations are explored.

4.2. Experimental

Sodium titanate nanotubes (NaTNTs) were prepared by alkali hydrothermal treatment of titania following a reported procedure (Chapter 2, section 2.2.1.2). The alkali and alkaline earth metal ion-exchanged titanate nanotubes were prepared form the pre-formed NaTNTs by simple ion-exchange method using aqueous solutions of alkali/alkaline earth metal nitrate precursors. These alkali and alkaline earth metal ion-exchanged titanate nanotubes are denoted as ATNTs (A= Li^+, Na^+, K^+, Cs^+, Mg^{2+}, Ca^{2+}, Sr^{2+} and Ba^{2+}; Chapter 2, section 2.2.1.3). ATNT-supported Au and Au-Pd catalysts were prepared by a deposition-precipitation (DP) method using 2 mM aqueous $HAuCl_4 \cdot 3H_2O$ and $Pd(OAc)_2$ as precursor solutions for gold and palladium, respectively and by maintaining the pH at 7 - 8. Bimetallic Au-Pd/NaTNT catalysts were prepared with three different compositions (0.5:1, 1:1 and 1:0.5 wt. ratio) of Au and Pd keeping the total metal loading as 2 wt.%. Detailed descriptions of synthesis and characterization procedures are presented in Chapter 2 (section 2.2.2.2. and 2.3). The method of conducting alcohol oxidation reactions is explained in Chapter 2 (section 2.4.1).

4.3. Results and Discussion

4.3.1. Au/NaTNT and Effect of Co-added Metal (Pd)

4.3.1.1 Catalyst Characterization

4.3.1.1.1 Elemental Analysis & XRD

The chemical composition of the catalysts was determined by inductively-coupled plasma-optical emission spectroscopy (ICP-OES). The Na/Ti mole ratio of NaTNTs (0.65) was found nearly the same as the theoretical value (0.67) indicating the composition of NaTNTs as $Na_2Ti_3O_7$. For supported metal catalysts, depending on their composition, 65-80% of input Au and 70-96% of Pd got deposited and remained in their final composition (Table 4.1). X-ray powder diffraction (XRD) showed typical peaks at 10.1, 24.3, 28.4 and 48.5° corresponding to reflections arising from (200), (110), (211) and (020) planes, respectively of NaTNT with $Na_2Ti_3O_7$ composition (JCPDS files: 31-1329 and 41-0192; Fig. 4.1). The peak at 10.1° is a signature for the nanotube morphology [18]. Metal deposition

didn't alter the support structure. No additional peaks due to Au^o/Pd^o (JCPDS files: 04-0784 and 05-068) were detected for Au/NaTNT and Au-Pd/NaTNT indicating that the particle sizes of Au and Pd were, perhaps, below the X-ray detection limit.
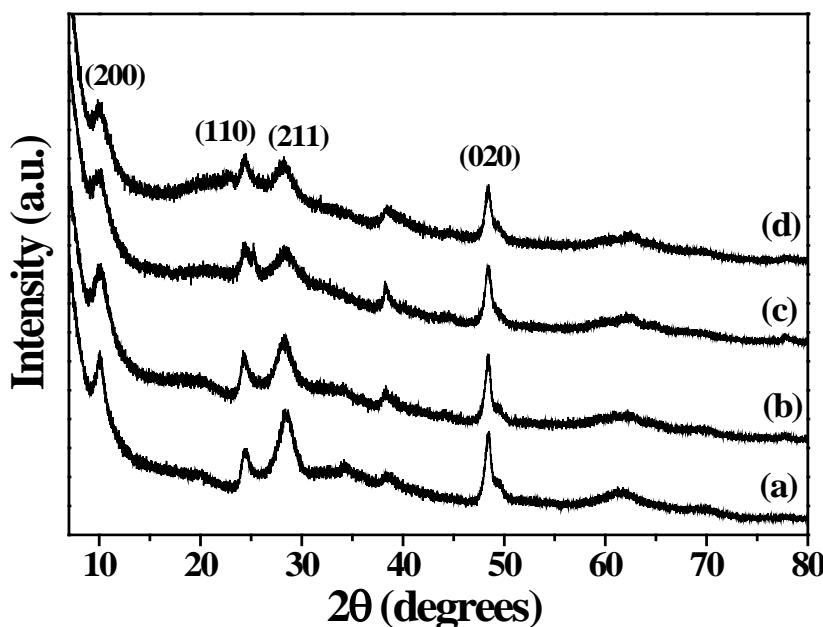
Fig. 4.1. XRD profiles of (a) NaTNT, (b) Au(2 wt.%)/NaTNT, (c) Au-Pd(2 wt.%, 1:1)/NaTNT and (d) spent Au-Pd(2 wt.%, 1:1)/NaTNT.

4.3.1.1.2. TEM

Transmission electron microscopic (TEM) images of supports (TiO_2 and NaTNT) and Au & Au-Pd supported catalysts are shown in Fig. 4.2 (a-e). Tubular morphology of NaTNT was confirmed with outer and inner diameters of the tubes being 9.8 and 4.8 nm, respectively (Fig. 4.2 (b)). The images have also confirmed the complete conversion of TiO_2 into $Na_2Ti_3O_7$ (Fig. 4.2 (a, b)). Metal particle size distribution pattern derived from TEM images indicated that the addition of Pd reduced the average particle size of Au from 2.3 nm (in Au(2 wt.%)/NaTNT) to 1.2 nm (in Au-Pd(2 wt.%, 1:1)/NaTNT) (Fig. 4.2 (c, d)). The average particle size of Au on Au-Pd(2 wt.%, 1:1)/TiO_2 was 1.5 nm (Fig. 4.2 (e)). Metal particles were evenly distributed on the surface of NaTNT in Au-Pd(2 wt.%, 1:1)/NaTNT (Fig. 4.2(d)). More number of lattice fringes corresponding to (111) plane of Au with an inter planar distance of 0.24 nm [25] were detected indicating that it is the most exposed metal plane ((Fig. 4.2(d)) inset). Pd is expected to form a monolayer on the surface of Au at certain concentrations and thereby control the size of Au particles. Also based on electrode

potentials, Pd leads to the reduction of Au which in turn hinders the growth of the nanoparticle.

4.3.1.1.3. N$_2$-physisorption

The nitrogen adsorption-desorption isotherms and BJH pore size distribution curves of as-prepared NaTNTs and NaTNT-supported Au, Pd, & Au-Pd are shown in Fig. 4.3 (a, b). The values of S$_{BET}$, pore volume, and pore diameter of the samples are listed in Table 4.1. These materials were mesoporous showing type IV nitrogen-isotherms with H$_2$-type hysteresis loop (Fig. 4.3). S$_{BET}$ of the catalysts was in the range of 149-200 m^2/g and pore diameter was between 5.9 and 7.0 nm. XRD, N$_2$-physisorption, and TEM suggest that metal deposition has negligible effect on microstructure of NaTNTs.

4.3.1.1.4. DR UV-vis Spectroscopy

Diffuse reflectance UV-vis spectra (Fig. 4.4) were recorded to study the changes in electronic structures of metal particles, in particular the influence of particle size and support on the localized surface plasmon resonance (LSPR) band of Au nanoparticles. Au(2 wt.%)/NaTNT showed a characteristic localized surface plasmon resonance at 540 nm. In the case of Au-Pd(2 wt.%, 1:1)/NaTNT, this band was broadened and shifted to 570 nm because of changes in the band structure of Au in the presence of Pd forming a bimetallic nano-composite and reduction in Au particle size. The variation in LSPR band position is in agreement with the change in gold particle size determined from TEM.
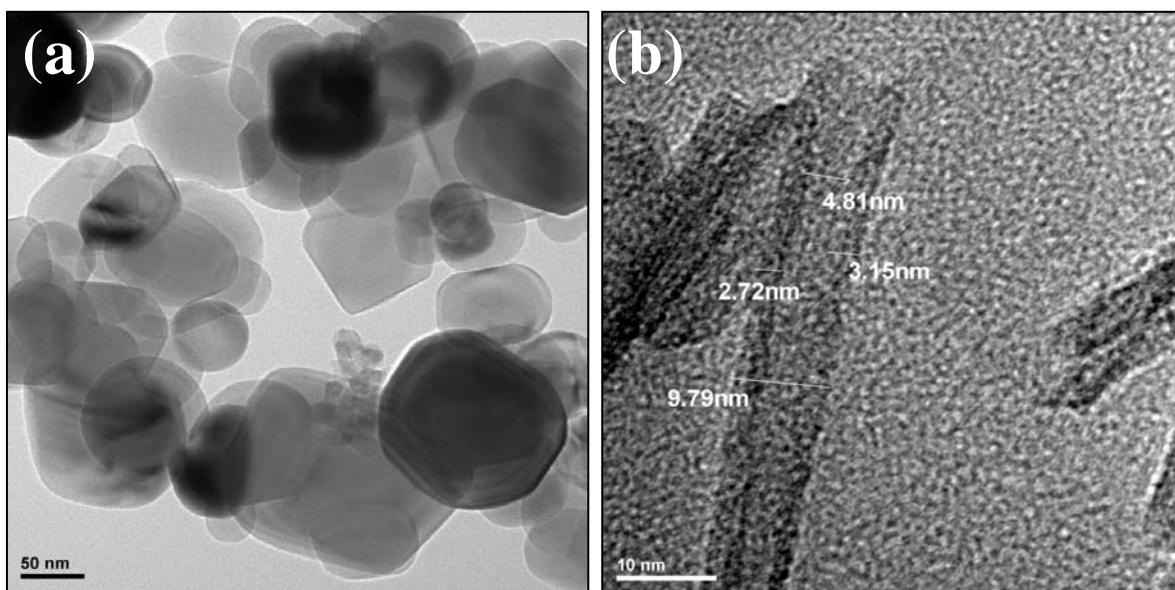
Fig. 4.2. TEM images: (a) anatase TiO$_2$, (b) NaTNT, (c) Au(2 wt.%)/NaTNT, (d) Au-Pd(2 wt.%, 1:1)/NaTNT and (e) Au-Pd(2 wt.%, 1:1)/TiO$_2$ (contd.).
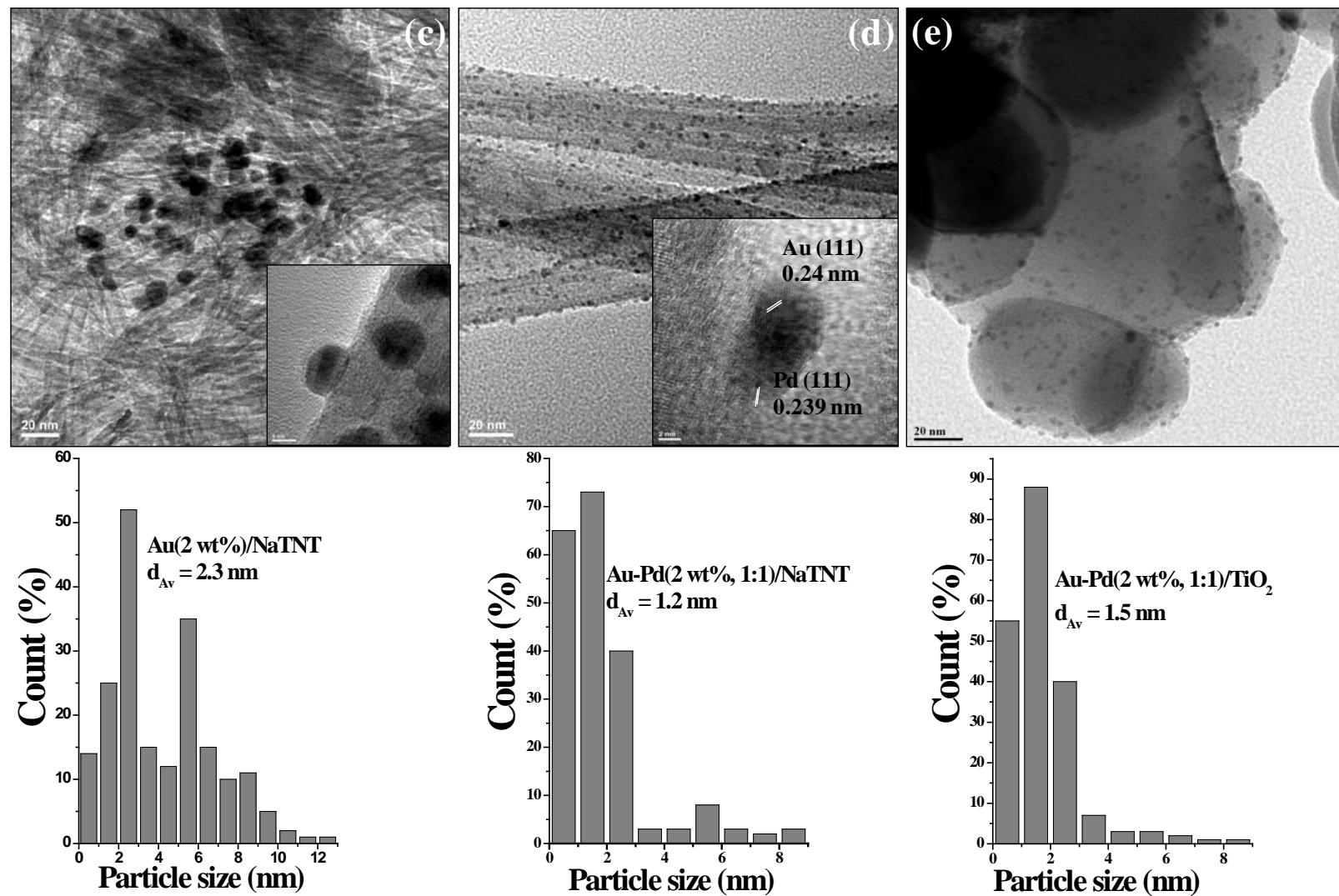
Fig. 4.2. TEM images: (a) anatase TiO_2, (b) NaTNT, (c) Au(2 wt.%)/NaTNT, (d) Au-Pd(2 wt.%, 1:1)/NaTNT and (e) Au-Pd(2 wt.%, 1:1)/TiO_2.
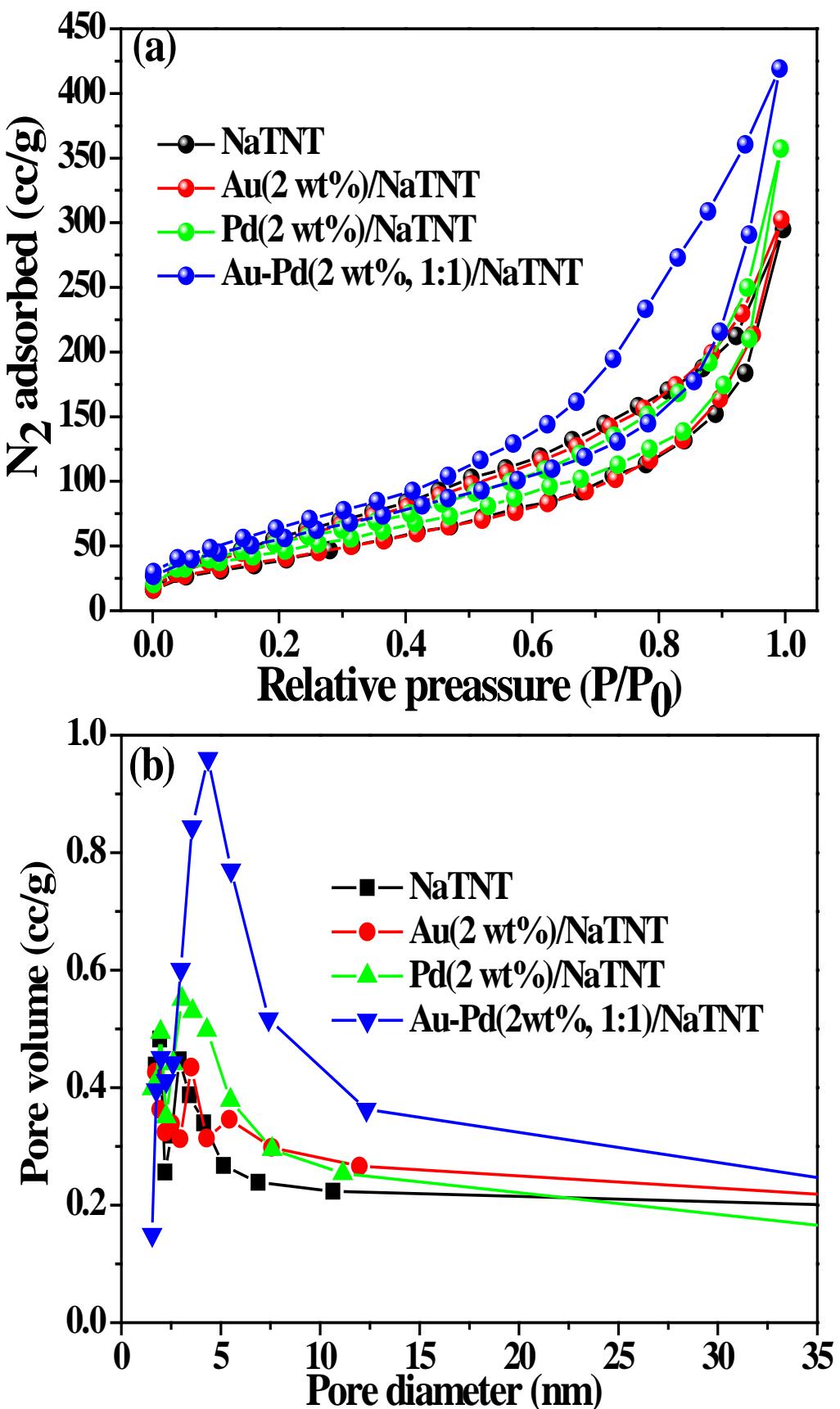
Fig. 4.3. (a) N_2-adsorption-desorption isotherms and (b) pore distribution curves of NaTNT, Au(2 wt.%)/NaTNT, Pd(2 wt.%)/NaTNT and Au-Pd(2 wt.%, 1:1)/NaTNT.

Table 4.1. Composition and textural properties of Au/NaTNT and Au-Pd/NaTNT

Catalyst	Metal content (output, wt.%; ICP-OES)			Au Particle size (nm; TEM)	Textural properties (N_2 physisorption)		
	Au	Pd	Na		S_{BET} (m^2/g)	Pore volume (cc/g)	Pore diameter (nm)
NaTNT	-	-	9.6	-	188	0.65	6.5
Au(1 wt.%)/NaTNT	0.80	-	6.90	2.2	180	0.60	6.0
Au(2 wt.%)/NaTNT	1.54	-	5.31	2.3	149	0.47	6.3
Au-Pd(2 wt.%, 3:1)/NaTNT	1.10	0.48	5.10	1.2	200	0.70	6.4
Au-Pd(2 wt.%, 1:1)/NaTNT	0.65	0.70	5.20	1.2	181	0.64	6.6
Au-Pd(2 wt.%, 1: 3)/NaTNT	0.35	1.20	6.60	-	153	0.55	5.9
Au-Pd(2 wt.%, 1:1)/TiO$_2$	0.67	0.95	-	1.5	23	0.08	7.0
Pd(2 wt.%)/NaTNT	-	1.3	7.03	-	157	0.45	5.68
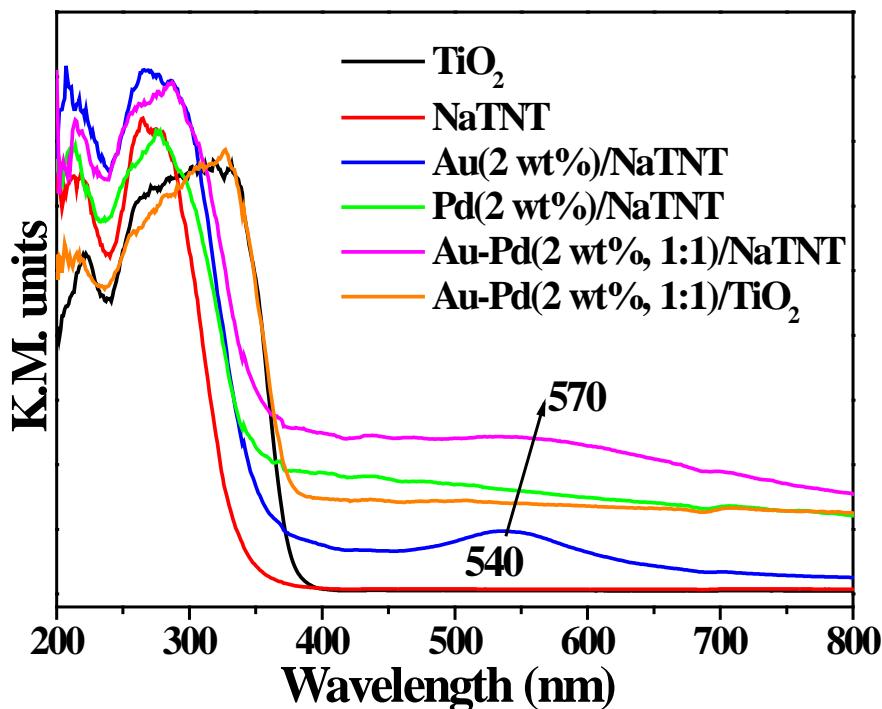
Fig. 4.4. DR UV-vis spectra of TiO_2, NaTNT & Au, Pd and Au-Pd/ NaTNT and TiO_2.

4.3.1.1.5. XPS

The X-ray photoelectron spectra (XPS) shown in Fig. 4.5 display the core level spectra of Au 4f and Pd 3d in Au-Pd(2 wt.%, 1:1)/TiO_2 and Au-Pd(2 wt.%, 1:1)/NaTNT catalysts. Au-Pd(2 wt.%, 1:1)/TiO_2 showed XPS lines at 83.4 and 87.1 eV for Au $4f_{7/2}$ and $4f_{5/2}$, respectively. Metallic gold shows $4f_{7/2}$ line at 84.0 eV [26]. For Au-Pd(2 wt.%, 1:1)/NaTNT, these spectral lines were weak and appeared at still lower BE values (82.8 and 86.5 eV, respectively). While weak intensity is indicative of the location of Au inside the nanotubes of NaTNT, their position at lower BE suggests a higher amount of electron density ($Au^{\delta-}$) as a consequence of electron transfer from NaTNT to Au. Reduction in particle size is an alternative reason for a lower BE value of Au on NaTNT compared to that on TiO_2. The lines for Pd^0 in Au-Pd(2 wt.%, 1:1)/TiO_2 appeared at 335.4 ($3d_{5/2}$) & 340.7 eV ($3d_{3/2}$) and in Au-Pd(2 wt.%, 1:1)/NaTNT at 335.3 & 340.4 eV, respectively.

Table 4.2. Binding energy values (eV)

Catalyst	Au		Pd		Ti		Na
	$4f_{7/2}$	$4f_{5/2}$	$3d_{5/2}$	$3d_{3/2}$	$2p_{3/2}$	$2p_{1/2}$	1s
Au-Pd(2 wt.%, 1:1)/NaTNT	82.8	86.5	335.3	340.4	458.4	464.0	1071
Au-Pd(2 wt.%, 1:1)/TiO_2	83.4	87.1	335.4	340.6	458.6	464.3	-
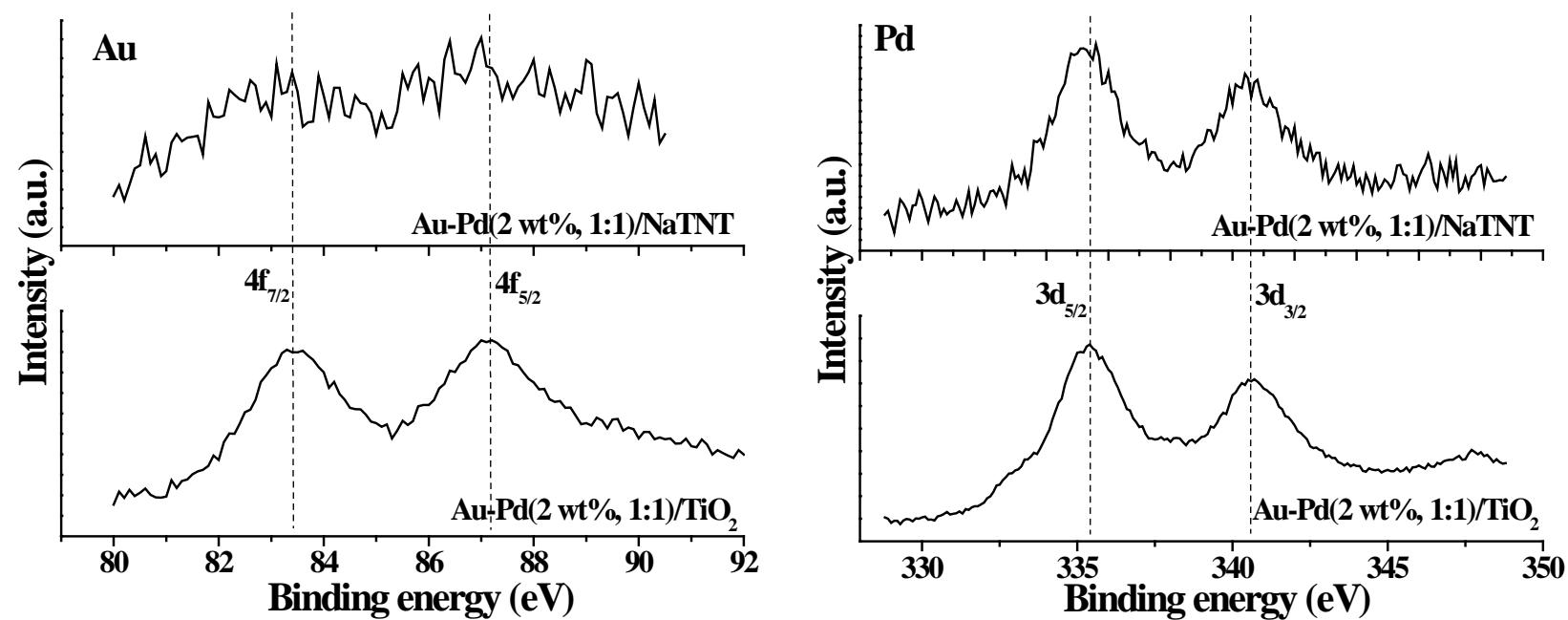
Fig. 4.5. XPS of Au-Pd(2 wt.%, 1:1)/TiO_2 and Au-Pd(2 wt.%, 1:1)/NaTNT.

4.3.1.2. Catalytic Activity

Au/NaTNT and Au-Pd/NaTNT catalyzed the oxidation of benzyl alcohol with aerial oxygen at 120 °C under solvent- and alkali-free conditions (Table 4.3). Benzaldehyde is the major product (selectivity = 70.2-98.5 wt.%) with benzoic acid, benzyl benzoate, benzene and toluene as minor products (Scheme 4.1). While benzaldehyde and benzoic acid formed via oxidation reaction, benzene formed by decarbonylation and toluene by the disproportionation of benzyl alcohol [27]. Benzyl benzoate is produced by the esterification of benzoic acid with benzyl alcohol [28]. At chosen experimental conditions (air = 1 atm, reaction temperature = 120 °C, reaction time=10 h), benzyl alcohol conversion was very little (1.5 wt.%) in the absence of a metal catalyst. The supported gold [Au(1 wt.%)/NaTNT] catalyzed this reaction yielding benzyl alcohol conversion of 15.2 wt.% and benzaldehyde selectivity of 98.5 wt.%. This value is comparable to the reports by others using erstwhile supports [7, 29]. With increasing Au content from 1 to 2 wt.%, the conversion of benzyl alcohol doubled (from 15.2 to 30.0 wt.%) but the selectivity for benzaldehyde decreased (from 98.5 to 94.3 wt.%); the selectivity for benzyl benzoate and benzene + toluene increased from 1.5 to 4 wt.% and 0 to 1.7 wt.%, respectively (Table 4.3; run nos. 1 and 2). Upon promotion with Pd, the conversion of benzyl alcohol raised from 15.2 to 63.0 wt.% and TOF increased from 187 to 318 h^{-1}; benzaldehyde selectivity decreased from 98.5 to 82.7% as more and more benzaldehyde converted to benzoic acid and benzyl benzoate (compare run nos. 1 and 4). The presence of Pd enhanced the selectivity of undesired products, although their overall content was low: benzene (from 0 to 6.4 wt.%) and toluene (from 0 to 1.1 wt.%). The activity of Au-Pd/NaTNT (TOF = 318 h^{-1} based on total metal content and 516 h^{-1} based on surface metal atoms) was superior to Au-Pd/TiO$_2$ (TOF = 240 h^{-1} based on total metal content and 470 h^{-1} based on surface metal atoms).

Selectivity for benzaldehyde was lower and toluene formation was higher on the latter (compare run nos. 4 and 6). The composition of Au-Pd affected benzyl alcohol conversion and benzaldehyde selectivity. A composition with 1:1 wt./wt. of Au and Pd was found to be highly active and selective. Such enhancement in catalytic activity is already known for Au-Pd on other supports [7, 29]. Higher activity of the present catalyst is due to the uniform dispersion and smaller size of metal particles (1.2 instead of 2.3 nm; TEM) as well as synergistic electronic effects between the metal and support. Au atoms draw electron density away from Pd and NaTNT. Enache et al. [6] and Chen et al. [30] have also made such observation in related systems. The smaller the particle size, the higher would be the

Table 4.3. Catalytic activity data for aerial oxidation of benzyl alcohol over NaTNT- and TiO_2-supported Au and Au-Pd catalysts[a]

Run No.	Catalyst	Conversion (wt.%)	TOF (h^{-1})	Product selectivity (wt.%)				
				Benzaldehyde	Benzoic acid	Benzyl benzoate	Benzene	Toluene
1	Au(1 wt.%)/NaTNT	15.2	187 (264)	98.5	0	1.5	0	0
2	Au(2 wt.%)/NaTNT	30.0	192 (283)	94.3	0	4.0	1.2	0.5
3	Au-Pd(2 wt.%, 3:1)/NaTNT	50.5	250 (419)	81.6	0.8	11.1	5.9	0.6
4	Au-Pd(2 wt.%, 1:1)/NaTNT	63.0	318 (516)	82.7	0.6	9.2	6.4	1.1
5	Au-Pd(2 wt.%, 1: 3)/NaTNT	53.9	206	70.2	1.0	20.1	7.2	1.5
6	Au-Pd(2 wt.%, 1:1)/TiO_2	57.0	240 (470)	75.6	5.7	2.6	1.1	15
7	Pd(2 wt.%)/NaTNT	50.2	205	78.8	2.2	10.7	5.3	3.0

[a]Reaction conditions: Catalyst = 50 mg, benzyl alcohol = 25 mmol, p(air) = 1 atm, reaction temperature = 120 °C, reaction time =10 h, Turnover frequency (TOF) = moles of benzyl alcohol converted per mole of total metal in the catalyst (ICP-OES) per hour. TOF values in parentheses are those calculated based on mole of benzyl alcohol converted per mole of surface metal atoms (estimated from TEM) per hour.

availability of surface active sites and interactions with the support which then can lead to a higher activity of the catalysts.
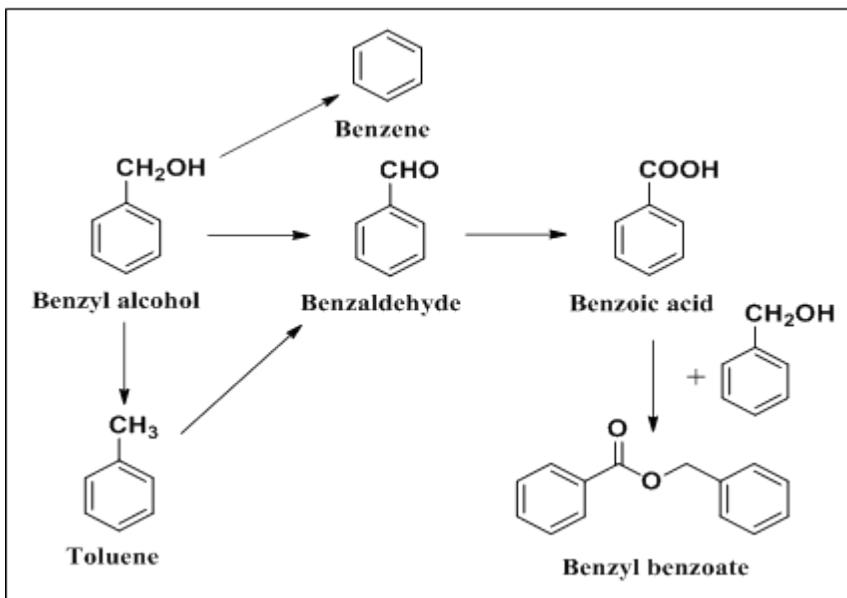
Scheme 4.1. Reaction products obtained in oxidation of benzyl alcohol.

4.3.1.2.1. *Effect of Reaction Conditions*

Benzyl alcohol conversion over Au-Pd(2 wt.%, 1:1)/TiO$_2$ and Au-Pd(2 wt.%, 1:1)/NaTNT increased with increasing reaction time (Fig. 4.6). However, benzaldehyde selectivity decreased at higher conversion levels due to the consecutive reaction of ester formation. At similar conversion levels, Au-Pd(2 wt.%, 1:1)/NaTNT showed higher selectivity for benzaldehyde than Au(2 wt.%)/NaTNT and Au-Pd(2 wt.%, 1:1)/TiO$_2$ (Fig. 4.7). TOF at the end of 1 h over TiO$_2$- and NaTNT-supported Au-Pd(2 wt.%, 1:1) was 964 and 1635 h^{-1} (based on total metal content), respectively. Metal particles on TiO$_2$ have an average diameter of 1.5 nm while those on NaTNT are of 1.2 nm (Fig. 4.2 (e)). The difference in metal particle sizes is the possible cause for difference in the catalytic activity of these two systems. This reaction occurred even at a temperature as low as 80 °C over Au-Pd(2 wt.%, 1:1) catalyst and benzyl alcohol conversion of 50% and benzaldehyde selectivity of 93% were obtained (Fig. 4.8).With a view to optimize the temperature, reactions were conducted at 80, 100 and 120 °C. Benzyl alcohol conversion increased with increasing reaction temperature, but a loss in selectivity for benzaldehyde was observed at higher temperatures (Fig. 4.8). Zhang and co-workers [31, 32] reported the application of silica-supported Au-Cu and Au-Ag alloy nanoparticles for the selective oxidation of alcohols at 80 °C. Benzyl alcohol conversion of 96% and benzaldehyde selectivity of > 99% were obtained.
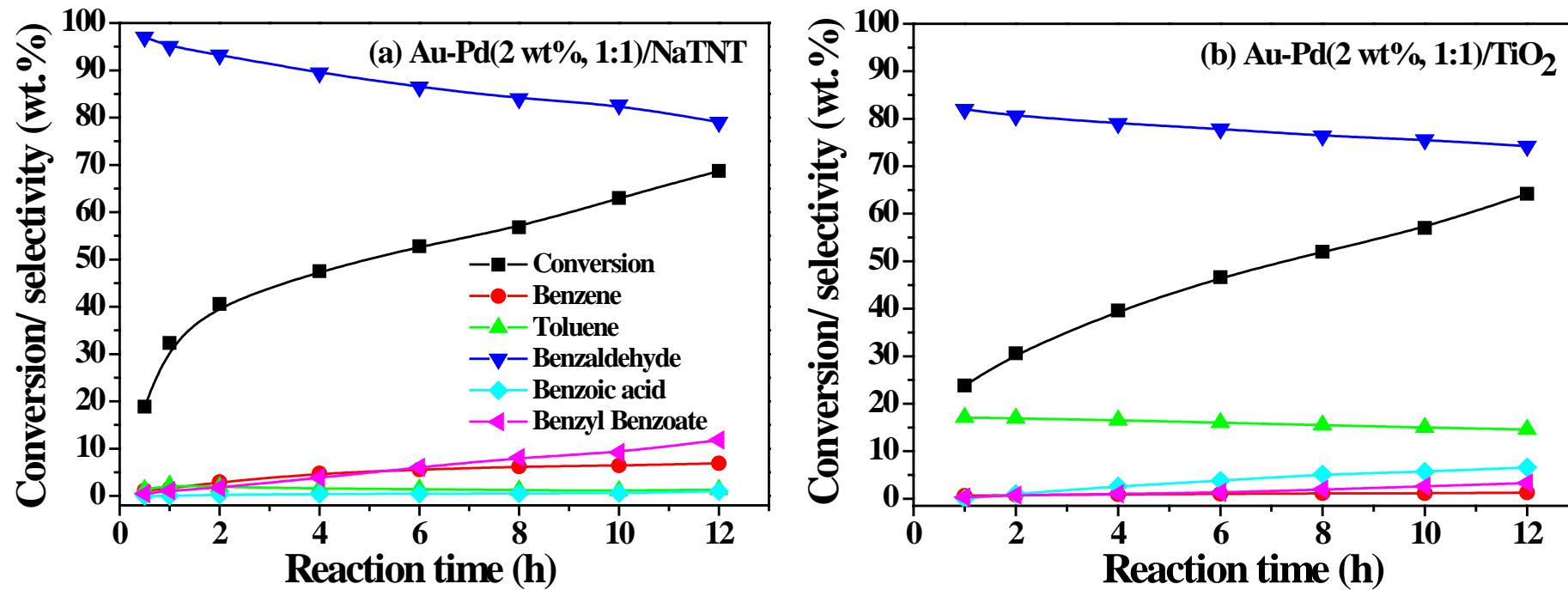
Fig. 4.6. Catalytic activity as a function of reaction time over (a) Au-Pd(2 wt.%, 1:1)/NaTNT and (b) Au-Pd(2 wt.%, 1:1)/TiO2.

Reaction conditions: Catalyst = 50 mg, benzyl alcohol = 25 mmol, p(air) = 1 atm, reaction temperature = 120 °C.
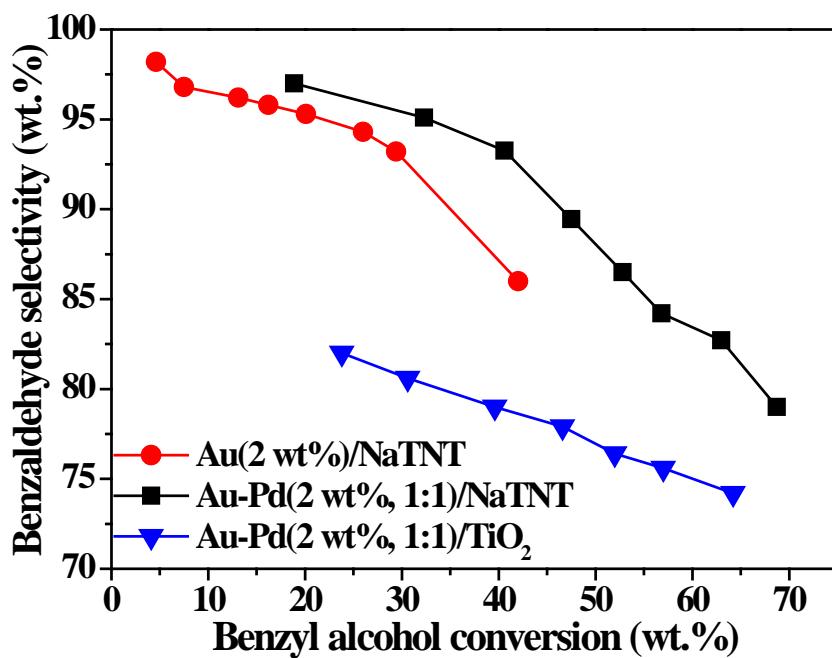
Fig. 4.7. Conversion Vs Selectivity plot.
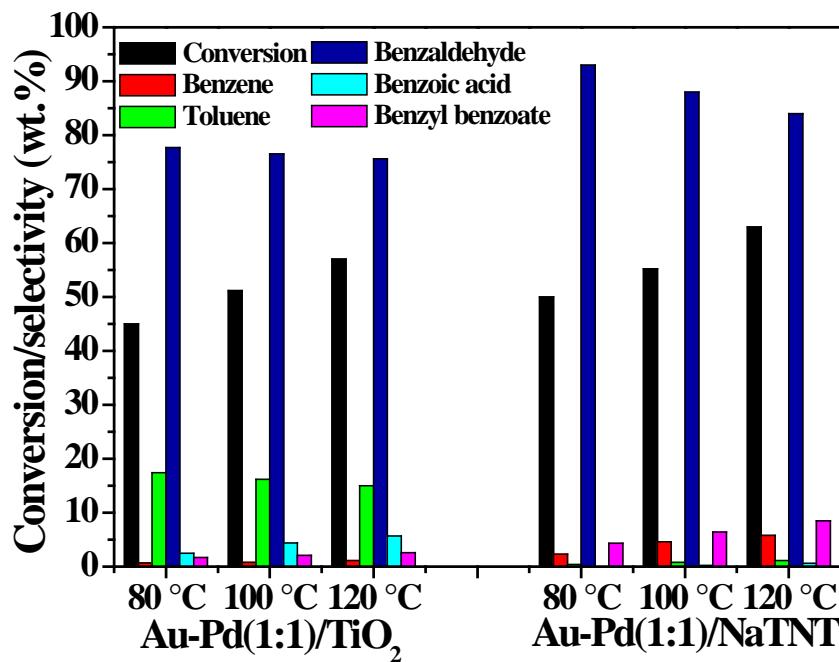
Fig. 4.8. Effect of temperature on performances of Au-Pd(2 wt.%, 1:1)/TiO$_2$ and Au-Pd(2 wt.%, 1:1)/NaTNT in benzyl alcohol oxidation. Reaction conditions: Catalyst = 50 mg, benzyl alcohol = 25 mmol, p(air) = 1 atm, reaction time =10 h.

But 50 times higher amount of the catalyst compared to that used in the present study was employed to achieve the reported conversion. Moreover, the catalyst needed reduction in between the recycles to maintain the conversion, which is not the case with the catalysts of the present study. The activity of Pd(2 wt.%)/NaTNT was higher (50.2 wt.%, TOF = 205 h^{-1}) than that of Au(2 wt.%)/NaTNT (30.0 wt.%; TOF = 192 h^{-1} based on total metal content). However, the selectivity for aldehyde on the former was lower (78.8 wt.%) than on the latter (94.3 wt.%). Bimetallic Au-Pd/NaTNT showed an enhanced activity (63.0 wt.%; TOF = 318 h^{-1}) than either of the monometallic catalysts. It was proposed [25, 33] that in the case of Pd the rate determining step is the transfer of H-atom from the β-carbon of the adsorbed alkoxide forming the aldehyde and a Pd-hydride species. For Au, it is the H-abstraction by an Au-superoxide species. Since Au draws electron density from Pd, it can activate molecular oxygen more easily than without Pd, forming a superoxide like active oxygen species which in turn initiates the reaction. At the same time, the electron depleted Pd (in the presence of Au) easily eliminates hydride species from the β-carbon of alkoxide. Thus, the co-presence of Pd with Au facilitates the oxidation rate. The scope of Au-Pd(2 wt.%, 1:1)/NaTNT for a range of structurally different alcohols was investigated (Table 4.4). The structure and substituent have a marked effect on alcohol conversion.

Table 4.4. Aerobic oxidation of alcohols over Au-Pd(2 wt.%, 1:1)/NaTNT catalyst[a]

Run No.	Alcohol	Alcohol conversion (wt.%)	Aldehyde/ Ketone selectivity (wt.%)
1	3- Methoxybenzyl alcohol	53.7	84.3
2	4- Methoxybenzyl alcohol	41.5	85.0
3	4- Methy benzyl alcohol	40.0	86.0
4	4- Chlorobenzyl alcohol	10.0	82.0
5	4-Nitrobenzyl alcohol	10.0	89.0
6	1-Phenylethanol	84.0	86.0
7	2-Phenylethanol	10.0	100
8	Cinnamyl alcohol	60.5	75.5
9	Crotyl alcohol	75.6	70.0
10	Furfuryl alcohol	18.8	65.0
11	Cyclohexanol	11.5	100

[a]Reaction conditions: Catalyst = 50 mg, alcohol = 25 mmol, p(air) = 1 atm, reaction temperature = 120 °C and reaction time =10 h.

4.3.1.2.2. Catalyst Recyclability

Catalyst recyclability test was conducted to check the stability of the catalyst in oxidation reactions. Upon reuse, Au-Pd(2 wt.%, 1:1)/NaTNT showed a marginal loss (by 5 wt.%) in benzyl alcohol conversion but no further loss in the activity was detected in subsequent recycles (Fig. 4.9). The structure of the catalyst was intact even after the 5th recycle (XRD, Fig. 4.1). ICP-OES analysis revealed a marginal loss in the metal content (500 ppm for Au and 200 ppm for Pd).
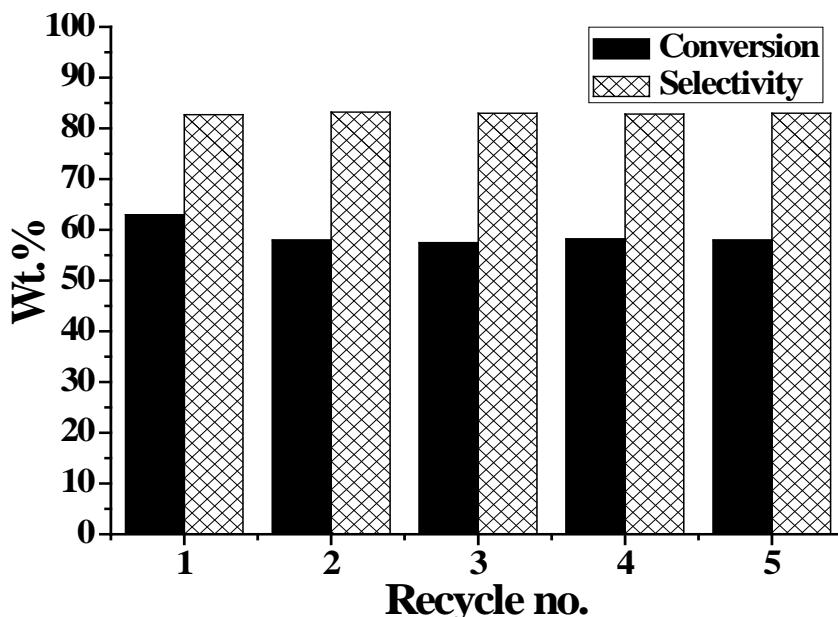
Fig. 4.9. Recycle study of Au-Pd(2 wt.%, 1:1)/NaTNT. Reaction conditions: Catalyst = 50 mg, benzyl alcohol = 25 mmol, p(air) = 1 atm, temperature = 120 °C, reaction time =10 h.

4.3.2. Au/ATNT: Effect of Alkali and Alkaline Earth Metal Ion Exchange
4.3.2.1. Catalyst Characterization
4.3.2.1.1 XRD

The XRD pattern of NaTNT (Fig. 4.10) showed peaks at 2θ = 10.1, 24.3, 28.4 and 48.5° corresponding to reflections from (200), (110), (211) and (020) planes, respectively (JCPDS files: 31-1329 and 41-0192). The ion-exchanged and Au loaded samples depicted similar XRD patterns indicating that they all have the same X-ray crystal structure as of NaTNT. The diffraction peak for (200) plane had, however, marginally shifted to a lower 2θ values (by 0.3°) when the cation in ATNT changed from Li^+ to Ba^{2+}. This shift in XRD peak position is due to increase in interplanar spacing with increasing size of the counter ion. But the positions of other peaks remained nearly the same. No additional peaks due to Au were

detected in 1 wt.% Au deposited samples (except for Au/CaTNT) indicating that the size of Au particles in all those catalysts was below the detection limit of X-rays.
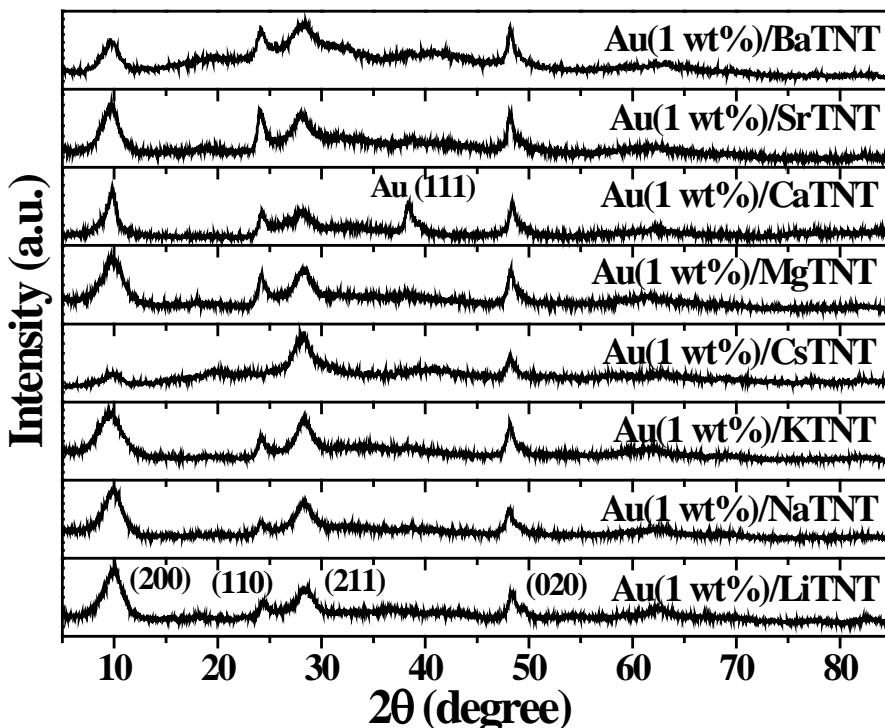
Fig. 4.10. XRD patterns of Au/ATNT catalysts.

4.3.2.1.2. TEM

The TEM images and Au particle size distribution curves of Au(1 wt.%)/ATNT catalysts are shown in Fig. 4.11. These images confirmed the presence of hollow tubular multi-walled morphology of the support titanate nanotube and the Au nanoparticles on the interior and outer surfaces of nanotubes. Moreover, the metal dispersions (D) were determined using eqs. (1) and (2)

$$D = \frac{6V_m}{a_m d_{av}} \tag{1}$$

$$d_{Av} = \frac{6 \sum n_i V_i}{\sum n_i A_i} \tag{2}$$

where V_m = volume occupied by Au atom (1.69 x 10^{-23} cc), a_m = area occupied by Au atom (0.869 x 10^{-15} sq.cm), d_{av} = mean particle size of Au (TEM), V_i = volume of ith particle (TEM) and A_i = area of ith particle (TEM). Mean particle size and percentage dispersion of Au estimated from TEM images are listed in Table 4.5. The characteristic peaks due to Au on Au(1 wt.%)/CaTNT were observed in XRD. The average crystallite size of Au determined using the Scherrer formula was 10 nm, which was comparable with the particle size of Au
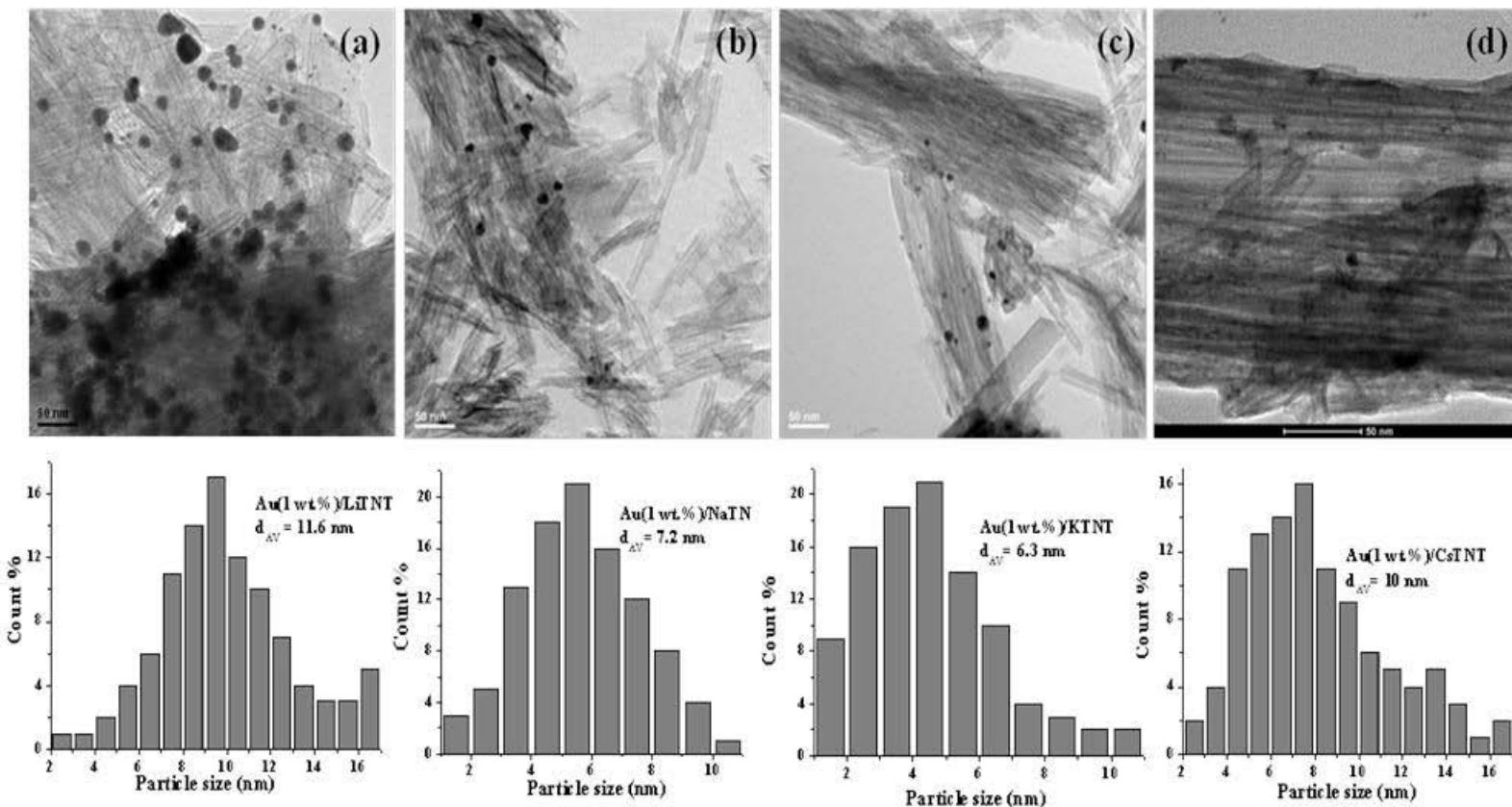
Fig. 4.11. TEM images and particle size distribution histograms of (a) Au(1 wt.%)/LiTNT, (b) Au(1 wt.%)/NaTNT, (c) Au(1 wt.%)/KTNT, (d) Au(1 wt.%)/CsTNT, (e) Au(1 wt.%)/MgTNT, (f) Au(1 wt.%)/CaTNT, (g) Au(1 wt.%)/SrTNT and (h) Au(1 wt.%)/BaTNT catalysts (contd.).
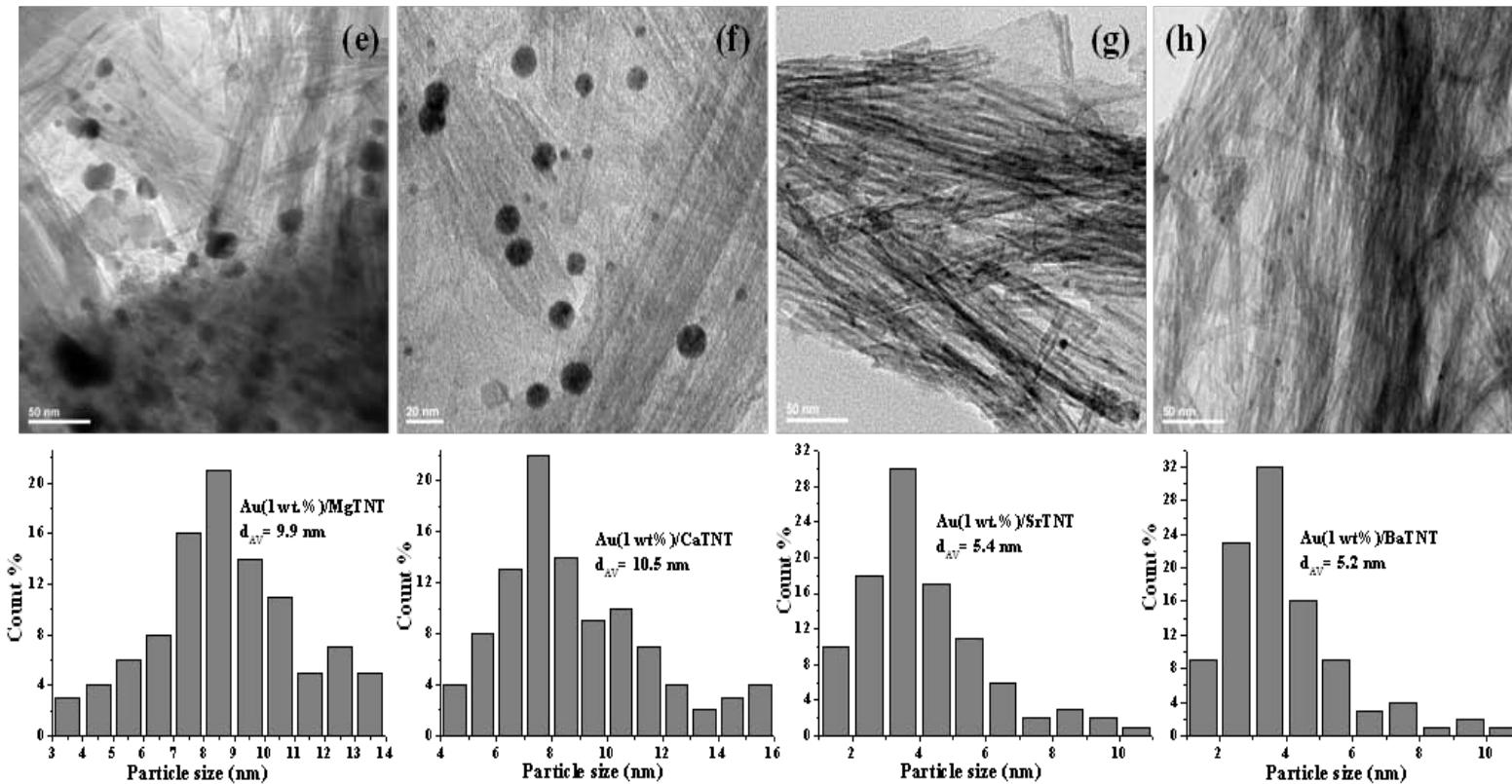
Fig. 4.11. TEM images and particle size distribution histograms of (a) Au(1 wt.%)/LiTNT, (b) Au(1 wt.%)/NaTNT, (c) Au(1 wt.%)/KTNT, (d) Au(1 wt.%)/CsTNT, (e) Au(1 wt.%)/MgTNT, (f) Au(1 wt.%)/CaTNT, (g) Au(1 wt.%)/SrTNT and (h) Au(1 wt.%)/BaTNT catalysts.

Table 4.5. Chemical composition and textural properties of supported Au catalysts

S. No.	Catalyst	Chemical composition (wt%)[a]			Au particle size (nm)[b]	Au dispersion (%)[b]	Textural properties[c]		
		Au	Alkaline ion	Na$^+$			S_{BET} (m^2/g)	Pore volume (cm^3/g)	Pore diameter (nm)
1	Au(1 wt.%)/LiTNT	0.62	2.21	0.92	11.6	10	178	0.56	5.1
2	Au(1 wt.%)/NaTNT	0.65	-	7.2	7.2	16	182	0.50	5.6
3	Au(1 wt.%)/KTNT	0.55	9.90	0.61	6.3	18	153	0.45	5.5
6	Au(1 wt.%)/CsTNT	0.52	16.42	2.6	10	11	126	0.32	4.1
7	Au(1 wt.%)/MgTNT	0.90	2.50	0.62	9.9	12	165	0.41	5.6
8	Au(1 wt.%)/CaTNT	0.91	4.22	0.61	10.5 (10.0^d)	11	175	0.50	5.4
9	Au(1 wt.%)/SrTNT	0.72	9.21	0.30	5.4	19	173	0.44	5.5
12	Au(1 wt.%)/BaTNT	0.68	13.81	0.42	5.2	20	155	0.37	5.4
13	Au(3 wt.%)/BaTNT	2.80	12.0	0.36	- (5.5^d)	-	146	0.36	5.3
14	Au(5 wt.%)/BaTNT	4.10	9.26	0.28	- (6.4^d)	-	140	0.35	5.1
15	Au-Pd(1:1, 2 wt.%)/BaTNT	0.70 (0.82)^e	11.82	0.30	4.2	25	149	0.37	5.2

[a]ICP-OES. Alkaline ion means A$^+$ ion in ATNT. [b]TEM. [c]N$_2$-physisorption. [d]Crystallite size from XRD. [e]Value in parentheses is the Pd content.

determined from the TEM analysis (Table 4.5). The value of d_{Av} for different Au(1 wt.%)/ATNT is in the range 5.2-11.6 nm and Au dispersion is between 10 and 20%.

4.3.2.1.3. ICP-OES

Chemical composition (Au, alkali/alkaline earth metal ion and Na^+ contents) of Au/ATNT catalysts was determined by ICP-OES (Table 4.5). The Na/Ti mole ratio of "bare" NaTNT was 0.65, which is nearly equal to the theoretical value of 0.67 confirming the molecular formula of NaTNT as $Na_2Ti_3O_7$. Ion-exchange with other alkali/alkaline earth metal ions occurs along the length of the nanotube. Na^+ ions in interlayer region were difficult to exchange and hence, reminiscence of non-exchangeable Na^+ may be noted in the compositions of Au/ATNT (Table 4.5).

4.3.2.1.4. N$_2$-physisorption

Representative N_2 adsorption-desorption isotherms along with pore size distributions curves of Au(1 wt.%)/ATNT catalysts are shown in Fig. 4.12. These materials showed N_2 physisorption isotherms typical of type IV with H_2-hysteresis loop. The isotherms represent mesoporosity with open-ended pore structure. The samples showed broad pore size distribution curves. Size of the alkali/alkaline earth metal ion had an influence on the textural properties. S_{BET} of Au/ATNT was in the range 122-182 m^2/g and average pore diameter was between 4.1 and 5.6 nm (Table 4.5). Bare supports had S_{BET} between 132 and 196 m^2/g and average pore diameter between 4.5 and 6.6 nm (Table 4.6).

Table 4.6. N_2 physisorption data for ATNT supports

| S.No.	Sample	Textural properties		
		S_{BET} (m^2/g)	Pore volume (cm^3/g)	Pore diameter (nm)
1	LiTNT	196	0.54	5.2
2	NaTNT	188	0.65	6.5
3	KTNT	194	0.47	4.5
4	CsTNT	132	0.36	4.8
5	MgTNT	179	0.41	6.6
6	CaTNT	185	0.55	6.2
7	SrTNT	182	0.48	5.8
8	BaTNT	175	0.40	6.0
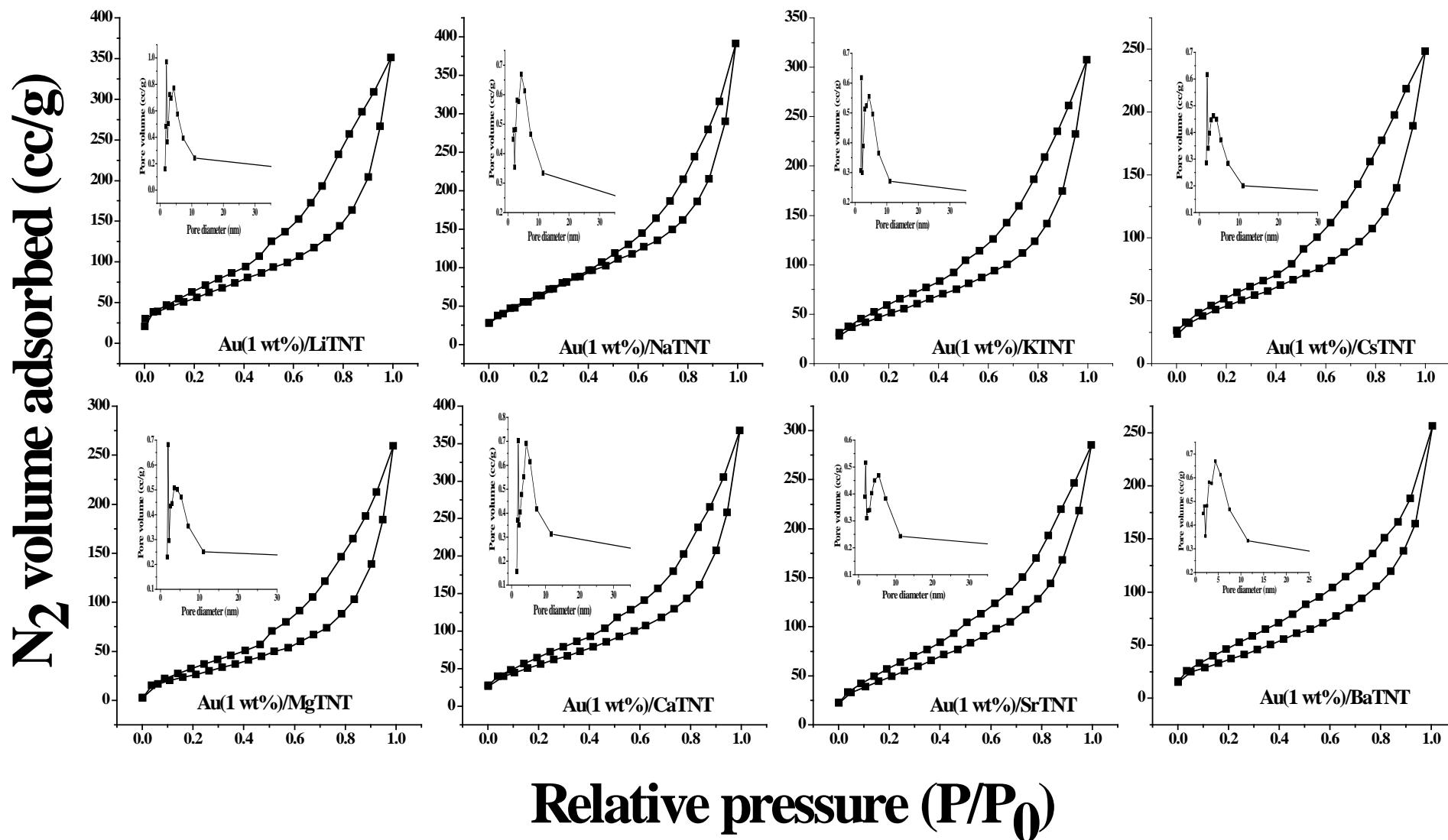
Fig. 4.12. N_2-physisorption isotherms and pore size distribution curves of Au(1 wt.%)/ATNTs.

A marginal decrease in specific surface area and average pore diameter was noted upon loading Au. A decrease in total pore volume of Au/ATNT compared to the supports was also observed.

4.3.2.1.5. CO_2-TPD

Carbon dioxide was used as a probe molecule to determine the basicity of Au/ATNT catalysts. The TPD profiles (Fig. 4.13) contained two desorption peaks, in the temperature regions 100-300 °C and 300-500 °C corresponding to weak and strong basic sites, respectively. Desorption temperature and the amount of CO_2 desorbed refer to the strength and density of basic sites. Basicity of the catalysts is reported in Table 4.7. In general, the alkaline earth metal ion exchanged titanates have higher basicity than the alkali metal ion exchanged catalysts. It appears that the amount of ions exchanged also determined the basicity value. Au(1 wt.%)/NaTNT showed an additional weak overlapping peak at 250-300 °C which is rather missing in other ATNT samples.

Basicity of the catalysts influenced the uptake and particle size of Au (Fig. 4.14). Among alkali ion exchanged Au/ATNT catalysts the uptake of Au (Au content in the catalyst) decreased with increasing basicity of the catalyst. Similar observation was found also for alkaline earth metal ion exchanged Au/ATNT catalysts. In general, the percentage Au uptake (with respect to the input value) is higher for alkaline earth metal ion than alkali ion exchanged ATNT. Also a decrease in the mean size (d_{Av}) of Au with increasing basicity of the catalyst was observed (Fig. 4.14) with the values of Au supported on Cs^+, Mg^{2+} and Ca^{2+}-exchanged NaTNT deviating from this relationship.
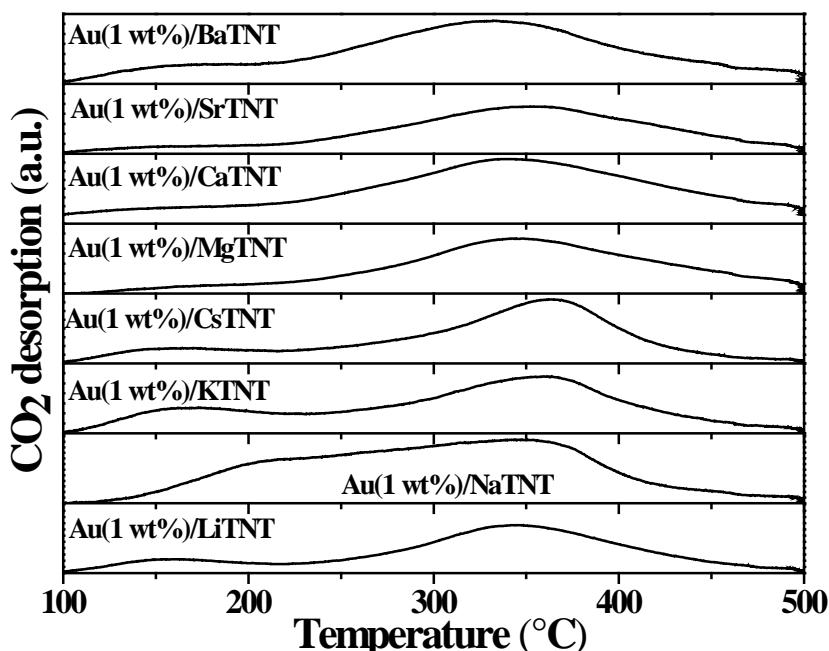

Fig. 4.13. CO_2-TPD profiles of Au (1 wt.%)/ATNT catalysts.

Table 4.7. Basicity of Au(1 wt.%)/ATNT catalysts.

S. No.	Catalyst	Basicity ($\mu mol/m^2$)		
		Weak[a]	Strong[b]	Total
1	Au(1 wt.%)/LiTNT	0.46	0.80	1.26
2	Au(1 wt.%)/NaTNT	0.43	0.87	1.29
3	Au(1 wt.%)/KTNT	0.43	1.05	1.70
4	Au(1 wt.%)/CsTNT	0.45	1.72	2.17
5	Au(1wt.%)/MgTNT	0.21	2.12	2.19
6	Au(1 wt.%)/CaTNT	0.28	2.84	3.12
7	Au(1 wt.%)/SrTNT	0.25	2.82	2.75
8	Au(1 wt.%)/BaTNT	0.21	2.79	3.00
9	Au-Pd (1:1, 2 wt.%)/BaTNT	0.66	1.79	2.45

[a]Weak (100-300 °C). [b]Strong (300-500 °C).

Reason for this abnormal behaviour is not clear at this point of time. However, it appears that strength of basicity and relative concentration strong acid sites may influence the metal particle size

4.3.2.1.6. DR UV- vis Spectroscopy

DR UV-vis spectroscopy provided evidence for the presence of Au nanoparticles by showing a typical localized surface plasmon resonance (LSPR) band at 480-580 nm (Fig. 4.15 (a)). The peak position of LSPR band (λ_{max}) is related to the Au mean particle size. It is also related to the shape of Au particle and dielectric function of the support material. As seen from Fig. 4.15 (b), λ_{max} of LSPR band increased with increasing particle size of Au. As seen above, the particle of Au has an inverse relation with the basicity of the catalyst. In other words, the spectral/electronic properties of Au are greatly influenced by the nature of the support and Au particle size. Similar observations were made also by other researchers [34].

4.3.2.1.7. XPS

X-ray photoelectron spectra of the Au(1 wt.%) supported on KTNT, SrTNT and BaTNT (Fig. 4.16) showed $4f_{7/2}$ line at 83.2, 83.0 and 82.8 eV, respectively. Metallic gold in gold foil shows this line at 84.0 eV [35]. This suggests that Au on ATNT is rich in electron density. The formation of such electron rich Au species was attributed to form through transfer of the electron density from the support [35, 36]. Arrii et al. [37] have reported the dependence of Au $4f_{7/2}$ binding energy on the nature of support.
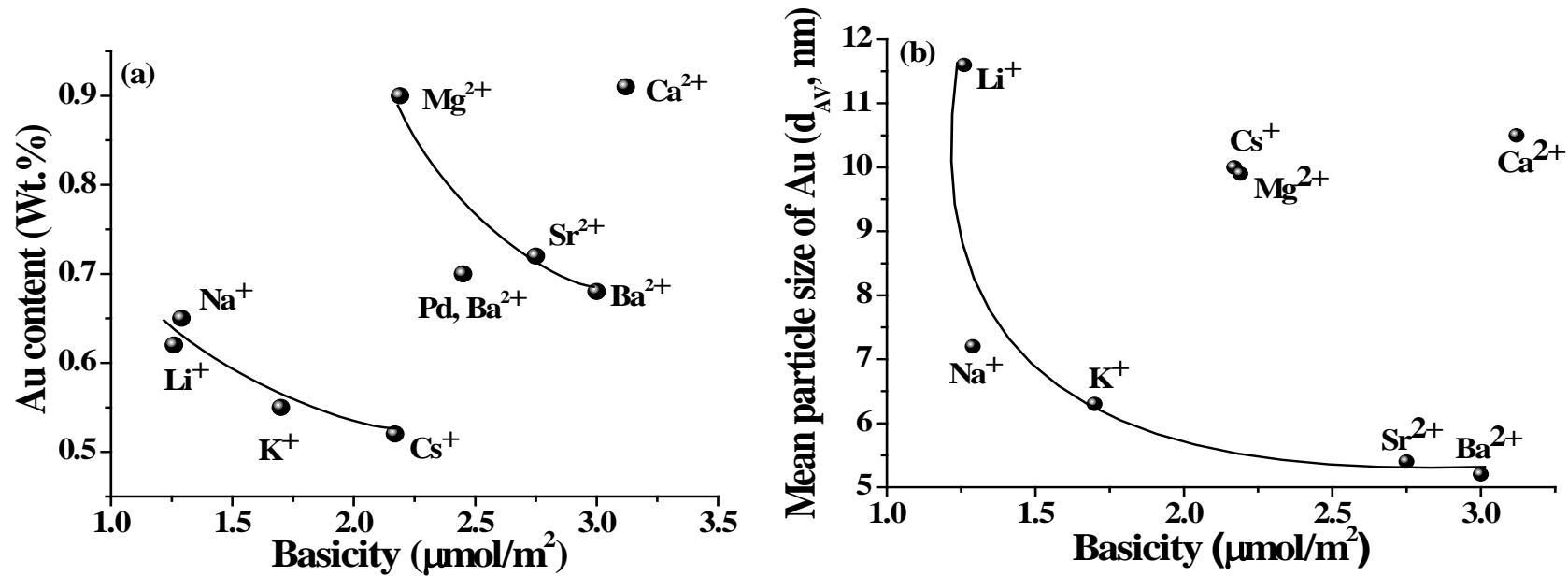
Fig. 4.14. Influence of basicity of the catalyst on (a) Au uptake and (b) mean particle size of Au.
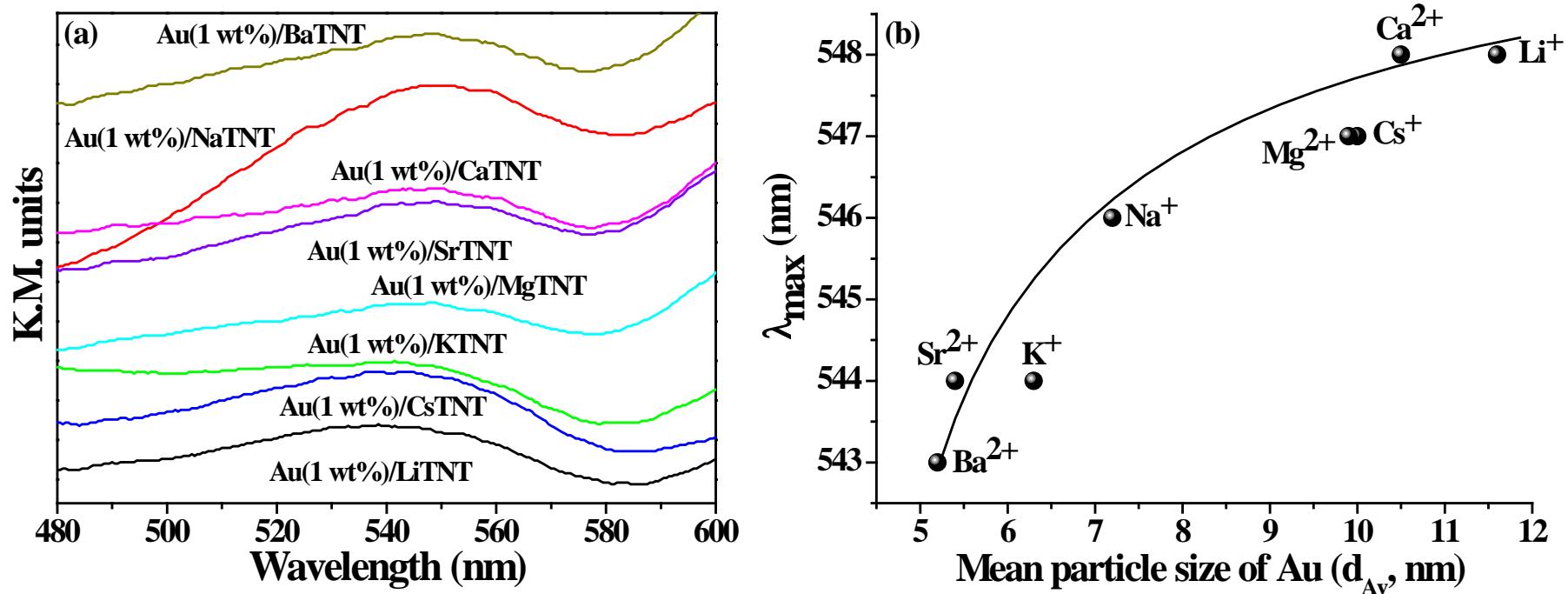
Fig. 4.15. (a) DR UV-vis spectra for Au(1 wt.%)/ATNT catalysts and (b) Variation of LSPR band position (λ_{max}) with the mean particle size (d_{Av}) of supported Au.
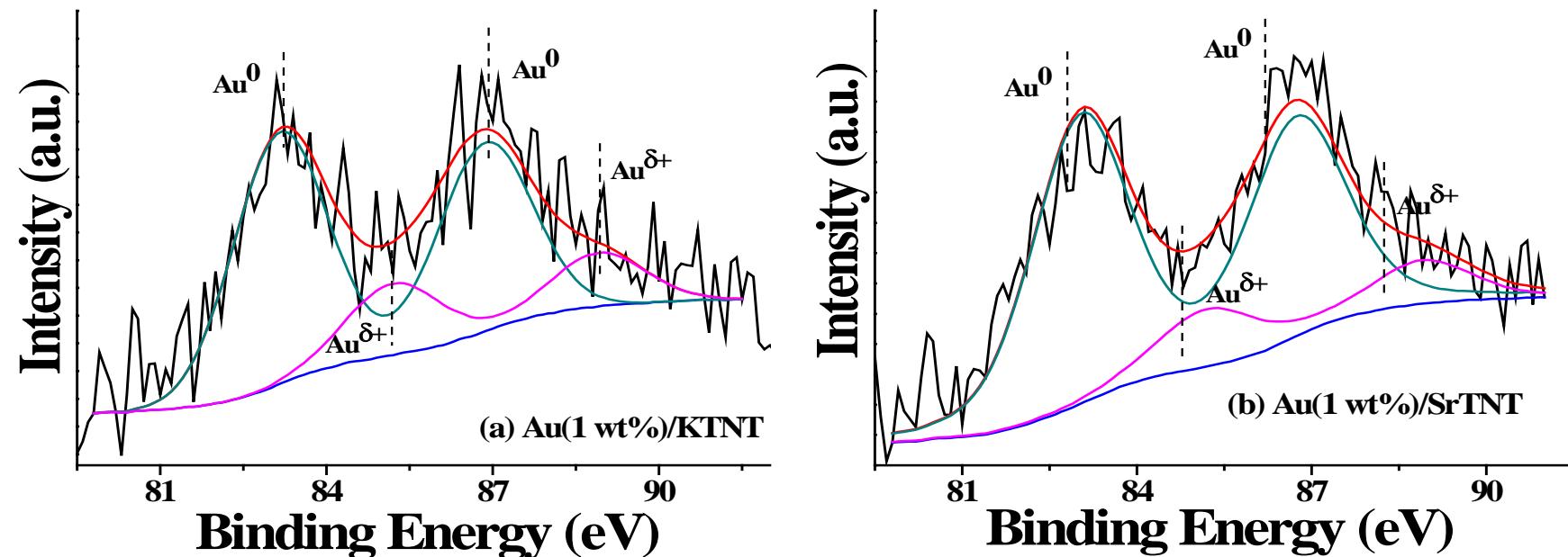
Fig. 4.16. XPS of Au 4f in (a) Au(1 wt.%)/KTNT, (b) Au(1 wt.%)/SrTNT and Au(1 wt.%)/BaTNT (contd.).
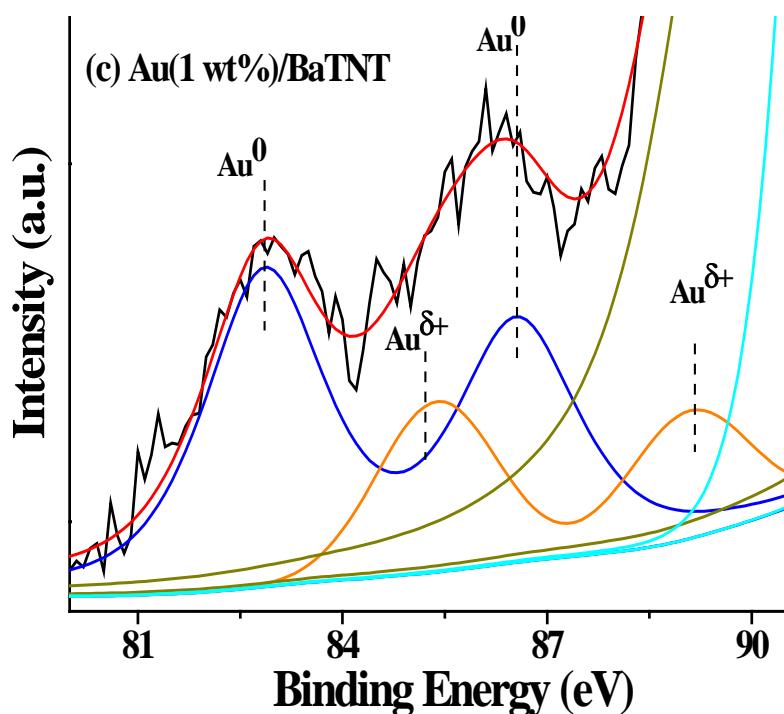
Fig. 4.16. XPS of Au 4f in (a) Au(1 wt.%)/KTNT, (b) Au(1 wt.%)/SrTNT and (c) Au(1 wt.%)/BaTNT.

They observed that the BE of Au $4f_{7/2}$ in Au/TiO_2 and Au/Al_2O_3 showed a negative shift by −0.6 and −0.9 eV, respectively.

A large shift up to −1.1 eV was observed for the spent Au/TiO_2 catalyst. When the cations were changed from K^+ to Sr^{2+} and Ba^{2+} in ATNT, the BE of Au signals shifted systematically downward (Table 4.8). This observation indicates that as the basicity of the support increased, the Fermi level of the metal particles shifted to a lower binding energy. Thus, the XPS points out electron transfer from ATNT to Au nanoparticles, the extent of which follows the order: BaTNT > SrTNT > KTNT. Deconvolution of the XPS lines in the Au binding energy region reveal the presence of another set of signals at higher BE values but with lower intensity assignable to $Au^{\delta+}$ ions. Pusztai et al. [35] reported that, on titanate nanowires, gold atoms can occupy ion exchange positions at lower loading. They observed a higher portion of Au^+/Au^0 on the catalyst after reduction with H_2 compared to reduction with $NaBH_4$. This may be a reason for the presence of a small quantity of $Au^{\delta+}$ species in ATNT samples. There are reports [9, 38], which argue that hydride transfer is involved in C–H bond activation, and the cationic gold is catalytically active. Abad et al. [9] have investigated the active sites on Au/CeO_2. Recently, Zhao et al. [39] have also reported the active sites on Au/Ni_2O_3 involved in oxidation of alcohol. They showed a direct correlation between the

Table 4.8. XPS data (B.E. values in eV) of supported Au catalysts

Catalyst	$\dfrac{Au^{\delta+}}{Au^0}$	Au^0		$Au^{\delta+}$	
		$4f_{7/2}$	$4f_{5/2}$	$4f_{7/2}$	$4f_{5/2}$
Au(1 wt.%)/KTNT	0.28	83.2	86.9	85.2	88.9
Au(1 wt.%)/SrTNT	0.27	83.0	86.7	85.2	88.9
Au(1 wt.%)/BaTNT	0.43	82.8	86.5	85.3	89

concentration of Au^+ or Au^0 species and catalyst supports. Au^+/Au^0 ratio in the present catalysts was determined (Table 4.8). Lower the BE value higher was the catalytic activity over Au/ATNT catalysts (Fig. 4.17). Weak intensity of these Au 4f lines indicate that a part of Au is located inside the titanate nanotubes.
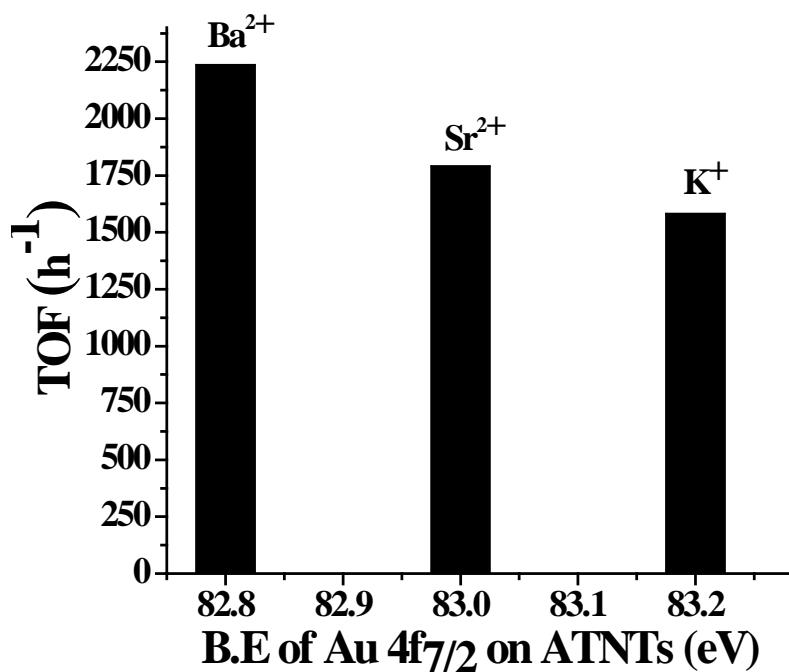
Fig. 4.17. Correlation between B.E. values and catalytic activity (TOF, h^{-1}) of Au.

115

4.3.2.2. Catalytic Activity

The catalytic activity of Au supported on ATNTs for benzyl alcohol oxidation with molecular oxygen as oxidant was studied at 120 °C and under solvent- and alkali-free conditions (Table 4.9). Benzaldehyde was the selective product (selectivity = 99 wt.%). While the support had little effect on benzaldehyde selectivity, a remarkable influence of it on benzyl alcohol conversion and turnover frequency (TOF) was observed (Table 4.9). Au (1 wt.%) supported on Ba^{2+} ion-exchanged NaTNT [Au(1 wt.%)/BaTNT] showed highest catalytic activity [benzyl alcohol conversion = 43 wt.% and TOF = 622 h^{-1} (based on total metal content) and 2237 h^{-1} (based on exposed surface metal atoms)]. This reaction occurred also with air instead of molecular oxygen over Au(1 wt.%)/BaTNT but then the conversion under same reaction conditions was 24.6 wt.% with benzaldehyde selectivity of 96.5 wt.% (Table 4.9; run no. 8b). Support (BaTNT) alone could not catalyze this reaction to a notable extent (benzyl alcohol conversion = 2.8 wt.%). Gold nanoparticles were smaller in size (d_{av} = 5.2 nm) and highly dispersed (metal dispersion = 20%) on BaTNT than on other supports (Table 4.5). Smaller the particle size, higher would be the number of exposed surface active sites and interaction with the support and higher would be the catalytic activity. The catalytic activity of Au(1 wt.%) supported on KTNT, SrTNT and BaTNT with almost similar Au particle size followed the order: Au(1 wt.%)/BaTNT > Au(1 wt.%)/SrTNT > Au(1 wt.%)/KTNT (Table 4.9, run nos. 3, 7 and 8a). This trend in catalytic activity parallels the variation in electron transfer from support to Au particles. With a view to see the influence of addition of Pd on the catalytic activity of Au, a Au-Pd (2 wt.%, 1:1)/BaTNT composition was prepared. Addition of Pd decreased the mean particle size of Au from 5.2 to 4.2 nm and metal dispersion increased from 20 to 25%. Au-Pd/BaTNT showed remarkably high catalytic activity than the catalyst without Pd content (benzyl alcohol conversion = 92.3 wt.% as against 43 wt.%). But the benzaldehyde selectivity dropped from 99 to 80.5 wt.%. Note that 92.3% of conversion on Au-Pd was achieved in just 5 h instead of 10 h. Hence, Au supported on NaTNT exchanged with larger cations exhibited higher catalytic activity due to higher amount of electron density at Au in those catalysts, which could easily activate molecular oxygen and enable the oxidation of benzyl alcohol [40]. Hsu et al. [18] observed such electronic effect on Pt catalysts with similar supports.

Table 4.9. Catalytic activity data of supported Au catalysts for oxidation of benzyl alcohol[a]

Run no.	Catalyst	Conversion (wt.%)	TOF (h^{-1})	Benzaldehyde selectivity (wt.%)[b]
1	Au(1 wt.%)/LiTNT	7.2	114 (689)	99.0
2	Au(1 wt.%)/NaTNT	17.0	257 (892)	99.0
3	Au(1 wt.%)/KTNT	21.9	392 (1005)	99.0
4	Au(1 wt.%)/CsTNT	8.8	166 (748)	99.0
5	Au(1 wt.%)/MgTNT	11.6	127 (692)	99.0
6	Au(1 wt.%)/CaTNT	13.4	147 (706)	99.0
7	Au(1 wt.%)/SrTNT	37.8	516 (1159)	99.0
8a	Au(1 wt.%)/BaTNT	43.0	622 (1277)	99.0
8b	Au(1 wt.%)/BaTNT	24.6	356 (730)	96.5
9	Au(3 wt.%)/BaTNT	62.5	220	97.0
10	Au(5 wt.%)/BaTNT	69.7	167	95.2
11	Au-Pd(1:1, 2 wt.%)/BaTNT[c]	92.3	819 (2213)	80.5

[a]Reaction conditions: Catalyst = 50 mg, benzyl alcohol = 25 mmol, p(O_2) = 1 atm, reaction temperature = 120 °C, and reaction time = 10 h, Turnover frequency (TOF) = moles of benzyl alcohol converted per mole of Au in the catalyst (ICP-OES) per hour.TOF values in parentheses are those calculated based on mole of benzyl alcohol converted per mole of surface metal atoms (estimated from TEM) per hour. Run no. 8a is performed with molecular oxygen, while run no. 8b was done with air. [b]Balance selectivity is benzyl benzoate. [c]For run no. 11, reaction time = 5 h and the product includes benzoic acid (1.0%), benzyl benzoate (10.2%), benzene (6.2%) and toluene (2.1%).

4.3.2.2.1. Structure-activity Correlations

Fig. 4.18 shows an interesting correlation between basicity and mean particle size/catalytic activity (TOF). Particle size of Au decreased with increasing basicity (basic sites per unit surface area) of the catalyst while TOF showed an increasing trend. In other words, basicity of the support, mean particle size of Au and catalytic activity are inter-related to each other. The points related to Au(1 wt.%) on CaTNT

and MgTNT have fallen away from this relation because there could be other factors like strength of basicity that would influence the values of particle size and TOF. Fig. 4.19 depicts the variation of oxidation activity of Au (TOF) as a function of its particle size.
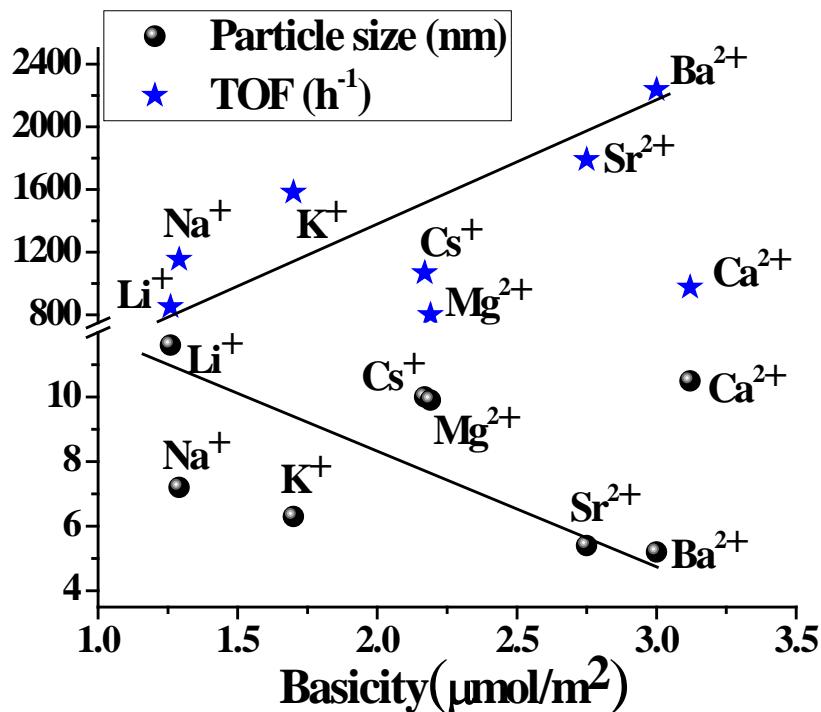

Fig. 4.18. Variation of mean particle size and TOF with the basicity for Au(1 wt.%)/ATNT. Reaction conditions: catalyst = 0.05 g, benzyl alcohol = 25 mmol, $p(O_2)$ = 1 atm, reaction temperature = 120 °C, and reaction time = 10 h.
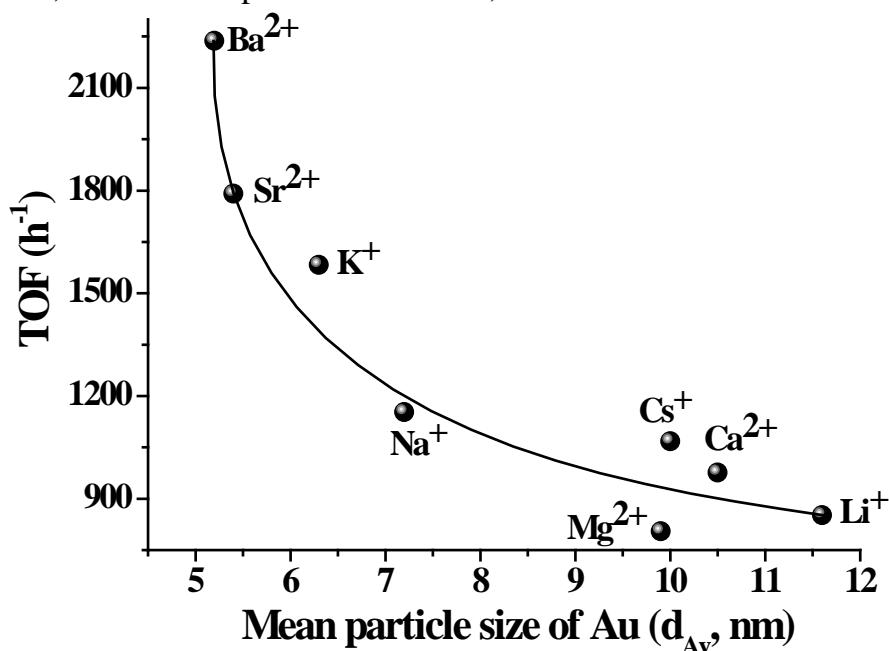

Fig. 4.19. Correlation between TOF and mean particle size of Au.

Catalytic activity increased with decreasing Au particle size. It is interesting to note that all the catalysts have followed this trend unlike that observed in Fig. 4.18. This clarifies that other than density, strength of basicity plays a crucial role. With increasing Au content from 1 to 5 wt.% on BaTNT, the conversion of benzyl alcohol increased from 43 to 69.7 wt.% but the selectivity for benzaldehyde decreased from 99 to 95.2 wt.% (Table 4.9).

4.3.2.2.2. Effect of Reaction Conditions

Catalytic activity increased with increasing reaction time (Fig. 4.20). Only a marginal drop in benzaldehyde selectivity was noted at higher conversions. Also an increase in activity with the amount of the catalyst was noted (Fig. 4.20). When the reaction temperature was raised from 80 to 100 and then to 120 °C, benzyl alcohol conversion on Au(1 wt.%)/BaTNT increased from 30.2 to 36.3 and then to 43 wt.%. This increase was from 8.4 to 15.2 and then to 17 wt.% over Au(1 wt.%)/NaTNT. Selectivity for benzaldehyde was 99 wt.% at all those conditions (Fig. 4.21).

4.3.2.2.3. Catalyst Reusability

After the first run, the catalyst was separated from the reaction mixture by filtration, washed with water, dried at 110 °C for 4 h and then, reused in the next recycle conducted at the same conditions. Such recycles were done for five times. The catalyst was recyclable (Fig. 4.22). ICP-OES analysis of spent catalyst showed no loss of Au content but a little loss of Ba^{2+} ion (0.6 wt.%) at the end of 5th recycle was detected. To confirm the heterogeneity of oxidation reaction over Au(1 wt.%)/BaTNT, the reaction at 120 °C was stopped after 2 h (when the conversion was 17.2 wt.%), catalyst was taken out and the reaction was continued without the catalyst for another 8 h and the reaction mixture was analyzed by GC. No detectable change in benzyl alcohol conversion was observed (Fig. 4.23) suggesting that the reaction is heterogeneous in nature.

4.3.3. Tentative Mechanism for Alcohol Oxidation over Au/ATNT Catalysts

Electro-oxidation of ethanol over Au supported on glassy carbon requires a partial coverage of Au surface with its oxide species. In CO oxidation, it was found that the oxidation activity increases with increase in the concentration of Au^+ species; but the presence of metallic Au (electron rich) was essential. According to these reports, the active sites consist of an ensemble of metallic Au atoms and a cationic Au^+ species [41-43]. In the present case, benzyl alcohol is activated on the support surface (as a consequence of its basic nature).
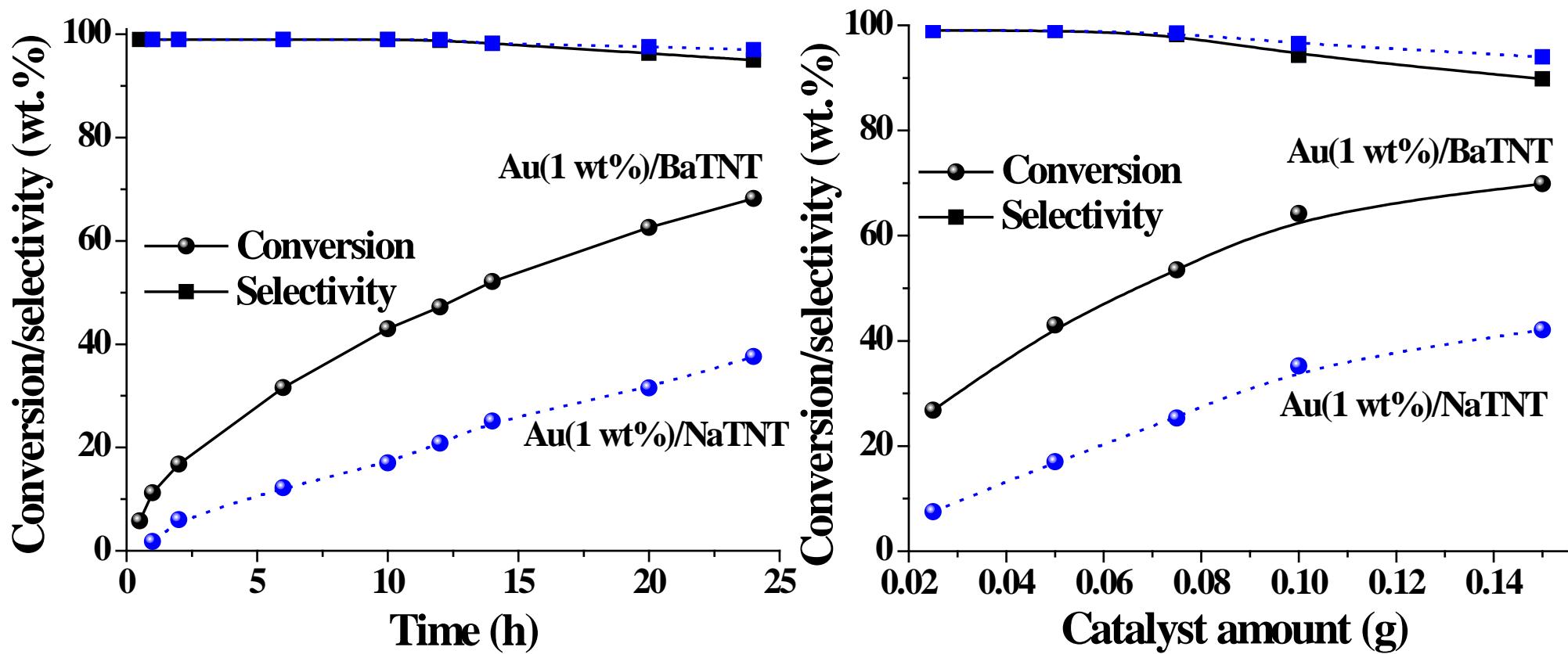
Fig. 4.20. Influence of reaction time and catalyst amount on conversion of benzyl alcohol and selectivity for benzaldehyde. Reaction conditions: Left - catalyst = 0.05 g, benzyl alcohol = 25 mmol, p(O$_2$) = 1 atm, reaction temperature = 120 °C, and reaction time = 0-25 h. Right - catalyst = 0.025-0.15 g, benzyl alcohol = 25 mmol, p(O$_2$) = 1 atm, reaction temperature = 120 °C, and reaction time = 10 h.
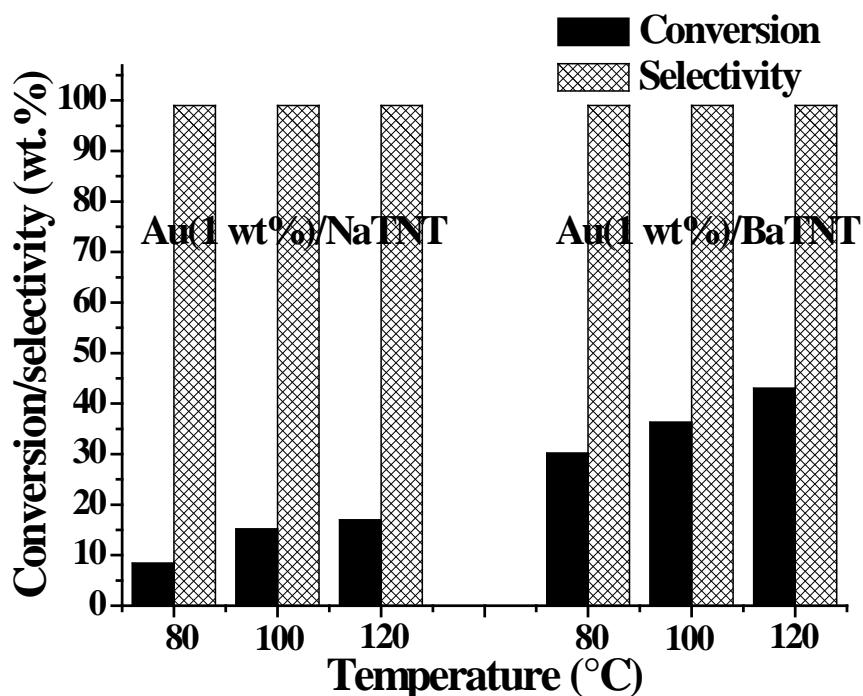
Fig. 4.21. Influence of reaction temperature on the conversion of benzyl alcohol and selectivity of benzaldehyde. Reaction conditions: catalyst = 0.05 g, benzyl alcohol = 25 mmol, p(O_2) = 1 atm, reaction temperature = 80-120 °C, and reaction time = 10 h.
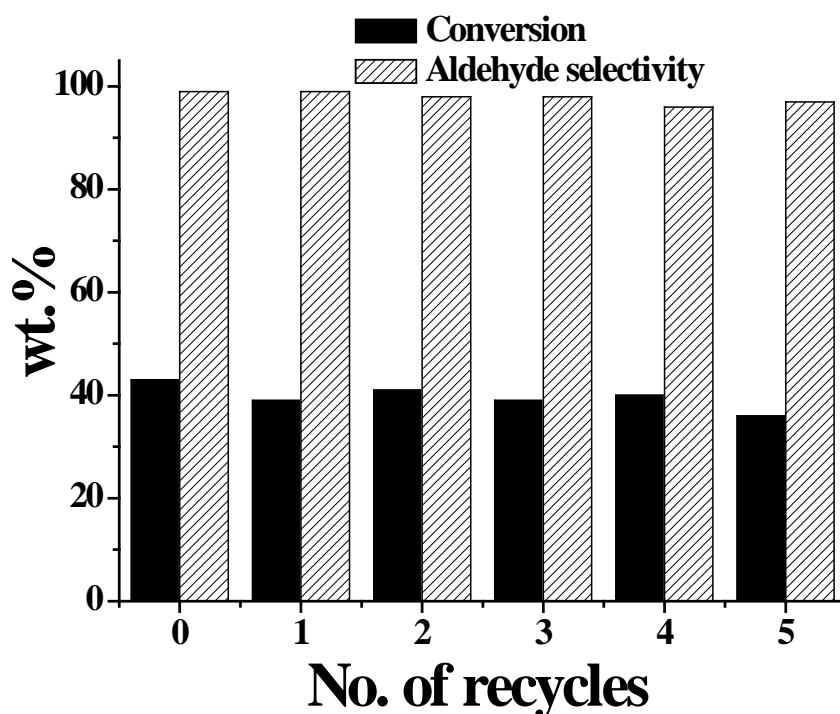
Fig. 4.22. Recyclability of Au(1 wt%)/BaTNT. Reaction conditions: catalyst = 0.05 g, benzyl alcohol = 25 mmol, p(O_2) = 1 atm, temperature = 120 °C, and reaction time = 10 h.

Then the abstraction of hydride ion is favoured at the metal-support interface (at coordinatively unsaturated sites/Au$^+$ ions).
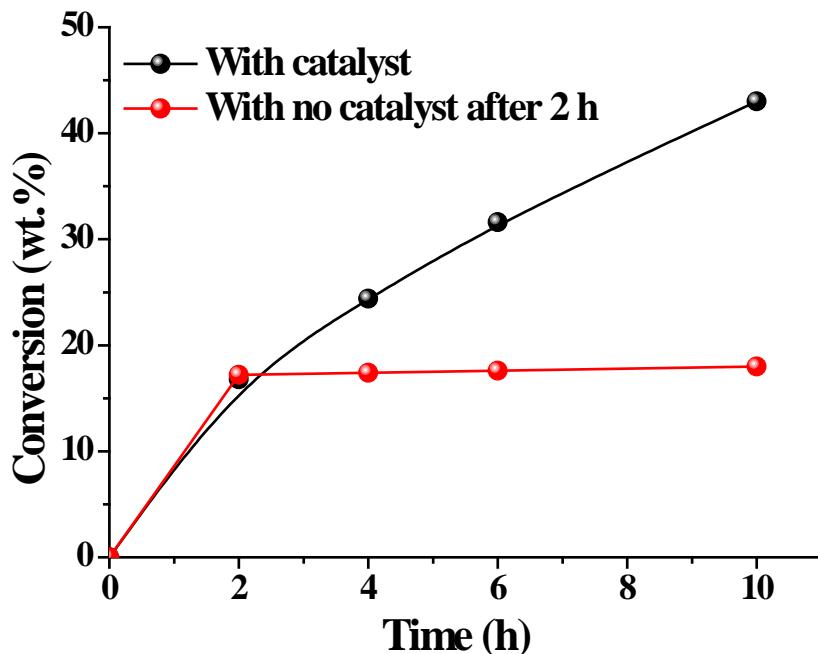
Fig. 4.23. Hot filtration test for oxidation of benzyl alcohol over Au(1 wt.%)/BaTNT. Reaction conditions: catalyst = 0.05 g, benzyl alcohol = 25 mmol, p(O$_2$) = 1 atm, reaction temperature = 120 °C, and reaction time = 10 h.

The electron rich Au nanoparticles activate molecular oxygen to produce activated oxygen species, which help removing H from AuH species to produce water as by-product. Meanwhile, the benzyloxy cation releases proton and forms the final product benzaldehyde [44, 45]. A schematic representation of reaction mechanism is shown in Fig. 4.24. Particle size of Au decreased with increasing basicity of the support while the catalytic activity had increased (Fig. 4.18). Higher the basicity higher would be the activation of benzyl alcohol and more would be the conversion. At the same time, lower the particle size of Au, higher would be the available surface area and support-Au interaction and higher would be activation of molecular oxygen and thereby, higher would be the catalytic activity. Thus, basicity has a direct (by way of activating benzyl alcohol) and indirect (by way of support-metal interaction) influence on the catalytic activity. The mean particle size of Au different supports decreased in the order: Au/BaTNT < Au/SrTNT < Au/KTNT. Smaller the particle size higher would be the SMSI effect, more would be the peripheral Au that are in δ+ state and hence, higher would be the hydride ion abstraction and thereby, higher would be the catalytic activity. This behavior is clearly evident from the XPS and catalytic activity data.

122
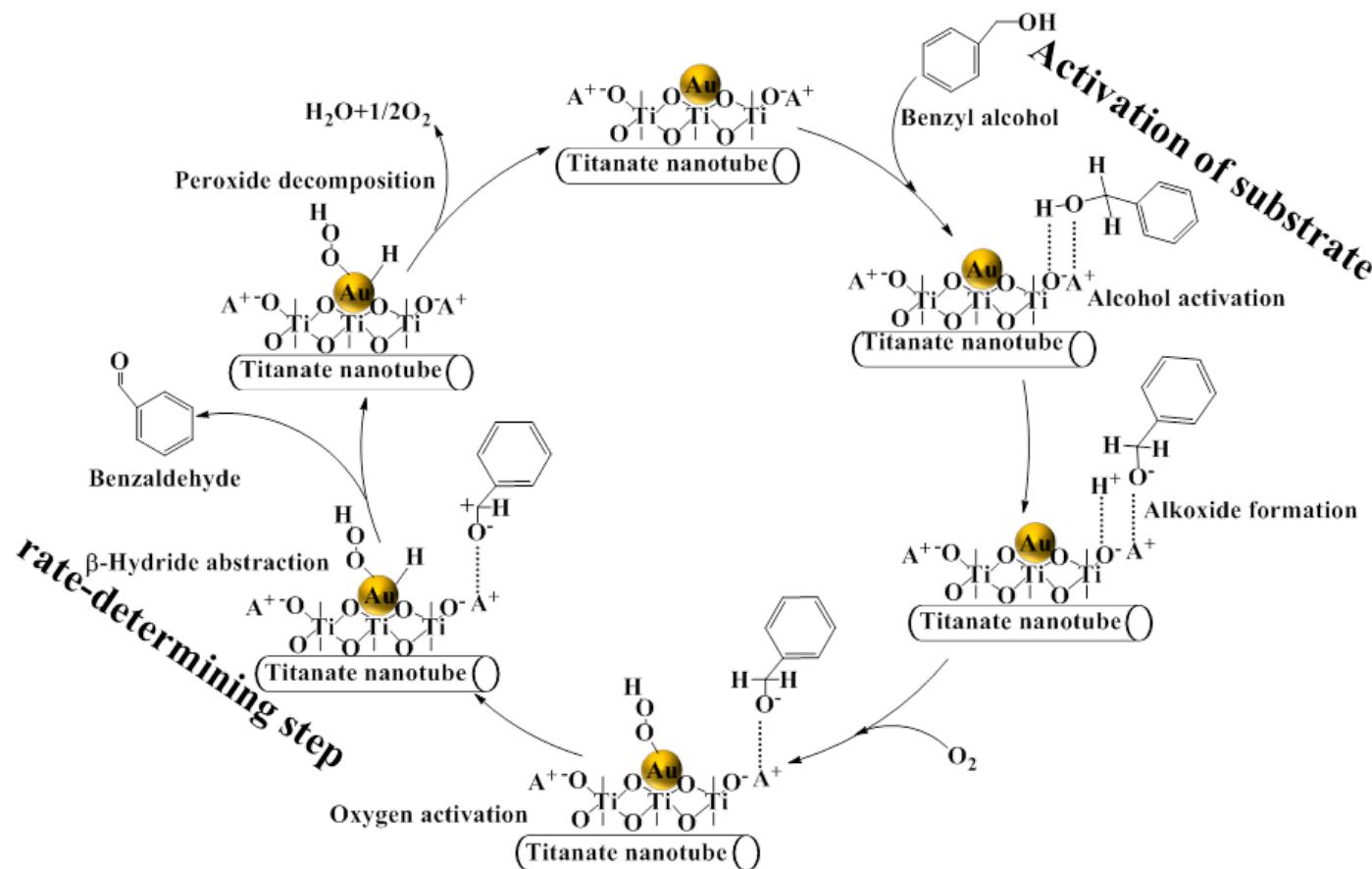
Fig. 4.24. Tentative mechanism for the oxidation of alcohols over Au/ATNT.

4.4. Conclusions

Catalytic application of Au-Pd/NaTNT for the selective aerial oxidation of alcohols was studied. The activity of this catalyst was found to be higher than Au/NaTNT, Pd/NaTNT and Au-Pd/TiO$_2$. Physicochemical studies revealed that the particles of Au were smaller and uniformly dispersed on the support in the presence of Pd. Au atoms on NaTNT in the presence of Pd were richer in electron density and thereby enhanced the activation of molecular oxygen enabling a higher oxidation activity. A range of 1° and 2°-alcohols were converted into corresponding carbonyl compounds.

Gold supported on alkali and alkaline earth metal ion-exchanged titanate nanotubes (ATNTs) were synthesized, characterized and their catalytic activities for benzyl alcohol oxidation with molecular oxygen/air were investigated. Oxidation of benzyl alcohol formed benzaldehyde with a selectivity of 99 wt.%. Alkali and alkaline metal ion exchange has a marked effect on the catalytic activity of titanate nanotubes. Among the catalysts investigated Au supported on BaTNT showed highest catalytic activity. Basicity of the support has an influence on the mean particle size and catalytic activity of Au. With increasing basicity, the particle size of Au has decreased while the activity of the catalyst has increased. This study teaches that catalytic activity of Au can be enhanced by altering the titanate support through exchanging with Ba^{2+} ions and by adding a co-metal like Pd. Since Au draws electron density from the basic support, it can activate molecular oxygen more easily forming superoxide like active oxygen species which in turn initiate the oxidation reaction.

4.5. References

[1]   Y. Zhang, X. Cui, F. Shi, Y. Deng, Chem. Rev. 112 (2012) 2467-2505.

[2]   R.A. Sheldon, J.K. Kochi, Metal-Catalyzed Oxidations of Organic Compounds, Academic Press, New York, 1981.

[3]   C. D. Pina, E. Falletta and M. Rossi, Chem. Soc. Rev. 41 (2012) 350-369.

[4]   S. J. Tauster, S. C. Fung, R. L. Garten, J. Am. Chem. Soc. 100 (1978) 170-175.

[5]   B. Hammer, J. K. Norskov, Adv. Catal. 45 (2000) 71-129.

[6]   D. I. Enache, J. K. Edwards, P. Landon, B. Solsona-Espriu, A. F. Carley, A. A. Herzing, M. Watanabe, C. J. Kiely, D. W. Knight, G. J. Hutchings, Science 311 (2006) 362-365.

[7]   N. Dimitratos, A. Villa, D. Wang, F. Porta, D. S. Su, L. Prati, J. Catal.244 (2006) 113-

121.

[8] W. Hou, N.A. Dehm, R.W.J. Scott, J. Catal. 253 (2008) 22-27.

[9] A. Abad, P. Conception, A. Corma, H. Garcia, Angew. Chem. Int. Ed. 44 (2005) 4066-4069.

[10] V. E. Herinch, P. A. Cox, The Surface Science of Metal, Cambridge University Press, Cambridge, 1996.

[11] A. Bruix, J. A. Rodriguez, P. J. Ram rez, S. D. Senanayake, J. Evans, J. B. Park, D. Stacchiola, P. Liu, J. Hrbek, F. Illas, J. Am. Chem. Soc. 134 (2012) 8968-8974.

[12] C. T. Campbell, Nat. Chem. 4 (2012) 597-598.

[13] M. Valden, X. Lai, D. W. Goodman, Science 281 (1998) 1647-1650.

[14] J. K. Nørskov, T. Bligaard, B. Hvolbæk, F. Abild-Pedersen, I. Chorkendorff, C. H. Christensen, Chem. Soc. Rev. 37 (2008) 2163-2171.

[15] C. Milone, R. Ingoglia, A. Pistone, G. Neri, S. Galvagno, Catal. Lett. 87 (2003) 201-209.

[16] T. Kasuga, M. Hiramatsu, A. Hoson, T. Sekino, K. Niihara, Langmuir 14 (1998) 3160-3163.

[17] X. Sun, Y. Li, Chem. Eur. J. 9 (2003) 2229-2238.

[18] C.-Y. Hsu, T.-C. Chiu, M.-H. Shih, W.-J. Tsai, W.-Y. Chen, C.-H. Lin, J. Phy. Chem. C 114 (2010) 4502-4510.

[19] M. Hodos, Z. Konya, G. Tasi, I. Kiricsi, React. Kinet. Catal. Lett. 84 (2005) 341-350.

[20] M. A. Khan, O. B. Yang, Catal. Today 146 (2009) 177-182.

[21] V. Idakiev, Z. Yuan, T. Tabakova, B. Su, Appl. Catal. A: Gen. 281 (2005) 149-155.

[22] T. A. Ntho, J. A. Anderson, M. S. Scurrell, J. Catal. 261 (2009) 94-100.

[23] L. C. Sikuvhihulu, N. J. Coville, T. Ntho, M. S. Scurrell, Catal. Lett. 123 (2008) 193-197.

[24] L. T. Murciano, Q. He, G. J. Hutchings, C. J. Kiely, D. Chadwick, ChemCatChem 6 (2014) 2531-2534.

[25] J. Feng, C. Ma, P.J. Miedziak, J.K. Edwards, G.L. Brett, D. Li, Y. Du, D.J. Morgan, G.J. Hutchings, Dalton Trans. 42 (2013) 14498-14508.

[26] P. Gobbo, M. C. Biesinger, M. S. Workentin, Chem. Commun. 49 (2013) 2831-2833.

[27] J. A. Lopez-Sanchez, N. Dimitratos, P. Miedziak, E. Ntainjua, J. K. Edwards, D. Morgan, A. F. Carley, R. Tiruvalam, C. J. Kiely, G. J. Hutchings, Phys. Chem. Chem. Phys. 10 (2008) 1921-1930.

[28] P. H.-Hipolito, M. G.-Castillejos, E. M.-Klimova, N. J.-Flores, A. G.-Cortes, T.E.

Klimova, Catal. Today 220-222 (2014) 4-11.

[29] S. K. Klitgaard, A. T. DeLa Riva, S. Helveg, R. M. Werchmeister, C. H. Christensen, Catal. Lett. 126 (2008) 213-217.

[30] H.-Y, Chen, S.-L. Lo, H.-H. Ou, Appl. Catal. B: Environ. 142-143 (2013) 65-71.

[31] W. Li, A. Wang, X. Liu, T. Zhang, Appl. Catal. A: Gen. 433-434 (2012) 146-151.

[32] X. Liu, A. Wang, X. Yang, T. Zhang, C.-Y. Mou, D.-S. Su, J. Li, Chem. Mater. 21 (2009) 410-418.

[33] A. Villa, N. Janjic, P. Spontoni, D. Wang, D. S. Su, L. Prati, Appl. Catal. A: Gen. 364 (2009) 221-228.

[34] P. Claus, A. Bruckner, C. Mohr, H. Hofmeister, J. Am. Chem. Soc. 122 (2000) 11430-11439.

[35] P. Pusztai, R. Puskas, E. Varga, A. Erdohelyi, A. Kukovecz, Z. Konyaad, J. Kiss, Phys. Chem. Chem. Phys. 16 (2014) 26786-26797.

[36] J. Y. Tsai, J. H. Chao, C. H. Lina, J. Mol. Catal. A: Chem. 298 (2009) 115-124.

[37] S. Arrii, F. Morfin, A. J. Renouprez, J. L. Rousset, J. Am. Chem. Soc. 126 (2004) 1199-1205.

[38] M. Wang, F. Wang, J. Ma, M. Li, Z. Zhang, Y. Wang, X. Zhang, J. Xu, Chem. Commun. 50 (2014) 292-294.

[39] G. Zhao, J. Huang, Z. Jiang, S. Zhang, L. Chen, Y. Lu, Appl. Catal. B: Environ. 140 (2013) 249-257.

[40] C. Santra, S. Rahman, S. Bojja, O. O. James, D. Sen, S. Maity, A. K. Mohanty, S. Mazumder, B. Chowdhury, Catal. Sci. Tech. 3 (2013) 360-370.

[41] T. Mallat, A. Baiker, Chem. Rev. 104 (2004) 3037-3058.

[42] G. C. Bond, D. T. Thompson, Gold Bull. 33 (2000) 41-50.

[43] M. S. Chen, D. W. Goodman, Catal. Today 111 (2006) 22-33.

[44] H. Liu, Y. Liu, Y. Li, Z. Tang, H. Jiang, J. Phys. Chem. C 114 (2010) 13362-13369.

[45] X. Zhang, X. Ke, H. Zhu, Chem. Eur. J. 18 (2012) 8048-8056.

Chapter - 5

Oxidation of Styrene over Au/BaTNT

5.1. Introduction

Oxidation of olefins (in particular, styrene) is an important industrial process. Products of this reaction (epoxide and aldehyde) serve as building block in the manufacture of plasticizers, perfumes, and pharmaceuticals [1]. Epoxides are conventionally prepared by halogen alcohol and peracid methods. These approaches are unsafe and generate a large amount of waste product. There have been several reports [2-5] on the catalytic use of supported gold and other metals for olefin oxidation with tert-butylhydroperoxide (TBHP). Choudhary et al. [6, 7] reported that Au NPs supported on a range of oxides including BaO are active for oxidation of styrene yielding styrene oxide with TBHP as oxidant. Supports play a crucial role in catalytic reactions providing anchoring sites to metal nanoparticles and influencing the reaction rates. Oxidations with aqueous H_2O_2 often lead to poor selectivity for styrene oxide (SO). Further, usage of molecular oxygen instead of peracids and peroxides in olefin epoxidation is a major challenge [8]. Haruta reported the direct oxidation of propene with molecular oxygen over Au/TS-1 catalyst [9]. Zhu et al. [10] described the catalytic activity of thiolate protected gold clusters in the oxidation of styrene using molecular oxygen; benzaldehyde was the major product in that study. Development of efficient and selective, solid catalysts for oxidation of styrene with molecular oxygen / H_2O_2 / TBHP is desired. Catalysis by gold nanoparticles supported on titanate nanotubes was explored by several research groups [11-15]. The titanate nanotubes are particularly attractive hosts for catalytically active metal nanoparticles because of their well-defined mesoporous one dimensional structure, high specific surface area and ion-exchange capability. Their semiconducting properties lead to strong metal-support interaction which could influence the catalytic performance. In this chapter, the catalytic performance of Au supported on barium titanate nanotubes (Au/BaTNT) in liquid-phase oxidation of styrene is reported. The influence of reaction parameters such as oxidant, solvent, loading of Au on BaTNT, amount of the catalyst, substrate/oxidant mole ratio, temperature and reaction time is systematically studied. The scope of Au(1 wt.%)/BaTNT for oxidation of a range of substituted styrenes is investigated. Reusability of the catalyst was also probed.

5.2. Experimental

BaTNTs were prepared by exchanging Na^+ ions in NaTNTs with Ba^{2+} ions employing a barium nitrate as precursor solution. Au of different loadings was supported on BaTNTs by deposition-precipitation (DP) method. A detailed procedure for synthesis and characterization of catalysts is described in Chapter 2 (sections 2.2.1.2, 2.2.1.3, 2.2.2.2 and 2.3). Reaction procedure for oxidation of styrene is presented in Chapter 2 (section 2.4.3).

5.3. Results and Discussion

5.3.1. Catalyst Characterization

5.3.1.1. XRD & ICP-OES

Fig. 5.1 shows the X-ray powder diffraction (XRD) patterns of BaTNT and Au/BaTNT. The diffraction peaks located at $2\theta = 10.1, 24.3, 28.4$ and $48.5°$ confirm the formation of titanate nanotubes (JCPDS files: 31-1329 and 41-0192) [25]. Catalyst samples containing 3 and 5 wt.% Au loading showed additional peaks at $38.2°$ and $44.6°$ due to (111) and (200) planes of metallic Au (JCPDS files: 04-0784 and 05-068; Fig. 5.1 (e and f)). Some loss in crystallinity of the support was observed at higher loadings of Au. A decrease in the intensity of (200) [relative to (020)] peak was noted at higher Au loadings (3 and 5 wt.%) [16]. This could be due to blockage of inter-planar spacing with Au nano-particles or structural deformation as a consequence of strong Au-support interaction. Chemical composition (Au, Ba^{2+} and Na^+ contents) of the catalysts was determined by inductively-coupled plasma-optical emission spectroscopy (ICP-OES; Table 5.1).
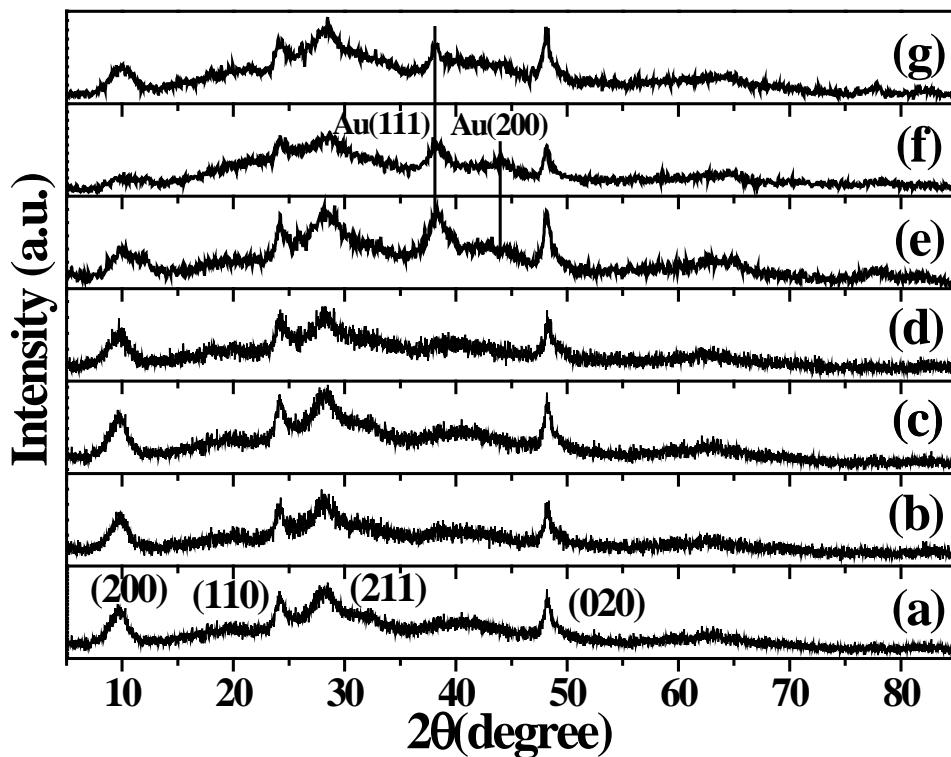
Fig. 5.1. XRD profiles: (a) BaTNT, (b) Au(0.5 wt.%)/BaTNT, (c) Au(1 wt.%)/BaTNT, (d) Au(2 wt.%)/BaTNT, (e) Au(3 wt.%)/BaTNT, (f) Au(5 wt.%)/BaTNT and (g) Spent Au(1 wt.%)/BaTNT (after 4th recycle).

129

Table 5.1. Physicochemical properties of Au/BaTNTs

S.No.	Catalyst[a]	Chemical composition (wt.%)[b]			Textural properties[c]			Au particle size (nm)[d]	Au dispersion (%)[d]	Basicity (μmol/m²)[e]		
		Au	Ba	Na	S_{BET}	V_p	d_p			Weak	Strong	Total
1	BaTNT	-	17.76	0.43	175	0.40	6.0	-	-	0.28	3.37	3.65
2	Au(0.5 wt.%)/BaTNT	0.30	15.64	0.42	162	0.39	5.6	5.0	22	0.30	2.94	3.24
3	Au(1 wt.%)/BaTNT	0.68	13.81	0.42	155	0.37	5.4	5.2	20	0.21	2.79	3.0
4	Au(2 wt.%)/BaTNT	1.46	12.97	0.40	150	0.36	5.4	5.9	19	0.27	2.36	2.63
5	Au(3 wt.%)/BaTNT	2.80	12.0	0.36	146	0.36	5.3	7.0	16	0.32	2.07	2.39
6	Au(5 wt.%)/BaTNT	4.10	9.26	0.28	140	0.35	5.1	7.4	15	0.42	1.72	2.06

[a]Values in parenthesis represent the nominal values of Au (input Au). [b]ICP-OES. [c]N_2-physisortion. S_{BET} = specific surface area (m²/g), V_p = pore volume (cc/g) and d_p = pore diameter (nm). [d]TEM. [e]CO_2-TPD.

5.3.1.2. N₂-physisorption

The textural properties of BaTNT and Au/BaTNT were characterized by the N_2-physisorption. The specific surface area (S_{BET}), pore volume (V_p) and mean pore diameter (d_p) of the samples are summarized in Table 5.1. Representative adsorption-desorption isotherms along with pore size distribution curves of BaTNT and Au/BaTNT are shown in Fig. 5.2. These isotherms are typical of type IV and exhibit H_2- hysteresis loops indicative of the presence of mesopores in the catalysts investigated. Upon Au loading, a marginal decrease in specific surface area and average pore diameter was observed. Further, a decrease in total pore volume of Au/BaTNT compared to bare BaTNT was also observed.

5.3.1.3. TEM

The morphology and particle size of the Au on BaTNT were determined by transmission electron microscopy (TEM). Representative TEM images are shown in Fig. 5.3. These images reveal the presence of Au nanoparticles on the inner and outer surfaces of tubular multi-walled BaTNT support. It was observed that the length of nanotubes range from several tens to hundreds of nanometers. The outer and inner diameters of nanotubes were around 10 and 5 nm, respectively [15]. The inner diameter value is quite close to the value determined from N_2-physisorption studies (~ 5-6 nm). Au nanoparticles are well dispersed on the walls of nanotubes. The mean particle size and percentage dispersion of Au estimated from TEM images are reported in Table 5.1. As the gold loading increased from 0.5 to 5 wt.%, a decrease in the dispersion of Au from 22 to 15 % was noted. Moreover, an increase in mean Au particle size from 5.2 to 6.9 nm was identified for Au(1 wt.%)/BaTNT after its reuse (for four times) in catalytic reaction.

5.3.1.4. DR UV-vis Spectroscopy

DR UV‑vis spectroscopy is a sensitive tool to probe the local environment of Au nanoparticles. Au/BaTNT showed a characteristic localized surface plasmon resonance (LSPR) band with maximum at 545-580 nm (Fig. 5.4(i)). With increase in particle size and decrease in Au dispersion, red shift and increase in intensity of the LSPR band were observed.

On contacting with acetonitrile (ACN, solvent), H_2O_2 (oxidant), ACN + H_2O_2/TBHP and ACN + H_2O_2/TBHP + styrene significant changes in the DR UV-visible spectrum of Au(2 wt.%)/BaTNT was noted (Fig. 5.4 (ii)). On contact with ACN or H_2O a new charge transfer band was observed at 280-300 nm characteristic of an octahedral Ti^{4+} species [17]. When the catalyst came in contact with oxidants like H_2O_2 or TBHP development of a new
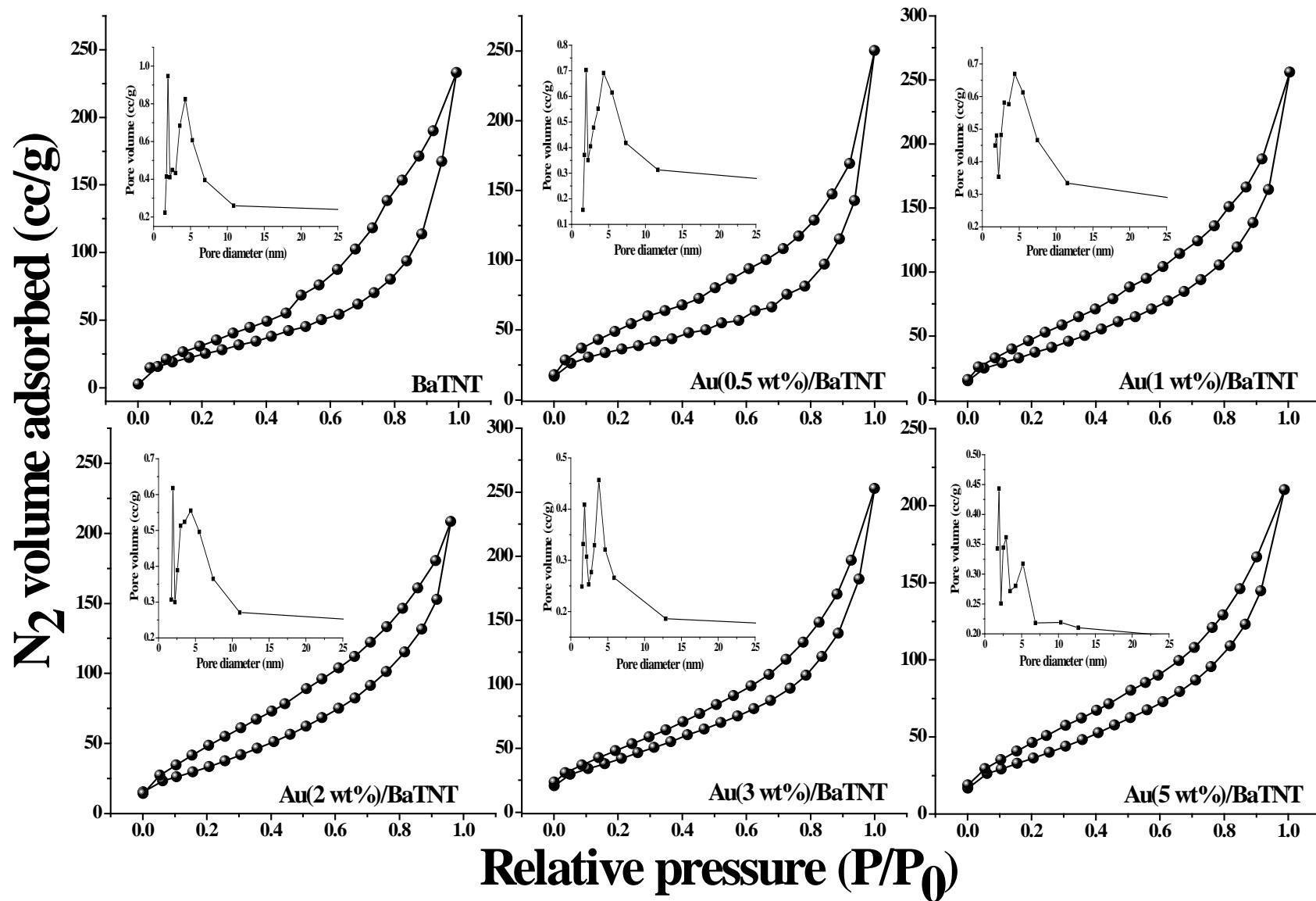
Fig. 5.2. N_2-adsorption-desorption isotherms and pore size distribution curves of BaTNT and Au/BaTNTs.
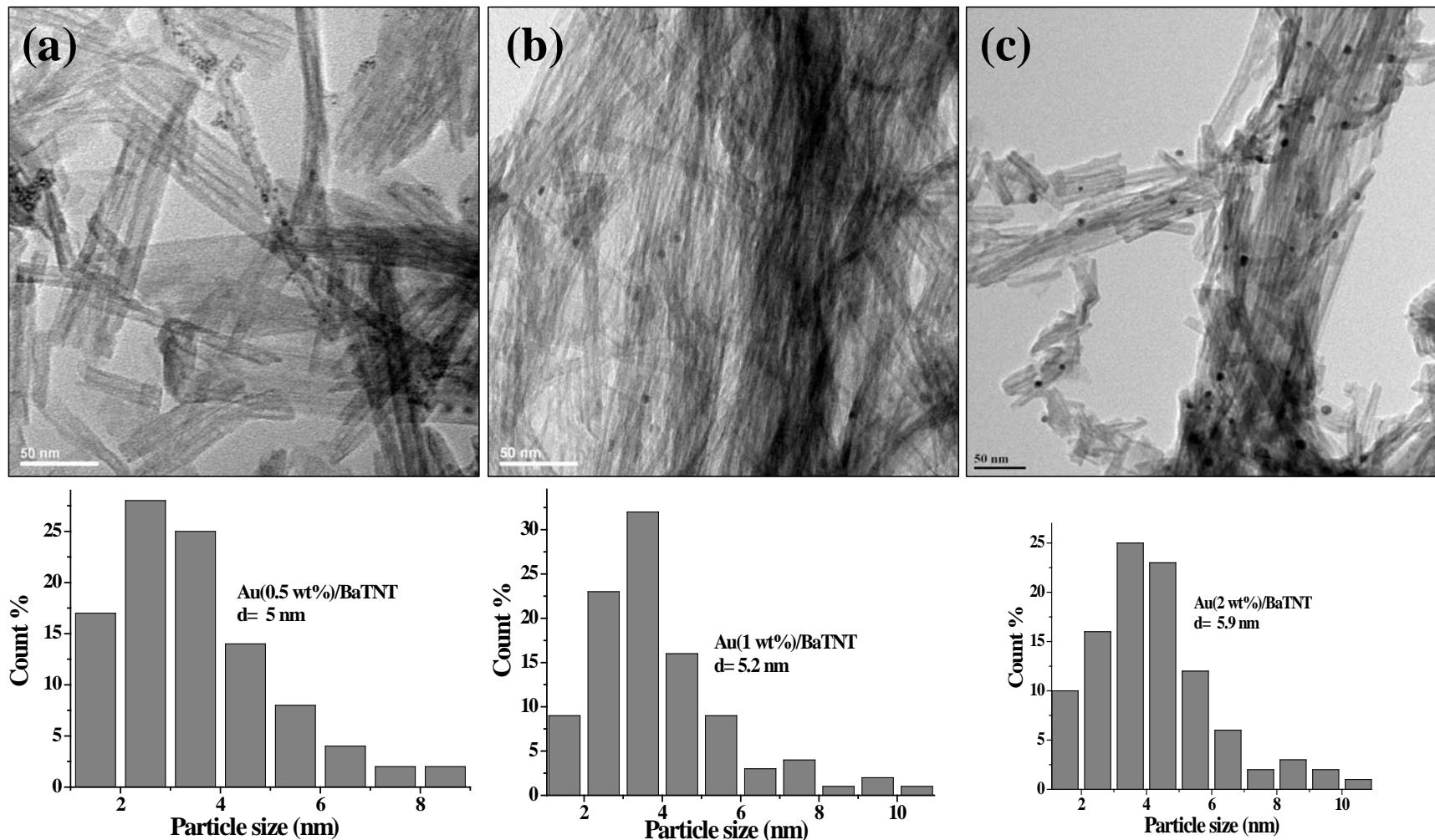
Fig. 5.3. TEM images and particle size distribution curves of Au/BaTNT catalysts (Contd.).
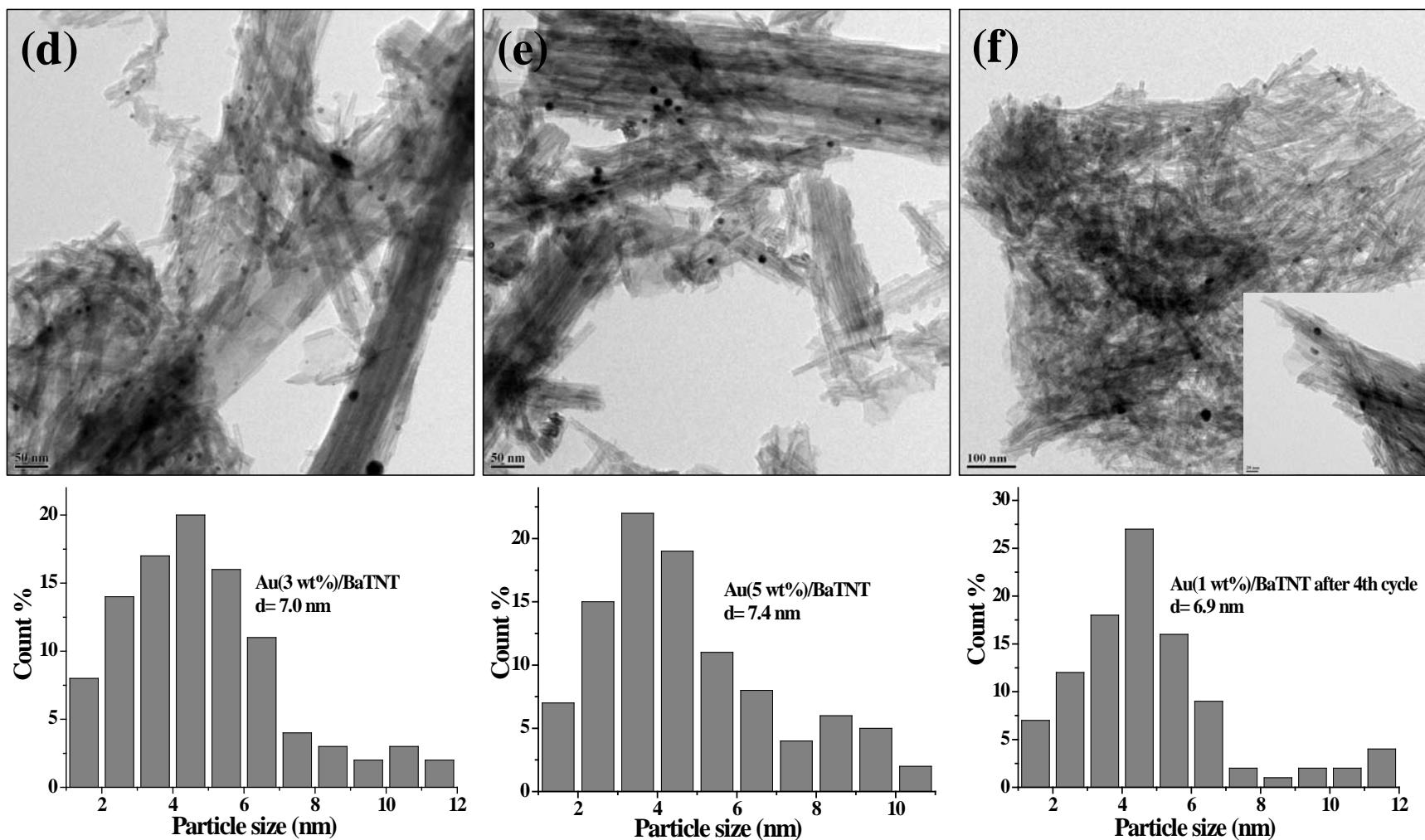
Fig. 5.3. TEM images and particle size distribution curves of Au/BaTNT catalysts.
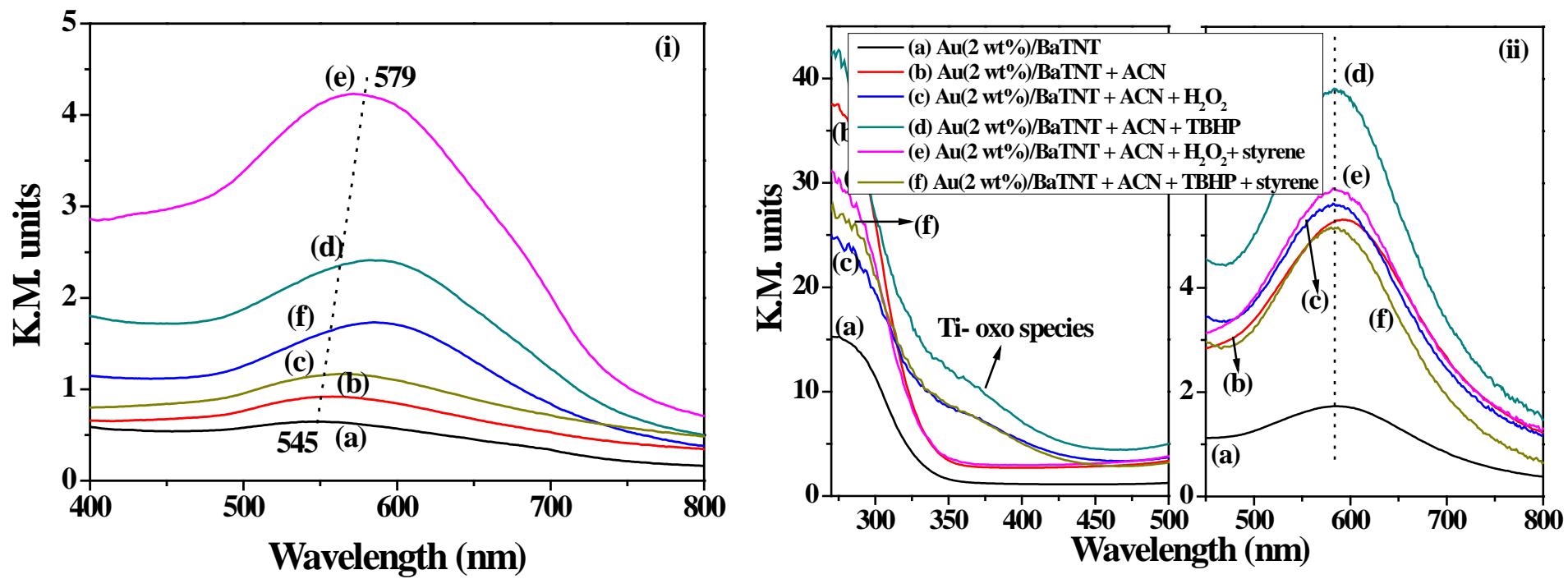
Fig. 5.4. DR UV-vis spectra: (i) Au(0.5 wt.%)/BaTNT (a), Au(1 wt.%)/BaTNT (b), Au(2 wt.%)/BaTNT (c), Au(3 wt.%)/BaTNT (d), Au(5 wt.%)/BaTNT (e) and spent Au(1 wt.%)/BaTNT after 4th recycle (f). (ii) Au (2 wt.%)/BaTNT contacted with ACN, H_2O_2, TBHP and styrene.

asymmetric band at around 360 nm typical of oxo-spcies was observed. When styrene (substrate olefin) was added intensity of oxo-band decreased indicate the role of oxo species in olefin oxidation reaction. Formation of oxo-species were detected also on bare BaTNT when it was contacted with H_2O_2/TBHP. But their concentration was much higher for Au/BaTNT than for bare BaTNT. Shift in LSPR band position when the catalyst was contacted with solvent / oxidant / substrate.

5.3.1.5. FT-Raman Spectroscopy

Anatase TiO_2 showed four main peaks in FT-Raman spectrum (Fig. 5.5(i)) at 141, 396, 517 and $641\,cm^{-1}$ corresponding to E_g, B_{1g} and A_{1g}, modes of vibration. BaTNT and Au(1 wt.%)/BaTNT showed characteristic peaks for the nanotubes at 275-290, 433-450 and 706 cm^{-1} [18]. Absence of anatase TiO_2 peaks in the spectrum of BaTNT and Au(1 wt.%)/BaTNT confirms that all the TiO_2 in the synthesis of those materials got converted into titanate nanotubes during the hydrothermal treatment with alkali. The band at 275-290 cm^{-1} is assigned to vibrations involving Ti-O-A (A is the interlayer cation, Ba^{2+}). Bands at 433-450 and 706 cm^{-1} are assigned to Ti-O bending vibrations in TiO_6 octahedron of titanate nanotubes [19]. On deposition of Au on BaTNT, the band at 890 cm^{-1} due to short Ti-O bond in TiO_6 octahedron disappeared and the band at 275-290 cm^{-1} assigned to long Ti-O bond shifted to higher frequency (i.e., lower wavenumber). The short and long Ti-O bonds correspond to central Ti atom-terminal O atom and Ti-bridging O atom, respectively. A new band at 150 cm^{-1} was observed for Au(1 wt.%)/BaTNT pointing out deformation of the titanate structure. Similar observations were reported also by Yang et al. [20].

Raman spectroscopy is a sensitive tool to detect the oxo-species (peroxo and superoxo) formed during reactions with peroxides. Fig. 5.5 (ii) shows the spectra of BaTNT and Au(1 wt.%)/BaTNT contacted with $ACN+H_2O_2$ and ACN+TBHP. An intense band at 877 cm^{-1} corresponding to peroxo species [21] was observed when bare BaTNT and Au(1 wt.%)/BaTNT were contacted with $ACN+H_2O_2$. Intensity of this band was higher for Au(1 wt.%)/BaTNT than for bare BaTNT indicating that Au nanoparticles enhance the formation of peroxo species. BaTNT and Au(1 wt.%)/BaTNT, when contacted with ACN+TBHP exhibited a new band at 747 cm^{-1}. Presence of this band was reported also by Chan et al. [22]. Difference in the position of this new band from that observed in the case of Au(1 wt.%)/BaTNT+ACN+H_2O_2 is attributed to difference in the type of oxidant (tert-butyl hydroperoxide versus hydrogen peroxide).
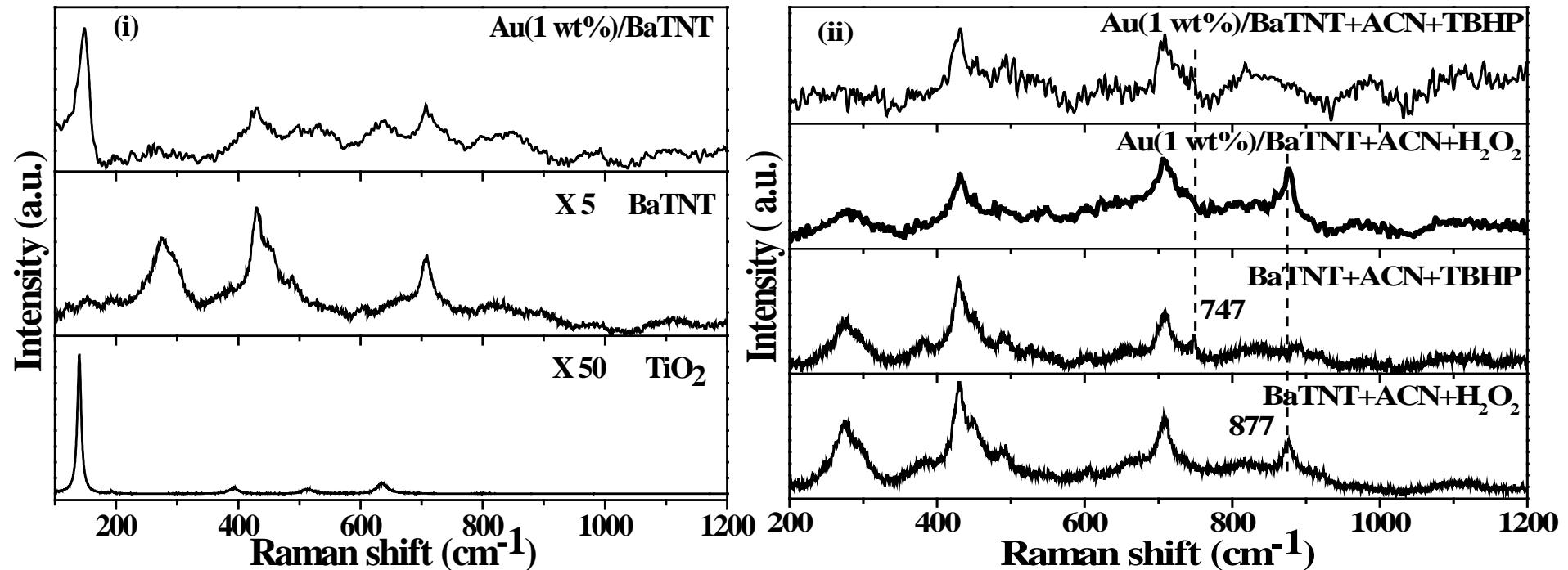
Fig. 5.5. FT-Raman spectra: (i) TiO$_2$, BaTNT and Au(1 wt.%)/BaTNT. (ii) BaTNT and Au(1 wt.%)/BaTNT contacted with ACN+H$_2$O$_2$ and ACN+TBHP.

5.3.1.6. CO$_2$-TPD

CO$_2$-temperature-programmed desorption measurements on Au/BaTNT (Fig. 5.6) showed two desorption peaks in the temperature regions 100-300 and 300-500 °C attributable to weak and strong basic sites, respectively. With increasing Au the overall basicity decreased. Also decrease in the amount of strong basic sites and increase in weak basic sites was observed. Stronger basic sites became more stronger (desorption peak shifted to higher temperatures) and weaker sites became more weaker (desorption peak shifted to lower temperatures). With decreasing basicity particle size increased and dispersion of Au decreased (Table 5.1).
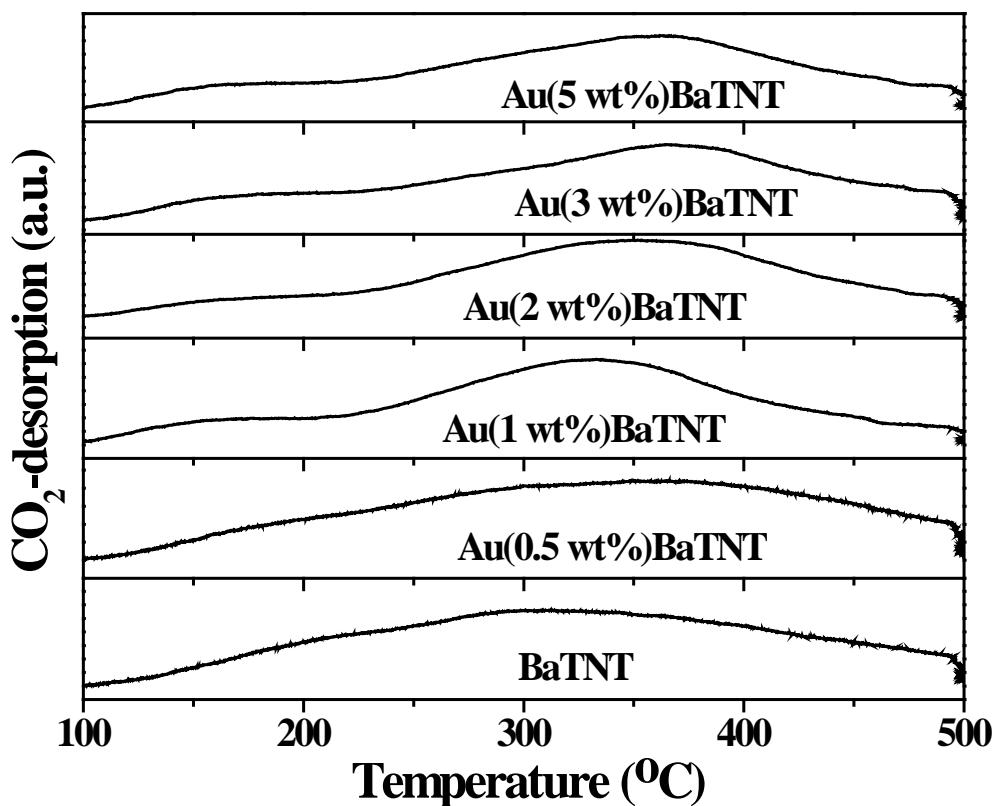
Fig. 5.6. CO$_2$-TPD profiles of Au/BaTNT catalysts.

5.3.2. Catalytic Activity

Catalytic activity data of Au(1 wt.%)/BaTNT in styrene oxidation with O$_2$, H$_2$+O$_2$, aq. H$_2$O$_2$ (30%), aq. TBHP (70%) and TBHP in n-decane (5.5 M) as oxidants are presented in Table 5.2. Styrene oxide (SO), benzaldehyde (Bzh), phenylacetaldehyde (PAA), 1-phenyl-1,2-ethanediol (Diol) and others including acids are the products of this oxidation reaction. This reaction did not proceed to an appreciable extent over Au (1 wt.%)/BaTNT when molecular oxygen was used as an oxidant (Table 5.2, Run No. 1; styrene conversion = 1 wt.% and selectivity for Bzh = 100%). With a view of understand the photocatalytic oxidation

activity of Au/BaTNT, reaction was performed at room temperature in presence of a solar simulator (Table 5.2, Run No. 2). No breakthrough in the oxidation activity was detected. When the reaction was carried out in presence of H_2+O_2 instead of O_2 alone a significant enhancement in styrene conversion from 1.0 to 19.3 wt.% with SO (selectivity = 35.8%), Bzh (53.6%) and others (10.6%) as products was observed (Run No. 3). In this experiment hydrogen peroxide is formed in situ from $H_2 + O_2$ over the supported Au catalyst and which in turn acts as an oxidant. When the reaction was carried out with 30% aq. H_2O_2 as oxidant instead of $H_2 + O_2$ styrene conversion increased to 34.4 wt.% (Run No. 4). Oxidation occurs with aq. H_2O_2 even in the absence of a catalyst, but styrene conversion was 10.1 wt.% only (Run No. 5). When 70% aq. TBHP in place of 30% aq. H_2O_2 was used as oxidant styrene conversion increased 46.8 wt.% and selectivity for SO increased from 22.8 to 70.9 wt.% (Run No. 6). When anhydrous TBHP (5.5 M; in decane) was used styrene conversion raised to 60.5 wt.% with selectivity for SO being 80.1 wt.% (Run No. 8). Styrene conversion in the absence of catalyst was low (Run Nos. 7 and 9). BaTNT could also catalyze the reaction to a low extent (styrene conversion = 22.5 wt.%) with poor selectivity for SO (43 wt.%). Comparison of the data (Run Nos. 8 - 10) reveal that presence of supported Au nanoparticle is essential for high activity and SO selectivity. When anhydrous TBHP along with O_2 (static -filled balloon or continuous flow) was used as oxidant, a maximum conversion of 72.2 - 75.8 wt.% was obtained but the selectivity for SO got lowered (34.0 - 56.1 wt.%; Run Nos. 11 and 12). In other words, oxygen or H_2O_2 promoted Bzh formation while TBHP facilitated SO formation. Oxidation activity (turnover frequency, TOF) of Au(1 wt.%)/BaTNT with different oxidants increased in the following order: TBHP > aq. TBHP > aq. H_2O_2 > H_2+O_2 > O_2. In the case of TBHP+O_2 oxidant system TBHP decomposes and forms $BuO^{\cdot}+^{\cdot}OH$ which in turn activate dioxygen to form superoxo-like species that are responsible for oxidation reaction [23]. Earlier, Shetti et al. [24] reported that hydroperoxy/peroxo species are responsible for selective epoxidation while superoxo-like species lead to non-selective products. Formation of the extent of peroxo species was higher with TBHP as oxidant as revealed by in situ DR UV-visible and FT-Raman studies and thus, higher amount of SO was obtained when TBHP instead of H_2O_2 was used as oxidant.

5.3.2.1. Effect of Reaction Conditions

5.3.2.1.1. Effect of Solvent

Solvent has a marked effect on oxidation of styrene at 80 °C over Au(1 wt.%)/BaTNT using TBHP (5.5 M; in decane) as the oxidant (Table 5.3). The solvents of varying polarity (toluene, dioxane, N,N-dimethylformamide (DMF) and acetonitrile (ACN)) were tested.

Table 5.2. Catalytic activity data of Au/BaTNT in the oxidation of styrene[a]

Run No.	Catalyst	Oxidant	Styrene conv.(wt.%)	Product selectivity (wt.%)					Yield of SO (%)	TOF[c] (h^{-1})	TOF[d] (h^{-1})
				SO	Bzh	PAA	Diol	Others			
1	Au (1 wt.%)/BaTNT	O$_2$	1.0	-	100	-		-	-	4	13
2	Au (1 wt.%)/BaTNT [b]	O$_2$	0.6	-	100	-		-	-	7	23
3	Au (1 wt.%)/BaTNT	H$_2$+O$_2$ (10 ml/min)	19.3	35.8	53.6	0	0	10.6	6.9	75	251
4	Au (1 wt.%)/BaTNT	H$_2$O$_2$	34.4	22.8	54.0	1.7	19.3	2.2	7.8	134	447
5	No catalyst	H$_2$O$_2$	10.1	17.1	61.2	5.5	12.7	3.5	1.7	-	-
6	Au (1 wt.%)/BaTNT	Aq. TBHP	46.8	70.9	18.9	4.8	0	5.4	33.2	182	608
7	No catalyst	Aq. TBHP	13.4	32.3	25.8	6.2	0	35.7	4.3	-	-
8	Au (1 wt.%)/BaTNT	TBHP	60.5	80.1	13.4	2.5	0	4.0	48.5	236	786
9	Au (1 wt.%)/BaTNT	TBHP+O$_2$ (stat)	72.2	34.0	59.9	2.3	0	3.8	24.5	281	938
10	Au (1 wt.%)/BaTNT	TBHP+O$_2$ (flow)	75.8	56.1	34.8	1.4	0	7.7	42.5	295	985
11	BaTNT	TBHP	22.5	43.0	41.2	6.0	0	9.8	15.1	-	-
12	No catalyst	TBHP	18.0	38.9	26.1	7.5	0	27.5	7.0	-	-

[a]Reaction conditions: catalyst = 50 mg, styrene = 10 mmol, solvent (acetonitrile, ACN) = 5 ml, reaction temperature = 80 °C, substrate/oxidant molar ratio = 1:1 (in the case of 30% aq. H$_2$O$_2$ and TBHP in n-decane (5.5 M)), reaction time =15 h. H$_2$O$_2$ refers to 30% aqueous H$_2$O$_2$, TBHP refers to TBHP in n-decane (5.5 M). Aq. TBHP refers to 70% aqueous TBHP. [b]Photocatalytic reaction at 25 °C for 5 h. [c]Turnover frequency (TOF) = moles of styrene converted per mole of total metal in the catalyst (ICP-OES) per hour. [d]TOF values based on moles of styrene converted per mole of surface metal atoms (estimated from TEM) per hour. SO = styrene oxide, Bzh = benzaldehyde, PAA = phenylacetaldehyde, Diol = 1-phenyl-1,2-ethanediol and others include acids.

Table 5.3. Influence of solvent on catalytic performance of Au (1 wt.%)/BaTNT[a]

Run No.	Solvent	Polarity	Styrene conversion (wt.%)	Product selectivity (wt.%)				Yield of SO (%)
				SO	Bzh	PAA	Others	
1	ACN	6.2	60.5	80.1	13.4	2.5	4.0	48.5
2	DMF	6.4	38.8	70.0	23.0	0	7.0	27.2
5	Dioxane	4.8	14.6	57.4	36.1	0	6.5	8.4
6	Toluene	2.4	15.4	39.6	48.8	4.4	7.2	6.1

[a]Reaction conditions: catalyst = 50 mg, styrene = 10 mmol, solvent = 5 ml, reaction temperature = 80 °C, substrate/ TBHP (5.5 M) (mol/mol) = 1:1, reaction time =15 h.

Table 5.4. Influence of Au loading on the oxidation of styrene[a]

Run No.	Au (wt.%)	Conversion (wt.%)	Selectivity (wt.%)				Yield of SO (%)	TOF[b] (h^{-1})	TOF[c] (h^{-1})
			SO	Bzh	PAA	Others			
1	0.5	31.0	75.8	14.0	3.4	6.8	23.5	273	879
2	1	60.5	80.1	13.4	2.5	4.0	48.5	236	786
3	2	72.8	74.2	13.8	5.6	6.4	54.0	132	500
4	3	77.2	69.4	14.1	9.9	6.6	53.6	73	328
5	5	80.0	64.6	16.1	12.5	6.8	51.7	52	246

[a]Reaction conditions: catalyst (Au(x wt.%)/BaTNT) = 50 mg, x = 0.5 - 5, styrene = 10 mmol, solvent (ACN) = 5 ml, reaction temperature = 80 °C, substrate/TBHP (5.5 M) (mol/mol) = 1:1, reaction time =15 h. [b]Turnover frequency (TOF) = moles of styrene converted per mole of total metal in the catalyst (ICP-OES) per hour. [c]TOF values are calculated based on mole of styrene converted per mole of surface metal atoms (estimated from TEM) per hour.

ACN with high polarity enabled high conversion of styrene. Polar solvents not only affected activity but also the selectivity for SO. Similar observations reported also by Liu et al. [25].

5.3.2.1.2. *Effect of Au Loading*

With increasing Au loading on BaTNT from 0.5 to 5 wt.%, a continuous rise in styrene conversion from 31 to 80 wt.% was observed (Table 5.4). Beyond 3 wt.% Au on BaTNT the increase in styrene conversion was marginal. TEM studies indicated that the mean particle size of Au increases from 5 to 7 nm, as the gold loading increases above 1 wt.%. While styrene conversion increases at higher Au loadings, selectivity to SO decreases

from 80.1 to 64.6 wt.%. The lower selectivity of Au(5 wt.%)/BaTNT could be associated with the large Au particles present in that catalyst.

5.3.2.1.3 Effect of Reaction Temperature, Catalyst Amount, Styrene/TBHP Ratio and Reaction Time.

Reaction temperature has a significant effect on the activity and selectivity of Au/(1 wt.%)BaTNT in the oxidation of styrene (Table 5.5). Oxidation of styrene with TBHP occurred even at 40 °C. But the conversion was 20 wt.% only. With increasing temperature from 40 to 85 °C, styrene conversion increased from 20 to 64.4 wt.%. An increase in SO selectivity from 58.4 to 80.1 wt.% was observed with rise in temperature from 40 to 80°C but above that it started decreasing. In other words, SO yield showed a maximum at 80 °C.

Table 5.5 Influence of reaction temperature on the oxidation of styrene[a]

Run No.	Temp. (°C)	Styrene conversion (wt.%)	Product selectivity (wt.%)				Yield of SO (%)	TOF[b] (h⁻¹)	TOF[c] (h⁻¹)
			SO	Bzh	PAA	Others			
1	40	20.0	58.4	18.2	1.2	22.2	11.7	78	260
2	60	31.4	69.4	16.8	3.0	10.8	21.8	122	408
3	80	60.5	80.1	13.4	2.5	4.0	48.5	236	786
4	85	64.4	73.6	13.8	2.8	9.8	47.4	251	837

[a]Reaction conditions: catalyst (Au/BaTNT) = 50 mg, styrene = 10 mmol, solvent (ACN) = 5 ml, substrate/ TBHP (5.5 M) (mol/mol) = 1:1, reaction time =15 h. [b]Turnover frequency (TOF) = moles of styrene converted per mole of total metal in the catalyst (ICP-OES) per hour. [c]TOF values are calculated based on mole of styrene converted per mole of surface metal atoms (estimated from TEM) per hour.

Figs. 5.7 and 5.8 demonstrate the effects of catalyst mass and substrate/TBHP molar ratio on the catalytic performance of Au(1 wt.%)/BaTNT. The styrene conversion increased from 31.8 to 82.4 wt.% with increasing catalyst mass from 0.025 to 0.1 g, which could be attributed to availability of more number of active sites. SO selectivity was 80.1 wt.% when the amount of catalyst taken was 0.05 g and the selectivity to SO decreasing while the catalyst amount was above 0.05 g. Hence, there is an upper limitation for the catalyst amount which is 0.05 g. Increase in oxidant concentration enhanced styrene conversion. However, the plot of SO selectivity revealed that a molar ratio of 1:1 for substrate/TBHP is ideal for getting high SO.
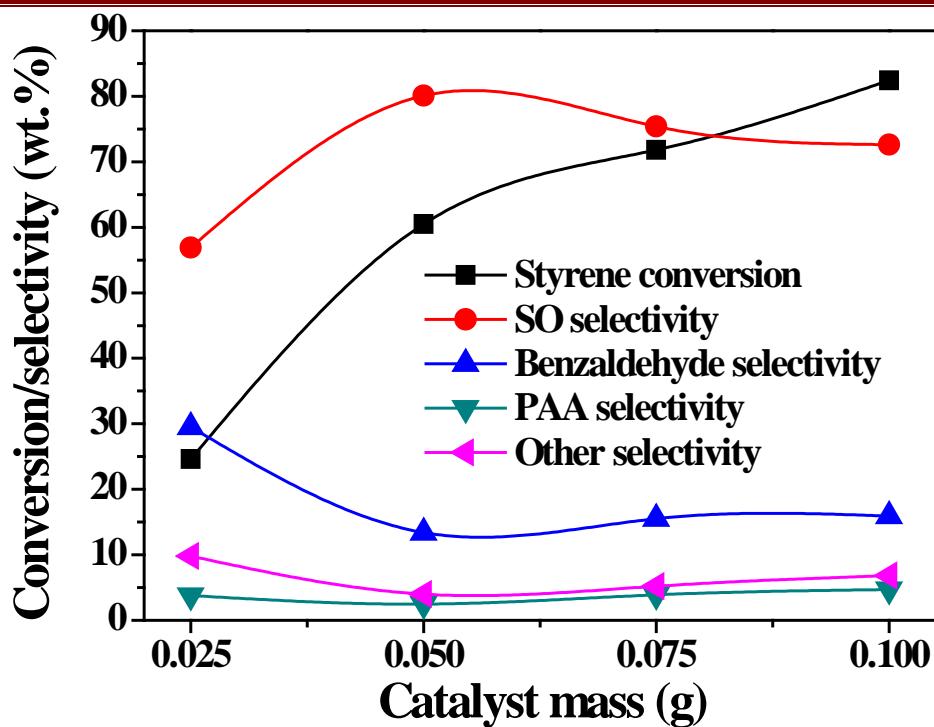
Fig. 5.7. Effect of catalyst mass on the catalytic performance of Au(1 wt.%)/BaTNT. Reaction conditions: styrene = 10 mmol, solvent (ACN) = 5 ml, temperature = 80 °C, substrate/TBHP (5.5 M in decane) (mol/mol) = 1:1 and reaction time =15 h.
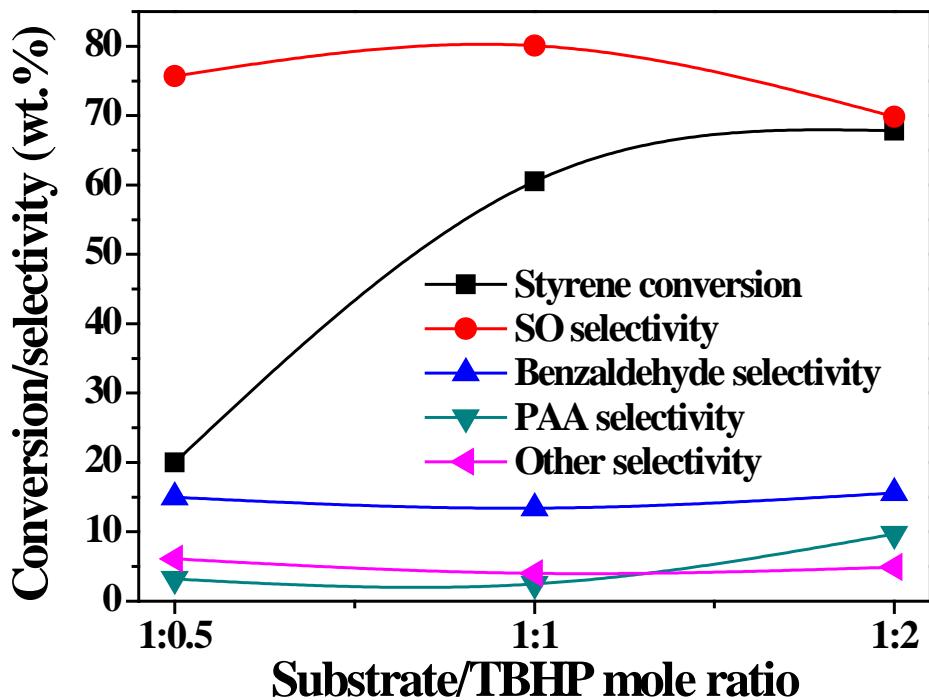


Fig. 5.8. Effect of substrate to oxidant (TBHP in decane) ratio over Au(1 wt.%)/BaTNT catalyst. Reaction conditions: catalyst = 50 mg, styrene = 10 mmol, solvent (ACN) = 5 ml, reaction temperature = 80 °C and reaction time =15 h.

Fig. 5.9 presents the effect of reaction time on styrene conversion and product selectivity over Au(1 wt.%)/BaTNT. Conversion of styrene increased with increasing reaction time. Styrene conversion of 78.8 wt.% was obtained after 24 h of run. Variation in product selectivity was noted as a function of reaction time. The selectivity for SO increased linearly with time up to 15 h and thereafter decreased continuously. The observed trends for the product selectivity point out that SO and Bzh are the primary products formed in parallel reactions. The selectivity for Bzh and PAA decreased with course of time as they underwent subsequent oxidation to corresponding acids. The study reveals that the oxidation of styrene is tough and requires at least 15 h for optimum yield of SO.
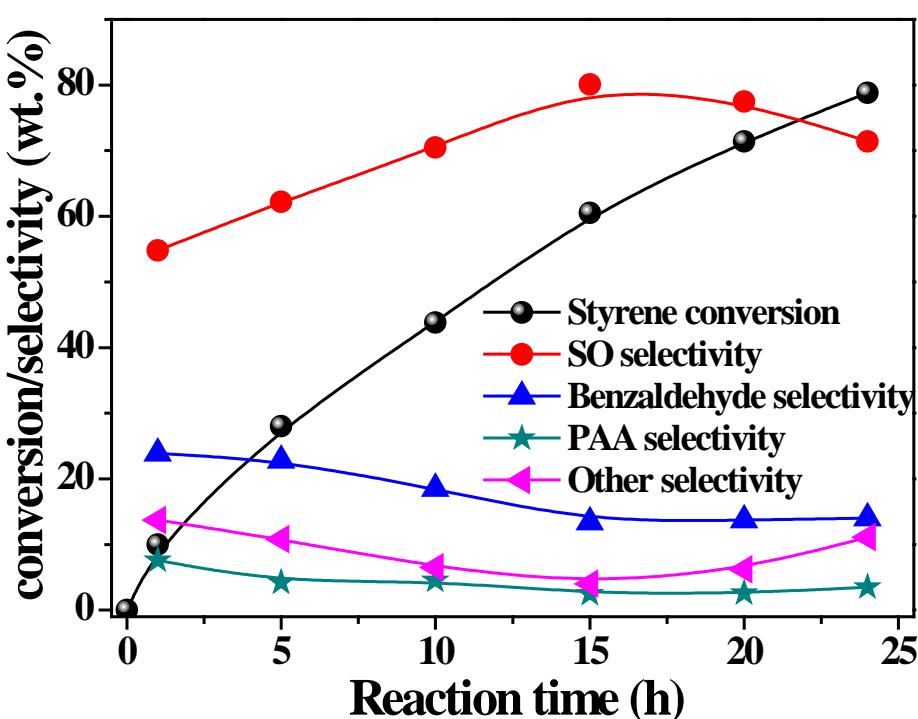

Fig. 5.9. Catalytic activity of Au(1 wt.%)/BaTNT was monitored with respect to the time. Reaction conditions: catalyst = 50 mg, styrene = 10 mmol, solvent (ACN) = 5 ml, reaction temperature = 80 °C and substrate/ TBHP (5.5 M in decane) (mol/mol) = 1:1.

5.3.2.1.4. Substrate Scope

In order to establish the general applicability of Au(1 wt.%)/BaTNT for epoxidation reactions, a variety of substituted styrenes were also tested under optimized reaction conditions (Table 5.6). The catalyst is active for oxidizing a range of substituted styrenes. In comparison to styrene (yield of epoxide = 48.5 %), α-methylstyrene and α,p-dimethylstyrene

afforded higher yields of epoxide (53.5% and 58.6%, respectively). Substituents on the aromatic ring do have a profound effect on conversion and epoxide selectivity. While diffusional effect is one reason for variation in conversion, electronic effects are the cause for the difference in epoxide selectivity.

Table 5.6. Epoxidation of substituted styrenes over Au(1 wt.%)/BaTNT[a]

R.No.	Substrate	Conversion (wt.%)	Selectivity (wt.%)				Yield of SO (%)
			SO	Bzh	PAA	Others	
1	Styrene	60.5	80.1	13.4	2.5	4.0	48.5
2	α -methylstyrene	64.8	82.6	9.5	2.0	5.8	53.5
3	p-methylstyrene	61.6	77.4	11.2	4.5	6.9	47.7
4	α, p-dimethylstyrene	68.5	85.5	8.6	3.4	2.5	58.6
5	p-chlorostyrene	48.8	61.2	28.0	4.4	6.4	29.9
6	p-nitrostyrene	38.1	54.3	35.1	4.1	6.5	20.7
7	p-methoxystyrene	32.8	68.3	15.9	6.3	9.5	22.4

[a]Reaction conditions: catalyst = 50 mg, substrate = 10 mmol, solvent (ACN) = 5 ml, reaction temperature = 80 °C, substrate/ TBHP (5.5 M) (mol/mol) = 1:1 and reaction time =15 h.

5.3.2.1.5. Catalyst Recyclability

With a view to probe the stability of Au(1 wt.%)/BaTNT in reactions, recyclability tests were conducted and the results of four recycles are shown in Fig. 5.10. After each run, the catalyst was separated from the reaction mixture by filtration, washed with acetonitrile, dried at 110 °C for 4 h and then, reused in the next recycle conducted at the same reaction conditions. A marginal decrease in styrene conversion from 60.1 to 55.4 wt.% was noticed after the fourth recycle. However, the selectivity towards styrene oxide remained constant in all the recycles. The decrease in styrene conversion was due to the increase in the mean particle size of supported Au from 5.2 to 6.9 nm (Fig. 5.3(f)). ICP-OES analysis confirmed the absence of leaching of gold into the liquid medium. XRD pattern of the spent Au(1 wt.%)/BaTNT (Fig. 5.1(g)) confirmed the structural integrity of the catalyst even after four reuses. These studies reveal that the catalyst is fairly stable in the oxidation of styrene with anhydrous TBHP as an oxidant.
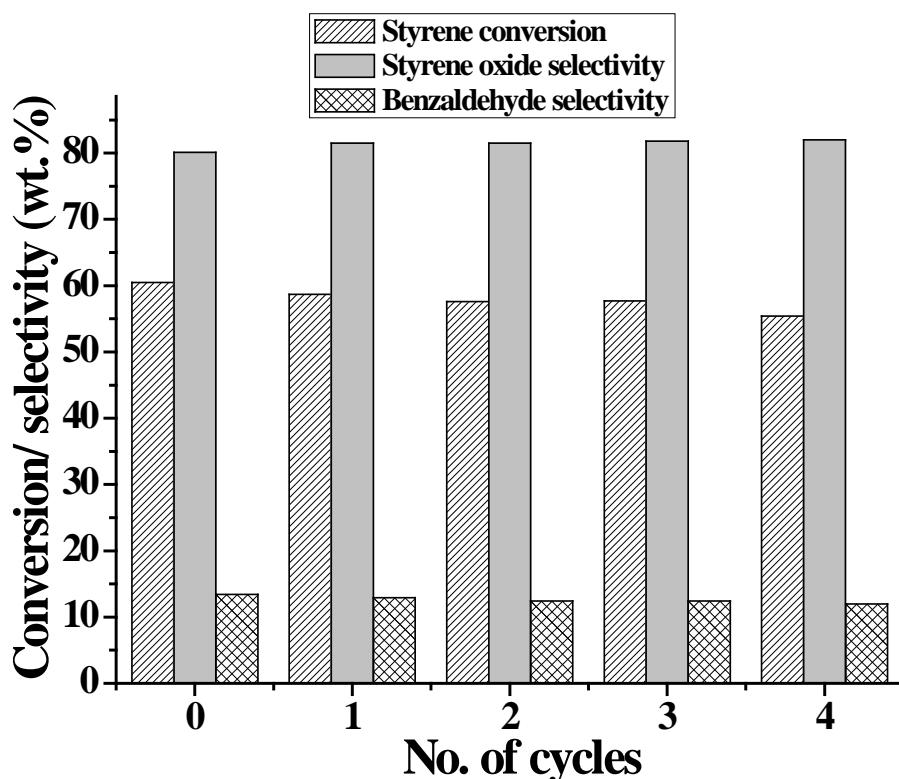
Fig. 5.10. Recyclability of Au(1 wt.%)/BaTNT for styrene oxidation. Reaction conditions: catalyst = 50 mg, styrene = 10 mmol, solvent (ACN) = 5 ml, reaction temperature = 80 °C, substrate/ TBHP (5.5 M in decane) (mol/mol) = 1:1 and reaction time =15 h.

5.3.2.2. Tentative Reaction Mechanism

A tentative reaction mechanism for the oxidation of styrene over Au/BaTNT is shown in Fig. 5.11. Oxidation of styrene occurs on the surface of gold [25-27]. When peroxides like H_2O_2 or TBHP interact with active Au, a metal-hydro/alkylperoxy species is formed. These peroxo species have been identified by DR UV-visible and FT-Raman spectroscopies (Figs. 5.4(b) and 5.5). These species by undergoing one electron reduction and loss of water molecule form Au-oxo species [8]. The first step in epoxidation is the addition of oxygen to the terminal double bond. Two kinds of intermediate oxametallacycles are formed in the case of styrene. Further conversion of oxametallacyclic species into products is considered as the rate determining step [26, 27], wherein epoxide is obtained from a metalloepoxy intermediate through transfer of oxygen to the olefinic bond and benzaldehyde from the breakage of the C-C bond. β-Hydride elimination from the oxametallacyclic species forms phenylacetaldehyde.
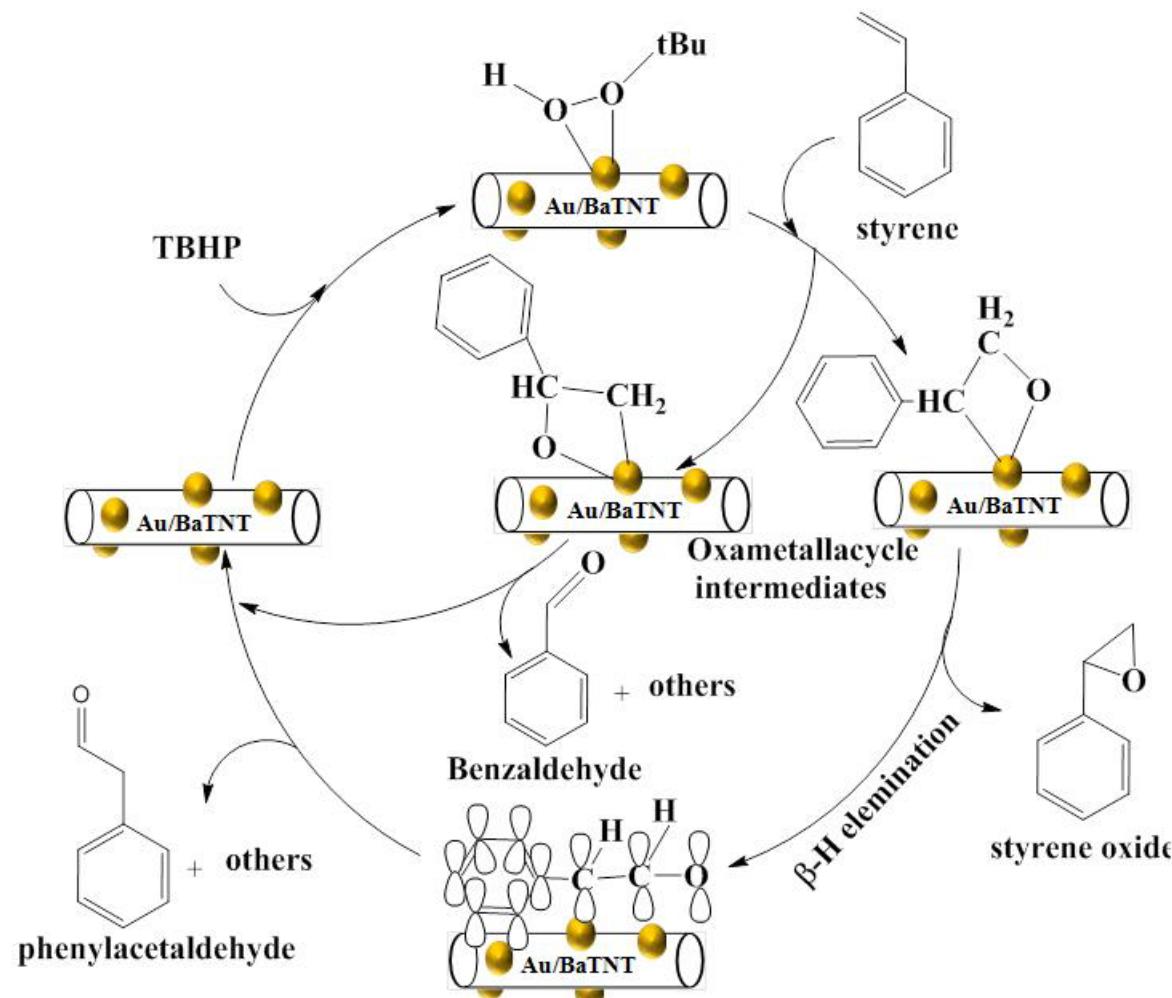
Fig. 5.11. Tentative mechanism for styrene oxidation

5.4. Conclusions

In summary, Au nanoparticles of varying amount 0.5 - 5 wt.% supported on barium ion-exchanged titanate nanotubes (BaTNT) were prepared, characterized and evaluated, for the first time, as catalysts for liquid-phase oxidation of styrene with O_2, H_2+O_2, aq. H_2O_2 and aq./non-aqueous TBHP as oxidants. Among the oxidants studied, TBHP (5.5 M, in decane) was found more effective resulting in high styrene conversion and styrene oxide selectivity in acetonitrile medium. Particle size and dispersion of Au showed a marked influence in the oxidation activity. At optimized conditions epoxide selectivity of 80.1 wt.% at styrene conversion of 60.5 wt.% was obtained. Au(1 wt.%)/BaTNT was reusable and effective for oxidation of a range of substituted styrenes.

5.5. References

[1]   O. D. Pavel, B. Cojocaru, E. Angelescu, V. I. Parvulescu, Appl. Catal. A: Gen. 403 (2011) 83-90.

[2]   V. R. Choudhary, D. K. Dumbre, N. S. Patil, B. S. Uphade, S. K. Bhargava, J. Catal. 300 (2013) 217-224.

[3]   I. Nongwe, V. Ravat, R. Meijboom, N. J. Coville, Appl. Catal. A: Gen. 466 (2013) 1-8.

[4]   E. Tebandeke, C. Coman, K. Guillois, G. Canning, E. Ataman, J. Knudsen, L. R. Wallenberg, H. Ssekaalo, J. Schnadt, O. F. Wendt, Green Chem. 16 (2014) 1586-1593.

[5]   B. Tyagi, U. Sharma, R. V. Jasra, Appl. Catal. A: Gen. 408 (2011) 171-177.

[6]   V. R. Choudhary, R. Jha, P. Jana, Green Chem. 8 (2006) 689-690.

[7]   N. S. Patil, B. S. Uphade, P. Jana, S. K. Bharagava, V. R. Choudhary, J. Catal. 223 (2004) 236-239.

[8]   M. Turner, V. B. Golovko, O. P. H. Vaughan, P. Abdulkin, A. B.-Murcia, M. S. Tikhov, B. F. G. Johnson, R. M. Lambert, Nature 454 (2008) 981-984.

[9]   B. Chowdhury, J. J. Bravo-Suárez, M. Daté, S. Tsubota, M. Haruta, Angew. Chem. Int. Ed. 118 (2006) 426-429.

[10]   Y. Zhu, H. Qian, M. Zhu, R. Jin, Adv. Mater. 22 (2010) 1915-1920.

[11]   J. Jiang, Q. Gao, Z. Chen, J Mol. Catal. A: Chem. 280 (2008) 233-239.

[12]   M. Toth, J. Kiss, A. Oszko, G. Potari, B. Laszlo, A. Erdohelyi, Top. Catal. 55 (2012) 747-756.

[13]   V. Idakiev, Z.-Y. Yuan, T. Tabakova, B.-L. Su, Appl. Catal. A: Gen. 281 (2005) 149-155.

[14]   T. Murciano, Q. He, G. J. Hutchings, C. J. Kiely, D. Chadwick, ChemCatChem 6 (2014) 2531-2534.

[15]   D. Nepak, D. Srinivas, Catal. Commun. 58 (2015)149-153.

[16]   D. Nepak, D. Srinivas, RSC Adv. 5 (2015) 47740-47748.

[17]   B. Chowdhury, J. J. Bravo-Suarez, N. Mimura, J. Lu, K. K. Bando, S. Tsubota, M. Haruta, J. Phys. Chem. B. 110 (2006) 22995-22999.

[18]   D. V. Bavykin, M. Carravetta, A. N. Kulak, F. C. Walsh, Chem. Mater. 22 (2010) 2458-2465.

[19]   T. Gao, H. Fjellvag, P. Norby, Inorg. Chem. 48 (2009) 1423-1432.

[20]   D. Yang, H. Liu, L. Liu, S. Sarina, Z. Zheng, H. Zhu, Nanoscale 5 (2013) 11011-11018.

[21]   P. Lakshmanan, F. Averseng, N. Bion, L. Delannoy, J.- M. Tatibouet, C. Louis, Gold Bull. 46 (2013) 233-242.

[22]   H.-Y. Chan, V. -H. Nguyen, J. C. S. Wu, V. C. -Casilda, M. A. Banares, H. Bai, Catalysts 5(2015) 518-533.

[23]   Y. Zhu, H. Qian, R. Jin, Chem. Eur. J. 16 (2010) 11455-11462.

[24]   V. N. Shetti, P. Manikandan, D. Srinivas, P. Ratnasamy, J. Catal. 216 (2003) 461-467.

[25]   J. Liu, F. Wang, T. Xu, Z. Gu, Catal. Lett. 134 (2010) 51-55.

[26]   X. Deng, C. Friend, J. Am. Chem. Soc. 127 (2005) 17178-17179.

[27]   R. Quiler, X. Liu, C. Friend, Chemistry – An Asian Journal 5 (2010) 78-86.

List of Publications

1. Direct synthesis of amides from amines using mesoporous Mn-SBA-12 and Mn-SBA-16 catalysts

   Anuj Kumar**, Devadutta Nepak** and D. Srinivas

   Catalysis Communications 37 (2013) 36-40.

2. Catalysis by supported nano-gold in liquid phase hydrogenation of cinnamaldehyde

   Devadutta Nepak, Bhogeswararao Seemala and D. Srinivas

   Science Letters 4 (2015) 106-110.

3. Selective aerobic oxidation of alcohols over Au-Pd/sodium titanate nanotubes

   Devadutta Nepak and D. Srinivas

   Catalysis Communications 58 (2015) 149-153.

4. Effect of alkali and alkaline earth metal ions on benzyl alcohol oxidation activity of titanate nanotubes-supported Au catalysts

   Devadutta Nepak and D. Srinivas

   RSC Adv. 5 (2015) 47740-47748.

5. Gold nanoparticles supported on barium-titanate nanotubes as efficient catalyst for selective oxidation of styrene

   Devadutta Nepak and D. Srinivas (to be communicated).

List of Patents

1. Process for producing amide compounds

   D Srinivas, Anuj Kumar and **Devadutta Nepak**

   US 0099900 A1 (2015)